HYDROGEN BONDING AND CRYSTAL PACKING IN MULTI-FUNCTIONAL MOLECULES

A Thesis
Submitted for the Degree of
Doctor of Philosophy

By

L. SREENIVAS REDDY

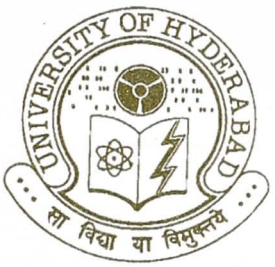

School of Chemistry
University of Hyderabad
Hyderabad 500 046
India

April 2006

Dedicated to
Amma & Nanna

STATEMENT

I hereby declare that the matter embodied in this thesis entitled **"Hydrogen Bonding and Crystal Packing in Multi-Functional Molecules"** is the result of investigations carried out by me in the School of Chemistry, University of Hyderabad under the supervision of Prof. Ashwini Nangia.

In keeping with the general practice of reporting scientific observations due acknowledgements have been made wherever the work described is based on the findings of other investigators.

Hyderabad
April 2006

L. Sreenivas Reddy

STATEMENT

I hereby declare that the matter embodied in this thesis entitled **"Hydrogen Bonding and Crystal Packing in Multi-Functional Molecules"** is the result of investigations carried out by me in the School of Chemistry, University of Hyderabad under the supervision of Prof. Ashwini Nangia.

In keeping with the general practice of reporting scientific observations due acknowledgements have been made wherever the work described is based on the findings of other investigators.

Hyderabad
April 2006

L. Sreenivas Reddy

CERTIFICATE

Certified that the work "**Hydrogen Bonding and Crystal Packing in Multi-Functional Molecules**" has been carried out by L. Sreenivas Reddy under my supervision and that the same has not been submitted elsewhere for a degree.

Dean
School of Chemistry

Prof. Ashwini Nangia
Thesis Supervisor

ACKNOWLEDGEMENT

I express my deep sense of gratitude and profound thanks to **Prof. Ashwini Nangia** for his inspiration, guidance and constant encouragement throughout the course of this research work.

I would like to thank Prof. Gautam R. Desiraju for his guidance on the project described in chapter 7.

I thank Prof. M. Periasamy, Dean, School of Chemistry and former Deans of the School and faculty for their co-operation in providing facilities in the School.

I would like to thank Dr. V.M. Lynch, University of Texas, Austin, USA, Prof. R. Boese, University of Essen, Germany, Prof. T.C.W. Mak, The Chinese University of Hong Kong, China, Prof. G.J. Kruger, University of Johannesburg, South Africa and Prof. J.-F. Nicoud, France for their help in collecting single crystal, powder X-ray diffraction data and SHG measurements on some of the compounds studied in this thesis.

I am very thankful to Dr. P. Pratap Reddy and Dr. A. Ram Reddy who encouraged me to join the Ph. D programme.

I am thankful to all the teachers and lecturers, who taught me throughout my career. My sincere thanks to late Sri P. Hanmi Reddy, who was my first teacher.

I am grateful to CSIR, New Delhi for fellowship support. I thank DST for providing single crystal X-ray diffractometer facility and UPE programme of UGC for infrastructure facilities.

I thank all the non-teaching staff of the School of Chemistry, CIL, COSIST building and the Computer Centre for their assistance on various occasions. I thank Mr. Raghavaiah and Satyanarayana for their help with X-ray data collection and NMR respectively.

I wish to thank my friendly and cooperative labmates Drs. Sanjay, R. Thaimattam, R.K.R. Jetti, V.S.S. Kumar, S. George, P. Vishweshwar, P.K. Thallapally, V.R. Vangala, S. Basavoju, Narendar, Srinivasulu and Mrs. Sairam, Bala Krishna Reddy, Malla Reddy, Binoy, Saikat, Sreekanth, Jagadeesh, Bipul, Ranjit and Naba Kamal for creating a cheerful working atmosphere in the lab. I also thank Dinabandu, Archan, Prashant, Aparna, Sunil, Tejendar, Pati, Sanjeev and Sandeep for their help on various occasions. My stay on this campus has been pleasant with the association of all the research scholars at the School of Chemistry, Srivardhan, Raghunath Reddy, Jaipal Reddy, Sastry, Sampath, Jagan, Bandaru, Siva, JK, Dharmanna, Vamsee Krishna, Chadra Sekhar, Pradeep, Senthil Kumar, Alchemie

99, Pavan Chicha, Gupta, Devender, Ravikanth, Maadhu, Anbu, Raju, Ramesh Reddy, Aravind, Shekar Reddy, Rajesh, Yadaiah, Krishna Rao, Bhuvan, Venu, Phani, Sridhar Reddy, Satish, Ramprasad, Mahipal Mama, Malli, Madan and others.

Special thanks to my labmates Dr. A. Srinivasulu and Saikat Roy for their assistance in DSC and TGA measurements. Jagadeesh Babu and Dr. Basavoju Srinivas for their help in synthesizing some of compounds discussed in this thesis. I also thank Rahul and Prasant for VT-PXRD measurements.

I thank my M.Sc. friends, Rajesh, Vidya Sagar, Prasad Reddy, V. Neelima, Neelima, Sangeetha, Uncle Rajendar, SM, Bhaskar Reddy, Uma, Nayeem, Srinivas, Jangaiah, Kurmaiah, Srinivas Reddy, Sridhar Reddy, Indra Sekhar and Nagendra Babu for their timely help and encouragement. I also thank G. Madhusudan Rao and Jagan Reddy for their help, when I was in IIT study circle.

It would be too formal to thank my personal friends at home Lotti, Anil, Prema, Peddodu, Koti, Ramanji, V. Dada, Nidroji, Venu, Ramana, Sodi Reddy, Yaram Srinu, Allu Srinivas Reddy and Gundu Srinu for their unreserved encouragement.

I thank my brother and sister-in-law, sisters and brothers-in-law and their families for support and encouragement. I thank my nieces, nephews and all the children in my family for their smiles and wishes, special thanks to Mohan Reddy, Narsi Reddy, Ramu, Anji Reddy and Venkat Reddy.

The blessings and best wishes of my parents keep me active throughout my life. They made me what I am and I owe everything to them. Dedicating this thesis to them is a minor recognition for their invaluable support and encouragement.

L. Sreenivas Reddy
April 2006

SYNOPSIS

This thesis entitled "**Hydrogen Bonding and Crystal Packing in Multi-Functional Molecules**" consists of nine chapters.

CHAPTER ONE

Supramolecular Chemistry and Crystal Engineering

Hydrogen bonding plays an important role in supramolecular chemistry, crystal engineering and biological recognition. To prepare a desired crystal structure of interest, one must first identify molecular functionalities that will generate predictable intermolecular interactions or synthons. It becomes more difficult in multi-functional molecules because of competition between similar strength donor/acceptor groups. Therefore, understanding the forces that govern recognition between multi-functional molecules is of fundamental importance in supramolecular molecular chemistry. With a knowledge of intermolecular interactions and their specificity in recognition (homosynthons and heterosynthons), organic crystal engineering is now geared towards synthesizing cocrystals using supramolecular reactions. Some recent advances in cocrystallization, hydrogen bond competition and polymorphism are discussed in chapter 1.

CHAPTER TWO

Hydrogen Bond Competition and Interplay of Weak Interactions in Crystal Structures of Nitro-Substituted Diphenylureas

The urea tape α-network of bifurcated N–H···O hydrogen bonds is a common motif in unsubstituted diarylureas. However diarylureas with electron-withdrawing and/or a hydrogen bond acceptor groups behave differently in terms of hydrogen bonding with itself and cocrystal and/or solvate formation. Alternative hydrogen bonding pattern and engineering of characteristic urea tape α-network are discussed in a series of *N*-(*p*-nitropheny)-*N*′-(*m/p*-X-phenyl)urea compounds (Scheme 1).

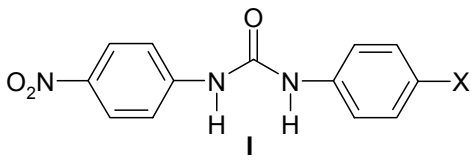

I

1: X = F **11**: X = $CONH_2$·DMSO

2: X = Cl
3: X = Br
4: X = CN
5: X = I(*m*-isomer)
6: X = Br(*m*-isomer)
7: X = H·DMF
8: X = CN·DMF
9: X = $CONH_2$·DMF
10: X = I·DMSO
12: X = Me·DMSO
13: X = Ac·DMSO
14: X = F (3,5-difluoro)·DMSO
15: X = OH(*m*-isomer)·H_2O
16: X = I
17: X = Ethynyl
18: X = $N(Me)_2$
19: X = 4-Iodophenyl
20: X = 4-Ethynylphenyl

Scheme 1. Compounds studied in chapter 2.

Crystal structures studied in this chapter can be divided into two categories: non-urea tape structures (structures which are not forming α-network, **1**–**15**), and urea tape structures (**16**–**19**). Compound **20** did not afford diffraction quality single crystals, but powder XRD pattern is similar to **19**. This study shows that the conformation and weak interactions are driving the strong hydrogen bonds in crystal formation and highlights the importance of understanding hydrogen bond pattern in a family of structures for reliable prediction of crystal packing.

CHAPTER THREE

Hydrogen Bond Competition and Interplay of Molecular Conformation in Crystal Structures of Pyridylureas

In the background of chapter 2, we have studied crystal structures of *N*,*N*′-bis(3-pyridyl)urea, **21**, which is electronically similar to *N*,*N*′-bis(3-nitrophenyl)urea (electron withdrawing group) but sterically unblocked (like phenyl group). *N*,*N*′-bis(3-pyridyl)urea crystallizes as two hydrates (**21**·(4/3)H_2O and **21**·2H_2O) and forms complexes with succinic and fumaric acids (**21**·SA and **21**·FA·H_2O). To activate *ortho* hydrogens for C–H···O interactions, bis pyridine *N*-oxide, **22**, and bis-*N*-methylpyridinium iodide, **23** were prepared (Scheme 2). Crystal packing in these structures is directed by N–H···$N_{pyridyl}$, N–H···O_{water}, N–H···O_{acid} N–H···O_{oxide} and N–H···I^- hydrogen bonds instead of the one-dimensional N–H···O_{urea} tape. This indicates that the planar conformation with intramolecular C–H···O

synthon is the cause for deviation from the α-network in crystal structures of dipyridyl and phenyl–pyridylureas.

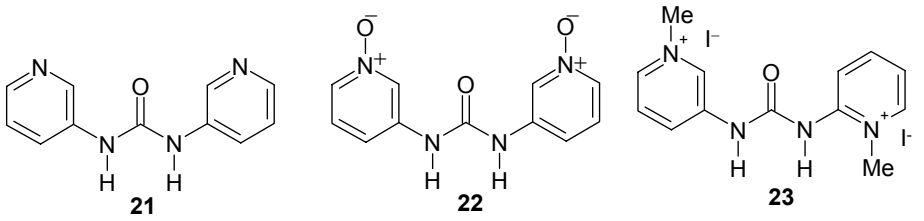

Scheme 2. Compounds studied in chapter 3.

CHAPTER FOUR

Phenyl–Perfluorophenyl Stacking and Supramolecular Reactivity in Multi-Component Cocrystals

Electron-deficient and electron-rich aromatic rings tend to stack because of favourable quadrupole–quadrupole interaction between aromatic rings with negative and positive quadrupole moment. The most remarkable example of phenyl–perfluorophenyl (Ph–Ph^F) stacking is the crystal structure of 1:1 complex of benzene-hexafluorobenzene. However, reliability of this synthon is only tested in the absence of strong hydrogen bonding functionalities. Considering that the energy of Ph–Ph^F synthon (4–5 kcal/mol) is half that of strong O–H···O, N–H···O hydrogen bonds (8-10 kcal mol^{-1}), we are interested to check the utility of this synthon in the presence of strong hydrogen bond functionalities, like carboxylic acids and amides. For this purpose X-ray crystal structures of **26**, **27**, and **28** are analyzed and compared with crystal structures of individual components. Complex **28** is not obtained under similar conditions. Mechanochemistry and supramolecular reactivity of these cocrystals is also studied by PXRD and VT-PXRD. Cocrystals **26** and **31** are formed by simple mechanical grinding at room temperature whereas in case of cocrystals **27** and **28** the cocrystal formation is incomplete at room temperature. As temperature increases the supramolecular reaction of cocrystal formation proceeds to completion about 100 °C in case of cocrystal **27** and 78 °C in cocrystal **28**. Molecular complexes are not formed in **29** and **30** even at high temperatures. Molecular complex **31** goes through a phase change on heating to form a stable new phase that does not change on cooling and substantial reheating.

$C_6H_5COOH{\cdot}C_6F_5COOH$, **26** $C_6H_5COOH{\cdot}C_6F_5CONH_2$, **29**

$C_6H_5CONH_2{\cdot}C_6F_5CONH_2$, **27** $C_6H_5COOH{\cdot}C_6H_5CONH_2$, **30**

$C_6H_5CONH_2 \cdot C_6F_5COOH$, **28** $C_6F_5COOH \cdot C_6F_5CONH_2$, **31**

CHAPTER FIVE

Phenazine and Acridine Stacks in Cocrystals With Multi-Functional Molecules

Aryl–aryl interactions between aromatic moieties are particularly useful in crystal engineering and supramolecular chemistry and can be used to manipulate the organization of molecular components in the crystalline state. To understand the nature and reliability of stacking in presence of strong hydrogen bonding functionalities, cocrystallization of phenazine and acridine with multi-functional molecules like phloroglucinol and 3,5-dihydroxybenzoic acid was attempted (Scheme 3).

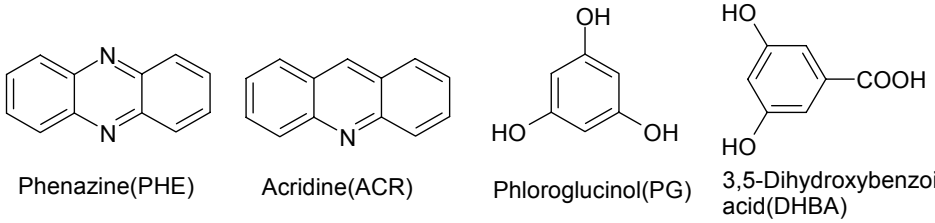

Phenazine(PHE) Acridine(ACR) Phloroglucinol(PG) 3,5-Dihydroxybenzoic-acid(DHBA)

37 = 1:1.5 (PG:PHE) **42** = 1:2 (PG:ACR)

38 = 2:3.5 (PG:PHE) **43** = 2:2:1 (DHBA:ACR:water)

39 = 0.5:1 (PG:PHE) **44**=1:3:1 (DHBA:ACR:acetonitrile)

40 = 1:2:1(PG:PHE:water) **45** = 1:3:1 (DHBA:ACR:ethanol)

41 = 1:1.5 (DHBA:PHE)

Scheme 3. Cocrystals and host-guest complexes studied in chapter 5.

Crystal structures **37** to **41** show a remarkable cooperation of hydrogen bonding, aromatic stacking and herringbone interactions in the formation of one-, two- and three-dimensional crystal structure. In **42**, both hydrogen bonding and stacking are in the same direction to form 2D layers. In the crystal structure of **43**, DHBA and water molecules form a 3D hexagonal channel structure and stacked acridine molecular columns fill in the channels as guest. Cocrystals **44** and **45** have similar structures. Acridine and DHBA form cavities with stacking and herringbone interactions and disordered guest molecules fill the cavities. All these crystal structures show that phenazine and acridine stacking is robust (as it always formed) and flexible (as stacking distances are varied) in presence of strong hydrogen functionalities like phenolic-OH and carboxylic acid groups.

CHAPTER SIX

Carboxamide···*N*-Oxide Heterosynthon and its Application in Cocrystal Design

A crystal structure is the result of a delicate balance between a range of intermolecular interactions. These interactions can be combined by the designed placement of functional groups in the molecular skeleton to generate supramolecular synthons. When there is a competition between acid–acid homosynthon and acid–pyridine heterosynthon the probability of the latter is 91%. But in case of amide-pyridine, out of 84 crystal structures containing primary amide and pyridine functionalities in CSD, only 4 structures have amide-pyridine heterosynthon. By taking advantage of the greater acceptor strength of *N*-oxide, carboxamide–*N*-oxide heterosynthon is designed and exploited in model API cocrystallization of barbiturate drugs with 4,4'-bipyridine-*N,N'*-dioxide (Scheme 4).

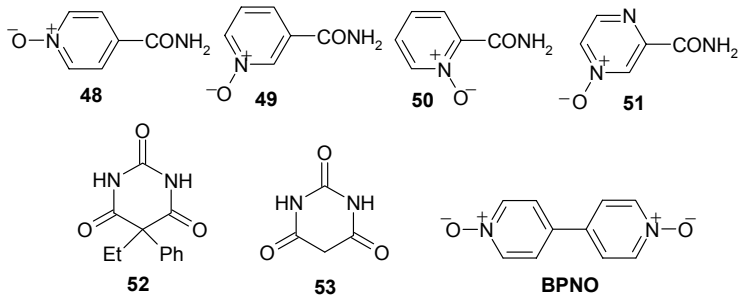

Scheme 4. Compounds studied in chapter 6.

CHAPTER SEVEN

Polymorphism in 6-Amino-2-phenylsulfonylimino-1,2-dihydropyridine and Derivatives

Polymorphism, the phenomenon that molecule can crystallize in more than one solid-state form, is a major challenge in our fundamental understanding of crystallization and is of immense practical importance in pharmaceuticals industry. Amino-2-phenylsulfonylimino-1,2-dihydropyridine, **54**, is a conformationally flexible molecule with two degrees of acyclic torsional freedom, is one of the three molecules supplied in CSP2001. Compound **54** exhibits synthon based polymorphism. Kinetic Form I is characterized by 2-point catemer synthon whereas thermodynamic Form II is characterized by 4-point dimer synthon (Scheme 5). But in derivatives of **54**, polymorphism was not found in a general sense exept in *p*-methyl derivative. Thermodynamic Form II is isolated with much difficulty and crystallizes only from nitromethane.

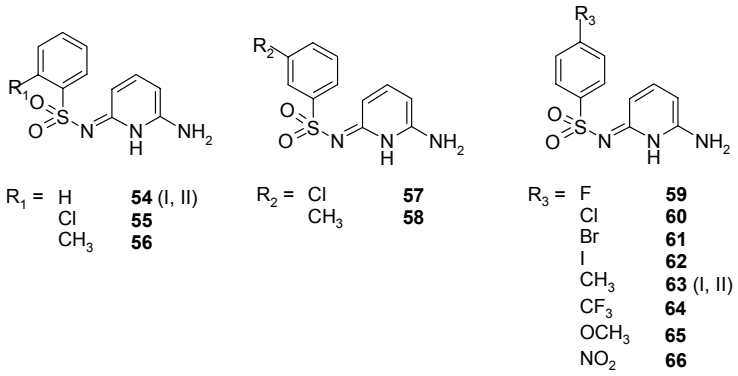

Scheme 5. Compounds studied in chapter 7.

CHAPTER EIGHT

Weak C–H···N Hydrogen Bond Mediated Network Structures

The description of crystal structures in terms of networks is one of the most promising of systematic approaches to communicate connectivity information in a precise fashion. The $SrAl_2$ net (Schläfli symbol $4^2.6^3.8$) is an uncommon topology among 4-connected interpenetrated nets, occurring in only five metal–organic structures out of 301 refcodes analyzed from the CSD. $SrAl_2$ network is generally formed by distorted tetrahedral nets. But surprisingly a pseudo-trigonal molecule **67** (Scheme 6) forms $SrAl_2$ with exclusively weak C–H···N interactions and its saturated analogue **68** forms expected trigonal network.

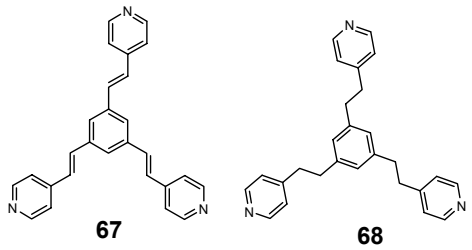

Scheme 6. Compounds studied in chapter 8.

CHAPTER NINE

Conclusions

A particular class of organic compounds will have a characteristic hydrogen bond pattern. N–H···O mediated α-network is the characteristic hydrogen bond motif in unsubstituted arylureas with twisted conformation. Alternation of hydrogen bonded motifs in some substituted aryl and pyridylureas are discussed in Chapter 2 and 3. When electron

withdrawing groups like nitro, pyridine-*N* are substituted, the crystal structures are dominated by planar conformation and intramolecular C–H···O synthon.

Weak interactions play an important role in crystal structure stabilization and assembly when strong interactions are absent. On the other hand there are seminal reports where weak interactions play major role in directing the strong interactions. Hence understanding the role of weak interactions in the presence of strong hydrogen bonds is crucial in crystal structure prediction and the design of novel materials. The role of aryl-perfluoroaryl and aryl-aryl stacking and their reliability in the presence of strong hydrogen bonding functionalities are studied in Chapter 4 and 5.

Design of materials with specific properties and controlling polymorphism require a knowledge of dominant synthons, because these synthons are primarily responsible for the arrangement of molecules in the crystal lattice. Heterosynthons considerably reduce the possibility of alternative hydrogen bond patterns, and hence control polymorphism. A novel amide-*N*-oxide heterosynthon is designed and exploited in model API cocrystals of barbiturate drugs in chapter 6.

From the structures discussed in Chapter 7, it can be concluded that though the polymorphs are predicted computationally, the experimental observation of these forms is very difficult. Prediction of polymorphs even in closely related molecules is not easy and substitution effect is minimum when molecules are capable of forming multiple complimentary hydrogen bonds.

The network representation is a useful and powerful concept and a simplifying aid for crystal engineering. Generally tetrahedral molecules like tetraphenylmethane and adamantane derivatives act as 4-connected tetrahedral node and form diamondoid networks. As discussed in Chapter 8, a pseudo trigonal molecule 1,3,5-tris[4-pyridyl(ethenyl)]benzene with cluster of five molecules forms a distorted tetrahedral node and propagation of these nodes results in a rare 3D $SrAl_2$ network mediated by weak C–H···N interactions. Thus, careful analysis of molecular packing and intermolecular interactions and judicious choice of nodes and node connections will lead to new examples of organic network architectures.

Salient crystallographic details of the crystal structures discussed in this thesis have been given in an appendix at the end of the thesis. A full list of atomic coordinates has been deposited with the University of Hyderabad and is available upon request from Prof. Ashwini Nangia (ashwini_nangia@rediffmail.com).

CONTENTS

CHAPTER FOUR

CHAPTER FIVE

CHAPTER 1

SUPRAMOLECULAR CHEMISTRY AND CRYSTAL ENGINEERING

"There is no more basic enterprise in chemistry than the determination of the geometrical structure of molecule. Such a determination, when it is well done, ends all speculation as to the structure and provides us with the starting point for the understanding of every physical, chemical and biological property of the molecule."

–R. Hoffman in *Determination of the Geometrical Structure of Free Molecules,* MIR Publishers: Moscow, 1983.

1.1 Introduction

For more than 150 years, synthetic organic chemists have accumulated an immense amount of knowledge about the rules that govern the fabrication and transformation of covalent molecular species. The level of understanding has presently reached a stage where even very complex target organic molecules can be synthesized. Molecular chemistry, thus, has established its power over the covalent bond. The field of covalent synthesis has perhaps reached the limit of what is synthetically achievable in terms of time requirements and yields. A complex molecule like palytoxin[1] an extraordinarily toxic natural product isolated from marine soft corals of the genus palythoa, with 65 disymmetric carbons and 10^{21} possible isomers weighing 2680 daltons, was synthesized in 10 years by over 100 researchers. The chemistry of the last 25 years has been largely dominated by the endeavor to master secondary noncovalent bonding. This has meant a substantial shift of interest, from focus on atoms and bonds between atoms to emphasis on molecules and bonds between molecules.[2] Beyond molecular chemistry based on the covalent bond there lies the field of supramolecular chemistry, wherein the goal is to gain control over the intermolecular bond. The term supramolecular chemistry and its basic concepts were introduced by J.-M. Lehn in 1978. [3] He defined supramolecular chemistry as the "*chemistry of molecular assemblies and of the intermolecular bond*'. In supramolecular chemistry, one makes higher level aggregates (supermolecules) from smaller entities (molecules) using intermolecular interactions as the glue (Scheme 1).[4] Supramolecular chemistry is one of the most vigorous and fast growing fields in chemical sciences and its interdisciplinary nature

has brought wide ranging collaborations between physicists, theorists, computational modellers, crystallographers, organic and inorganic solid state chemists, biochemists and biologists. It is also a relatively young discipline. Its concepts and roots may be traced from the beginning of modern chemistry itself. There are three main branches of supramolecular chemistry: one in which hydrogen bonding plays a key role,[5] another in which weaker noncovalent interactions, such as stacking of aromatic rings, are the main forces, and a third in which coordination of ligands to metal ions is the central idea.[6] Supramolecular chemistry has always been associated with new materials and applications with the study of structure as a necessary first step towards the achievement of that goal. Investigations on the assembly of small organic molecules in solution and solid state are important in designing well-defined supramolecular architectures.

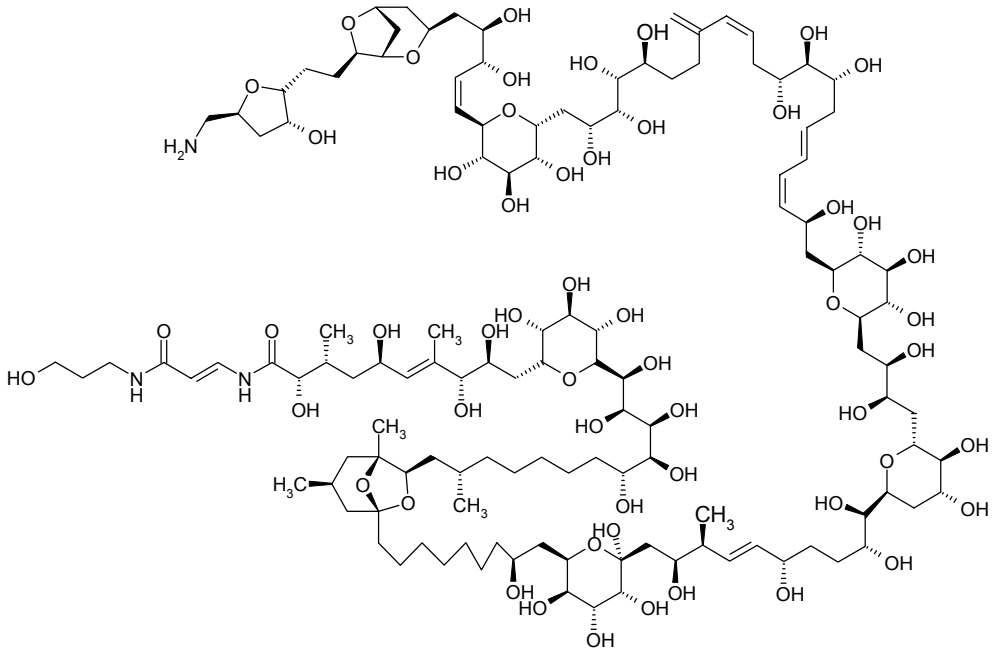

Palytoxin

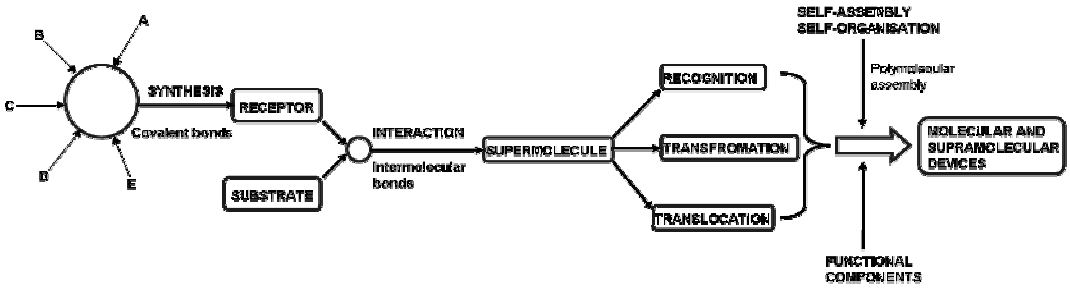

Scheme 1. From molecular to supramolecular chemistry: molecules, supermolecules, molecular and supramolecular devices (taken from ref. 2).

The word "Crystal Engineering" was first introduced by Pepinsky[7] in 1955 and was elaborated by Schmidt during the period 1960 to 1970 to address the issue of crystal packing in the context of organic solid state photochemical reactions of cinnamic acids and amides.[8] The meaning of term was extended by Desiraju who defined crystal engineering as "*the understanding of intermolecular interactions in the context of crystal packing and the utilization of such understanding in the design of new solids with desired physical and chemical properties*".[9] Analysis and design are the two principal components of crystal engineering. Analysis means examination of various intermolecular interactions that govern the crystal packing. This is mainly carried out by the analysis of structural data archived in the Cambridge Structural Database (CSD)[10] and through computational methods. Design involves utilization of the knowledge thus gained in the synthesis of new structures. Crystal engineering is an interdisciplinary field that seeks to develop protocols for predicting and controlling the structure and functional properties of solids. Such properties range from the commonplace (colour, melting point) to those of great relevance to materials scientists and physicists (polarity, porosity, conductivity) and pharmaceutical development (active drug form, bioavailability, stability). Some of the key research areas under the purview of crystal engineering include: catalysis, optical materials, conducting and magnetic materials, nanotechnology, electronic materials and sensors, nano and microporous materials, supramolecular devices, protein-receptor, binding molecular modeling and drug design.[11]

1.2 Intermolecular interactions

The properties of a crystalline material are the result of molecular arrangement in the crystal lattice, which is controlled by intermolecular interactions (Scheme 2). The crystal structure of a molecule is the free energy minimum resulting from the optimization of several attractive and repulsive intermolecular interactions with varying strengths, directional preferences and distance-dependence properties. Hence, understanding the nature and strength of intermolecular interactions is of fundamental importance in supramolecular chemistry. Intermolecular interactions in organic compounds can be classified as isotropic, medium-range forces, which define molecular shape, size and close packing; and anisotropic, long-range forces, which are electrostatic and involve heteroatom interactions.[12] In general, isotropic forces include C···C, C···H and H···H interactions and anisotropic interactions include ionic forces, strongly directional hydrogen bonds (O–H···O, N–H···O), weakly directional hydrogen bonds (C–H···O, C–H···N, C–H···X, where X is a halogen, and

O–H···π) and other weak heteroatom interactions such as halogen···halogen, nitrogen···halogen, sulfur···halogen and so on. Among all intermolecular interactions hydrogen bonding is the most reliable directional interaction and it has a fundamental role in crystal engineering.[13] The characteristic qualities of transferability and reproducibility make it the interaction *par excellence* in crystal engineering.[14] Hydrogen bonds are classified into three categories based on their strength as very strong, strong and weak hydrogen bonds (Table 1).[15]

Halogen bond (XB)[16] is the noncovalent interaction between halogen atoms (Lewis acids) and neutral or anionic Lewis bases, emerging as a parallel paradigm to hydrogen bonding in recent years. Practically all the energetic and geometric features known for hydrogen bond (HB) complexes are encountered in XB complexes as well. The XB interaction energy spans over a very wide range, from 1 to 35 kcal/mol, the weak Cl···Cl interaction between chlorocarbons and the very strong $I^-\cdots I_2$ interaction in I_3^- being the extremes. Due to its strength, XB can prevail over HB in selecting the modules to be involved in competitive recognition processes.[17]

Table 1. Some properties of very strong, strong and weak hydrogen bonds.

	Very strong	Strong	Weak
Bond energy (–kcal/mol)	15–40	4–15	< 4
Bond lengths	H–A ≈ X–H	H···A > X–H	H···A >>X–H
Lengthening of X–H (Å)	0.05–0.2	0.01–0.05	≤ 0.01
D(H···A) range (Å)	1.2–1.5	1.5–2.2	2.0–3.0
D(X···A) range (Å)	2.2–2.5	2.5–3.2	3.0–4.0
θ(X–H···A) range (°)	175–180	130–180	90–180
IR ν, relative shift	> 25%	5–25%	< 5%
Effect on crystal packing	strong	distinctive	variable
Covalency	pronounced	weak	vanishing
Electrostatics	significant	dominant	moderate

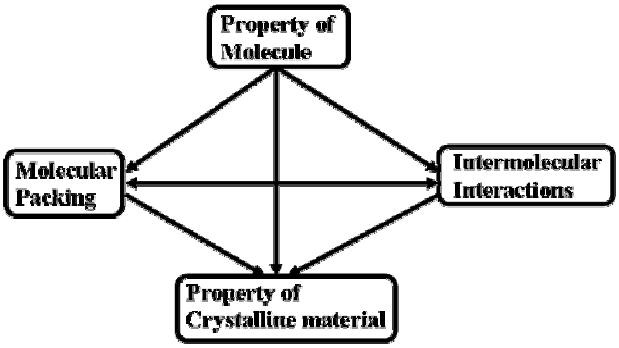

Scheme 2

1.3 Molecular recognition: Supramolecular synthons

Every crystal structure is the result of a delicate balance between a range of intermolecular interactions and study of an individual crystal structure leads to the identification of these interactions related to a specific crystal structure. The geometrical attributes of intermolecular interactions and their chemical characteristics can be studied reliably by statistical analysis. Directionality is a prerequisite of reproducibility, only if the topological properties of a given interaction persist in different structural environments; i.e., on passing from one solid supermolecule to another, the interaction is useful in the construction of new solids. This concept is elaborated in the idea of supramolecular synthon.

Corey introduced the term 'synthon' in 1967 to simplify the synthesis of complex natural products and other molecules.[18] Recognizing that crystal engineering is the solid state equivalent of supramolecular synthesis, Desiraju defined supramolecular synthons as *structural units within supermolecules which can be formed and/or assembled by known or conceivable synthetic operations involving intermolecular interactions*.[19] A synthon is usually smaller and less complex than the target structure and yet contains most of the information required to synthesize the target substance. Synthons represent a carry-over of structural information between crystal structures and as the size increases the information content increases; so larger synthons are potentially more useful than smaller ones. But as the synthon size increases, its occurrence becomes less frequent. The advantage of using the synthon approach is that it offers a simplification in the understanding of crystal structures. Zaworotko sub-classified synthons as homosynthons and heterosynthons based on the interacting functional groups. If supramolecular synthon is formed between the same functional group it is a homosynthon, if it forms between two different functional groups it is called as heterosynthon.[20] Some homosynthons and heterosynthons are shown in scheme 3.

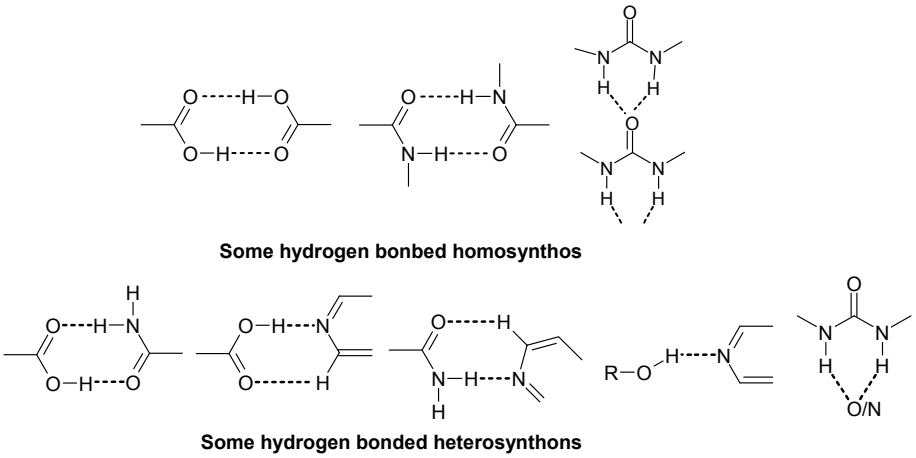

Scheme 3. Some of the homosynthons and heterosynthons studied in this thesis.

1.4 Role of weak interactions in organic crystals

Strong hydrogen bonds are well exploited in crystal engineering due to their inherent strength and reliability. However, crystal engineering studies are incomplete without considering weaker interactions due to their greater abundance in crystal structures.[21] The role of weak interaction can vary from unimportant to supportive to one that is actually driving the crystal structure. In this last case, the weak interactions may actually distort and modify the topology and arrangement of the conventional and stronger interactions. Weak interactions include C–H···O and C–H···N hydrogen bonds,[21a] C–H···π,[22] Hal···Hal interactions.[23] C–H···O and C–H···N hydrogen bonds are important in a wide variety of chemical and biological systems. They are electrostatic in nature and have long-range distance character (Table 1). Among weaker interactions, C–H···O hydrogen bonds gained much popularity due to the common presence of C–H groups and O-atoms in organic molecules. Furthermore, it was also shown that C–H···O hydrogen bonds are capable of exhibiting all the properties that are similar to strong hydrogen bonds such as dependence on the acidity and basicity of acceptor and donor strengths and near linearity of the interaction and lone-pair directionality of the acceptor. A typical example, where C–H···O hydrogen bonds direct the strong hydrogen bonding is the benzene clathrate of 1,3-cyclohexane dione (enol form). 1,3-Cyclohexane dione exists in two unsolvated polymorphs,[24] where infinite O–H···O hydrogen bond dominates the crystal structure (Figure 1a). It also crystallizes with benzene in 1:6 ratio, which form hexameric hydrogen bonded rings and benzene sits in the ring as guest and interacts with the host *via* weak C–H···O hydrogen bonds (Figures 1b, 1c).

Hexameric ring formation is observed only in the presence of benzene indicating the importance of C–H···O hydrogen bonds and guest size.[24a] Ohkita and coworkers[25] have synthesized the elusive graphyne network using weak C–H···N hydrogen bonds (Figure 2). Here the weak C–H···N hydrogen bond plays a directing role in determining the crystal structure.

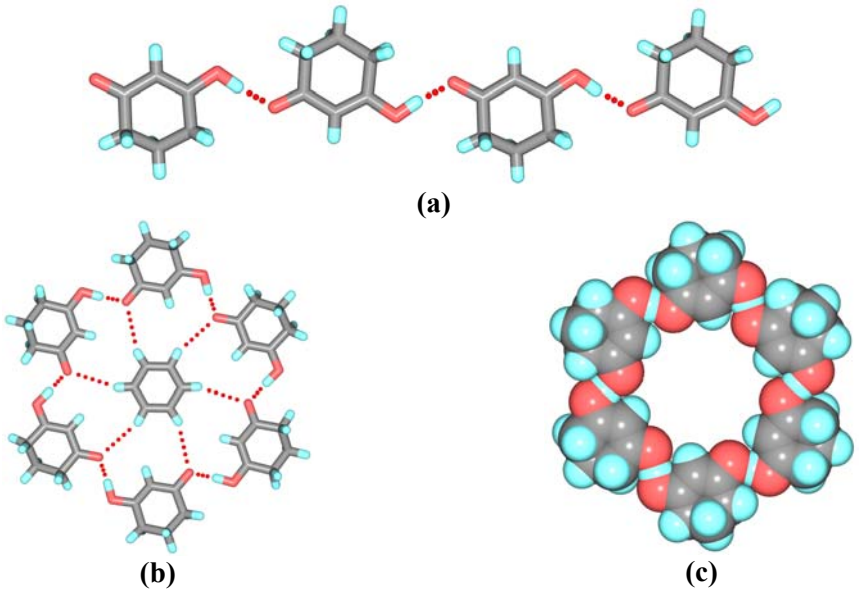

Figure 1. (a) Infinite O–H···O hydrogen bonded tapes in unsolvated 1,3-cyclohexane dione. (b) Benzene solvate of 1,3-cyclohexane dione. Note that the presence of C–H···O hydrogen bonds. (c) CPK model of hexameric hydrogen bonded ring, which is the emblem of *CrystEngComm* journal.

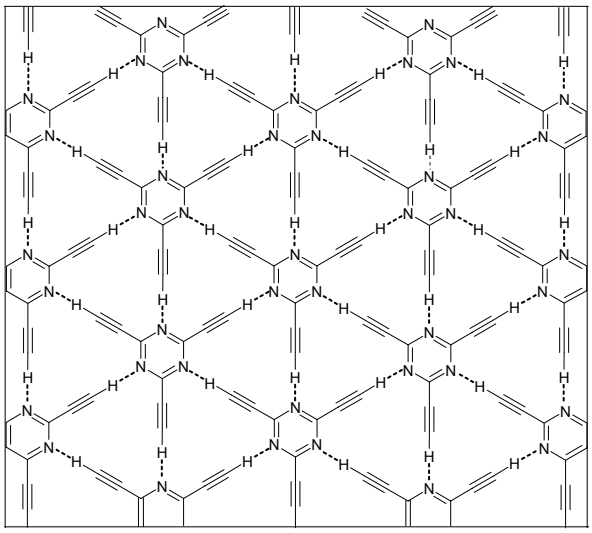

Figure 2. The two-dimensional hexagonal network structure formed by 2,4,6-triethynyl-1,3,5-triazine, a structure dominated by weak hydrogen bonds.

1.5 Hydrogen bond competition–Etter rules

To prepare a desired crystal structure of interest, one must first identify molecular functionalities that will generate predictable intermolecular interactions or synthons. It becomes more difficult in multi-functional molecules because of competition between similar strength donor/acceptor groups. To understand hydrogen bonding and competition in organic compounds, Etter proposed three hydrogen bond rules. In the case of reasonably strongly hydrogen-bonded systems, in which there is a single interaction that dominates the crystal packing of regularly shaped small molecules, it is possible to make some predictions about the resulting crystal structures. A fundamental rule is that "*all acidic hydrogens available in a molecule will be used in hydrogen bonding in the crystal structure of that compound*."[26] A second rule, corresponding to the first one, is that "*all good proton acceptors will be used in hydrogen bonding when there are available hydrogen-bond donors*."[27] The third rule is that "*the best hydrogen-bond donor and the best hydrogen acceptor will preferentially form hydrogen bonds to one another*."[28] If there is possibility of forming six-membered intramolecular hydrogen bond ring, it will usually form in preference to intermolecular hydrogen bonds. The hydrogen bond rules provide useful information about the preferred connectivity patterns, hydrogen bond competition and stereoelectronic properties of hydrogen bonds for a particular functional group or for sets of functional groups. The methods of ranking solid-state hydrogen bond preferences are based on functional group competitions in homomeric crystals or heteromeric cocrystals. The procedure involves analyzing which donors are selected by a limited number of acceptors or *vice versa* during crystallization. For example, it was observed that when benzoic acid is cocrystallized with 2-amino-4-chloro-6-methylpyrimidine (CMAP), the best hydrogen bond donor (BHD), carboxylic acid O–H, preferentially bonded to the best hydrogen bond acceptor (BHA), N(1), whose electron density is enhanced by the electron donating adjacent methyl group. The electron density on N(2) is decreased by the electron withdrawing nature of chlorine atom. Hence, the second best hydrogen bond donor (SBHD), the amine N–H hydrogen bonded to the second best hydrogen bond acceptor (SBHA), N(2), thus following the hierarchy of hydrogen bonding (Scheme 4a).

Aakeröy and coworkers have synthesized many ternary cocrystals by exploiting differences in acidity and basicity of different hydrogen bond acceptors and donors in a well planned manner.[29,30] For example, in 1-((3-pyridyl)methyl) benzimidazole there are two hydrogen bond acceptors with two different pKa values. When 1-[(3-pyridyl)methyl]

benzimidazole is cocrystallized with 3,5-dintrobenzoic acid and 4-nitrobenzoic acid in 1:1:1 ratio (Scheme 4b), the BHD, 3,5-dintrobenzoic acid interacts with the BHA, benzimidazol-1-yl moiety (pKa: 5.72) and the SBHD, 4-nitrobenzoic acid interacts with SBHA, the pyridyl moiety (pKa: 4.71).[29] Very recently they also tested the hydrogen bond competition and hierarchy of hydrogen bonding in a family of amide derivatives (Scheme 5) with carboxylic acids.[30] However, hierarchy may at times not be followed in simple to complex systems. For example, Nangia and coworkers showed that hydrogen bonding in 1:2 cocrystals of aliphatic dicarboxylic acid and isonicotinamide obeys hierarchy rules whereas in 1:1 cocrystals the hydrogen bonding does not follow the best donor–best acceptor order.[31] Similar trend is observed in 2:1 cocrystals of *cis*-itraconazole and 1,4-dicarboxylic acids (Scheme 5). In the crystal structures, BHD (carboxylic acid) interact with N acceptor of triazole (SBHA) instead of piperazine (BHA), which is a stronger base.

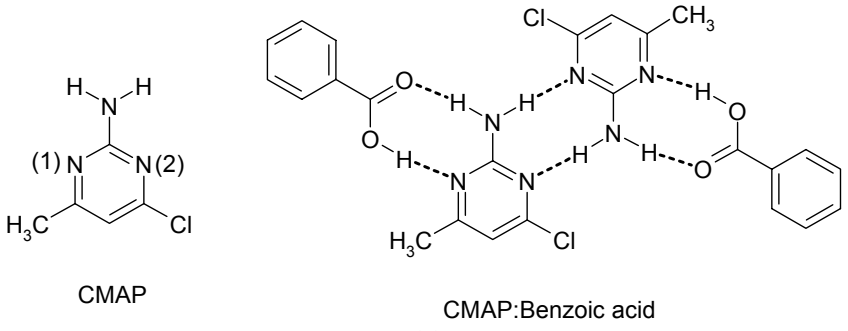

(a)

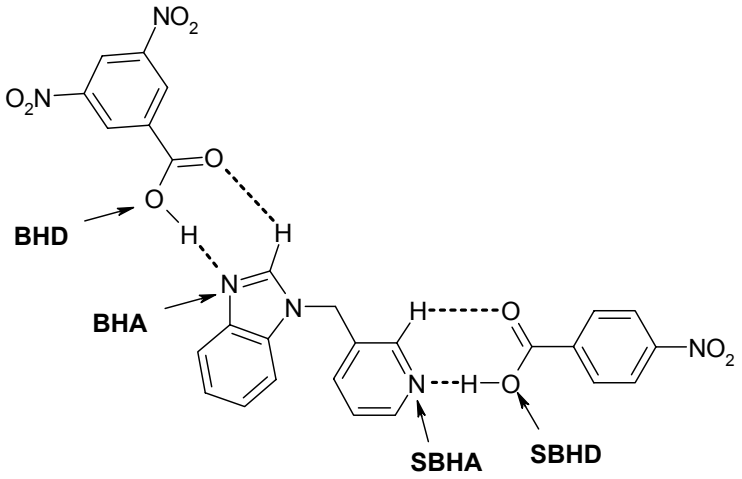

(b)

Scheme 4. (a) Hydrogen bond competition in 1:1 cocrystal of CMAP and benzoic acid. (b) Hierarchy of hydrogen bonding in 1:1:1 ternary cocrystal of 1-((3-pyridyl)methyl)benzimidazole, 3,5-dinitrobenzoic acid and 4-nitrobenzoic acid.

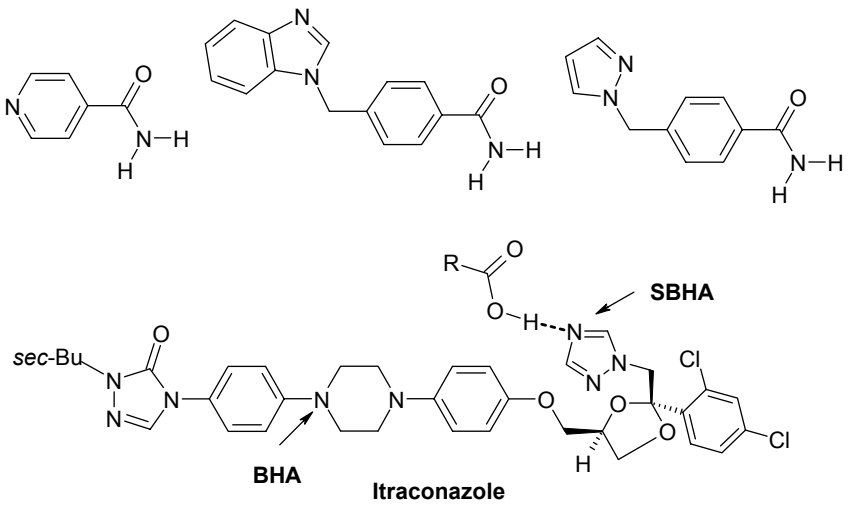

Scheme 5

1.6 Cocrystallization

Molecular recognition is typically associated with molecules in solution, but such events are also responsible for organizing molecules in the solid state. The formation of a cocrystal is favoured when intermolecular interactions between molecules of different components are stronger than those in the homomeric crystal. The cocrystal can be defined as an electrically neutral material, which consists of different molecular species in definite stoichiometric amounts that are held together by intermolecular interactions.[32] There is debate on the term cocrystal in recent years.[33] Cocrystallization is very useful in various fields of chemistry to prepare novel NLO materials, in designing extended supramolecular architectures, solid-state photodimerisation reactions, enantio separation of racemic compounds and pharmaceuticals. The majority of organic molecular cocrystals have been assembled *via* strong hydrogen bonds. But weak hydrogen bonds[34] and many other intermolecular interactions such as halogen bond,[16] nitro···iodo,[35] ethynyl···nitro[36] are also found to be broadly useful tools for construction of cocrystals. Zaworotko *et al*.[20] emphasized the importance of understanding supramolecular synthons in synthesizing cocrystals containing pharmaceutical agents. A recent study of adducts of acetaminophen (paracetamol) with ethers and amines provides additional examples of supramolecular synthons for cocrystal formation.[37] The specificity of carboxylic acid···pyridine recognition has been extensively used to synthesize 1D, 2D and 3D network structures.[38] Zaworotko and coworkers reported the highest fold interpenetration (18-fold) in a 2:3 binary cocrystal of 1,3,5-benzeneteicarboxylic acid (TMA) and bipyridylethane (BPE) using acid···pyridine

heterosynthon.[39] Recently, Nangia and coworkers[40] developed a novel ternary cocrystal, which is formed among 1,3,5-cyclohexanetricarboxylic acid (CTA) and two different pyridine bases, 4,4'-bipyridine (BP) and bipyridylethane (BPE). The crystal structure of CTA·BP·$(BPE)_{0.5}$ shows infinite helices of acid···BP O–H···N hydrogen bonds along the *y*-axis, and such helices are connected *via* BPE base. The interaction of CTA with BP and BPE gives a hexagonal network of 25 × 32 Å voids (Figure 3a), which are filled in the triply parallel-interpenetrated (6,3) network (Figure 3b). MacGillivray's group has employed rigid bifunctional molecules, such as 1,3-dihydroxybenzene and 1,8-naphthalenedicarboxylic acid that function as linear templates to organize reactants, such as trans-1,2-bis(4-pyridyl)ethylene, through hydroxy···pyridine and acid···pyridine heterosynthons for single and multiple photo induced [2+2] cycloaddition reactions.[41] They also prepared carcerand like capsules *via* hydroxy···pyridine heterosynthon by cocrystallization of *C*-methylcalix[4]resorcinarene with BP in the presence of nitrobenzene guest molecules.[42]

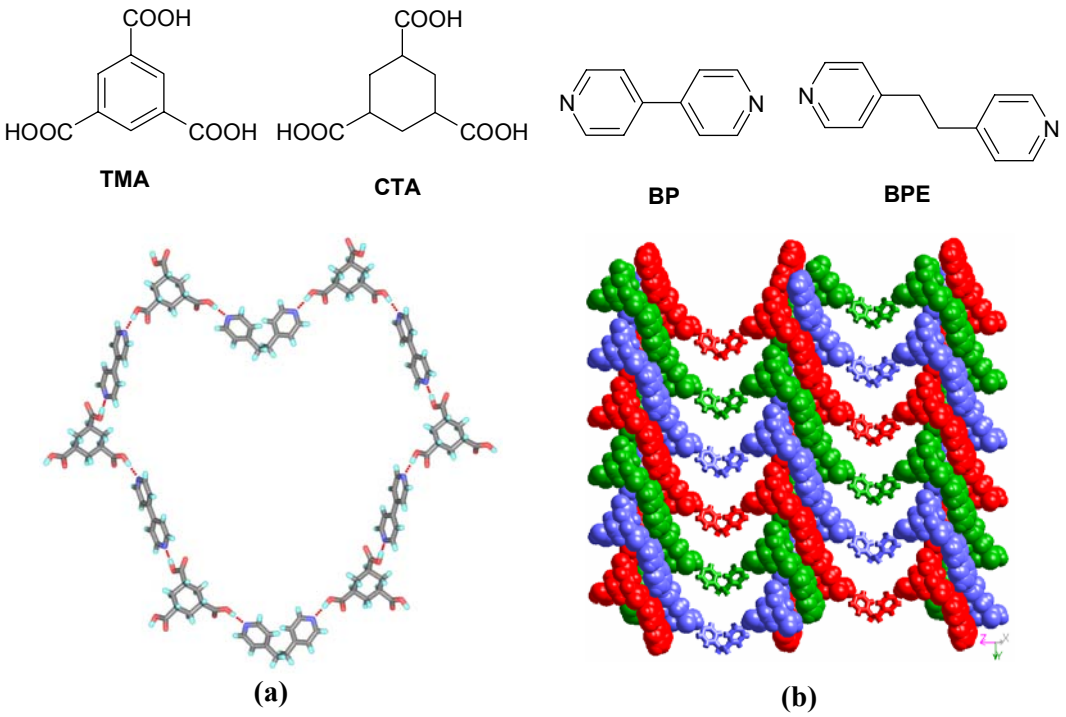

Figure 3. (a) COOH···BP and COOH ···BPE heterosynthons aggregating in the shape of a molecular necklace with voids of 25 × 32 Å in crystal structure CTA·BP·$(BPE)_{0.5}$. (b) Triply interpenetrated network.

Halogen bonding is also successfully used in cocrystallization of several activated halocarbons and heterocyclic compounds particularly pyridine heterocyclic compounds.

Haloperfluoroalkanes are particularly robust tectons[43] and they are nicely tailored to XB based supramolecular chemistry. The XB interactions that they form are particularly short and directional, thus allowing structural control of supramolecular aggregates. Resnati *et al.* synthesized binary cocrystals between diiodoperfluoroalkanes (**IFA**) and dicyanoalkanes (**CA**), which show highly consistent geometric characteristics (Figure 4). The donor and acceptor modules alternate in infinite chains the pitch of which shows a very good linear correlation with the number of the methylene groups in **CA** and the number of the difluoromethylene groups in **IFA**. The halogen bonding mediated cocrystallization useful in the topochemically controlled stereoselective photocyclization of olefins, synthesis of liquid crystalline materials and in the non-covalent fluorous coating of polymers.[44] Resnati *et al.* recently reported spontaneous resolution in a halogen bonded supramolecular architecture of 1,8-diiodoperfluorooctane and *N,N,N9,N9*-tetramethyl-*p*-phenylenediamine.

Cocrystals can also be prepared by solid-state grinding of individual components together.[45] For example, Hollingsworth *et al.*[46] demonstrated the utility of the grinding approach in preparing a cocrystal material not initially accessible from solution. The researchers aimed to prepare a series of cocrystals with *α,w*-dinitriles of the formula $NC(CH_2)_nCN$ with urea, with varying aliphatic chain lengths (*n*). Success was achieved in growing from solution a number cocrystals of different chain lengths; however, the *n*=3 (glutaronitrile) derivative could not be prepared from solution. On the other hand, solid-state grinding of the two components, afforded cocrystal formation in greater than 98% yield. Cocrystallization by simple grinding is not always successful. However, cocrystallization is significantly accelerated by the addition of small amounts of solvent, known as kneading. The solvent facilitates mutual contact and reactivity between the molecular species.

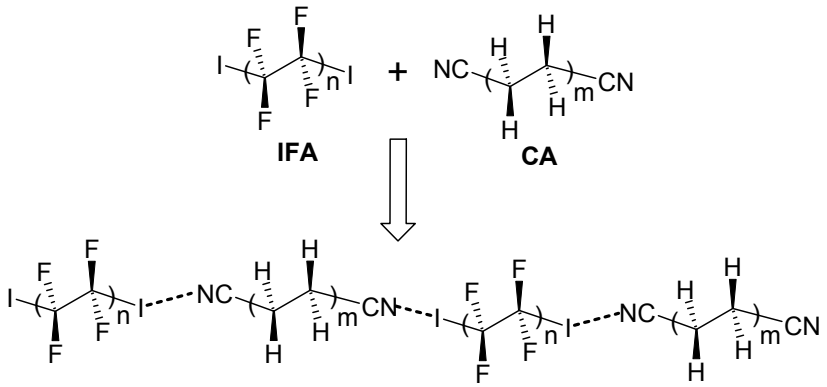

Figure 4. Halogen bonding mediated cocrystals formed between diiodoperfluoroalkanes and dicyanoalkanes.

1.7 Substitution effect on crystal structure

The observed three-dimensional architecture of a compound is the result of the interplay between the geometrical factors whose magnitude is proportional to the size of the molecule, and chemical factors whose strengths are related to donor atom acidities and acceptor group basicities. These factors also depend on substitution on the molecule. Substitution exerts both steric and electronic effects on the structure and reactivity, but separation of these two effects is difficult. Furthermore supramolecular behaviour of a particular functional group depends on the nature and location of other groups in the molecule. For example, the crystal structure of 4-aminobenzonitrile (ABN) is dominated by N–H···N and N–H···π interaction, which lead to zig-zag tape structure (Figure 5a). On the other hand, when *ortho*-positions of amine are substituted with methyl groups the crystal structure and the hydrogen bonding pattern changes drastically to a layered structure (Figure 5b).[47] The crystal structures of 2-oxaandrost-4-ene-3,17-dione (**6HAS**) and 6α-hydroxy-2oxaandrost-4-ene-3,17-dione (**6OHAS**) are isostructural, although there is an additional strong hydrogen bonding functionality present in **6OHAS**. The above two examples indicate that steric factors drive crystal structures in earlier case whereas geometrical factors control in latter cases (Figures 5c, 5d).[48] The azo dye 3-hydroxy-6-(4'-nitro)phenylazopyridine (3H4NPAP), crystallizes in a channel structure that include a number of molecules such as ethanol, methanol, isopropanol and ethylacetate[49] whereas its 3'-nitro analogue[50] (3H3NPAP) does not form solvates, indicating the position of functional group also plays role in the supramolecular behavior of that compound. Custelcean and coworkers have used steric control to manipulate the primary hydrogen bonding structure of crystalline organic solids. N,N'-dialkylthioureas can form two different hydrogen bonding motifs (Scheme 6) with completely different connectivity in the solid state: dimers (**A**) and chains (**B**). But the substitution of thiourea with bulky organic groups strongly favors the formation of the chain motif (**B**) due to steric hindrance.[51]

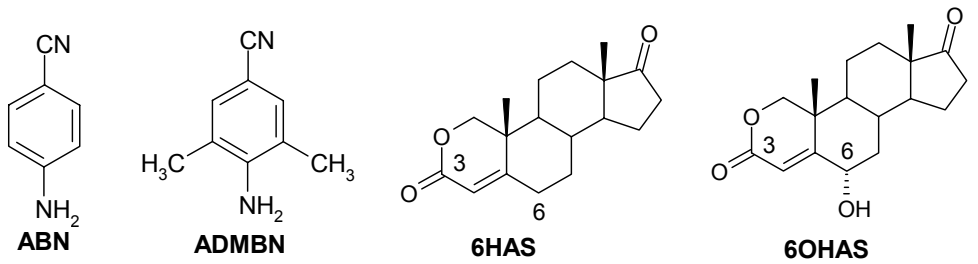

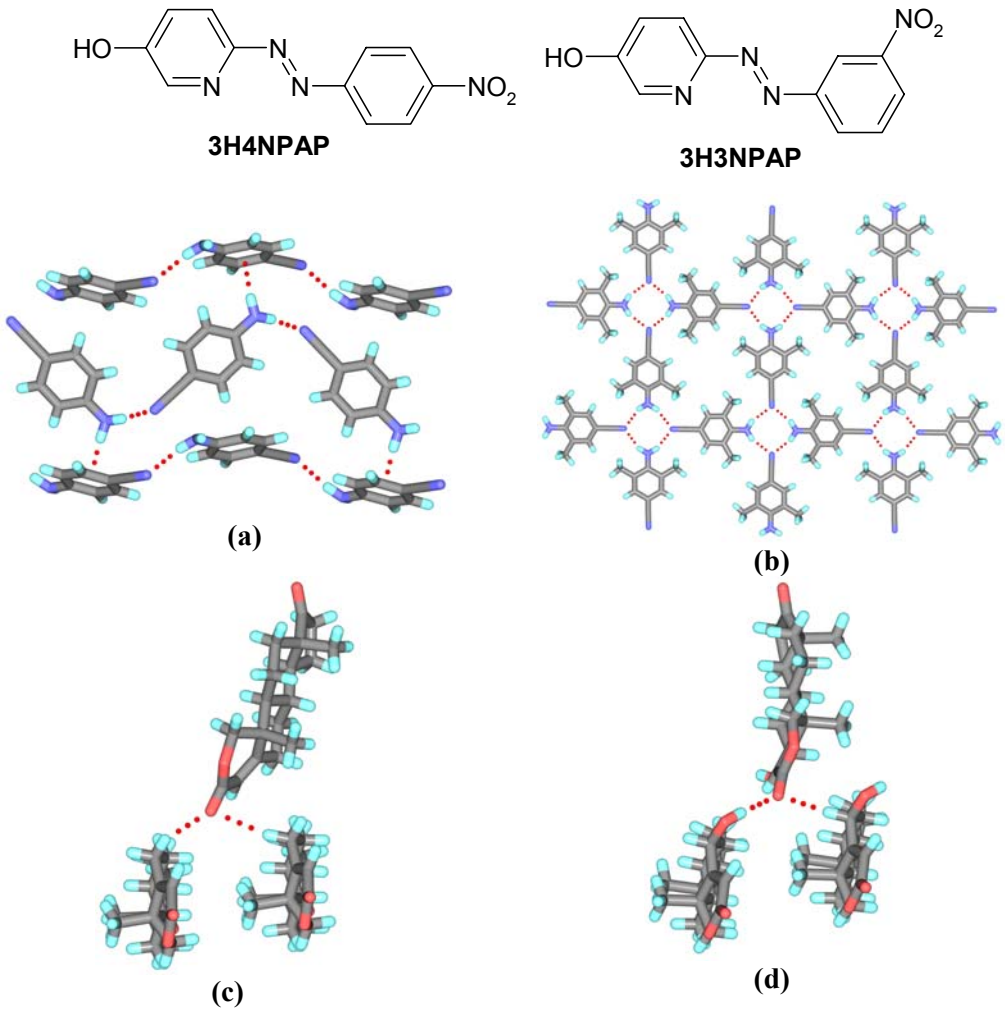

Figure 5. (a) Crystal structure of ABN (CSD refcode: BERTOH01). (b) Crystal structure of 3,5-dimethy-4-aminobenzonitrile (CSD refcode: WESBAX). (c) 2-Oxa-4-androstene-3-17-dione, (6HAS), (d) 6α-Hydroxy-2-oxa-4-androstene-3,17-dione, (6OHAS). Note that the change in structures due to substitution in (a) and (b) and isostructurality in (c) and (d).

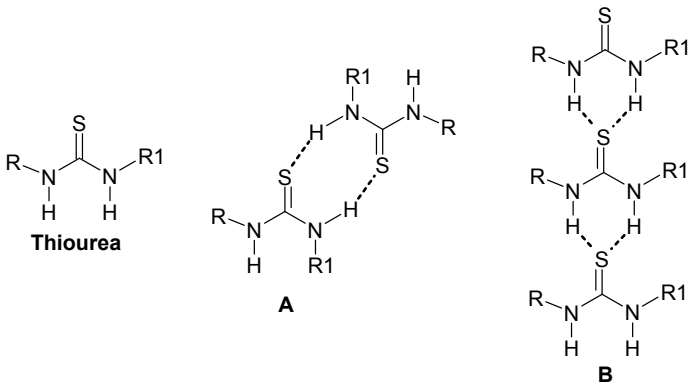

Scheme 6

1.8 Hydrogen bonding in ureas

The urea group is a self-complementary moiety in which both NH groups may interact with the oxygen atom of the carbonyl group of an adjacent molecule through the formation of strong bifurcated N–H···O hydrogen bonds. This specific and robust recognition is used in the synthesis of urea inclusion compounds,[52] urea based supramolecular polymers,[53] two-dimensional layered solids,[54] nanotubular structures based on bis-urea macrocycles[55] and more recently in the preparation of gelators.

Fowler and Lauher have shown that two-dimensional layered structures can be assembled using strong O–H···O and N–H···O hydrogen bond networks with urea-based building blocks, where two independent sets of one-dimensional self-complementary hydrogen bonded chains are oriented in orthogonal arrays.[56] The urea portion of these molecules form the α-network and these α-networks are cross-linked *via* carboxylic acid···amide heterosynthon to form two-dimensional layered structure (Figure 6a). Nangia *et al.*[57] showed strong and weak hydrogen bond mimicry in a family of *meta*-phenyl pyrimidinone derivatives, which on hydrogen bonding and close packing arguments would self-assemble in a manner similar to the α-network in urea crystal structures. In the crystal structures of *meta*-phenyl pyrimidinones translation-related molecules are connected by the weak C–H···O hydrogen bond chain synthon along the *a*-axis and C–H···X interaction connects such chains in the lateral direction to produce two-dimensional polar layered structures (Figure 6b).

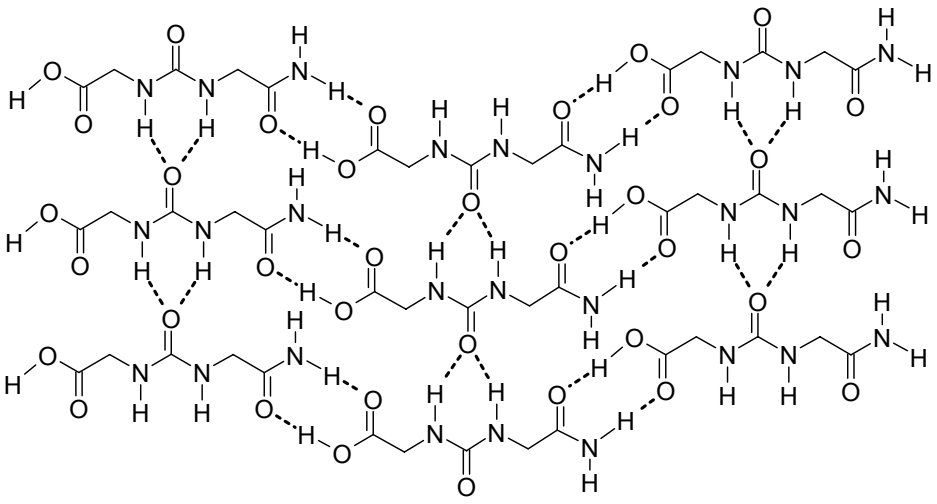

(a)

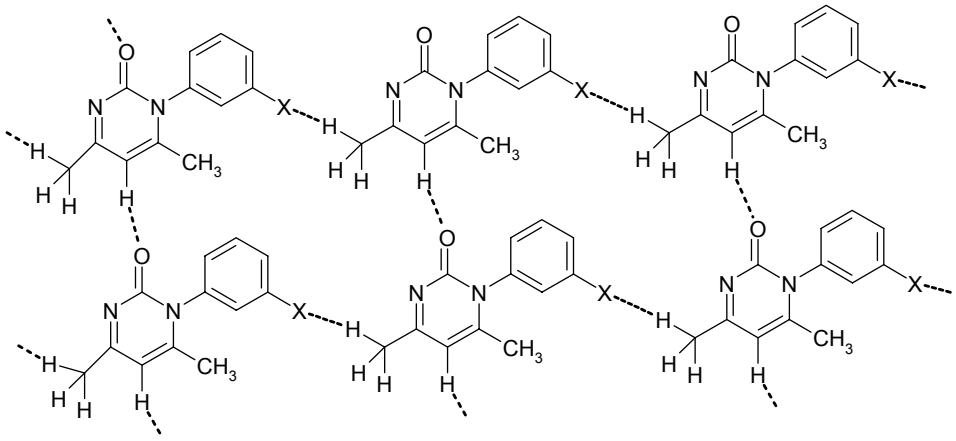

(b)

Figure 6. (a) Layered structure formed by the molecule through the N–H···O α-network and acid···amide heterosynthon in *N*-(carbamoylmethyl)-*N*'-(2-carboxymethyl)urea and (b) C–H···O and C–H···Br interactions mediated polar layered structure in *meta*-phenyl pyrimidinone derivatives. Note the similarities in (a) and (b), in latter case strong hydrogen bonds of (a) are replaced by weak interactions.

1.9 Polymorphism

Polymorphism is defined as the ability of a molecule to adopt more than one crystalline form in the solid-state. Mitscherlich recognized the phenomenon of polymorphsim in 1822.[58] This phenomenon occurs widely among organic compounds where several crystal packing possibilities exist *via* variations in intermolecular hydrogen bonding of functional groups and changes in conformation. Different packing arrangements of organic molecules result in different physical properties such as melting point, solubility, hardness, and density. Therefore, in many industries in which crystallization is often used for purification and isolation, controlling the crystallization process and ensuring the isolation of the correct polymorph is crucial.[59] For example, Abbott Laboratories had to rapidly reformulate the anti-HIV drug Ritonavir[60] when a more stable polymorph suddenly appeared in an established manufacturing process, with a different conformation and much lower solubility.[61] Because polymorphs have different physical properties, controlled preparation and characterization of polymorphs has become one of the major issues of modern crystal engineering and solid-state chemistry.[62] This is not only because of the commercial issues arising from drug patent litigations but also because studies of polymorphism afford fundamental information on molecular recognition, crystal nucleation, crystallization, and the relationship between solid phases.[63] Recently some novel techniques

such as, epitaxial growth,[64] crystallization in capillaries,[65] confinement within porous materials[66] crystallization with tailor made soluble additives,[67] using polymers as heteronuclei,[68] laser induced nucleation,[69] solid-state grinding[70] and high-throughput crystallization[71] have been reported for selective growth of a particular polymorph. Very recently meta-stable polymorphs of tolbutamide were trapped with cyclodextrin derivatives.[72] Swift and coworkers[73] have selectively grown different polymorphs of 1,3-bis(*m*-nitrophenyl) urea (MNPU) by exploiting chemical and geometric interactions at two-dimensional self-assembled monolayer (SAM) interfaces bearing different functionalities. MNPU exists in three polymorphic form and a monohydrate, α-, β-, δ- and γ-from respectively and crystallizes from solution in various concomitant combinations. Introduction of gold-thiol SAMs of substituted 4'-X-mercaptobiphenyls (X = H, I, and Br) into the crystallization solution selectively template the nucleation and growth of α-, β- and γ-froms, respectively (Figure 7). Polymorph control in the presence of SAM surfaces persists under a variety of solution conditions and consistently results in crystalline materials with high phase purity.

Incorporation of solvent into the lattice of crystalline solids results in the formation of molecular adducts known as solvates or pseudopolymorphs.[74] If water is included, it is called as hydrate.[75] Inclusion of solvent changes the physical and chemical properties that are analogous to those associated with polymorphs, and therefore the phenomenon is often referred to as pseudopolymorphism. The usage of the term pseudopolymorph is part of an ongoing debate.[76] In a recent commentary Nangia has argued to retain the term pseudopolymorph for scientific, legal and practical considerations.[76f]

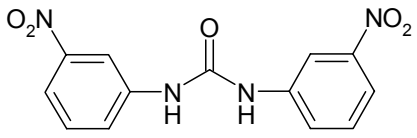

MNPU

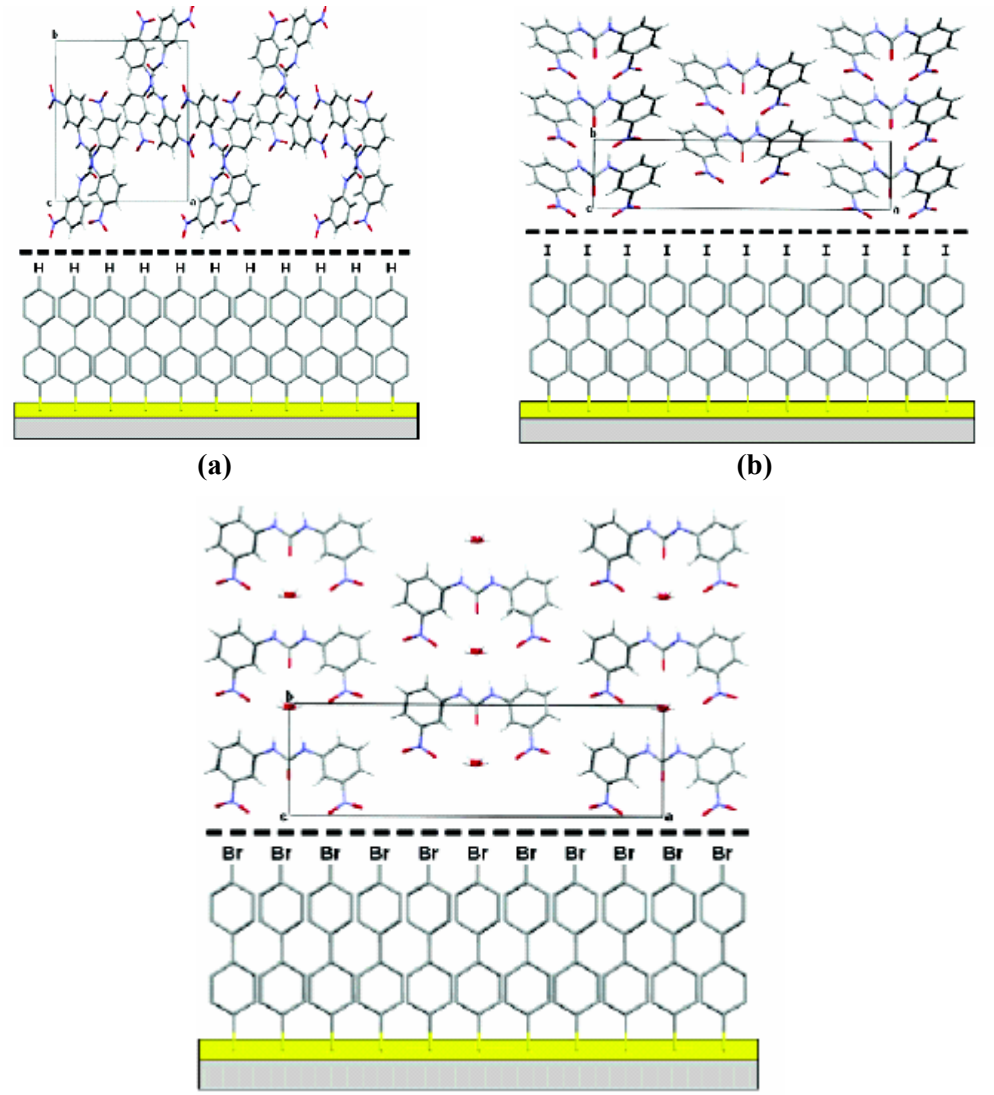

Figure 7. Selective nucleation and growth of polymorphs of MNPU (a) α-form on a 4-mercaptobiphenyl SAM template. (b) β-form on a 4'-iodo-4- mercaptobiphenyl SAM template. (c) γ-form on a 4'-bromo-4-mercaptobiphenyl SAM template.

1.10 References

1. (a) R.W. Armstrong, J.-M. Beau, S.H. Cheon, W.J. Christ, H. Fujioka, W.-H. Ham, L.D. Hawkins, H. Jin, S.H. Kang, Y. Kishi, M.J. Martinelli, W.W. McWhorter, M. Mizuno, M. Nakata, A.E. Stutz, F.X. Talamas, M. Taniguchi, J.A. Tino, K. Ueda, J. Uenishi, J.B. White and M. Yonaga *J. Am. Chem. Soc.*, **1989**, *111*, 7530. (b) E.M. Suh and Y. Kishi, *J. Am. Chem. Soc.*, **1994**, *116*, 11205.

2. J.-M. Lehn, *Supramolecular Chemistry: Concepts and Perspectives*, VCH: Weinheim, **1995**.
3. J.-M. Lehn, *Pure Appl. Chem*., **1978**, *50*, 871.
4. G.R. Desiraju, *Curr. Science*, **2001**, *81*, 1038.
5. (a) J.C. MacDonald and G.M. Whitesides, *Chem. Rev*., **1994**, *94*, 2383. (b) L.J. Prins, D.N. Reinhoudt and P. Timmerman, *Angew. Chem., Int. Ed*., **2001**, *40*, 2382. (c) A. Casnati, F. Sansone and R. Ungaro, *Acc. Chem. Res*., **2003**, *36*, 246.
6. (a) J.P. Sauvage, *Acc.Chem. Res*., **1998**, *31*, 611. (b) M. Fujita, *Acc. Chem. Res*., **1999**, *32*, 53. (c) D.L. Caulder and K.N. Raymond, *Acc. Chem. Res*., **1999**, *32*, 975. (d) P.J. Stang, *Chem. Rev*., **2000**, *100*, 853. (e) M.J. Zaworotko, *Chem. Commun*., **2001**, 1. (f) B. Moulton and M.J. Zaworotko, *Chem. Rev*., **2001**, *101*, 1629. (g) K. Biradha, *CrystEngComm*, **2003**, *5*, 374. (h) E.R.T. Tiekink and J.J. Vittal (Eds.), *Frontiers in Crystal Engineering*, Wiley, **2006**.
7. R. Pepinsky, *Phys. Rev*., **1955**, *100*, 52.
8. G.M.J. Schmidt, *Pure Appl. Chem.,* **1971**, *27*, 647.
9. G.R. Desiraju, *Crystal Engineering: The Design of Organic Solids,* Elsevier: Amsterdam, **1989**.
10. (a) F.H. Allen, *Acta Crystallogr*., **2002**, *B58*, 380. (b) A. Nangia, *CrystEngComm*, **2002**, *4*, 93.
11. (a) I. Weissbuch, M. Lahav and L. Leiserowitz, *Cryst. Growth Des*., **2003**, *3*, 125. (b) C.V.K. Sharma, *Cryst. Growth Des*., **2002**, *2*, 465.
12. A.I. Kitaigorodski, "*Molecular Crystals and Molecules*," Academic Press, New York, **1973.**
13. (a) G.A. Jeffrey and W. Saenger, *Hydrogen Bonding in Biological Structures*, Springer-Verlag, Berlin, **1991**. (b) L.J. Prins, D.N. Reinhoudt and P. Timmerman, *Angew. Chem. Int. Ed.*, **2001**, *40*, 2382. (c) G. Gilli and P. Gilli, *J. Mol. Struct.*, **2000**, *552*, 1. (d) T. Steiner, *Angew. Chem. Int. Ed.*, **2002**, *41*, 48; (e) G.R. Desiraju, *Acc. Chem. Res.*, **2002**, *35*, 565. (f) D. Braga, F. Grepioni, K. Biradha, V.R. Pedireddi and G.R. Desiraju, *J. Am. Chem. Soc.*, **1995**, *117*, 3156.
14. D. Braga, L. Brammer and N.R. Champness, *CrystEngComm*, **2005**, *7*, 1.
15. G.R. Desiraju and T. Steiner, *The Weak Hydrogen Bond in Structural Chemistry and Biology*, Oxford University Press, Oxford, **1999**.
16. P. Metrangolo, H. Neukirch, T. Pilati and G. Resnati, *Acc. Chem. Res.*, **2005**, *38*, 386.

17. E. Corradi, S.V. Meille, M.T. Messina, P. Metrangolo and G. Resnati, *Angew. Chem., Int. Ed.*, **2000**, *39*, 1782.
18. E.J. Corey, *Pure Appl. Chem*., **1967**, *14*, 19.
19. (a) G.R. Desiraju, *Angew. Chem*., *Int. Ed. Engl.,* **1995**, *34*, 2311. (b) A. Nangia and G.R. Desiraju, *Top. Curr. Chem.*, **1998**, *198*, 57.
20. (a) R.D.B. Walsh, M.W. Bradner, S. Fleishman, L.A. Morales, B. Moulton, N.R. Hornedo and M.J. Zaworotko, *Chem. Commun*., **2003**, 186. (b) S.G. Fleischman, S.S. Kuduva, J.A. McMahon, B. Moulton, R.D.B. Walsh, N.R. Hornedo and M.J. Zaworotko, *Cryst. Growth Des.,* **2003**, *3*, 909.
21. (a) R. Boese, M.T. Kirchner, W.E. Billups and L.R. Norman, *Angew. Chem*., *Int. Ed*., **2003**, *42*, 1961. (b) R. Taylor and O. Kennard, *J. Am. Chem. Soc.,* **1982**, *104*, 5063. (c) Z.S. Derewenda, L. Lee and U. Derewenda, *J. Mol. Biol.,* **1995**, *252*, 248. (d) G.R. Desiraju, *Acc. Chem. Res.,* **1996**, *29*, 441. (e) G.R. Desiraju, *Acc. Chem. Res.,* **2002**, *35*, 565. (f) G.R. Desiraju, *Chem. Commun.,* **2005**, 2995. (g) M.C. Wahl and M. Sundaralingam, *Trends Biochem. Sci.,* **1997**, *22*, 97. (h) Y. Mandel-Gutfreund, H. Margalit, R.L. Jernigan and V.B. Zhurkin, *J. Mol. Biol.,* **1998**, *277*, 1129.
22. (a) M. Nishio, M. Hirota and Y. Umezawa, *The C–H/π Interaction*, Wiley, New York, **1988**. (b) M. Nishio, *CrystEngComm,* **2003**, *7*, 130. (c) H. Suezawa, T.Yoshida, S. Ishihara, Y. Umezawa and M. Nishio, *CrystEngComm*, **2003**, *7*, 514.
23. (a) N. Ramasubbu, R. Parthasarathy and P. Murray-Rust, *J. Am. Chem. Soc*., **1986**, *108*, 4308. (b) S.L. Price, A.J. Stone, J. Lucas, R.S. Rowland and A.E. Thornley, *J. Am. Chem. Soc*., **1994**, *116*, 4910.
24. (a) M.C. Etter, Z. Urbanczyk-Lipkowska, D.A. Jahn and J.S. Frye, *J. Am. Chem. Soc.*, **1986**, *108*, 5871. (b) A. Katrusiak, *J. Mol. Struct.*, **1992**, *269*, 329.
25. M. Ohkita, M. Kawano, T. Suzuki and T. Tsuji, *Chem. Commun*., **2002**, 3054.
26. J. Donohue, *J. Phys. Chem*., **1952**, *56*, 502.
27. M.C. Etter, *J. Am. Chem. Soc*., **1982**, *104*, 1095.
28. (a) M.C. Etter, *Acc. Chem. Res*., **1990**, *23*, 120. (b) M.C. Etter, *J. Phys. Chem*., **1991**, *95*, 4601.
29. C.B. Aakeröy, J. Desper and J.F. Urbina, *Chem. Commun.*, **2005**, 2820.
30. (a) C.B. Aakeröy, J. Desper and J.F. Urbina, *Chem. Commun.*, **2006**, 1445. (b) C.B. Aakeröy, A.M. Beatty, B.A. Helfrich and M. Nieuwenhuyzen, *Cryst. Growth Des.,*

2003, *3*, 159. (c) C.B. Aakeröy, A.M. Beatty and B.A. Helfrich, *Angew. Chem. Int. Ed.*, **2001**, *40*, 3240.

31. P. Vishweshwar, A. Nangia and V. M. Lynch, *Cryst. Growth Des*., **2003**, *3*, 783.
32. C.B. Aakeröy and D.J. Salmon, *CrystEngComm*, **2005**, *7*, 439.
33. (a) G.R. Desiraju, *CrystEngComm*, **2003**, 5, 466. (b) J.D. Dunitz, *CrystEngComm*, **2003**, *5*, 506.
34. (a) M.T. Kirchner, R. Boese, A. Gehrke and D. Bläser, *CrystEngComm*, **2004**, *8*, 360. (b) V.R. Thalladi, A. Gehrke and R. Boese, *New J. Chem.*, **2000**, 463.
35. R. Thaimattam, P.J. Langley, J. Hulliger and G.R. Desiraju, *New. J. Chem*., **1998**, 1307.
36. J.M.A. Robinson, D. Philip, B.M. Kariuki and K.D.M. Harris, *Chem. Commun*., **1999**, 329.
37. I.D.H. Oswald, D.R. Allan, P.A. McGregor, W.D.S. Motherwell, S. Parsons, C.R. Pulham, *Acta Crystallogr.*, **2002**, *B58*, 1057.
38. (a) C.V.K. Sharma and M.J. Zaworotko, *Chem. Commun*., **1996**, 2655. (b) N. Shan, A.D. Bond, W. Jones, *Cryst. Eng*., **2002**, *5*, 9. (c) E. Batchelor, J. Klinowski and W.J. Jones, *J. Mater. Chem*., **2000**, *10*, 839. (d) S. Varughese and V.R. Pedireddi, *Chem. Eur. J.*, **2006**, *12*, 1597.
39. T.R. Shattock, P. Vishweshwar, Z. Zang and M.J. Zaworotko, *Cryst. Growth Des*., **2005**, *5*, 2046.
40. B.R. Bhogala, S. Basavoju and A. Nangia, *Cryst. Growth Des*., **2005**, *5*, 1683.
41. (a) X. Gao, T. Friščić and L.R. MacGillivray, *Angew. Chem. Int. Ed.,* **2004**, *43*, 232. (b) D.B. Varshney, G.S. Papaefstathiou and L.R. MacGillivray, *Chem. Commun.*, **2002**, 1964. (c) L.R. MacGillivray, *CrystEngComm*, **2002**, *7*, 1. (d) X. Gao, T. Friščić and L.R. MacGillivray, *Chem. Commun.*, **2003**, 1306.
42. (b) L.R. MacGillivray, P.R. Diamente, J.L. Reid and J.A. Ripmeester, *Chem. Commun.*, **2000**, 359.
43. (a) D.D. Burton, F. Fontana, P. Metrangolo, T. Pilati and G. Resnati, *Tetrahedron Lett.*, **2003**, *44*, 645. (b) F. Fontana, A. Forni, P. Metrangolo, W. Panzeri, T. Pilati and G. Resnati, *Supramol. Chem*., **2002**, *14*, 47.
44. (a) P. Metrangolo, T. Pilati, G. Resnati and A. Stevenazzi, *Chem. Commun*., **2004**, 1492. (b) T. Caronna, R. Liantonio, T.A. Logothetis, P. Metrangolo, T. Pilati and G. Resnati, *J. Am. Chem. Soc*., **2004**, *126*, 4500. (c) H.L. Nguyen, P.N. Horton, M.B. Hursthouse, A.C. Legon and D.W. Bruce, *J. Am. Chem. Soc.,* **2004**, *126*, 16. (d) R. Bertani, P.

Metrangolo, A.Moiana, E. Perez, T. Pilati, G. Resnati, I. Rico-Lattes and A. Sassi, *Adv. Mater.,* **2002**, *14*, 1197. (e) H. Neukirch, E. Guido, R. Liantonio, P. Metrangolo, T. Pilati and G. Resnati. *Chem. Commun*., **2005**, 1534.

45. N. Shan, F. Toda and W. Jones, *Chem. Commun*., **2002**, 2372.
46. (a) M.D. Hollingsworth, B.D. Santarsiero, H. Oumar-Mahamat and C.J. Nichols, *Chem. Mater*., **1991**, *3*, 23. (b) M.D. Hollingsworth, M.E. Brown, B.D. Santarsiero, J.C. Huffman and C.R. Goss, *Chem. Mater.*, **1994**, *6*, 1227.
47. A. Heine, R. Herbst-Irmer, D. Stalke, W. Kuhnle and K.A. Zachariasse, *Acta Crystallogr.*, **1994**, *B50*, 363.
48. (a) A. Anthony, M. Jaskólski, A. Nangia and G.R. Desiraju, *Chem. Commun.*, **1998**, 2537. (b) A. Anthony, M. Jaskólski and A. Nangia, *Acta Crystallogr*., **2000**, *B58*, 512.
49. (a) P. Ramachandra, T.S.R. Krishna and G.R. Desiraju, *Proc. Indian Acad. Sci., Chem. Sci.*, **1989**, *101*, 327. (b) J.A. Moore and F.J. Marascia, *J. Am. Chem. Soc*., **1959**, *81*, 6049.
50. G.R. Desiraju and T.S.R. Krishna, *Mol. Cryst. Liq. Cryst.*, **1988**, *159*, 277.
51. R. Custelcean, M.G. Gorbunova and P.V. Bonnesen, *Chem. Eur. J.*, **2005**, *11*, 1459.
52. (a) M.F. Benger, *Ger. Pat. Appl.*, OZ 123438, **1940**. (b) K.D.M. Harris and J.M. Thomas, *J. Chem. Soc., Faraday Trans.*, **1990**, *86*, 2985. (c) K.D.M. Harris, *Chem. Soc. Rev.*, **1997**, *26*, 279.
53. S. Boileau, L. Boutellier, F. Lauprete and F. Lortie, *New J. Chem,*. **2000**, 854.
54. T.L. Hguyen, A. Scott, B. Dinkelmeyer, F.W. Fowler and J.W. Lauher, *New J. Chem.* **1998**, 129.
55. (a) L.S. Shimizu, M.D. Smith, A.D. Hughes and K.D. Shimizu, *Chem. Commun.* **2001**, 1592. (b) L.S. Shimizu, A.D. Hughes, M.D. Smith, M.J. Davis, P. Zhang, H.-C. zur Loye and K.D. Shimizu, *J. Am. Chem. Soc.,* **2003**, *125*, 14972. (c) L.S. Shimizu, A.D. Hughes, M.D. Smith, S.A. Samuel and D. Ciurtin-Smith, *Supramol. Chem.*, **2005**, *17*, 27.
56. Y.-L. Chang, A.-N. West, F.W. Fowler and J.W. Lauher, *J. Am. Chem. Soc.*, **1993**, *115*, 5991.
57. S. George, A. Nangia, M. Bagieu-Beucher, R. Masse and J.-F. Nicoud, *New J. Chem.*, **2003**, 568.
58. E. Mitscherlich, *Ann. Chim. Phys*., **1822**, *19*, 350.

59. J. Bernstein, *Polymorphism in Molecular Crystals*; Oxford Science Publications: OUP, Oxford, U.K., 2002.
60. S.R. Chemburkar, J. Bauer, K. Deming, H. Spiwek, K. Patel, J. Morris, R. Henry, S. Spanton, W. Dziki, W. Porter, J. Quick, P. Bauer, J. Donaubauer, B.A. Narayanan, M. Soldani, D. Riley and K. McFarland, *Org. Process Res. Dev.,* **2000**, *4*, 413.
61. J. Bauer, S. Spanton, R. Henry, J. Quick, W. Dziki, W. Porter and J. Morris, *J. Pharm. Res.,* **2001**, *18*, 859.
62. (a) J. Bernstein, R.J. Davey and J.-O. Henck, *Angew. Chem., Int. Ed.*, **1999**, *38*, 3440. (b) N. Bladgen and R.J. Davey, *Chem. Br.*, **1999**, *35*, 44.
63. (a) J. Dunitz and J. Bernstein, *Acc. Chem. Res.*, **1995**, *28*, 193. (b) D. Braga and F. Grepioni, *Chem. Soc. Rev.*, **2000**, *4*, 229. (c) N. Blagden and R.J. Davey, *Cryst. Growth Des.*, **2003**, *3*, 873. (d) R.J. Davey, K. Allen, N. Blagden, W.I. Cross, F.H. Lieberman, M.J. Quayle, S. Righini, L. Seton and G.J.T. Tiddy, *CrystEngComm*, **2002**, *4*, 257.
64. (a) S.J. Bonafede and M.D. Ward, *J. Am. Chem. Soc.,* **1995**, *117*, 7853. (b) C.A. Mitchell, L. Yu and M.D. Ward, *J. Am. Chem. Soc.,* **2001**, *123*, 10830.
65. (a) L.J. Chyall, J.M. Tower, D.A. Coates, T.L. Houston and S.L. Childs, *Cryst. Growth Des.,* **2002**, *2*, 505. (b) J.L. Hilden, C.E. Reyes, M.J. Kelm, J.S. Tan, J.G. Stowell and K.R. Morris, *Cryst. Growth Des.,* **2003**, *3*, 921.
66. J.M. Ha, J.H. Wolf, M.A. Hillmyer and M.D. Ward, *J. Am. Chem. Soc.,* **2004**, *126*, 3382.
67. P.K. Thallapally, R.K.R. Jetti, A.K. Katz, H.L. Carrell, K. Singh, K. Lahiri, S. Kotha, R. Boese and G.R. Desiraju, *Angew. Chem. Int. Ed.*, **2004**, *43*, 1149.
68. (a) M.D. Lang, A.L. Grzesiak and A.J. Matzger, *J. Am. Chem. Soc.,* **2002**, *124*, 14834. (b) C.P. Price, A.L. Grzesiak and A.J. Matzger, *J. Am. Chem. Soc.*, **2005**, *127*, 5512.
69. J. Zaccaro, J. Matic, A. S. Myerson and B. A. Garetz, *Cryst. Growth Des.*, **2001**, *1*, 5.
70. A.V. Trask, N. Shan, W.D.S. Motherwell, W. Jones, S. Feng, R.B.H. Tan and K.J. Carpenter, *Chem. Commun.,* **2005**, 880.
71. (a) S.L. Morissette, S. Soukasene, D.A. Levinson, M.J. Cima and Ö. Almarsson, *Proc. Natl. Acad. Sci (USA).,* **2003**, *100*, 2180. (b) M.L. Peterson, S.L. Morissette, C. McNulty, A. Goldsweig, P. Shaw, M. LeQuesne, J. Monagle, N. Encina, J. Marchionna, A. Johnson, M.J. Cima and Ö. Almarsson, *J. Am. Chem. Soc.,* **2002**, *124*, 10958. (c) Ö. Almarsson, M.B. Hickey, M.L. Peterson, S.L. Morissette, S. Soukasene, C. McNulty, M. Tawa, J.M. MacPhee and J.F. Remenar, *Cryst. Growth Des.*, **2003**, *3*, 927.

72. (a) Y. Sonoda, F. Hirayama, H. Arima, Y. Yamaguchi, W. Saengerb and K. Uekama, *Chem. Commun.*, **2006**, 517. (b) Y. Sonoda, F. Hirayama, H. Arima, Y. Yamaguchi, W. Saenger and K. Uekama, *Cryst. Growth Des.*, **2006**, ASAP. DOI: 10.1021/cg060001o.
73. R. Hiremath, J.A. Basile, S.W. Varney and J.A. Swift, *J. Am. Chem. Soc.*, **2005**, *127*, 18321.
74. (a) T.L. Threlfall, *Org. Process Res. Dev.*, **2000**, *4*, 384. (b) Y.-S. Kim and R.W. Rousseau, *Cryst. Growth Des.*, **2004**, *4*, 1211. (c) T. Hosokawa, S. Datta, A.R. Sheth, N.R. Brooks, V.G. Young and D.J.W. Grant, *Cryst. Growth Des.*, **2004**, *4*, 1195. (d) S. Dutta and D.J.W. Grant, *Nat. Rev. Drug Discovery*, **2004**, *3*, 42.
75. (a) B.K. Saha and A. Nangia, *Chem. Commun.*, **2005**, 3024. (b) B.K. Saha and A. Nangia, *Chem. Commun.*, **2006**, DOI:10.1039/b600348f. (c) D.A. Haynes, W. Jones and W.D.S. Motherwell, *CrystEngComm*, **2005**, 462. (d) B.-Q. Ma, H.-L. Sun and S. Gao, *Angew. Chem. Int. Ed.*, **2004**, *43*, 1374. (e) B. Sreenivasulu and J.J. Vittal, *Angew. Chem. Int. Ed.*, **2004**, 43, 5769. (f) J.L. Atwood, L.J. Barbour, T.J. Ness, C.L. Raston and P.L. Raston, *J. Am. Chem. Soc.*, **2001**, *123*, 7192. (g) A.L. Gillon, N. Feeder, R.J. Davey and R. Storey, *Cryst. Growth Des.*, **2003**, *3*, 663.
76. (a) G.R. Desiraju, *CrystEngComm*, **2003**, *5*, 466. (b) J.D. Dunitz, *CrystEngComm*, **2003**, *5*, 506. (c) K.R. Seddon, *Cryst. Growth Des.*, **2004**, *4*, 1087. (d) J. Bernstein, *Cryst. Growth Des.*, **2005**, *5*, 661. (e) G.R. Desiraju, *Cryst. Growth Des.*, **2004**, *4*, 1089. (f) A. Nangia, *Cryst. Growth Des.*, **2006**, *6*, 2.

CHAPTER 2

HYDROGEN BOND COMPETITION AND INTERPLAY OF WEAK INTERACTIONS IN CRYSTAL STRUCTURES OF NITRO-SUBSTITUTED DIPHENYLUREAS

2.1 Introduction

The design and development of new materials with desired physical and chemical properties using organic, inorganic and organo-metallic hybrid molecules is of great interest where small to large molecular mass is important.[1] A popular method for the design of supramolecular assemblies is to use intermolecular interactions such as hydrogen bonds to guide the smaller molecules into larger ordered aggregates. Since interactions arise from molecular functionalities it is important to identify common hydrogen bond patterns or synthons in a family of crystal structures. With an enhanced knowledge of hydrogen bond synthons in crystals, novel strategies may be designed for the self-assembly of supramolecular architectures from multifunctional molecules. However, in multifunctional molecules it is difficult to predict the way molecules self-assemble, because one functional group can influence the other functional group in many ways[2] and even change in position of functional groups can result in an entirely different crystal structure. The situation is further complicated when there is competition for hydrogen bonding between functional groups. In this context one needs to establish which synthon is favoured over a competing motif for a reliable prediction of the final crystal structure. For example the design of novel protein ligands often involves functional group replacements and these bioisosteric replacements are performed to alter a molecular framework while retaining its hydrogen bonding or to enhance hydrogen bonding in a well planned and tailored fashion.

To examine the effect of substitution in multifunctional molecules, one has to look at an entire series of crystal structures so that hydrogen bonding competition, chemical and geometrical effects of functional groups may be assessed. Ward *et al.* studied the influence of steric and competitive hydrogen bonding on the crystal structures of guanidinium arenesulfonate networks (**GS**), where they showed that the substitution of carboxy and nitro groups on arenesulfonyl moiety disturbs the robust quasihexagonal two-dimenstional **GS** network, which is observed in about 30 structures.[3] Desiraju *et al.* examined a series of

crystal structures in two closely related structural families, the 4-substituted cubanecarboxylic acids and phenylpropiolic acids to probe steric and electronic effects of substituent groups on the hydrogen bonding pattern and concluded that in the cubane acids, the substituent groups mainly exert a steric effect, and the electronic effect is not critical whereas in the phenylpropiolic acids, both steric and electronic effects are very important.[4]

2.2 Substitution effect on hydrogen bonding pattern in diarylureas: An overview

The urea functional group is well exploited in crystal engineering to make target networks in channel inclusion compounds, nonlinear optical materials and modular assembly of hydrogen-bonded complexes.[5] The dominant recognition motif in unsubstituted *N,N'*-diarylureas is the α-network, a chain of bifurcated N–H···O hydrogen bonds between NH donors and the C=O acceptor (Synthon **A**, Scheme 3). But substitution on aryl ring plays a major role on the hydrogen bond pattern of diarylureas. Etter and co-workers have extensively studied the substitution effect on the hydrogen bond pattern and cocrystallization property of diarylureas.

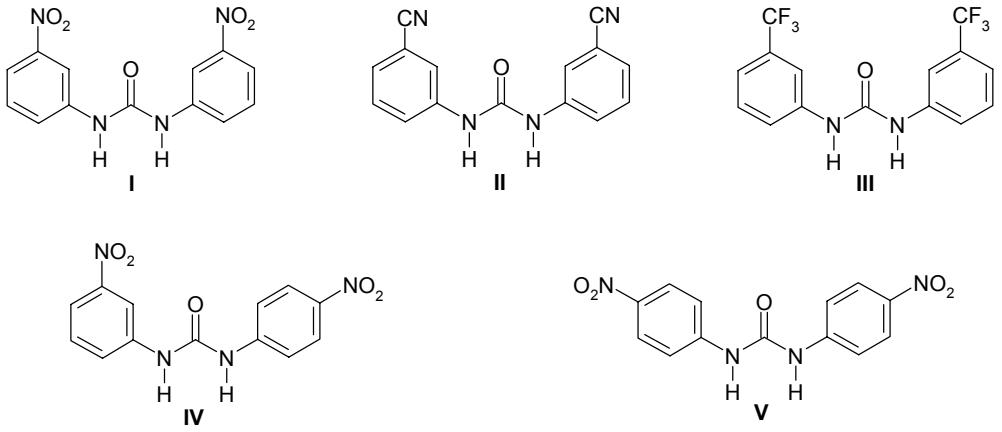

Scheme 1. Some electron withdrawing group substituted ureas in literature.

N,N'-Bis(*m*-nitrophenyl)urea, **I** (Scheme 1) exists in three concomitant polymorphic forms, namely α-form, β-form and δ-form of different colours.[6] It also forms many solvates and cocrystals with compounds having strong to moderate hydrogen bond acceptors and a monohydrate.[6f,7] Hydrogen bonding analysis of these polymorphs and solvates indicate that the characteristic α-network of diarylureas is generally absent in this family of structures and is observed in only the metastable β-form (Figure 1b). In more stable α-polymorph,

compound **I** adopts a quasi-planar conformation (C–C_{aryl}–N–$C_{carbonyl}$ torsion angles, 1.6, 24.8°) with respect to the urea carbonyl and forms a layered structure with nitro O-acceptor disrupting the α-network *via* synthon **B** (Figure 1a). The hydrogen bonding pattern of δ-form reveals that it is an intermediate crystal structure to α- and β-forms (Figures 1c, 1d). Though nitro group is a weak hydrogen bond acceptor when compared to the urea carbonyl, in both α- and δ-forms it successfully competes for hydrogen bonding with urea carbonyl *via* synthon **B** (Scheme 3). In all solvates including hydrate, the α-network is disrupted by competing solvent hydrogen bond acceptors and compound **I** adopts nearly planar conformation in all structures (Figures 1e, 1f, Table 3). Compound **III** also form solvates or cocrystals but only with very strong hydrogen bonding acceptor containing molecules like DMSO and triphenylphosphine oxide. Etter[7] proposed that compounds **I** and **III** behave primarily as a proton donor and its hydrogen bond acceptor ability is drastically reduced, possibly because of two weak intramolecular C–H···O interactions, which reduce the electron density on urea carbonyl in planar conformation. She suggested that only diarylureas with *meta*-substituted electron withdrawing groups have this property of solvent inclusion or cocrystal formation.

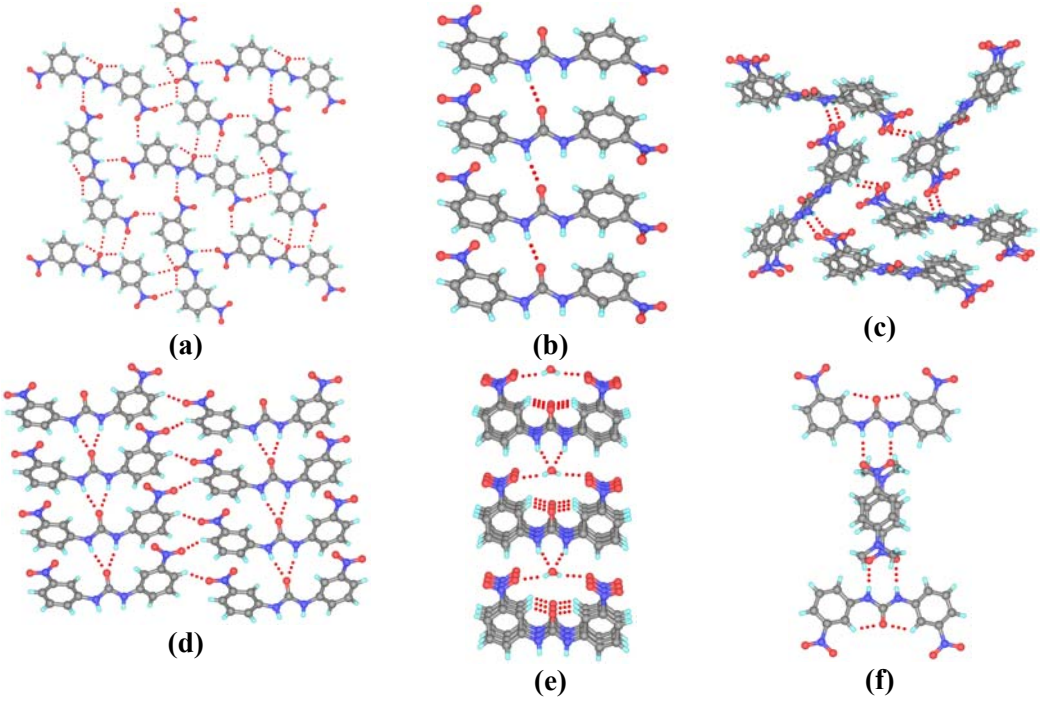

Figure 1. Crystal structures of **I** (a) α-form (SILTOW) (b) δ-form (c) δ-form along stacking axis (d) β-form (SILTOW01) (e) γ-form or monohydrate and (f) solvate of *N,N′*-dimethyl-*p*-nitroaniline (GIMRUP10). Note: Whenever α-network is absent compound **I** adopts planar

conformation with intramolecular C–H···O hydrogen bonds. CSD refcodes are given in brackets. α- and β-forms were reported by Etter *et. al*. (ref. 6e) and δ-and γ- or monohydrate forms were identified only recently by Price *et. al*. (ref. 6f).

Custelcean *et al.* determined crystal structures of compound **II** and its monohydrate as part of their study on anion coordination in metal-organic frameworks.[8] In these structures also α-network is absent. Crystal structure of anhydrous form shows that one of the two NH donors interacts with weak cyano acceptor and the other interacts with urea carbonyl and molecule adopts a twisted conformation ($C–C_{aryl}–N–C_{carbony}$, 27.3, 30.8°), whereas in the crystal structure of monohydrate the α-network is disrupted by water and the urea molecule adopts quasi-planar conformation (5.6, 21.0°). Recently Boiocchi *et al*.[9] have studied the hydrogen bonding of oxoanions with compound **V**. Crystal structures of $[Bu_4N][\mathbf{V}\cdot CH_3COO]$ and $[Bu_4N][\mathbf{V}\cdot HCO_3]\cdot 2H_2O$ show that the strong carboxylate disrupts the α-network and the molecule **V** adopts a planar conformation with intramolecular C–H···O hydrogen bond (Figures 2a, 2b). Compound **IV** forms DMSO solvate, where DMSO acts as a spacer between two urea molecules and thus disrupting the α-network and molecule **IV** exits in planar conformation stabilized by intramolecular C–H···O hydrogen bonds (Figure 2c).[7b] Urea-carboxylate synthon is also exploited in urea based chemosensors development.[10]

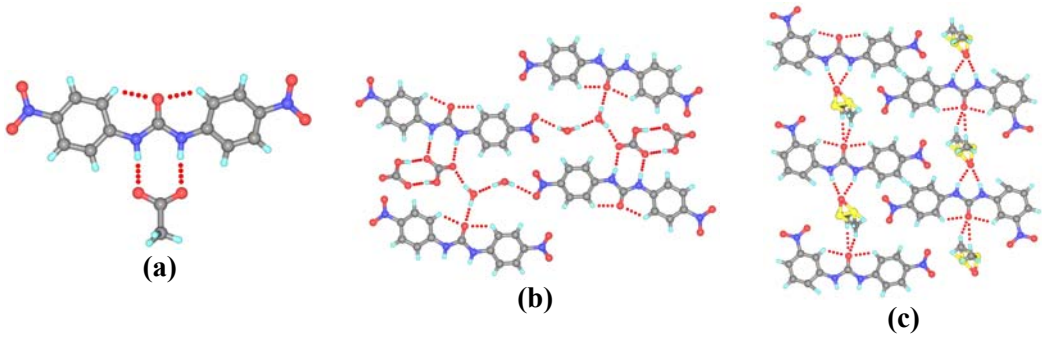

Figure 2. (a) Hydrogen bonding pattern of **V** in $[Bu_4N][\mathbf{V}\cdot CH_3COO]$ (FEMQEU). (b) Crystal structure of $[Bu_4N][\mathbf{V}\cdot HCO_3]\cdot 2H_2O$ (FEMQIY). (c) Crystal structure of DMSO solvate of IV (SILVOY). Note: $N–H\cdots O_{carboxylate}$ (synthon **E**) and intramolecular C–H···O hydrogen bonds in (a) and (b) and Bu_4N is removed for clarity.

2. 3 Hydrogen bonding pattern in *para*-nitro substituted diarylureas

In a recent thesis from our laboratory Sumod[11] observed that the α-network is not the common hydrogen bonding motif in *para* nitro-substituted diarylureas. Here I have further extended this study to understand the factors influencing the hydrogen bond pattern by keeping *para*-nitrophenyl moiety constant and changing the substituents on the other phenyl group (Scheme 2). All compounds studied in this chapter are prepared by the condensation of *p*-nitrophenyl isocyanate with the corresponding *m*/*p*-X-aniline in dry benzene. *Meta*-substituted compounds were synthesized to check the effect of position of functional groups on crystal structures. Some of the compounds crystallized only with solvent of crystallization. After characterizing all compounds by satisfactory NMR and IR spectra their crystal structures were determined by X-ray diffraction. All these crystal structures can be divided into two families. Non-urea tape structures and urea tape structures (Scheme 3). Crystallographic data of compounds studied in this chapter is given in appendix.

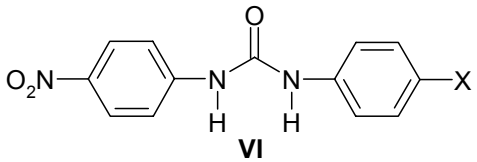

VI

1: X = F
2: X = Cl
3: X = Br
4:X = CN
5: X = I(m-isomer)
6: X = Br(m-isomer)
7: X = H·(DMF)
8: X = CN·(DMF)
9: X = $CONH_2$·(DMF)
10: X = I·(DMSO)
11: X = $CONH_2$·(DMSO)
12: X = Me·(DMSO)
13: X = Ac·(DMSO)
14: X = F (3,5-difluoro)·(DMSO)
15: X = OH(m-isomer)·(H_2O)
16: X = I
17: X = Ethynyl
18: X = $N(Me)_2$
19: X = 4-Iodophenyl
20: X = 4-Ethynylphenyl

Scheme 2. Compounds studied in this chapter.

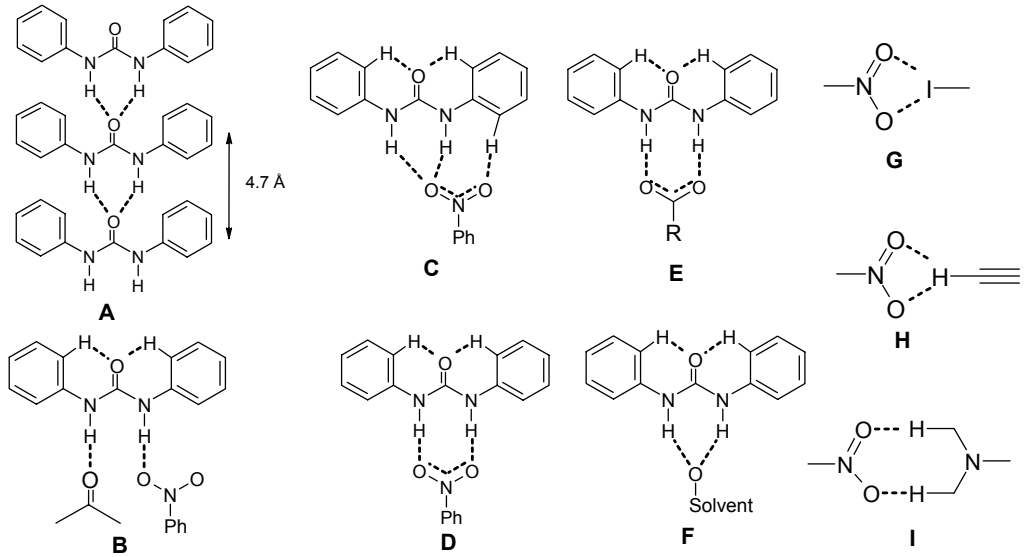

Scheme 3. Synthons observed in crystal structures studied in this chapter.

Table 1. Hydrogen bond geometries of compounds studied in this chapter.

Compound	Interaction[a]	*d*/Å	*D*/Å	θ/°
1	N1–H1···O2	2.22	3.135(3)	149.3
	N2–H2···O2	1.90	2.871(3)	160.3
	C3–H3···O1	2.25	2.915(3)	117.5
	C13–H13···O1	2.24	2.913(3)	118.2
2	N2–H2B···O1	1.94	2.913(2)	160.8
	N3–H3B···O1	2.13	3.069(2)	154.1
	C3–H3A···O3	2.25	2.917(2)	117.9
	C15–H15A···O3	2.25	2.926(2)	118.3
3	N2–H2B···O1	1.97	2.936(5)	159.9
	N3–H3B···O1	2.12	3.064(4)	155.4
	C3–H3A···O3	2.24	2.913(5)	118.2
	C15–H15A···O3	2.24	2.912(5)	118.0
4	N1–H1···O2	2.14	3.033(3)	146.9
	N2–H2···O2	1.94	2.908(3)	160.0
	C3–H3···O1	2.26	2.929(3)	118.1
	C9–H9···O1	2.25	2.924(3)	118.0
5	N1–H1···O3	2.01	3.021(7)	175.0
	N2–H2···O2	2.06	3.110(7)	154.3
	C12–H12···O1	2.61	3.583(8)	149.6
	C3–H3···O1	2.22	2.879(7)	116.6
	C9–H9···O1	2.19	2.876(7)	118.7
6	N1–H1···O3	2.04	3.032(4)	168.5
	N2–H2···O2	2.02	2.992(4)	160.0
	C3–H3···O1	2.23	2.875(5)	116.0
	C9–H9···O1	2.20	2.875(5)	118.2

7	N1–H1A···O4	1.88	2.844(4)	159.4
	N2–H1A···O4	1.90	2.853(4)	157.0
	C2–H2B···O1	2.29	2.943(5)	116.5
	C9–H9···O1	2.25	2.917(5)	117.4
8	N1–H1···O4	1.90	2.865(4)	159.6
	N2–H2···O4	1.89	2.846(3)	157.6
	C12–H12···N3	2.53	3.458(4)	142.8
	C10–H10···O1	2.25	3.295(4)	160.3
	C3–H3···O1	2.13	2.815(3)	118.6
	C9–H9···O1	2.14	2.825(4)	118.5
9	N1–H1···O5	1.98	2.918(3)	153.9
	N2–H2···O5	1.91	2.856(3)	154.9
	N3–H3A···O1	2.31	3.286(3)	161.2
	N3–H3B···O4	1.93	2.936(3)	173.1
	C16–H16A···O4	2.58	3.511(4)	144.0
	C17–H17A···O3	2.42	3.495(4)	169.3
	C3–H3···O1	2.40	3.040(3)	116.3
	C10–H10···O1	2.35	3.001(3)	116.7
10	N1–H1···O4	1.94	2.892(11)	157.1
	N2–H2···O4	1.95	2.901(11)	156.8
	N4–H4···O8	1.95	2.907(11)	157.2
	N5–H5···O8	2.08	3.019(11)	160.5
	C3–H3···O1	2.29	2.924(13)	115.3
	C9–H9···O1	2.24	2.878(12)	115.3
	C18–H18···O5	2.22	2.882(13)	117.0
	C24–H24···O5	2.27	2.922(12)	116.5
11	N1–H1···O5	1.88	2.876(4)	168.4
	N2–H2···O5	2.14	3.097(4)	158.2
	N4–H4A···O4	1.98	2.984(4)	173.3
	N4–H4B···O5	2.05	3.002(4)	156.2
	C7–H7···O1	2.18	2.860(4)	118.1
	C13–H13···O1	2.18	2.852(5)	118.1
12	N2'–H2B'···O4	2.01	2.818(4)	156.8
	N3'–H3B'···O4	2.10	2.902(4)	155.1
	N3–H3B···O4'	2.05	2.860(4)	156.4
	N2–H2B···O4'	1.99	2.818(4)	160.4
	C3'–H3'A···O3'	2.28	2.840(4)	118.9
	C153'–H15B···O3'	2.35	2.887(4)	116.5
	C3–H3A···O3	2.35	2.920(4)	118.9
	C15–H15A···O3	2.46	2.954(4)	113.6
13	N1–H1···O5	1.96	2.877(3)	148.8
	N2–H2···O5	1.85	2.796(3)	155.0
	C7–H7···O3	2.25	2.918(3)	117.5
	C13–H13···O2	2.23	2.898(3)	117.9
14	N1–H1···O4	1.81	2.777(2)	159.6
	N2–H2···O4	1.92	2.858(2)	153.7

	C3–H3···O1	2.22	2.876(2)	116.8
	C13–H13···O1	2.19	2.846(2)	116.3
15	N1–H1···O5	1.93	2.888(3)	158.2
	N2–H2···O5	1.92	2.880(3)	158.3
	O2–H2A···O3	2.07	2.778(3)	127.5
	O2–H2A···O4	2.43	3.416(3)	175.1
	O5–H5A···O1	1.76	2.743(3)	172.5
	O5–H5B···O2	1.89	2.850(3)	163.9
	C3–H3···O1	2.25	2.919(2)	118.1
	C9–H9···O1	2.30	2.949(2)	116.6
16	N3–H3···O3	2.13	2.931(5)	153.3
	N2–H2···O3	2.13	2.933(6)	155.0
	C11A–I1···O2		3.286	169.0
	C11A–I1···O1		3.618	154.3
17	N1–H1···O1	2.11	2.914(4)	156.2
	N2–H2···O1	2.12	2.919(4)	155.1
	C14–H14···O3	2.41	3.325(7)	167.6
	C14–H14···O2	3.04	3.833(7)	143.8
18	N5–H5···O6	2.21	3.057(6)	166.5
	N8–H8···O6	2.39	3.18(6)	153.4
	N6–H6···O5	2.28	3.103(6)	159.4
	N7–H7···O5	2.29	3.104(6)	157.4
	C1–H1···O4	2.74	3.463(9)	133.0
	C4–H4···O2	2.96	3.873(9)	159.7
19	N1–H1···O1	1.98	2.890(6)	148.8
	N2–H2···O1	2.09	3.011(7)	150.8
	C17–I1···O2		3.978	160.6
	C17–I1···O3		3.432	157.8

[a]All the N–H, C–H and O–H distances are neutron normalized to 1.009,1.083 and 0.983 Å respectively.

Table 2. Some structural features of compounds studied in this chapter.

Compound	Intramolecular C–H···O (Å)	Torsion angles ($C\text{-}C_{aryl}\text{-}N\text{-}C_{carbonyl}$ °)	H-bond motif (synthon)
1	2.33, 2.31	5.1, 4.6	**C**
2	2.32, 2.33	7.0, 5.9	**C**
3	2.32, 2.32	7.2, 5.9	**C**
4	2.33, 2.33	6.6, 5.9	**C**
5	2.30, 2.27	12.9, 3.8	**D**
6	2.30, 2.28	14.7, 3.0	**D**
7	2.32, 2.37	9.4, 12.8	**F**
8	2.21, 2.22	2.7, 6.8	**F**
9	2.43, 2.47	4.2, 8.1	**F**
10	2.26, 2.25	0.1, 11.0	**F**

11	2.30, 2.34, 2.36, 2.31	4.6, 5.7, 14.0, 14.6	**F**
12	2.28, 2.35, 2.35, 2.46	19.1, 20.7, 14.8, 31.1	**F**
13	2.33, 2.30	5.2, 2.4	**F**
14	2.28, 2.26	9.3, 15.2	**F**
15	2.32, 2.37	0.7, 9.3	**F**
16	2.62, 2.69	46.0, 49.0	**A** and **G**
17	2.64, 2.70	48.5, 49.0	**A** and **H**
18	2.16, 2.79, 2.33, 3.33	27.3, 51.5, 20.6, 88.0	**A** and **I**
19	2.42, 3.02	24.8, 63.0	**A** and **G**

2.4 Non-urea tape structures

Compounds **1**–**15** come under this family. Crystal structures of **1**–**6** are unsolvated and have similar structures with *para* and *meta*-substitutions while compounds **7**–**15** are solvates of DMSO and DMF.

2.4.1 Crystal structure of unsolvated *para*-substituted compounds, 1–4

The fluoro derivative **1** represents crystal structures of **1**–**4**. It crystallizes in the centrosymmetric space group $P2_1/n$ with one molecule in the asymmetric unit. The molecule adopts a flat planar molecular conformation stabilized by intramolecular C–H···O hydrogen bonds (2.33, 120.9, 2.32 Å, 121.5°) and resonance. The hydrogen bonding pattern reveals that the characteristic α-network is absent. Glide related urea molecules interact *via* synthon **C** in which one of the oxygen atom in the nitro group acts as a bifurcated acceptor to form one dimensional zig-zag tape and these tapes are further connected by C–H···O (2.60 Å, 170.6°) hydrogen bond and form a layered structure (Figure 3a). Adjacent layers are held together by weak van der Waals interactions. It is interesting to note that the nitro group, which is a weak hydrogen bond acceptor competes with urea carbonyl and succeeds by forming strong N–H···O (Table 1) hydrogen bonds. Urea carbonyl, a strong hydrogen bond acceptor is not participating in any strong hydrogen bonds. The fluorine atom in the molecule is not involved in any short contacts. Structures **1**–**4** are isostructural and isomorphous. Hydrogen bonding and crystal packing in these structures is very similar, with only slight differences in distances, angles and orientation of substituents. These crystal structures are displayed in figure 3.

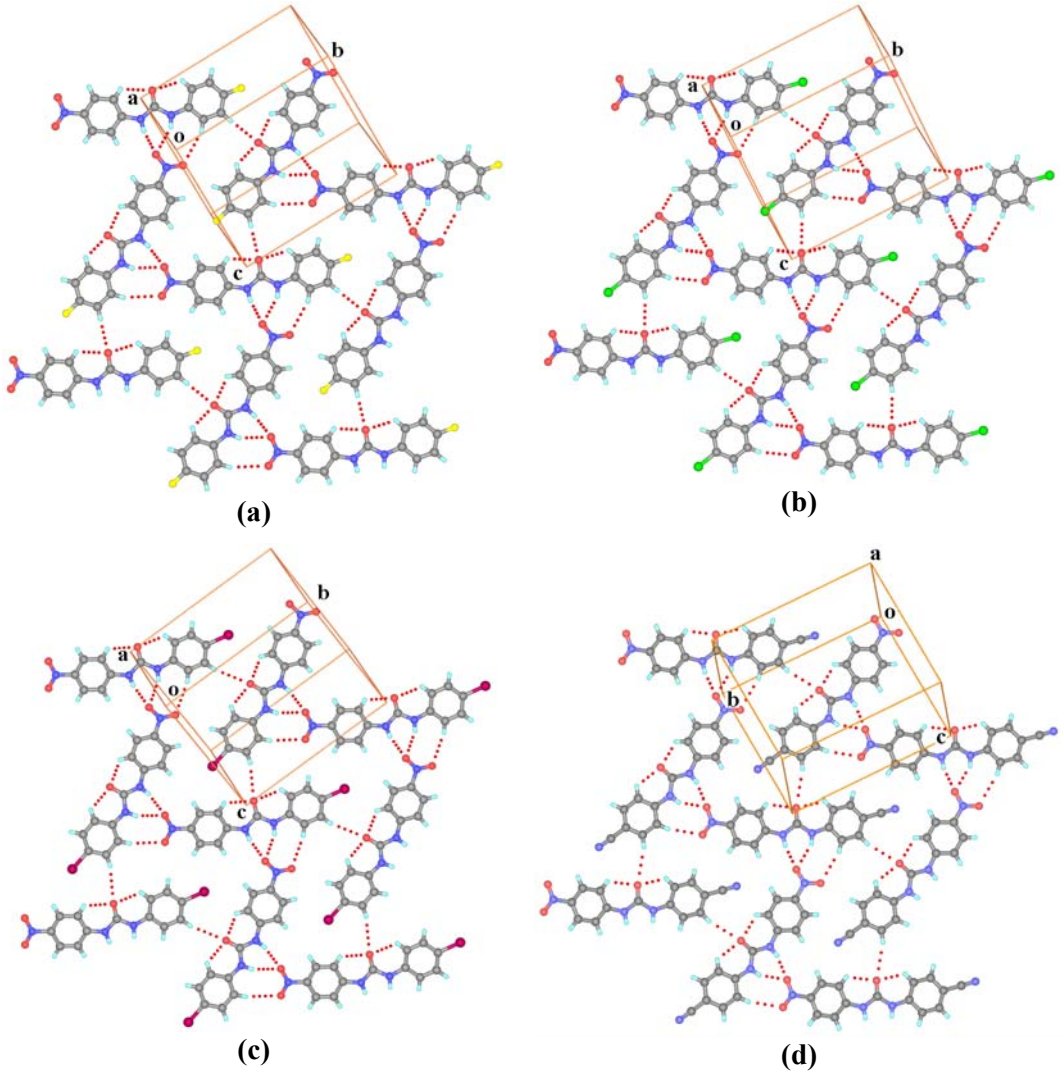

Figure 3. N–H···O_{nitro} (non-urea tape synthon **C**) and intramolecular C–H···$O_{carbonyl}$ interactions in crystal structures of (a) *p*-fluoro derivative, **1** (b) *p*-chloro derivative, **2** (c) *p*-bromo derivative, **3** and (d) *p*-cyano derivative, **4**. Notice the similarities in crystal packing.

2.4.2 Crystal structures of unsolvated *meta*-substituted compounds, 5–6

Meta-substituted derivatives, iodo **5** and bromo **6** are isostructural. Compound **5** crystallizes in the space group $P2_1/n$ with one molecule in the asymmetric unit and adopts a planar conformation stabilized by intramolecular C–H···O hydrogen bonds (2.30 120.0, 2.27 Å, 122.1°) and because of resonance between phenyl rings and urea group. Molecules hydrogen bonded *via* synthon **D** pack in a herringbone fashion in the crystal lattice (Figure 4). The hydrogen atom *meta* to the iodine forms a weak C–H···O with a glide related molecule, thus forming a planar layer in the [101] plane. There is a weak C–H···I (3.029 Å,

136.5°) interaction between the activated hydrogen (*ortho* to the nitro group) and the iodine atom. Adjacent layers are held together by weak van der Waals interactions. Similar to earlier crystal structures, urea carbonyl moiety in these crystal structures forms only weak C–H···O hydrogen bonds. The difference between **1**–**4** and **5**–**6** is in the mode of hydrogen bonding of the nitro group. In **1**–**4** nitro group interacts with urea NH donor *via* synthon **C** whereas in **5**–**6** it interacts *via* synthon **D** (Scheme 3).

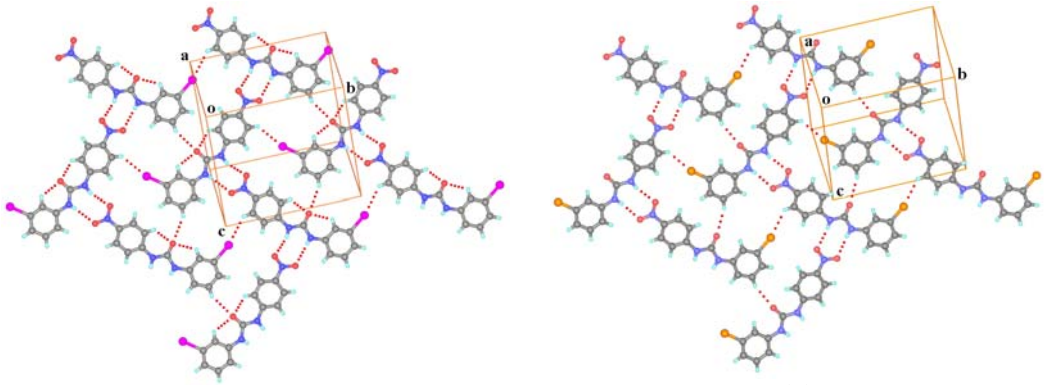

(a) **(b)**

Figure 4. N–H···O_{nitro} (non-urea tape synthon **D**) and intramolecular C–H···$O_{carbonyl}$ interactions in crystal structures of (a) *m*-iodo derivative, **5** and (b) *m*-bromo derivative, **6**. Note the similarities in the packing pattern and hydrogen bonding in both structures.

2.4.3 Crystal structures of solvates

Why solvents get included in crystal lattice is not yet properly understood. Nangia and Desiraju[12] showed that when solvent molecules are attached to solute molecules in a multi-point manner *via* either strong (O/N–H···O) or weak (C–H···O) hydrogen bonds, the extrusion of solvent from the aggregates may become sufficiently disadvantageous from an enthalpic viewpoint with the result that the solvent remains as an integral part of the nucleating crystal. Hence DMF and DMSO have the highest probability (corrected occurrence, O_{corr}, 5.69 and 4.73 respectively) of inclusion among common organic solvents in the crystal lattice. Some compounds in the present study failed to crystallize in pure form and crystallized with solvent of crystallization. Some compounds are crystallized in pure form as well as solvated form. The solvents which have stronger hydrogen bond acceptor than nitro-O and urea carbonyl like DMSO and/or DMF are included in the crystal lattice of compounds **7**–**15**.

2.4.4 DMF solvates, 7–9

Compounds **7**–**9** crystallize with DMF molecule in the crystal lattice. Though they belong to different crystal systems and space groups (**7**, $P2_1/c$; **8**, $P\bar{1}$; **9**, $P\bar{1}$), the hydrogen bonding pattern is same in these three crystal structures. Urea molecules adopt nearly planar conformation stabilized by intramolecular C–H···O hydrogen bonds and maximisation of resonance (for torsion angle and C–H···O hydrogen bond parameters, see Table 2). In crystal structure **7**, O-acceptor of DMF molecule competes with urea carbonyl and nitro groups for urea NH donors and forms strong N–H···O hydrogen bonds (Table 1) with a bifurcated synthon **F** (Figure 5a). Surprisingly nitro group is not involved in any strong hydrogen bonding. As described in structures **1**–**6**, urea carbonyl is forming only intra and intermolecular C–H···O hydrogen bonds and nitro group is involved in strong N–H···O hydrogen bonds. Crystal structure of **8** shows that DMF disrupts the α-network and form N–H···O hydrogen bonds. Cyano group involve in C–H···N dimer (2.66 Å, 144.8°) and nitro group accepts weak C–H···O hydrogen bonds from DMF solvent (Figure 5b). In crystal structure **9**, DMF interacts with urea NH and amide functionality forms a centrosymmetric homodimer (1.94 Å, 173.2°) as shown in figure 5c. The *anti* NH of amide interacts with urea carbonyl with N–H···$O_{carbonyl}$ hydrogen bond.

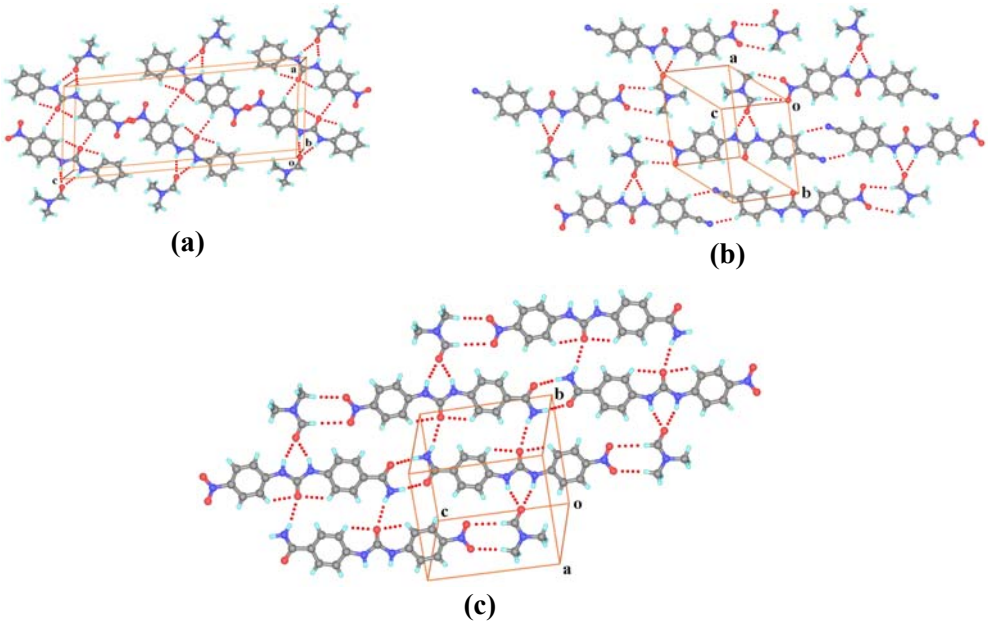

Figure 5. N–H···O_{DMF} (synthon **F**) and intramolecular C–H···$O_{carbonyl}$ interactions in DMF solvates of (a) Unsubstituted compound, **7** (b) *p*-cyano derivative, **8** and (c) *p*-amide derivative, **9**. Note that urea carbonyl interacts with *anti* NH with N–H···$O_{carbonyl}$ and amide dimer in (c).

2.4.5 DMSO solvates, 10–14

As DMF successfully competed for urea NH donors in structures **7**–**9**, DMSO too competes with urea carbonyl and nitro groups in crystal structures **10**–**14**. The crystal structure of **10** has two molecules of **10** and DMSO in the asymmetric unit. The sulfoxide oxygen in DMSO molecule acts as a bifurcated acceptor by accepting two N–H···O hydrogen bonds donated by the urea moiety (Figure 6a). One of the methyl groups are bonded to the oxygen of nitro group through a C–H···O (2.5 Å, 165.2˚) hydrogen bond. DMSO acts as a spacer between two urea molecules. Here DMSO molecule is sitting in between the urea molecule and it does not have any direct contacts with another DMSO molecule. In **11**, amide form centrosymmetric N–H···O homodimer and DMSO acts as spacer between urea molecules with a bifurcated N–H···O hydrogen bond (Synthon **F**) and forms a 2D layered structure (Figure 6b). Adjacent layers are connected through N–H···O hydrogen bonds. In crystal structures **12**, **13** and **14** the characteristic α-network is disrupted by DMSO molecules (Figure 6). In DMSO solvates **10**–**14**, the urea molecules are having nearly planar conformations with urea carbonyl forming both intra and intermolecular C–H···O hydrogen bonds (Table 2). Urea carbonyl and nitro groups accept only weak C–H···O hydrogen bonds.

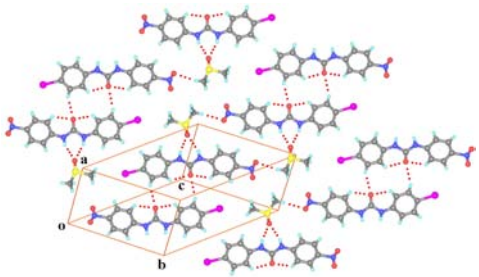

(a)

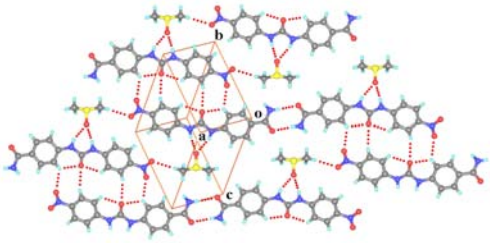

(b)

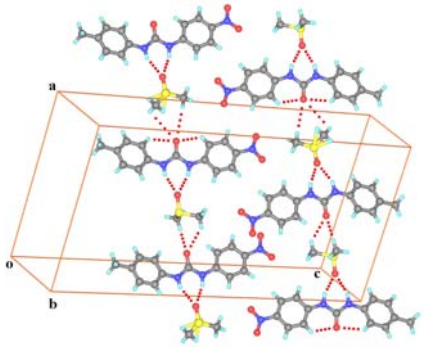

(c)

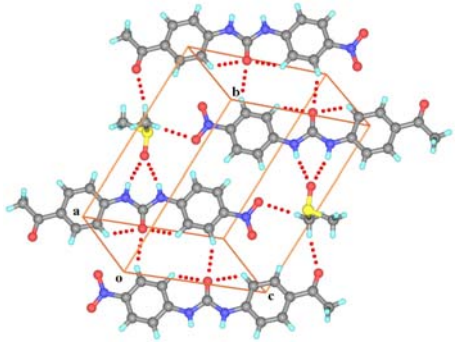

(d)

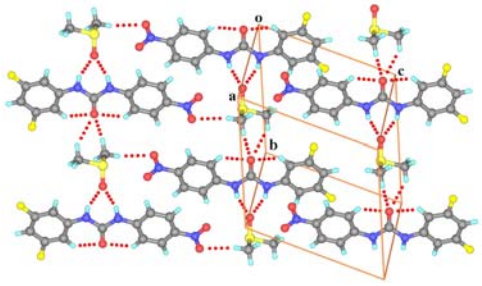

(e)

Figure 6. DMSO solvates of (a) *p*-iodo derivative, **10**, (b) *p*-amide derivative, **11**, (c) *p*-methyl derivative, **12**, (d) *p*-acetyl derivative, **13** and (e) 3,5-difluoro derivative, **14**. Note that in all structures α-network is disrupted by DMSO molecules and planar conformation of urea molecules.

2.4.6 Crystal structure of monohydrate, 15

The anhydrous form of *meta*-hydroxy derivative is not obtained but single crystals of a monohydrate are formed when crystallized from methanol at room temperature. It crystallizes in triclinic $P\bar{1}$ space group with one molecule of each in the asymmetric unit. Urea molecule adopts nearly planar conformation (0.7, 9.3°). Water O-acceptor interacts with urea NH donor in a bifurcated N–H···O motif (synthon F) and thus disrupts the α-network. Hydroxy group donates a bifurcated O–H···O (2.15, 2.57 Å, 130.4, 175.3°) to nitro acceptor and form a layered structure (Figure 7). These layers are connected by water OH donor and the urea carbonyl acceptor with O–H···O (1.83 Å, 172.7°) hydrogen bonds. The urea carbonyl participates in strong hydrogen bonding with water unlike DMF and DMSO solvates because of excess strong hydrogen bond donors of water present in the crystal lattice.

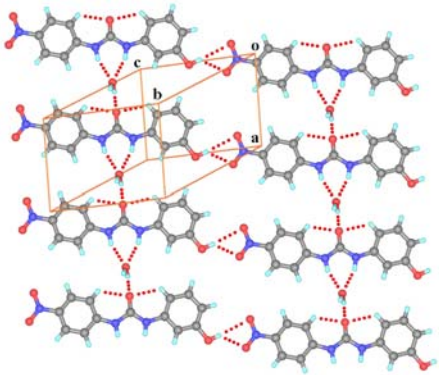

Figure 7. Crystal structure of *meta*-hydroxy derivative **15**, where water is disrupting the α-network and form one dimensional tape and these tapes are connected by O–H···O_{nitro} hydrogen bonds to form a layered structure.

2.5 Urea tape structures, 16–20

Para iodo, ethynyl, *N,N*-dimethylamino, *p*-iodophenyl and *p*-ethynylphenyl derivatives **16**–**20** come under this family. Compound **16** crystallizes in the polar space group *Cc* with one molecule in the asymmetric unit. Self assembly in **16** occurs *via* N–H···O (synthon **A)** hydrogen-bonding networks in one dimension, while the iodine atoms are in close contact with the nitro group with synthon **G** (3.61, 3.28 Å; 154.3, 169.6º)[13] controlling the alignment in the second dimension and leading to a two dimensional structure along *b*-axis (Figure 8). The carbonyl group is aligned along the short *b*-axis, 4.67 Å of the unit cell and the aryl groups are twisted out of the urea plane (49.1, 45.6°) to adjust to the α-network. Ethynyl derivative **17** crystallizes in space group *Cc* and is isostructural with iodo derivative **16,** confirming the observation that the iodo to ethynyl exchange does not generally disturb the crystal packing.[14] Figure 9 shows translation related molecules connected through N–H···O (2.11, 2.10 Å; 154.6, 156.3º) hydrogen bonds resulting in the α-network and such glide related tapes are in turn connected laterally through synthon **H** (2.40, 3.05 Å; 167.8, 142.9º). The aryl rings are twisted out of the urea plane by 48.8 and 47.3°. In the crystal structures of **16** and **17**, urea molecules adopt twisted conformation and have nearly the same conformation in the crystals. Compound **16** solid sample shows strong quadratic non-linear efficiency, with a green signal intensity (530 nm) equal to that of the benchmark compound 3-methyl-4-nitropyridine-1-oxide (POM).[15] The SHG activity of iodo derivative **16** is 13 times that of urea and ethynyl derivative **17** was found to have efficiency 1.2 times that of urea.

The crystal structure of **18** was determined to confirm the structure directing ability of the weak interactions over the strong N–H···O in this family of compounds. The *N,N*-dimethylamino derivative **18** crystallizes in the space group $P\bar{1}$ with two molecules in the asymmetric unit. Here also the N–H···O tape (Table 1) is reproduced faithfully. Weak C–H···O (2.74, 2.96 Å; 133.1, 159.6º) interactions between the $N(Me)_2$ group and the oxygen atom of the nitro group[16] give the auxiliary support for the α-network as indicated in figure 10. Chains along the *c*-axis are aligned antiparallel to each other. The phenyl rings are twisted out of the urea plane with angle 27.3, 51.5, 20.6, 88.0 53.4º. It does not show any SHG activity as it crystallizes in the centrosymmetric packing. Taking advantage the biphenyl moiety with extended ring conjugation compared to phenyl moiety there by anticipating an increase in SHG activity, biphenyl derivatives **19** and **20** were prepared.

Unfortunately compound **19** crystallizes in the centrosymmetric space group $P2_1/c$ with one molecule in the asymmetric unit. The characteristic α-network is formed via the urea tape N–H···O synthon **A** to form one dimensional polar tapes and these tapes are connected with I···NO_2 interaction in second dimension to form 2D polar layered structure (Figure 11). Two adjacent inversion related layers are connected by van der Walls interactions. In this crystal structure molecule **19** adopts twisted conformation (24.8, 63.0º) to facilitate the structure requirement of the α-network. Compound **20** failed to give diffraction quality single crystals and comparison of PXRD pattern with **19** indicates that it also belongs to the α-network structure category (Figure 12). Iodophenyl and ethynylphenyl derivatives **16** and **17** crystallizes in non-centrosymmetric space group *Cc* whereas *N,N*-dimethyl and iodobiphenyl derivatives **3** and **4** have a centrosymmetric packing. Yet the hydrogen bond networks in these structures are nearly identical. Crystal engineering of 1D chains and 2D layers is possible but the final 3D arrangement in a crystal is still very difficult to predict, particularly centrosymmetric vs. non-centrosymmetric crystal packing.

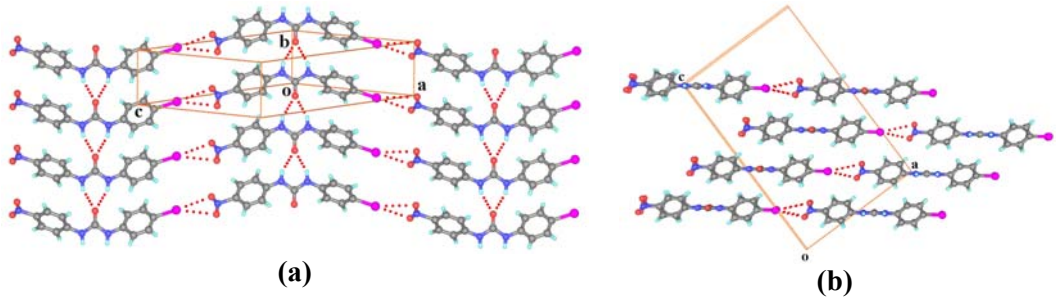

Figure 8. (a) N–H···O urea tapes along the *b*-axis and synthon **G** in *p*-iodo derivative, **16**. (b) View down the *b*-axis showing the parallel arrangement of polar chains.

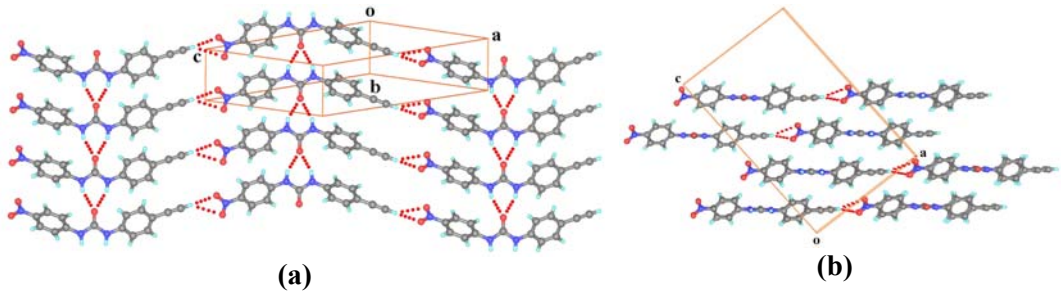

Figure 9. (a) The α-network observed in *p*-ethynyl derivative, **17** which is supported by the synthon **H** along the *b*-axis. (b) The parallel alignment of the chains down the *c*-axis

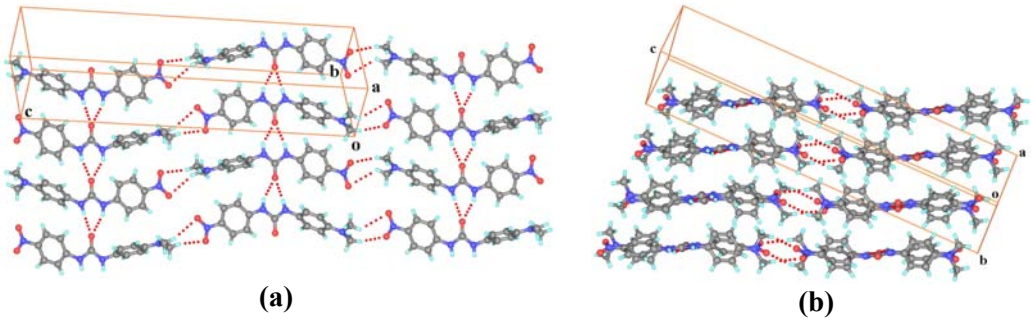

Figure 10. (a) The α-network observed in the crystal structure of *N,N*-dimethylamino derivative, **18** and the lateral C–H···O interaction. (b) The alignment of the chains.

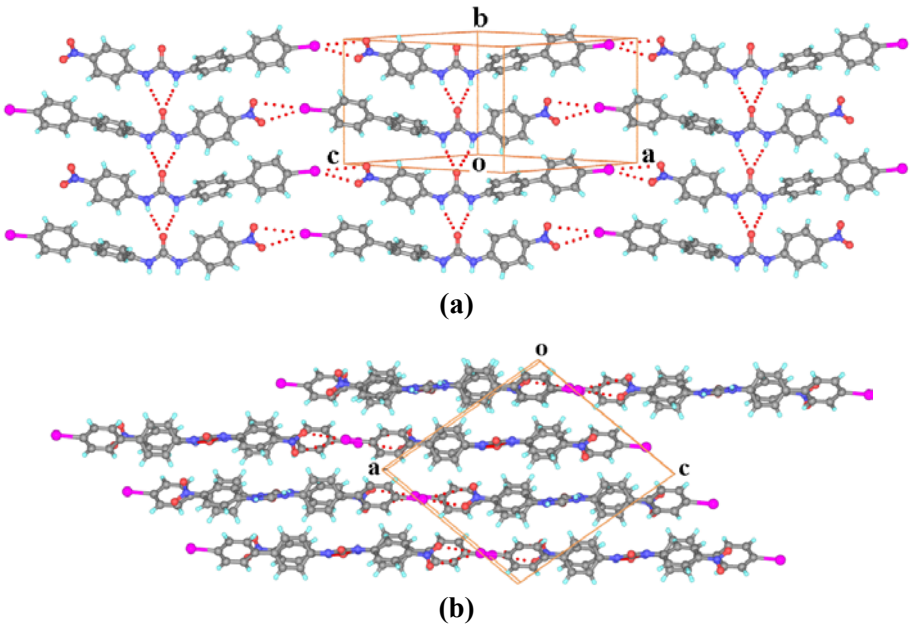

Figure 11. (a) Packing diagram showing urea α-network along the *b*-axis and synthon **G** in **19**. (b) View down the *b*-axis.

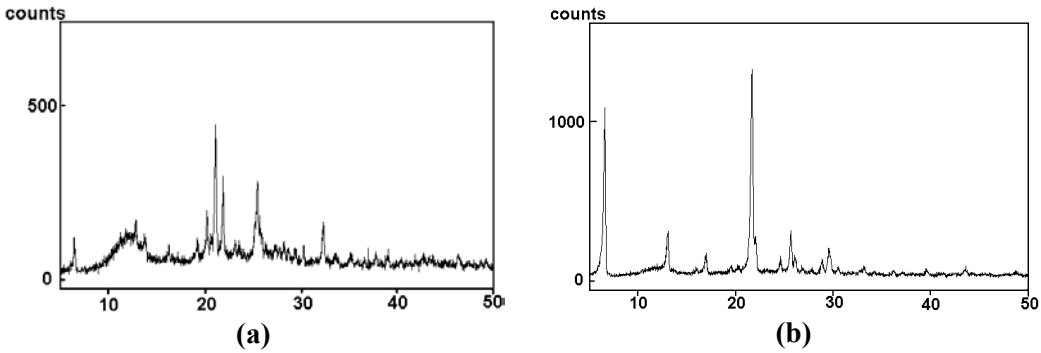

Figure 12. Experimental powder XRD pattern of (a) *p*-iodophenyl derivative, **19**. (b) *p*-ethynylphenyl derivative **20**. Note the similarities in intense peak positions.

2.6 Energy calculations

2.6.1 Synthon energy

Calculations were performed on simple model systems like *N,N*'-dimethyl urea homodimer and nitromethane···*N,N*'-dimethyl urea heterodimer (Scheme 4). Synthon energies were calculated in RHF/6-31G* basis set by geometry optimisation in PC Spartan Pro 1.0.[17] Interaction energies resulting from the N–H···O hydrogen bonds within the dimers were computed as the difference in energy between the dimer, on one hand, and the sum of isolated monomers. The urea dimer synthon has an energy –8.4 kcal/mol and the urea···NO_2 synthon energy is to –5.9 kcal/mol. Although synthon energy of urea tape is more than urea-nitro synthon, the latter is preferred in structures **1**–**6**.

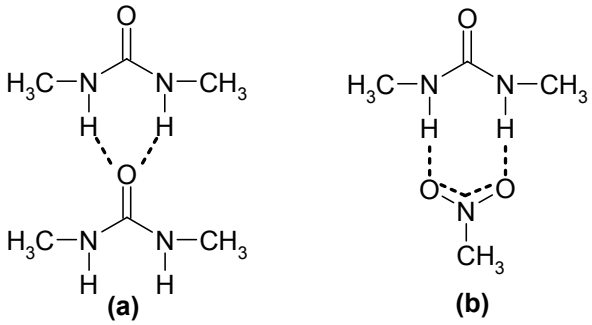

Scheme 4. The model systems on which Spartan calculations was performed (a) urea homodimer (b) urea···nitro heterodimer.

2.6.2 Energy profiles and electrostatic potential (ESP) calculations

The energy and atomic charge on diphenylurea was calculated as a function of aryl–N–C=O torsion angle (Figure 13). The energy profile in figure13 shows that the planar conformation of diphenylurea (τ = 0, 180°) is more stable than the twisted conformation (τ = 90°) by 9.0 kcal/mol, an energy difference that is in agreement with a recent calculation on torsional parameters about the urea amide bond.[18] The planar conformation of diarylurea is more stable because of two additive effects: conjugation of urea N with electron-withdrawing phenyl ring and intramolecular C–H···O interactions. Analysis of figure 13 leads to the following points. (1) The charge on urea O is sensitive to the aryl–N–C=O torsion angle, it being more electron-rich (better HB acceptor) when the aryl group is twisted and less negative (poorer HB acceptor) when it is planar. (2) The electron density on urea O in the experimental twisted conformation of diphenylurea is much greater than the charge in the minimized planar conformation (–50.8 vs. –38.6 kcal/mol). A weakening of

the C=O acceptor strength changes H-bonding in the structure from urea α-network to other motifs.

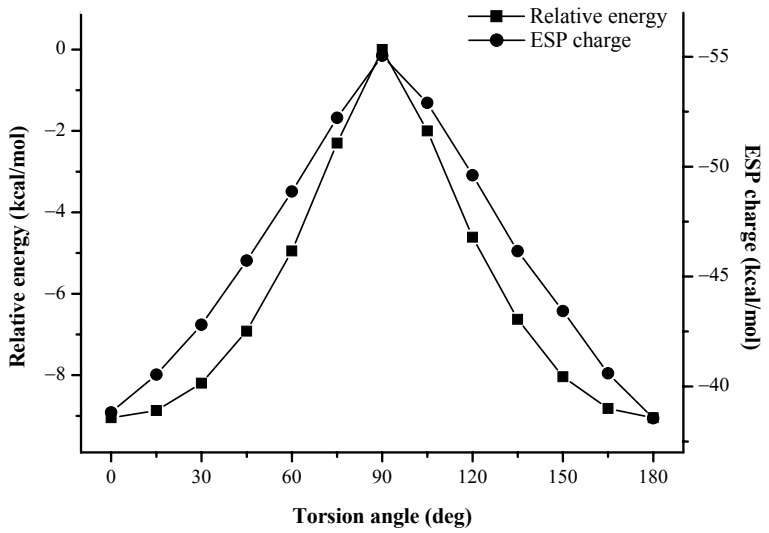

Figure 13. Spartan computations (DFT-B3LYP/6-31G*) on diphenylurea as a function of aryl–N–C=O torsion angle. Relative energy is plotted such that the highest energy conformer is fixed at 0. The planar molecular conformation is stable. Note that the ESP charge on urea O-atom is higher (better hydrogen bond acceptor) in the twisted conformation.

2.7 Nuclear Overhauser Enhancement (nOe) experiment

In order to find out the conformation of diphenylureas in solution, difference nOe ^{1}H NMR experiments were performed in DMSO-d_6. Irradiation of NH proton of diphenylurea at 8.71 shows nOe to the *ortho*-H signal at δ 7.48 (22%), implying that it is in a planar conformation (Figure 14). Similarly *p*-methyl and *p*-iodo derivatives also show nOe to the *ortho*-protons indicating the planar conformation. Variable-temperature NMR of diphenylurea in MeOH-d_4 (300-200 K) shows no change in peak positions, which means that the conformation remains the same upon cooling to 200 K and is in agreement with the higher stability of the planar conformation in the gas phase (DFT calculations, Figure 13). When NMR spectra were recorded at varying concentrations (0.005-0.5 M in MeOH-d_4) there is no change in the peak position, implying that the urea molecule aggregates with solvent but there is no evidence of dimeric species at higher concentration. NMR spectra in MeOH-d_4 and DMSO-d_6 are virtually identical in δ and *J* values. The nOe experiment was carried out in DMSO-d_6 because the NH protons exchange rapidly in MeOH-d_4. On the other hand, the variable temperature and concentration-dependent NMR studies had to be

done in MeOH-d_4. These data suggest that diphenylurea aggregation in NMR solvents perhaps resemble the related solvates of diarylureas.

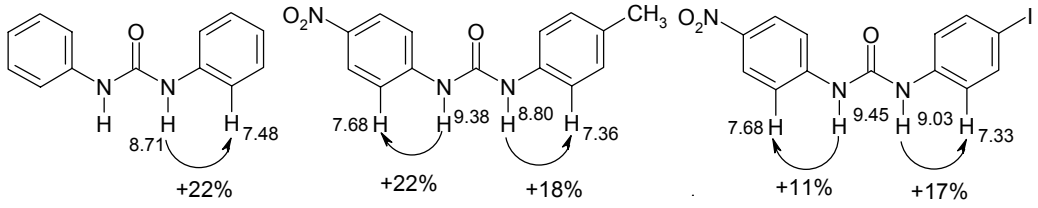

Figure 14. ^{1}H NMR nOe of diphenylurea, *p*-methyl derivative and *p*-iodo derivative in DMSO-d_6. This experiment indicates that all these ureas exist in planar conformation.

2.8 Discussion

In unsolvated structures **1**–**6**, the dominant hydrogen bonding is synthon C or synthon D with urea molecules adopting planar conformation with intramolecular C–H···O hydrogen bonds. Generally urea carbonyl (pK_{HB} of tetramethylurea is 2.44 and tertraphenylurea is 1.74)[19] is a better hydrogen bond acceptor than nitro (pK_{HB} of nitrobenzene is 0.30 and activated *N,N*-dimethyl-*p*-nitro-aniline is 0.83) acceptors. But due to planar conformation and intramolecular C–H···O, the electron density on carbonyl acceptor is reduced considerably and hence it becomes weak acceptor than nitro group. Therefore the best acceptor available in the molecule, which is nitro group, interacts with better urea NH donors and thus disrupting the urea tape.[20] Crystal structures of solvates **7**-**15** reveal that urea molecules act as only hydrogen bond donor in the flat conformation. Solvents like DMF and DMSO (pK_{HB} 2.10, 2.58) which are better hydrogen bond acceptors than urea carbonyl and nitro groups compete for NH donors and the dominant pattern in these structures is synthon **F**. In crystal structures **16**–**19** competing nitro group is trapped with complimentary interactions like nitro···iodo (synthon **G**), nitro···ethynyl (synthon **H**) and nitro···N,N-dimethylamine (synthon **I**), there is no acceptor left for urea NH donors and therefore urea molecules twist to a metastable conformation and form the urea tape.

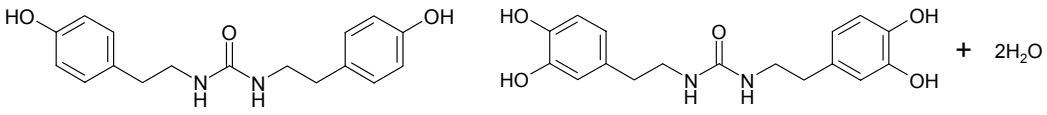

4-HPEU 3,4-DHPEU

Although they represent two different families, all crystal structures studied in this chapter can be compared with literature structures, *N,N*′-bis(4-hydroxyphenylethyl)urea (4-

HPEU) and *N,N′*-bis(3,4-dihydroxyphenylethyl)urea (3,4-DHPEU) dehydrate, in terms of hydrogen bonding and competition. Figure 15a shows the crystal structure of SEPQEJ, in which urea tape is disrupted by phenolic acceptor. Phenolic OH is a better hydrogen bond donor and weak acceptor. Urea carbonyl, which is better acceptor in this case (because there is no resonance and intramolecular C–H···O hydrogen bonds) interacts with better phenolic OH donor and forms strong O–H···O hydrogen bonds. In the dihydrate 3,4-DHPEU, phenolic OH is engaged in hydrogen bonding with water and the urea tape is reproduced (Figure 15b). It is interesting to note that the conformation of urea molecule in 4-HPEU is entirely different from that of 3,4-DHPEU.[21]

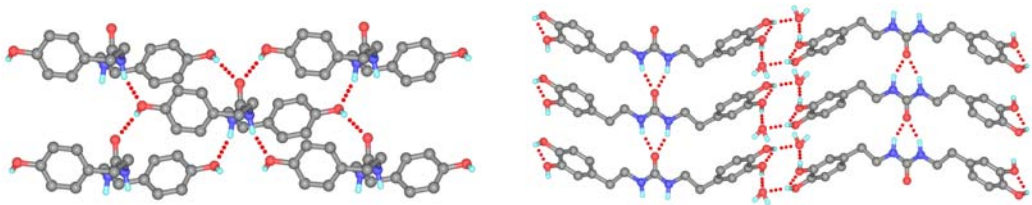

Figure 15. (a) O–H···$O_{carbonyl}$ and N–H···$O_{hydroxy}$ hydrogen bonds in the crystal structure of 4-HPEU (SEPQEJ), urea tape is disrupted by phenolic OH. (b) Crystal structure of 3,4-DHPEU (SEPQOT), when phenolic OH form strong O–H···O hydrogen bonds with water molecules urea tape is reproduced. Hydrogens which are not forming hydrogen bonds are removed for clarity.

Table 3. CSD refcodes and structural summary of diarylureas extracted from the CSD.

Entry No.	Structural Formula	Refcode	Torsion Angle (C–C–N–C)/°	H-bond Motif
1	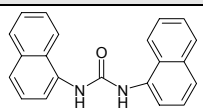	AMAFEZ	42.5, 49.6	urea tape
2	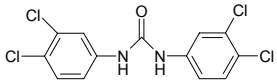	DCPHUR	20.2, 31.3, 30.9, 46.6	urea tape
3	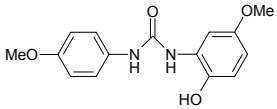	DEVVUV	59.0, 68.0	urea tape
4	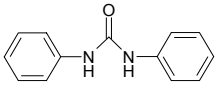	DPUREA	39.9, 44.0	urea tape
5	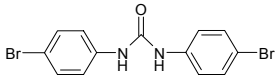	ETOBIY	51.3, 51.3	urea tape
6	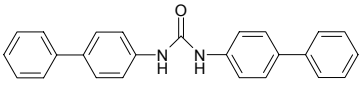	HAHCOJ	37.1, 57.1	urea tape

7	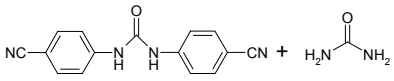	HEZTEL	39.3, 39.3	urea tape
8	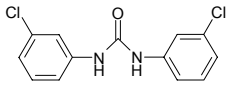	QQQAGA01	47.4, 47.4	urea tape
9	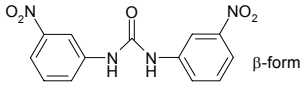	SILTOW01	32.6, 32.6	urea tape
10	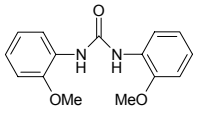	SILTUC	44.6, 44.6	urea tape
11	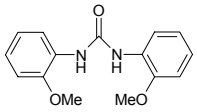	SILTUC01	24.4, 24.4	urea tape
12	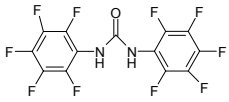	TUDLUZ	50.0, 50.1	urea tape
13	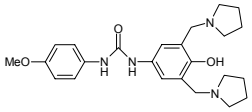	VIMYEV	40.3, 62.6	urea tape
14	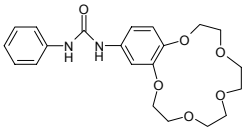	ILICAH	40.3, 62.6	urea tape
15	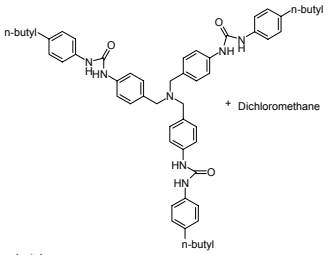	EGRFER	23.9,54.7, 33.5, 55.5, 18.1, 65.9	urea tape
16	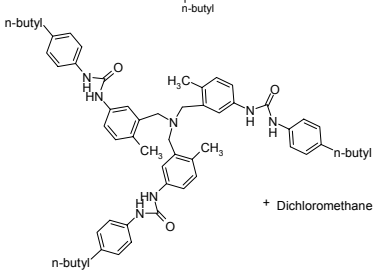	IXEMON	13.6, 60.0	urea tape
17	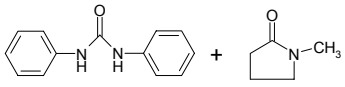	QAZXUK	4.2, 10.1	non-urea tape
18	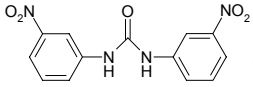	SILTOW	1.6, 24.8	non-urea tape
19	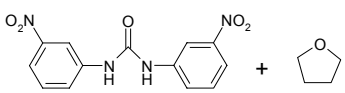	GIRROJ10	3.0, 6.3	non-urea tape

20	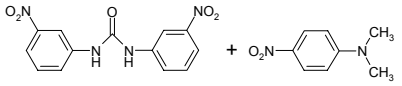	GIMRUP10	2.1, 2.1	non-urea tape
21	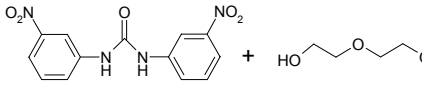	GIMSAW10	5.2, 12.2	non-urea tape
22	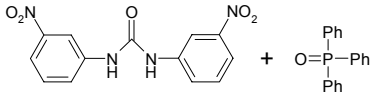	GIMSEA10	2.1, 22.9	non-urea tape
23	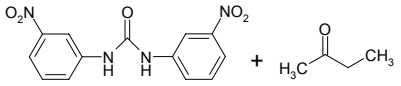	SILVAK	3.3, 4.6	non-urea tape
24	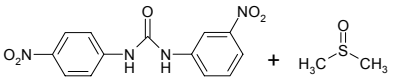	SILVOY	0.5, 16.7	non-urea tape
25	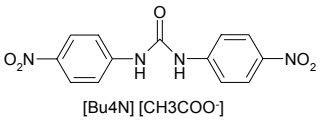	FEMQEU	6.6, 7.3	non-urea tape
26	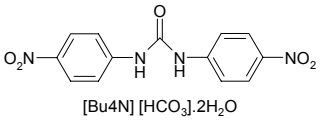	FEMQIY	1.5, 4.1	non-urea tape
27	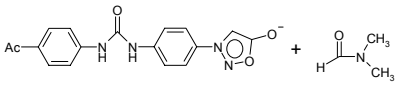	EWOZUL	0.5, 7.3	non-urea tape

2.9 Conclusion

Crystal structures studied here can be divided into two categories as non-urea tape structures (structures which are not forming α-network, **1**–**15**) and urea tape structures (**16**–**19**). Compound **20** failed to give diffraction quality single crystals, however by comparing PXRD patterns of **19** and **20** it is confirmed that the compound **20** forms the crystal structure similar to that of **19**. Hydrogen-bonding in diarylureas having electron-withdrawing groups irrespective of position, is different from that of diarylureas with neutral or electron-donating groups. The N–H group of the urea preferentially form N–H···O hydrogen bonds with the nitro oxygen rather than the carbonyl in compounds **1**–**6**, thus preventing the formation of α-network. The acceptor strength of urea C=O depends on the molecular conformation and the intramolecular C–H···O interactions, it is a better hydrogen bond acceptor in the twisted conformation than in the planar conformation. Because of the reduced acceptor strength of urea carbonyl with two intramolecular C–H···O hydrogen bonds in planar conformation, the strong NH donors approach other acceptors like solvent O

or nitro O atoms. The energy of forming α-network with the two N–H···O's (carbonyl) can be equalled by two N–H···O (nitro) and two weak intramolecular C–H···O (carbonyl) hydrogen bonds with an alternate packing. It is indicative from crystal structures **1**–**15**, where urea carbonyl is not involving in any kind of strong hydrogen bonding. Whenever interfering nitro group is engaged with complimentary interactions like iodo···nitro, ethynyl···nitro and *N,N*-dimethylamine···nitro, the characteristic α-network is observed in crystal structures **16**–**19**. Because bromo···nitro and chloro···nitro interactions are not that specific when compared to iodo···nitro, α-network is not observed in crystal structures of **2** and **3**. Analysis of table 3 and crystal structures of **16**–**19** reveal that to from α-network urea molecules have to twist (C–C–N–C, 30–60°) to a meta-stable conformation (1–1.5 kcal/mol from stable rotamer) to facilitate the approach of two urea molecules.

From *ab initio* calculations and nOe experiment (Figures 13, 14) on diphenylurea and crystal structure of it solvate (entry no. 17 in table 3, refcode, QAZXUK) with *N*-methyl-2-pyrrolidinone, it can be concluded that diphenylurea is more stable in planar conformation, which is stabilized by intramolecular C–H···O interactions and maximization of resonance. But in solid state it forms α-network with twisted conformation. Because there is no other hydrogen bond acceptor available in the molecule, diphenylurea twists to a less stable conformation and form N–H···O tape, whereas in *N*-methyl-2-pyrrolidinone solvate solvent molecule has strong hydrogen bond acceptor and interacts with urea NH donors and therefore diphenylurea retains its planar conformation (C–C–N–C torsion angles, 4.2, 10.1°) even in solid state. The planar conformation of *p*-iodo and *p*-methyl derivatives in their DMSO solvates is also confirmed by nOe experiment. The position of the functional groups also plays a major role in complimentary recognition.[22] For example crystal structures of meta iodo derivative **5** and of para iodo derivative **16** are entirely different in terms of hydrogen bonding. Characteristic α-network is observed in **16** due to the complimentary recognition of synthon **G,** whereas in crystal structure of **5** synthon **G** is absent thus result in a non urea tape structure.

The following conclusions may be drawn. (1) Molecular conformation and weak interactions direct the strong hydrogen bonding in diarylureas with electron withdrawing groups. (2) Arylureas exist in planar conformation irrespective of substitution in gas phase stabilized by weak intramolecular C–H···O hydrogen bonds and maximization of resonance. (3) Electron withdrawing groups activate phenyl CH donors and form stronger C–H···O

interactions when compared to unsubstituted and electron-donating group substituted diarylureas and therefore it retains planar conformation in solid state also. (4) Electron-withdrawing group containing diarylureas have the property of forming cocrystals or solvates irrespective of *meta* or *para* position in stable planar conformation. (5) The position of functional groups in the molecule is equally important in molecular recognition.

2.10 Experimental Section

Synthesis: All compounds are characterized by IR and NMR. ^{1}H NMR spectra (δ scale in ppm, *J* coupling constant in Hz) were recorded on Bruker 200 MHz and Bruker Avance at 400 MHz and FT-IR spectra (ν in cm^{-1}) on Jasco 5300 spectrophotometer. Melting points were recorded on Fisher–Johns apparatus.

***N*-4-Flourophenyl-*N*'-4'-nitrophenylurea, 1:** Compound was crystallized from THF/Ethanol mixture. ^{1}H NMR (DMSO-d_6): δ 9.417 (s, 1H), 8.93 (s, 1H), 8.16 (d, *J* = 8, 2H), 7.66 (d, *J* = 8, 2H), 7.45 (d, *J* = 8, 2H), 7.10 (d, *J* = 8, 2H). IR (KBr): 3406, 1724, 1618, 1408 cm^{-1}. M. p. Above 250 °C.

***N*-4-Chlorophenyl-*N*'-4'-nitrophenylurea, 2:** Compound was crystallized from THF and ethanol mixture. ^{1}H NMR (DMSO-d_6): δ 9.46(s, 1H), 9.05(s, 1H), 8.17 (d, *J* = 8, 2H), 7.66 (d, *J* = 8, 2H), 7.48 (d, *J* = 8, 2H), 7.33 (d, *J* = 8, 2H). IR (KBr): 3369, 1724, 1595, 1415 cm^{-1}. M. p. Above 250 °C.

***N*-4-Bromophenyl-*N*'-4'-nitrophenylurea, 3:** Compound was crystallized from THF, ethanol and benzene mixture. ^{1}H NMR (DMSO-d_6): δ 9.47 (s, 1H), 9.06 (s, 1H), 8.31 (d, *J* = 8, 2H), 7.70 (d, *J* = 8, 2H), 7.47 (s, 4H). IR (KBr): 3368, 1726, 1614, 1417 cm^{-1}. M. p. Above 250 °C.

***N*-4-Cyanophenyl-*N*'-4'-nitrophenylurea, 4**: Compound was crystallized from THF and ethanol mixture. ^{1}H NMR (DMSO-d_6): δ 9.62 (s, 1H), 9.42 (s, 1H), 8.2 (d, *J* = 8, 2H), 7.6 (m, 6H). IR (KBr): 3412, 2220, 1728, 1597, 1531, 1413 cm^{-1}. M. p. above 250 °C.

***N*-*Meta*-iodophenyl-*N*'-4'-nitrophenylurea, 5:** Compound was crystallized from DMSO. ^{1}H NMR (DMSO-d_6): δ 9.49 (s, 1H), 9.043 (s, 1H), 8.17 (d, *J* = 8, 2H), 8.01 (s, 1H), 7.67 (d, *J* = 8, 2H), 7.35 (d, *J* = 8, 2H), 7.10 (t, *J* = 6, 1H). IR (KBr): 3380, 1640, 1410 cm^{-1}. M. p. Above 250 °C.

***N*-*Meta*-bromophenyl-*N*'-4'-nitrophenylurea, 6:** Compound was crystallized from THF. ^{1}H NMR (DMSO-d_6): δ 9.52 (s, 1H), 9.043 (s, 1H), 8.31 (d, *J* = 8, 2H), 8.10 (s, 1H), 7.70 (d,

J = 8, 2H), 7.30 (d, *J* = 8, 2H), 7.00 (t, *J* = 6, 1H). IR (KBr): 3410, 3368, 1614, 1417 cm^{-1}. M. p. Above 250 °C.

***N*-Phenyl-*N*'-4'-nitrophenylurea, 7:** Compound was crystallized from DMF. ^{1}H NMR (DMSO-d_6): δ 9.42 (s, 1H), 8.91 (s, 1H), 8.17 (d, *J* = 8, 2H), 7.66 (d, *J* = 8, 2H), 7.45 (d, *J* = 8, 2H), 7.27 (t, *J* = 8, 2H), 7.018 (t, *J* = 6, 1H). IR (KBr): 3298, 1649, 1698, 1562, 1446 cm^{-1}. M. p. 226-229 °C.

***N*-4-Carboxamidophenyl-*N*'-4'-nitrophenylurea, 9:** Compound crystallized from DMSO and DMF. ^{1}H NMR (DMSO-d_6): δ 9.52 (s, 1H), 9.17 (s, 1H), 8.31 (d, *J* = 8, 2H), 7.86 (d, *J* = 8, 2H), 7.68 (d, *J* = 8, 2H), 7.56 (d, *J* = 8, 2H), 7.23 (s, 2H). IR (KBr): 3460, 3431, 3341, 1709, 1537, 1413 cm^{-1}. M. p. Above 250 °C.

***N*-4-Tolyl-*N*'-4'-nitrophenylurea, 12:** Compound was crystallized from DMSO. ^{1}H NMR (DMSO-d_6): δ 9.38 (s, 1H), 8.80 (s, 1H), 8.16 (d, *J* = 8, 2H), 7.69 (d, *J* = 8, 2H), 7.33 (d, *J* = 8, 2H), 7.13 (d, *J* = 8, 2H), 2.25 (s, 3H). IR (KBr): 3302, 1647, 1512, 1408 cm^{-1}. M. p. 238 °C.

***N*-(4-Acetyl)phenyl-*N*'-4'-nitrophenylurea, 13:** Compound was crystallized from DMSO. ^{1}H NMR (DMSO-d_6): δ 9.54 (s, 1H), 9.32 (s, 1H), 8.19 (d, *J* = 8, 2H), 7.91 (d, *J* = 8, 2H), 7.69 (d, *J* = 8, 2H), 7.59 (d, *J* = 8, 2H). IR (KBr): 3317, 1649, 1520, 1403 cm^{-1}. M. p. Above 250 °C.

***N*-(3,5-Difloro)phenyl-*N*'-4'-nitrophenylurea, 14:** Compound was crystallized from DMSO. ^{1}H NMR (DMSO-d_6): δ 9.60 (s, 1H), 9.30 (s, 1H), 8.22 (d, *J* = 8, 2H), 7.78 (d, *J* = 8, 2H), 7.21 (d, *J* = 8, 2H), 6.91 (t, *J* = 5, 1H). IR (KBr): 3364, 1616, 1572, 1437 cm^{-1}. M. p. Above 250 °C.

***N*-*Meta*-hydroxyphenyl-*N*'-4'-nitrophenylurea, 15:** Crystallized from methanol. ^{1}H NMR (DMSO-d_6): δ 9.40 (s, 1H), 9.35 (s, 1H), 8.81 (s, 1H), 8.22 (d, *J* = 8, 2H), 7.70 (d, *J* = 8, 2H), 7.07 (m, 1H), 6.84 (d, *J* = 6, 1H), 6.44 (d, *J* = 6, 1H). IR (KBr): 3369, 1707, 1618, 1412 cm^{-1}. M. p. 210-212 °C.

***N*-4-Iodophenyl-*N*'-4'-nitrophenylurea, 16:** Compound was recrystallized from THF. ^{1}H NMR (DMSO-d_6): δ 9.45 (s, 1H), 9.03 (s, 1H), 8.23 (d, *J* = 8, 2H), 7.71 (d, *J* = 8, 2H), 7.63 (d, *J* = 8, 2H), 7.31 (d, *J* = 8, 2H). IR (KBr): 3308, 1647, 1388 cm^{-1}. M. p. Above 250 °C.

***N*-4-Ethynylphenyl-*N*'-4'-nitrophenylurea, 17:** Ethynyl derivative **17** was prepared by protecting the 4-iodoaniline using trimethylsilylacetylene and condensing it with the *p*-nitrophenylisocyanate followed by deprotection to obtain the product.

Preparation of 4-(2-trimethylsilyl-1-ethynyl)aniline: Trimethylsilylacetylene (3.425 mmol, 335.6 mg, 0.48 ml) was added into 4-iodoaniline (500 mg, 2.283 mmol) taken in 7 ml Et_3N in presence of cuprous iodide and palladium catalyst [($PdCl_2(PPh_3)$] at 0°C under nitrogen atmosphere and the reaction mixture was allowed to stir in RT for 12 h. Et_3N was removed and the product was purified by column chromatograpy using neutral silica with hexane eluent. ^{1}H NMR (DMSO-d_6): δ 0.24 (s, 9H), 5.51 (s, 2H), 6.54 (d, J = 8, 2H), 7.11 (d, J = 8, 2H). IR (KBr): 3464, 2146, 1622, 1510 cm^{-1}. M. p. 99-101 °C.

Preparation of *N*-4-(2-trimethylsilyl-1-ethynyl)phenyl-*N*'-4'-nitrophenylurea: A mixture of 4-(2-trimethylsilyl-1-ethynyl)aniline (294 mg, 1.55 mmol) and 4-nitrophenyl isocyanate (306 mg, 1.87 mmol) in 12 ml benzene was heated to reflux until there was no starting material remained by TLC. ^{1}H NMR (DMSO-d_6): δ 0.25 (s, 9H), 7.22 (d, J = 8, 2H), 7.41 (d, J = 8, 2H), 7.73 (d, J = 8, 2H), 8.33 (d, J = 8, 2H), 9.21 (s, 1H), 9.55 (s, 1H). IR (KBr): 3364, 2156, 1680, 1595, 1408 cm^{-1}. M. p. Above 250 °C.

Deprotection of *N*-4-(2-trimethylsilyl-1-ethynyl)phenyl-*N*'-4'-nitrophenylurea to *N*-4-ethynylphenyl-*N*'-4'-nitrophenylurea, 17: To the protected urea derivative *N*-4-(2-trimethylsilyl-1-ethynyl)phenyl-*N*'-4'-nitrophenylurea (344 mg) taken in 15 ml MeOH was added 10 ml K_2CO_3 in MeOH. The reaction mixture was stirred for 1 h. ^{1}H NMR (DMSO-d_6): δ 9.61 (s, 1H), 8.90 (s, 1H), 8.20 (d, J = 8, 2H), 7.75 (d, J = 8, 2H), 7.54 (d, J = 8, 2H), 7.45 (d, J = 8, 2H), 4.1 (s, 1H). IR (KBr): 3260, 1647, 1585, 1502, 1408 cm^{-1}. M. p. Above 250 °C.

***N*-4-(*N*,*N*-Dimethyl)phenyl-*N*'-4'-nitrophenylurea, 18:** Compound was crystallized from ethylacetate/hexane mixture. ^{1}H NMR (DMSO-d_6): δ 9.3 (s, 1H), 8.55 (s, 1H), 8.19 (d, J = 8, 2H), 7.64 (d, J = 8, 2H), 7.25 (d, J = 8, 2H), 6.68 (d, J = 8, 2H), 2.84 (s, 6H). IR (KBr): 3310, 1643, 1612, 1406 cm^{-1}. M. p. sublimed at 246 °C.

Preparation of 4-iodo-4'-nitrobiphenyl: This compound was prepared using literature procedure.[23] To a powdered mixture of diphenyl (900 mg, 6 mmol) and iodone (450 mg, 3.5 mmol) in acetic acid (10 mL) and conc. HNO_3 was slowly added over a period of 0.5 h and resulting mixture was refluxed for 2 h. The cold mixture was then poured in to water (100 mL) and the yellow solid was filtered, and washed with water and extracted with boiling EtOH (2 × 50 mL). ^{1}H NMR ($CDCl_3$): δ 8.32 (d, J = 9, 2H), 7.86 (d, J = 9, 2H), 7.72 (d, J = 9, 2H), 7.38 (d, J = 9, 2H). M. p. 202-203 °C.

Preparation of 4-iodo-4'-aminobiphenyl: 4-iodo-4'-nitrobiphenyl (1 gm, 3 mmol) was dissolved in acetic acid and to the reflexing solution Fe powder (450mg excess) was added slowly for 10 min. After heating for 15 minutes, cooled to room temperature and poured in crushed ice. Pale yellow compound precipitated form the solution. ^{1}H NMR ($CDCl_3$): δ 7.71 (d, *J* = 9, 2H), 7.37 (d, *J* = 9, 2H), 7.28 (d, *J* = 9, 2H), 7.73 (d, *J* = 9, 2H). IR (KBr): 3408, 3290, 1602, 1477 cm^{-1}.

***N*-4-Iodobipheny-*N*'-4'-nitrophenylurea, 19:** It was prepared by the condensation of *p*-nitrophenylisocyanate and preparation of 4-iodo-4'-aminobiphenyl in dry benzene and crystallized from THF. ^{1}H NMR (DMSO-d_6): δ 9.47 (s, NH), 9.05 (s, NH), 8.20 (d, *J* = 9, 2H), 7.78 (d, *J* = 9, 2H), 7.70 (d, *J* = 9, 2H), 7.63 (d, *J* = 9, 2H), 7.57 (d, *J* = 9, 2H), 7.46 (d, *J* = 9, 2H). IR (KBr): 3314, 3265, 1649, 1113 cm^{-1}. M. p. Above 250 °C.

***N*-4-Ethynylbipheny-*N*'-4'-nitrophenylurea, 20:** It was prepared by ethynylation of **19** by trimethylsilylacetylene followed by deprotection with K_2CO_3 in MeOH. ^{1}H NMR (DMSO-d_6): δ 9.53 (s, NH), 9.10 (s, NH), 8.20 (d, *J* = 9, 2H), 7.64-7.70 (m, 6H), 7.58 (d, *J* = 9, 2H), 7.53 (d, *J* = 9, 2H), 4.21 (s, 1H). IR (KBr): 3344, 3296, 3018, 1640, 1204 cm^{-1}. M. p. Above 250 °C.

Data collection and crystal structure determination: The cell parameters, space groups and crystal structures were determined from single crystal X-ray diffraction data collected at ambient temperature on Enraf-Nonius CAD-4 diffractometer and Bruker Smart Apex CCD diffractometer at University of Hyderabad, Hyderabad and The Chinese University, Hong Kong. The incident radiation is Mo-Kα X-ray radiation (λ = 0.71073 Å) on both inustraments. Data reduction was performed using the Xtal 3.5[24] and SAINT. Structures were solved using the direct methods using SHELXS-97.[25] Analysis was carried out in PLATON[26] on Silicon Graphics workstation. Empirical absorption correction using SADABS[27] and semi empirical[28] was applied for **2**, **3**, **5**, **10**, **16** and **19**. Powder pattern was collected on Philips X-ray diffractometer (Cu-Kα, λ = 1.5405 Å) at University of Hyderabad.

^{1}H–^{1}H NMR difference nOe: Diphenylurea and substituted diphenylureas (8-10 mg) were dissolved in 0.5 ml of DMSO-d_6 and the samples were degassed with dry N_2 under vacuum. The built-in program for difference nOe spectroscopy in Bruker Avance 400 was used: power 50 db, relaxation delay 6 s, 128 scans. The percentage enhancement was calculated as the ratio of enhanced signal to the irradiated peak.

2.11 References

1. (a) J.-M. Lehn, *Proc. Natl. Acad. Sci*., *U.S.A*., **2002**, *99*, 4763. (b) G.M. Whitesides and M. Boncheva, *Proc. Natl. Acad. Sci*., *U.S.A*., **2002**, *99*, 4769.
2. (a) L. Leiserowitz and F. Nader, *Acta Crystallogr*., **1977**, *B33*, 2719. (b) P.L. Wash, E. Maverick, J. Chiefari and D.A. Lightner, *J. Am. Chem. Soc*., **1997**, *119*, 3802. (c) Y. Chang, M. West, F.W. Fowler and J.W. Lauher, *J. Am. Chem. Soc*., **1993**, *115*, 5991. (d) J.N. Moorthy, R. Natarajan, P. Mal and P. Venugopalan, *J. Am. Chem. Soc*., **2002**, *124*, 6530. (e) P.W. Baures, J.R. Rush, A.V. Wiznycia, J. Desper, B.A. Helfrich and A.M. Beatty, *Cryst. Growth Des*., **2002**, *2*, 653.
3. (a) V.A. Russel, M.C. Etter and M.D. Ward, *Chem. Mater*., **1994**, *6*, 1206. (b) V.A. Russel and M.D. Ward, *J. Mater. Chem*., **1997**, *7*, 1123.
4. (a) S.S. Kuduva, D.C. Craig, A. Nangia and G.R. Desiraju, *J. Am. Chem. Soc.*, **1999**, *121*, 1936. (b) D. Das, R.K.R. Jetti, R. Boese and G.R. Desiraju, *Cryst Growth Des.*, **2003**, *3*, 675.
5. (a) K.D.M. Harris, in *Encyclopedia of Supramolecular Chemistry*, J.L. Atwood, J.W. Steed (Eds.), Marcel Dekker, New York. **2004**, pp.1538-1548. (b) J.J. van Gorp, J.A. J.M. Vekemans, E.W. Meijer, *J. Am. Chem. Soc.,* **2002**, *124*, 14759. (c) L.S. Shimizu, A.D. Hughes, M.D. Smith, M.J. Davis, B.P. Zhang, H.-C. zur Loye and K.D. Shimuzu, *J. Am. Chem. Soc.,* **2003**, *125*, 14972.
6. (a) A. Offret and H. Vittenet, *Bull. Soc. Chim. Fr.,* **1899**, *21*, 152. (b) A. Offret and H. Vittenet, *Bull. Soc. Chim. Fr.,* **1899** *21*, 788. (c) A. Offret and H. Vittenet, *Bull. Soc. Chim. Fr.,* **1899** *22*, 627. (d) P.H.R. Groth, *An Introduction to Chemical Crystallography* (trans. H. Marshall), Gurnery & Jackson: London, **1906**, pp 28-31. (e) K.H. Huang, D. Britton, M.C. Etter and S.R. Byrn, *J. Mater. Chem.,* **1995**, *5*, 379. (f) M. Rafilovich, J. Bernstein, R.K. Harris, D.C. Apperley, P.G. Karamertzanis and S.L. Price, *Cryst. Growth Des.*, **2005**, *5*, 2197.
7. (a) M.C. Etter and T.W. Panunto, *J. Am. Chem. Soc.,* **1988**, *110*, 5896. (b) M.C. Etter, Z. Urbańczyk-Lipkowska, M. Zia-Ebrahimi and T.W. Panunto, *J. Am. Chem. Soc.,* **1990**, *112*, 8415.
8. R. Custelcean, B.A. Moyer, V.S. Bryantsev and B.P. Hay, *Cryst. Grouth Des.*, **2006**, *6*, 555.
9. M. Boiocchi, L. Del Boca, D.E. Gómez, L. Fabbrizzi, M. Licchelli and E. Monzani, *J. Am. Chem. Soc.*, **2004**, *126*, 16507.

10. T.W. Bell and N.M. Hext, *Chem . Soc . Rev.,* **2004**, *33*, 589.
11. (a) S. George, A. Nangia, C.-K. Lam, T.C.W. Mak and J.-F. Nicoud, *Chem. Commun.,* **2004**, 1202. (b) S. George, Ph.D. Thesis, University of Hyderabad, 2004.
12. A. Nangia and G.R. Desiraju, *Chem. Commun.*, **1999**, 605.
13. (a) J.A.R.P. Sarma, F.H. Allen, V.J. Hoy, J.A.K. Howard, R. Thaimattam, K. Biradha and G.R. Desiraju, *Chem. Commun*., **1997**, 101. (b) N. Masciocchi, M. Bergamo and A. Sironi, *Chem. Commun*., **1997**, 1347. (c) R. Thaimattam, C.V.K. Sharma, A. Clearfield and G.R. Desiraju, *Cryst. Growth Des*., **2001**, *1*, 103. (d) C.J. Kelly, J.M.S. Skakle, J.L. Wardell, S.M.S. Wardell, J.N. Low and C. Glidewell, *Acta Crystallogr*., **2002**, *B58*, 94. (e) P.K. Thallapally, S. Basavoju, G.R. Desiraju, M. Bagieu-Beucher, R. Massé and J.-F. Niçoud, *Current Science*., **2003**, *85*, 995.
14. (a) H.-C. Weiss, R. Boese, H.L. Smith and M.H. Haley, *Chem. Commun*., **1997**, 2403. (b) J.M.A. Robinson, B.M. Kariuki, K.D.M. Harris and D. Philp, *J. Chem. Soc., Perkin Trans. 2*., **1998**, 2459. (c) P.J. Langley, J. Hulliger, R. Thaimattam and G.R. Desiraju, *New. J. Chem*., **1998**, 1307. (d) J.M.A. Robinson, B.M. Kariuki and K.D.M. Harris, *Chem. Commun*., **1999**, 329.
15. J. Zyss, D.S. Chemla and J.-F. Niçoud, *J. Chem. Phys*., **1981**, *74*, 4800.
16. C.V.K. Sharma, K. Panneerselvam, T. Pilati and G.R. Desiraju, *Chem. Commun*., **1992**, 832.
17. *PC Spartan Pro 1.0* Wavefunction Inc., Irvine, CA, USA, **1999.**
18. H. Tang, R. J. Doerksen, G. N. Tew, *Chem. Commun.* **2005**, 1537.
19. C. Laurence and H. Berthelot, *Perspect. Drug Discovery Des.*, **2000**, *18*, 39.
20. M.C. Etter, *J. Phys. Chem.*, **1991**, *95*, 4601.
21. T.L. Nguyen, A. Scott, B. Dinkelmeyer, F.W. Fowler and J.W. Lauher, *New J. Chem.*, **1998**, 129.
22. K. Merz, *Acta Crystallogr*., **2003**, *C59*, 65.
23. J. Harley-Mason and F.G. Mann, *J. Chem. Soc*., **1940**, 1379.
24. Xtal 3.5. Manual, University of Western Australia, Australia, Geneva, Switzerland and Maryland, U.S.A., eds. S.R. Hall, H.D. Flack and J.M. Stewart, **1995**.
25. SHELX-97. G.M. Sheldrick, Program for the Refinement and Solution of Crystal Structures, University of Gottingen, Germany, **1997.**
26. PLATON. A. L. Spek, Bijvoet Centre for Biochemical Research, Vakgroep Kristal-en Structure-Chemie, University of Utrecht, The Netherlands.

27. (a) T. Higashu, ABSCOR: *An Empirical Absorption Correction Based on Fourier Coefficient Fitting*; Rigaku Corporation: Tokyo, **1995. (b)** G.M. Sheldricks, SADABS: Program for Empirical Absorption of Area Detector Data; University of Göttingen, Germany, **1996** (c) G. Kopfmann and R. Huber, *Acta Crystallogr*., **1968**, *A24*, 348.
28. A.C.T. North, D.C. Phillips and F.S. Mathew, *Acta Crystallogr*., **1968**, *A24*, 351.

CHAPTER 3

HYDROGEN BOND COMPETITION AND INTERPLAY OF MOLECULAR CONFORMATION IN CRYSTAL STRUCTURES OF PYRIDYLUREAS

3.1 Introduction

As discussed in chapter 2, the common hydrogen bond pattern in electron withdrawing group substituted diarylureas is not the N–H···O tape (α-network). In three polymorphs of *N,N'*-bis(3-nitrophenyl)urea, α-network was observed only in the least stable β-polymorph. In the crystal structures of solvates, NH donors interact with solvent of crystallization (THF, DMSO) or with an acceptor molecule such as $Ph_3P{=}O$. In a family of *para*-nitro substituted diarylureas, the urea N–H···O tape could be engineered in five out of 19 crystal structures by engaging the interfering NO_2 group in complimentary interactions such as I···O_2N, ethynyl···O_2N or N(Me)$_2$···O_2N. This result suggested that molecular conformation and specific directional interactions, even if they are weak (energy 1–4 kcal/mol), can direct the strong hydrogen bond network (energy 5–15 kcal/mol) in crystal structures. Despite sustained efforts by several groups for more than a decade, the connection between molecular functional groups and crystal packing in the solid-state is still an elusive goal.[1] Non-urea tape hydrogen bond motifs are found in pyridylurea based plant-growth inhibitors, organo-gelators, anion receptors and as models for DNA complexes.[2] Because it is still impossible to predict the crystal structure accurately using computational methods, examination of hydrogen bonding and crystal packing in related compounds will help in understanding the factors influencing crystal nucleation and growth. Therefore, we analyze strong and weak hydrogen bonds in crystal structures of *N,N'*-bis(3-pyridyl)urea **21**, its hydrates, molecular complexes and derivatives **22** and **23** in this chapter (Scheme 1).

Dipyridylurea **21** was selected for the following reasons. (1) The intramolecular C–H···O interactions and planar conformation observed in structures of nitrophenylureas is likely in **21** because the proximal CH donors are activated in the 3-pyridyl ring, similar to the hydrogens of 3 or 4-nitrophenyl group. Electron-withdrawing groups increase the acidity of donor hydrogen and consequently their hydrogen bond strength. (2) Dipyridylurea **21** is a symmetrical molecule isosteric with *N,N'*-diphenylurea. Hence, steric effects are minimal and differences in hydrogen bonding may be understood through the pyridyl functional

group. The crystal structure of *N*-3-pyridylurea[3] is very different from *N*-phenylurea.[4] Crystal structure of 3-pyridylurea contains a corrugated tape of N–H_{syn}···O and N–H_{anti}···O hydrogen-bond dimers along *a*-axis (Figure 1a). Screw-axis related molecules are connected *via* N–H···$N_{pyridyl}$ hydrogen bond. In the crystal structure of phenylurea, *c*-translation related molecules are linked together by a bifurcated N–H···O hydrogen bond to form a ribbon along *c*-axis (Figure 1b). These ribbons are held together by another N–H···O hydrogen bond between the molecules related by a twofold screw axis to form a sheet parallel to (100). The crystal structure of phenylurea has the typical α-network repeat of 4.7 Å whereas pyridylurea behaves like a primary amide with the characteristic 5.1 Å axis (Figure 1).

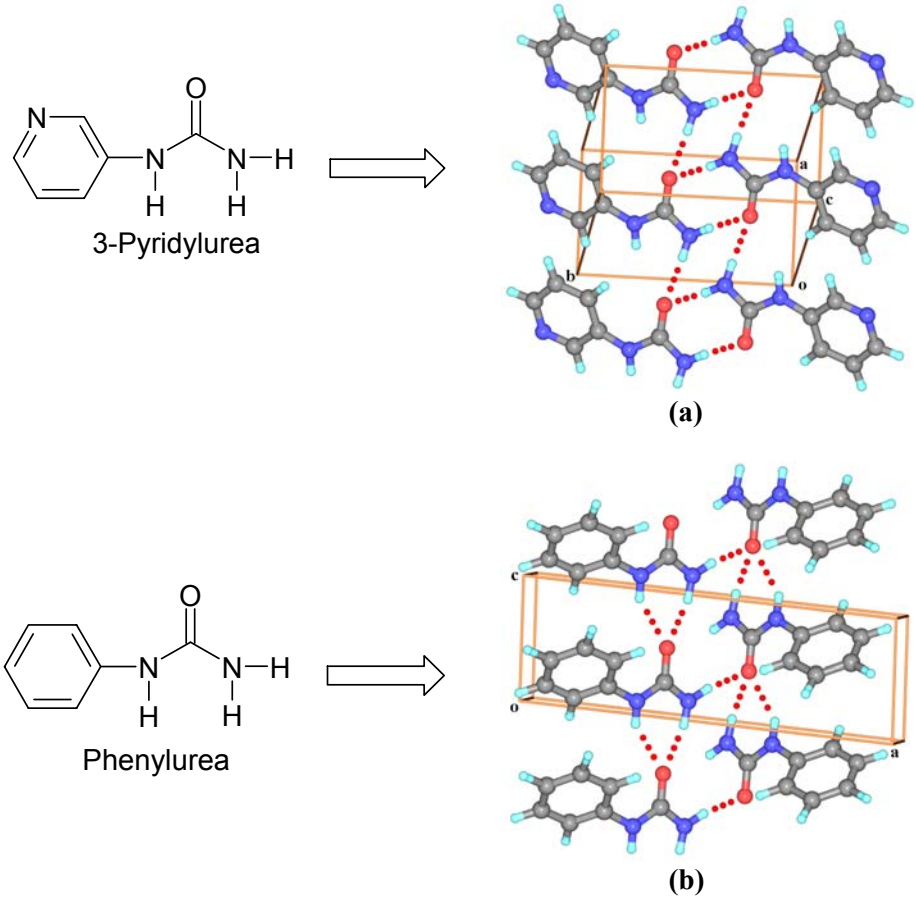

Figure 1. (a) N–H···O dimers in crystal structure of pyridylurea, notice the typical amide type hydrogen bonding. (b) N–H···O urea tape network in the crystal structure of phenylurea.

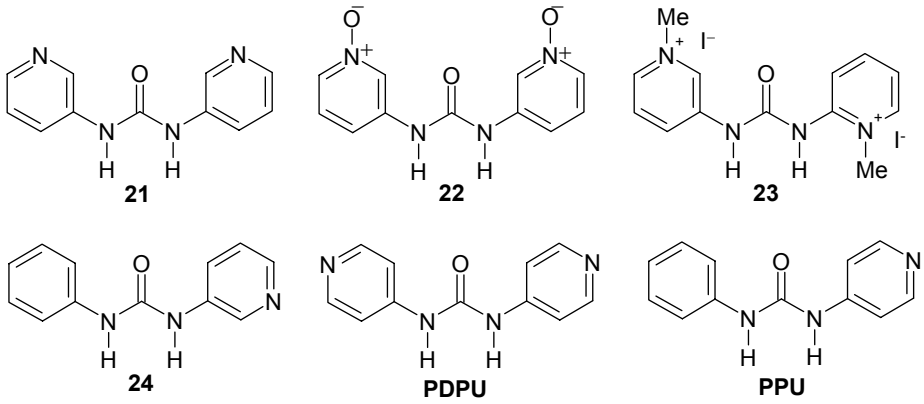

Scheme 1. Urea compounds studied in this chapter.

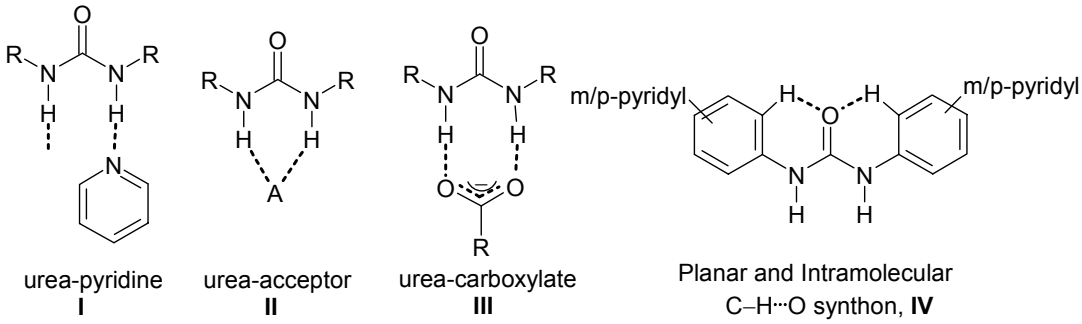

Scheme 2. Synthons discussed in this chapter.

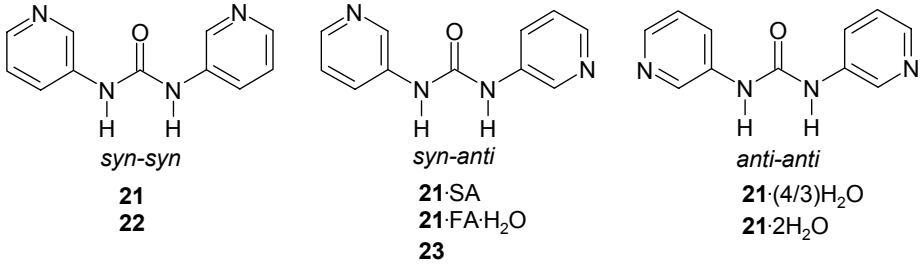

Scheme 3. Conformations of dipyridylurea in crystal structures discussed.

Table 1. Geometrical parameters of hydrogen bonds.

Urea	Interaction[a]	D–H···A (Å)	D···A (Å)	θ (°)
21	N1–H1···N2	2.08	3.064(4)	163.7
	C3–H3···O1	2.48	3.190(4)	122.3
	C6–H6···O1	2.18	2.807(4)	123.7
21·(4/3)H_2O	N1–H1···O3	2.16	3.057(2)	147.5
	N2–H2···O3	1.84	2.819(2)	162.2
	N5–H5A···O4	1.90	2.832(2)	152.1
	O4–H4A···O1	1.86	2.831(2)	167.6

	O3–H3B···N6	1.88	2.831(2)	162.3
	O3–H3A···N4	1.90	2.861(2)	165.3
	O4–H4B···N3	1.85	2.828(2)	175.4
	C5–H5···O2	2.55	3.479(2)	143.4
	C16–H16···O1	2.45	3.376(2)	143.4
	C6–H6···O1	2.22	2.875(2)	116.2
	C11–H11···O1	2.22	2.863(2)	115.7
	C17–H17···O2	2.33	2.902(2)	119.2
21·2H$_2$O	N1–H1···O2	2.30	3.162(3)	141.8
	N2–H2···O2	1.78	2.767(3)	164.9
	O2–H2B···N4	1.83	2.814(3)	175.9
	O2–H2A···O3	1.71	2.613(8)	159.9
	O3–H3A···N3	1.89	2.810(5)	154.6
	O3–H3B···O1	1.94	2.761(9)	138.9
	C9–H9A···O1	2.51	3.407 (3)	138.9
	C3–H3···O1	2.19	2.853(3)	116.8
	C8–H8···O1	2.24	2.885(3)	116.2
21·SA	O5–H5A···N1	1.66	2.637(3)	169.3
	N3–H3A···O2	1.78	2.772(3)	166.1
	N4–H4A···O2	2.14	3.024(3)	145.1
	N4–H4A···O3	2.55	3.151(3)	159.9
	N2–H2A···O3	1.56	2.563(3)	173.4
	C5–H5···O4	2.44	3.207(3)	126.7
	C1–H1···O5	2.37	3.415(4)	162.5
	C10–H10···O3	2.47	3.471(3)	153.8
	C9–H9A···O3	2.32	3.314(3)	151.8
	C8–H8···O1	2.16	2.821(3)	117.2
	C5–H5···O1	2.16	2.848(3)	118.7
21·FA·H$_2$O	O5–H5A···N1	1.58	2.556(4)	168.7
	N3–H3A···O2	1.74	2.742(4)	171.9
	N4–H4A···O3	1.82	2.817(4)	170.3
	N2–H2A···O6	1.64	2.639(4)	167.6
	O6–H6B···O4	1.85	2.796(5)	160.7
	O6–H6A···O3	1.72	2.683(4)	164.4
	C10–H10···O3	2.50	3.346(5)	134.5
	C2–H2···O2	2.32	3.398(6)	173.2
	C3–H3···O2	2.54	3.350(5)	130.8
	C6–H6···O5	2.39	3.463(5)	169.1
	C7–H7···O1	2.17	3.170(5)	152.3
	C5–H5···O1	2.08	2.785(5)	119.6
	C8–H8···O1	2.11	2.780(5)	117.0
22·H$_2$O	N2–H2···O2	1.81	2.735(2)	150.4
	N3–H3···O2	1.80	2.767(2)	157.3
	O4–H4A···O3	1.80	2.781(2)	171.4
	O5–H5A···O3	1.79	2.769(3)	172.2
	C5–H5···O5	2.20	3.202(3)	151.9

	C4–H4···O3	2.38	3.319(3)	144.0
	C10–H10···O4	2.36	3.183(3)	131.0
	C6–H6···O1	2.16	2.839(2)	118.3
	C11–H11···O1	2.19	2.870(2)	118.4
23	N1–H1···I1	2.70	3.664(3)	159.5
	N2–H2···I1	2.47	3.477(3)	176.7
	C6–H6···O1	2.12	2.815(4)	119.5
	C9–H9···O1	2.18	2.843(4)	117.4
24	N2–H2···N1	2.46	3.343(2)	145.4
	N3–H3···N1	1.92	2.922(2)	170.2
	C2–H2A···O1	2.20	3.138(2)	143.0
	C4–H4···O1	2.25	2.882(2)	115.0
	C8–H8···O1	2.24	2.903(2)	117.3

[a]All the N–H, C–H and O–H distances are neutron normalized to 1.009,1.083 and 0.983 Å respectively.

Table 2. Some structural features of compounds studied in this chapter.

Compound	Intramolecular C–H···O (Å)	Torsion angles ($C\text{-}C_{pyridyl}\text{-}N\text{-}C_{carbonyl}$ °)	H-bond motif (synthon)
21	2.18	4.5	**I**
21·(4/3)H_2O	2.22, 2.22, 2.33	9.0, 9.9, 10.8	**II**
21·2H_2O	2.19, 2.24	1.7, 5.1	**II**
21·SA	2.16, 2.16	0.9, 0.9	**III**
21·FA·H_2O	2.08, 2.11	0.7, 4.5	**III**
22·H_2O	2.16, 2.19	7.7, 16.1	**II**
23	2.12, 2.18	2.1, 6.0	**II**
24	2.25, 2.24	1.9, 15.5	**II**

3.2 Results

Dipyridylurea **21** was prepared by the solid-phase transamidation of urea with 3-aminopyridine.[5] Diffraction quality single crystals of **21** were obtained from hot EtOAc. Crystallization from MeOH and EtOH afforded hydrates of different stoichiometry, **21**·(4/3)H_2O and **21**·2H_2O respectively. The pyridine moiety was utilized to cocrystallize **21** with succinic and fumaric acids (SA and FA), which afforded equimolar complexes, **21**·SA and **21**·FA·H_2O. Smooth oxidation of the pyridine ring with *m*-CPBA gave bis *N*-oxide as a crystalline monohydrate, **22**·H_2O. *N*-methylation of the pyridyl ring (CH_3I) gave pyridinium salt **23**. After characterizing all new compounds by satisfactory NMR and IR spectra their crystal structures were determined by X-ray diffraction. Crystallographic data of compounds studied in this chapter is given in appendix.

3.2.1 Crystal structure of bis(3-pyridyl)urea, 21

Dipyridylurea **21** crystallizes in the orthorhombic space group *Aba*2 (No. 41). The molecule resides on the 2-fold axis such that pyridyl N-atoms are *syn* to the urea carbonyl. The activated CH donors (*ortho* to pyridyl N) form short intramolecular C–H···O (2.18 Å) interactions of motif **IV** (scheme 2) in the *syn-syn* conformation (Scheme 3) with the pyridyl moiety lying in a coplanar orientation with the urea carbonyl group (torsion angle $C–C_{pyridyl}–N–C_{carbonyl}$ 4.5°, Table 2). Pyridyl N acceptors compete with urea carbonyl for NH donors and form N–H···N hydrogen bond through short and linear interaction **I** (Figure 2). Thus, $N–H···N_{pyridyl}$ hydrogen bonding disrupts the robust N–H···O tape α-network of urea in **21** while the urea carbonyl accepts intra- and intermolecular C–H···O interactions. To complete the crystal packing, glide related molecules produce layers mediated *via* N–H···N and C–H···O interactions and such layers are connected through N–H···N hydrogen bonds, listed in Table 1.

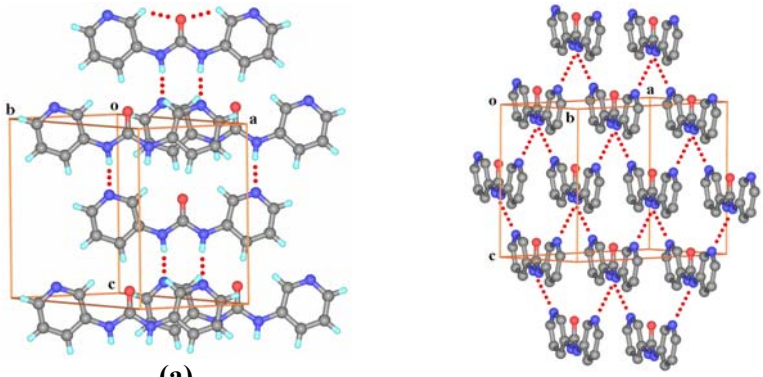

(a) **(b)**

Figure 2. (a) $N–H···N_{pyridyl}$ hydrogen bonds and intramolecular $C–H···O_{urea}$ interactions in the crystal structure of dipyridylurea **21**. Note the absence of urea tape. (b) Hydrogen bonding in 2D sheet. Hydrogen atoms are removed for clarity.

3.2.2 Crystal structures of bis(3-pyridyl)urea hydrates

The inclusion of water in organic crystals is a common phenomenon for structural chemists and crystal engineers[6] and yet it is not fully understood when and why water is included in crystal structures. Hydration is favored in small molecules which have an excess of acceptor groups because the inclusion of water, a donor-rich partner, compensates this imbalance to give a strongly hydrogen-bonded hydrate.

Crystallization of **21** from MeOH afforded single crystals of a hydrate, **21**·$(4/3)H_2O$. X-ray diffraction and structure solution in the monoclinic space group *C*2/*c* gave an asymmetric unit with 1.5 molecules of **21** and two water molecules. The pyridyl moiety

and urea carbonyl are roughly coplanar (C–$C_{pyridyl}$–N–$C_{carbonyl}$ ~10º) with pyridine N-atoms being *anti* to the urea carbonyl (Figure 3a). Two symmetry independent molecules of **21** adopt planar conformation, which is stabilized by intramolecular C–H···O (Table 2) interaction motif **IV**. Though water is considered to be good hydrogen bond donor but a moderate acceptor, water O-acceptor successfully competes with better hydrogen bond acceptors pyridyl N and urea carbonyl for NH donors and disrupts the characteristic α-network. One of the water molecules form a N–H···O_{water} bifurcated motif **II**. H atoms of water bond to different pyridyl moieties. In the crystallographically independent pair of **21** and water, one of the urea NHs and the adjacent phenyl CH form a bifurcated motif with water O and the water hydrogens donate to pyridyl N and urea O acceptors. All hydrogen bonds are in the usual distance–angle range (Table 1). Water is bonded to pyridylurea but there are no water···water hydrogen bonds.

A dihydrate, **21**·2H_2O, was crystallized from EtOH in space group $P2_1/c$ with one molecule of dipyridylurea, **21** and two water molecules in the asymmetric unit. One of the water molecules is disordered over two orientations with about equal occupancy (0.52, 0.48). The pyridyl moiety and urea carbonyl are in the same plane (Table 2). Figure 3b shows the role of water molecule in disrupting the urea α-network. The ordered water forms a bifurcated N–H···O and also connects the remaining structure *via* O–H···$N_{pyridyl}$ and O–H···$O_{disordered\ water}$ hydrogen bonds. The disordered water molecule connects to pyridine and urea carbonyl moieties and form 2D layers. These layers are connected by water. When X-ray reflections were collected at 100 K to minimize water disorder but no improvement in the disordered nature of the crystal structure was observed.

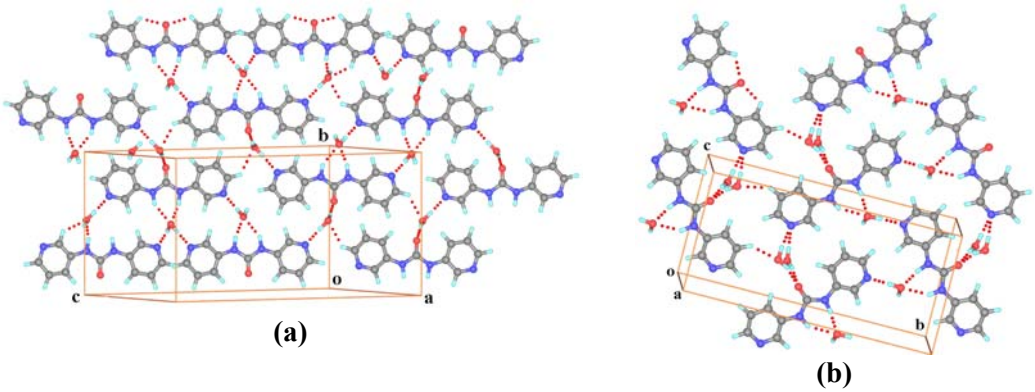

Figure 3. (a) N–H···O_{water}, O–H···O_{urea} and O–H···$N_{pyridyl}$ hydrogen bonds and auxiliary C–H···O interactions in hydrate **21**·(4/3)H_2O. (b) N–H···O_{water}, O–H···O_{urea} and O–H···$N_{pyridyl}$ hydrogen bonds in hydrate **21**·2H_2O. Note that one water molecule is ordered and the other is disordered over two positions.

3.2.3 Crystal structure of monohydrate of bis-*N*-oxide, 22

Having obtained three non-urea tape structures with the common synthon **IV**, we decided to activate the pyridyl CH donors of **21** by oxidation to bis *N*-oxide **22**. Pyridine *N*-oxide, N^{+}–O^{-}, is a very strong hydrogen bond acceptor group. The hydrate structure, **22**·H_2O, contains one molecule of **22** and two 0.5 water molecules in the asymmetric unit (space group *C*2/*c*). Both pyridine *N*-oxide rings and urea carbonyl groups are roughly in the same plane (Table 2). The activated CH donors participate in intramolecular C–H···O synthon **IV** (2.16, 2.19 Å) with both *N*-oxide groups being *syn* to the urea carbonyl (Scheme 3). Because *N*-oxide is better acceptor than urea carbonyl, one of the *N*-oxides interacts with urea NHs in a bifurcated motif **II** *via* N–H···O^{-} bond whereas the other *N*-oxide is engaged in hydrogen bonding with a water molecule (Figure 4). Translation related molecules are arranged in offset tapes with N–H···O^{-} Hydrogen bonds and C–H···O^{-}, C–H···O_{water} interactions connect such glide related tapes.

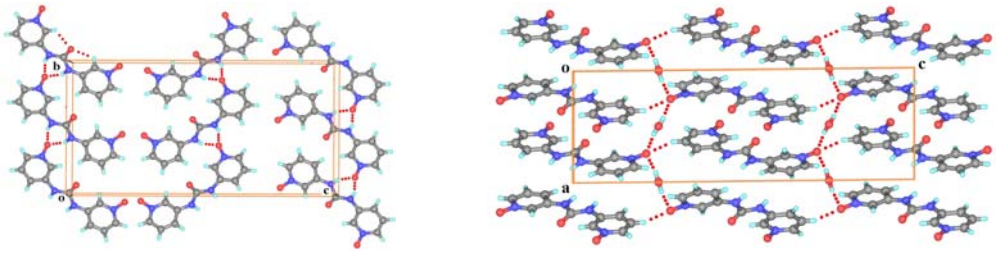

(a) **(b)**

Figure 4. (a) N–H···O_{oxide} hydrogen bonding disrupts the urea α-network in **22**·H_2O. (b) The N-oxide accepts hydrogen bonds from different water molecules.

3.2.4 Crystal structure of iodide, 23

Inorder to block the pyridine N from behaving as a hydrogen bond acceptor for the urea NHs, dipyridylurea **21** was *N*-methylated. Since the pyridyl N is quaternized as pyr-N^{+}–Me it cannot accept hydrogen bonds. CH donors, on the other hand, are strengthened in the electropositive pyridyl ring and so the likelihood of C–H···O synthon **IV** is favored. The crystal structure of **23** shows bifurcated N–H···I^{-} hydrogen bonds with the soft counter ion along with C–H···I^{-} interactions to the second iodide (Figure 5). The more activated CH (*ortho* to pyrN^{+}Me, *syn*) makes a shorter interaction with urea C=O compared to the *anti* pyridyl ring (synthon **IV**: 2.12, 2.18 Å) in the planar *syn–anti* conformation (Scheme 3). The structure of **23** shows that the strong NH donors seek out the best available acceptor even as the urea C=O consistently participates in intramolecular C–H···O interactions with pyridyl CH donors.

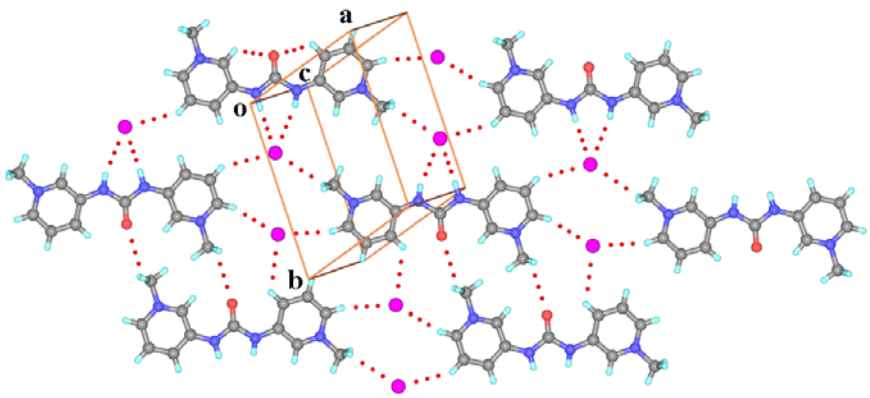

Figure 5. N–H···I⁻ hydrogen bonds with the counterion along with C–H···I⁻ interactions to the second iodide in the crystal structure of pyridinium salt **23**.

3.2.5 Crystal structures of molecular complexes

A crystal engineering approach to favour formation of the α-network in dipyridylurea would be to engage the interfering pyridyl group in COOH···pyridine hydrogen bonding.[7] The acid···pyridine synthon, stabilized *via* O–H···N hydrogen bond and auxiliary C–H···O interaction, has >90% probability of occurrence in crystals structures. For example, molecular complexes of *meta*-dipyridylmethylurea (3-PMU) and *para*-dipyridylmethylurea (4-PMU) with *N,N'*-dicarboxymethylurea (DCMU) have urea N–H···O tape and acid···pyridine O–H···N synthons in roughly orthogonal directions (Figure 6).[8]

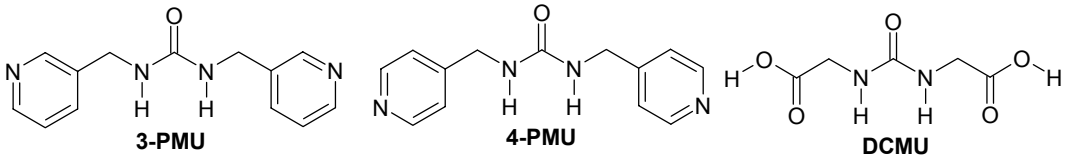

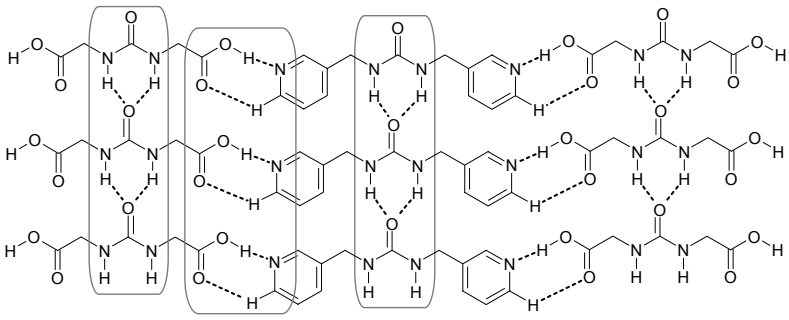

(a)

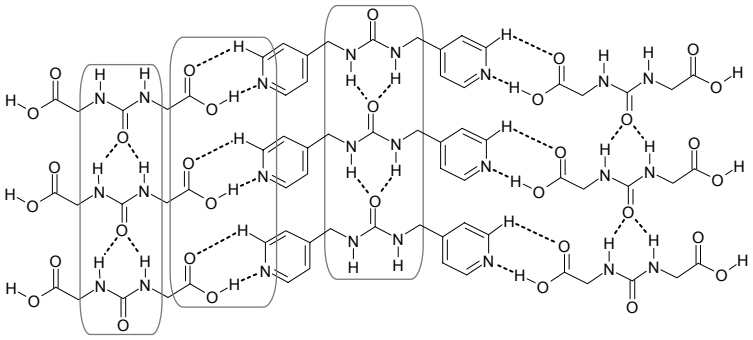

(b)

Figure 6. Acid···pyridine heterosynthon and urea tape synthon in (a) Cocrystal of *meta*-pyridylmethylurea and DCMU (CAJQOU). (b) Cocrystals of *para*-pyridylmethylurea and DCMU (CAJRIP).

Custelcean *et al*.[9] studied a series of metal-organic frameworks (MOFs) functionalized with urea hydrogen bonding groups to evaluate the efficacy of anion coordination by urea within the structural constraints of the MOFs. Various oxoanions with a wide range of basicities, such as SO_4^{2-}, NO_3^-, $CH_3SO_3^-$ and $CF_3SO_3^-$ interacts with urea NH donors and urea molecules generally adopt planar conformation. But in the crystal structure of $[Zn(\mathbf{21})_2](ClO_4)_2$, two pyridine rings of **21** are significantly twisted out of the urea plane by 34.5° and 41.1°, and the urea groups self-associate by N–H···O hydrogen bonding (α-network). Because ClO_4^- anion is weakly basic and pyridine-N is engaged in coordination with zinc there are no additional acceptors available for urea NH donors other than the urea carbonyl, therefore it twists to unstable conformation, in which urea carbonyl becomes better acceptor at the expense of intramolecular C–H···O interactions, forming an α-network (Figure 7).

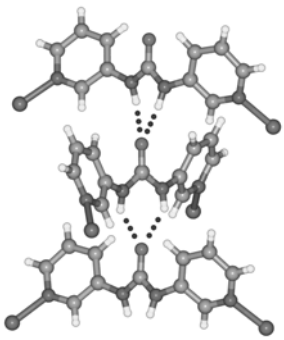

Figure 7. Orthogonal N–H···O urea tape in the crystal structure of $[Zn(\mathbf{21})_2](ClO_4)_2$, counterion is removed for clarity. Note that pyridyl N is engaged in coordination with Zn.

Cocrystallization of **21** with dicarboxylic acids such as oxalic acid, malonic acid, succinic acid, glutaric acid, adipic acid, maleic acid and fumaric acid was attempted to

restore the α-network by engaging interfering pyridyl N acceptor with strong acid···pyridine heterosynthon. But only molecular complexes of succinic acid (SA) and fumaric acid (FA) were obtained. Crystallization of 1:1 mixtures from EtOH afforded complexes, **21**·SA and **21**·FA·H_2O.

In **21**·SA (space group *C*2/*c*), the pyridylurea molecule resides in a perfectly planar conformation ($C–C_{pyridyl}–N–C_{carbonyl}$ <1º) with one pyridyl N *syn* to the urea C=O and the other *anti* (Scheme 3). The carboxylic acid groups of succinic acid adopt a rare conformation in which one of the COOH groups is *syn* and the other is *anti*; furthermore, the ethylene chain is in a *gauche* conformation (Figure 8a). As anticipated, both COOH donors hydrogen bond with the pyridyl residues of **21** but there are important differences: one of the acid–pyridine heterosynthons (*syn* COOH) has neutral O–H···N interaction whereas partial proton transfer occurs in *anti* COOH to give $N^+–H···O^-$ Hydrogen bond (1.56 Å, 173.4º). The NH donors preferentially bond to the *anti* COOH carbonyl acceptor instead of urea C=O because the former is a like a strong carboxylate acceptor (Figure 8b). The supramolecular architecture of this molecular complex is a helical assembly of acid···pyridine hydrogen bonds along the *b*-axis and such helices are interwoven to form a triple helix[10] via urea···COO^- hydrogen bonds (Figures 8c, 8d).

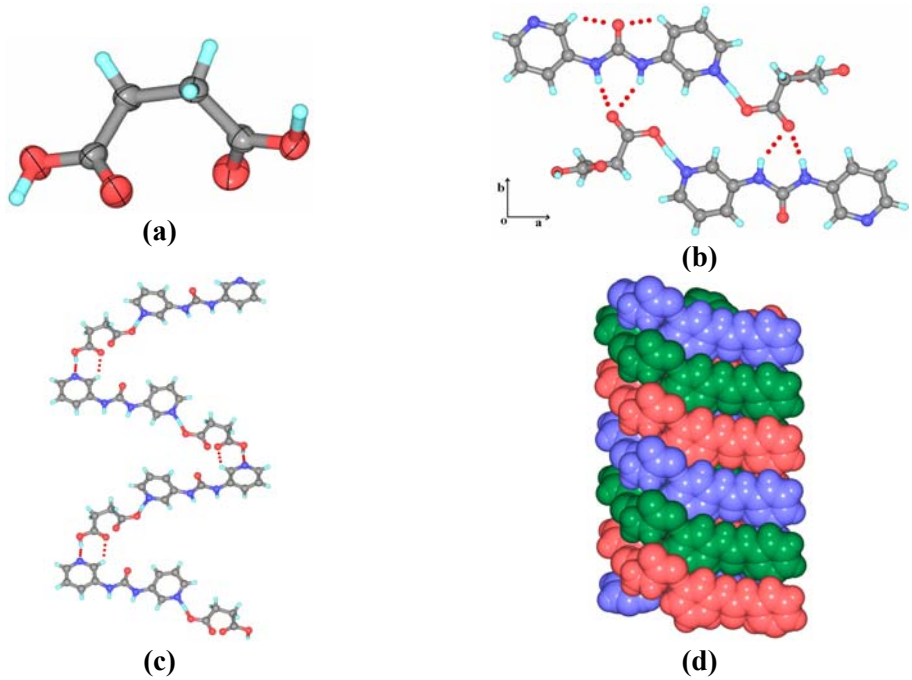

Figure 8. Crystal structure of **21**·SA (a) *Syn* and *anti* conformations of COOH groups. (b) Urea···acid hydrogen bonds. (c) Helical assembly of in **21**·SA along the *b*-axis mediated by COOH···pyridine heterosynthons. (d) Triple helix architecture.

In **21**·FA·H_2O (space group *P*-1), the urea molecule resides in a planar *syn–anti* conformation, as in the previous cocrystal. In comparison to partial proton transfer in **21**·succinic acid the stronger fumaric acid (1st pK_a: SA 4.16, FA 3.03) completely transfers one of its acidic protons to the pyridine base. In addition to urea··· carboxylate hydrogen bonding, $pyrNH^+$ is connected to water. The network of COOH···pyridine, water hydrogen bonds with COOH and COO^- groups, and urea hydrogen bonds are shown in figure 9. Even though there are significant differences in the strong hydrogen bond networks of **21**·COOH complexes, the C–H···O synthon **IV** is present in both structures. The urea tape, however, is absent because of N–H···O_{acid} hydrogen bonding. Recently Gale and coworkers[11] examined urea-carboxylate recognition in both solid and solution state in some bis ureas. They proposed that bis diphenylureas selectively binds to carboxylate anions with four N–H···O hydrogen bonds and adopt planar conformation with intramolecular C–H···O synthon **IV** (Figure 10).

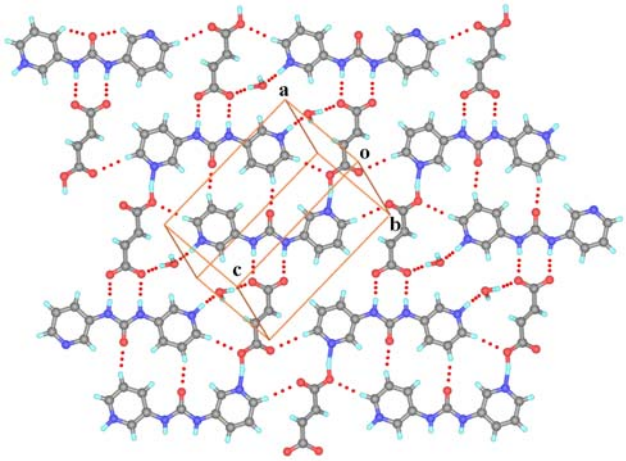

Figure 9. Layered structure of fumaric acid hydrate, **21**·FA·H_2O, stabilized by urea···COO^- and water O–H···O hydrogen bonds.

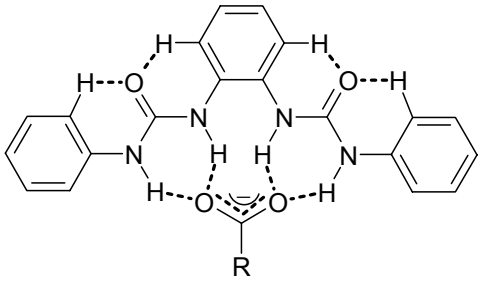

Figure 10. A proposed hydrogen bonding array formed between bis urea and carboxylate anions in solution and observed in solid-state.

3.3 Crystal structures of *para*-dipyridylureas

Dastidar and coworkers[12] studied the hydrogelation properties of bis-(4-pyridyl)urea (PDPU, Scheme 1). PDPU also crystallizes with its gelling solvents ethyleneglycol (EG) and water in 1:1:1 ratio. Crystal structure reveals that PDPU adopts planar conformation with intramolecular C–H···O synthon **IV** and ethyleneglycol disrupts the α-network (Figure 11a). Both the pyridine nitrogen atoms participate in hydrogen bonding with water and the EG molecule. They also reported the crystal structure of PDPU·HCl·xH_2O (x = 1.66). In the asymmetric unit, two monoprotonated urea, three water molecules and two chloride ions are located in general positions. The monoprotonated PDPU molecules are held together by a N–H···N hydrogen bond in planar conformation with synthon **IV**, resulting in 1D hydrogen bonded chains. In this crystal structure also chloride ion interacts with urea NH donors and thus results in non-urea tape structure (Figure 11b). Hydrogen atoms of one of the water molecules interacting with urea carbonyl are not located. Lee *et al.*[13] studied the hydrogen bonding in the crystal structure of calcium-trifluoromethanesulfonate-PDPU-methanol (1:2:2:4). In the crystal structure PDPU exits in planar conformation with synthon IV and sulfonate-O acceptors successfully compete with pyridyl N and urea carbonyl for NH donors (Figure 11c). Pyridine N interacts with methanol molecules.

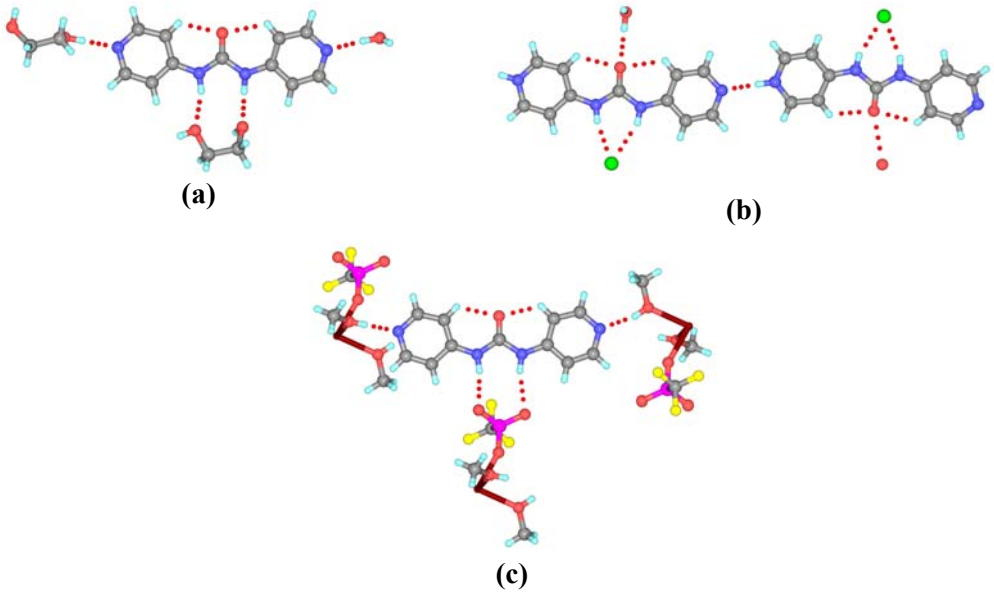

Figure 11. (a) N–H···O_{EG} hydrogen bonds disrupt urea tape in crystal structure of PDPU, ethyleneglycol (EG) and water in 1:1:1 ratio (GASMUJ). (b) N–H···Cl^- and O–H···O_{urea} hydrogen bonds in PDPU·HCl·xH_2O (x = 1.66, GASNAQ). (c) Crystal structure of calcium-trifluoromethanesulfonate-PDPU-methanol (1:2:2:4, EKJAF). Note the presence of intramolecular C–H···O synthon **IV** in all structures.

3.4 Crystal structures of phenyl–pyridylureas

The reported crystal structure[14] of *N*-phenyl-*N′*-(3-pyridyl)urea, **24** in space group $P2_1/n$ (CSD refcode MEPXEK) appears to be erroneous, so this crystal structure was redetermined. In the crystal structure (space group *Pbca*) urea molecule adopts a quasi-planar conformation through intramolecular C–H···O synthon **IV** (τ ~2, 15°; 2.24, 2.25 Å). The pyridyl acceptor group competes with urea carbonyl and forms a bifurcated N–H···N interaction which disrupts the characteristic urea α-network (Figure 12a). In the crystal structure of *N*-(4-pyridyl)-*N′*-phenylurea (PPU, Scheme 1)[14] the lack of urea tape is noted and molecule exits in planar conformation with synthon **IV** (Figure 12b). There are several phenyl–*m/p*-pyridylureas in the Cambridge Structural Database (CSD)[15], where N–H···O_{urea} tape α-network is generally disrupted by N–H···$N_{pyridyl}$ hydrogen bonding (Table 5). Many of these molecules having *meta*-pyridyl or *para*-pyridyl rings share common structural features to dipyridylurea **21**: (1) a planar molecular conformation stabilized by C–H···O synthon **IV**; (2) absence of one-dimensional urea tape and (3) NH donors hydrogen bond with other electronegative acceptor atoms instead of the urea carbonyl.

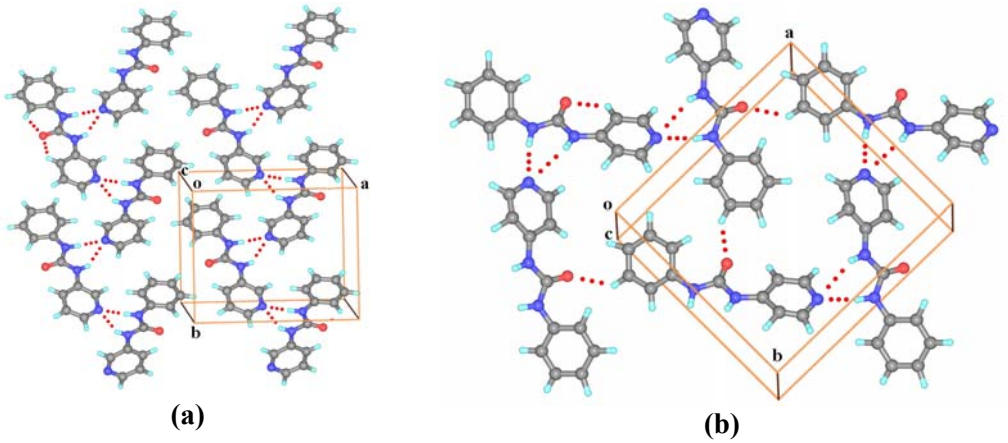

(a) **(b)**

Figure12. (a) Bifurcated N–H···$N_{pyridyl}$ mediated helical structure of **24.** (b) Layered structure of PPU (MEPXAG). Note the lack of urea tape in these structures.

Recently Abad and coworkers[16] have studied hydrogen bonding pattern of **25** by systematically changing the position and number of fluorine atoms. Crystal structures show that in compounds **25a**–**25g** pyridyl N acceptor disrupts the urea tape and molecules adopt planar conformation with synthon **IV** (Figure 13a). In crystal structure of **25h** molecule adopts twisted conformation (torsion angles, 16.3, 65.2°) due to the presence of fluorine atoms in *ortho*-positions. Because of one of the phenyl is twisted about 65.2°, one of

intramolecular C–H···O interactions breaks and urea carbonyl becomes slightly better acceptor than in planar conformation, interacts with one of the NH donors *via* N–H···O hydrogen bond. The other NH form N–H···N hydrogen bond with pyridyl N acceptor. In the crystal structure of **25i** and **25j,** molecules adopt twisted conformation (39.4, 90.0, 24.0, 61.9°). In this conformation molecule looses resonance as well as intramolecular C–H···O interactions, therefore urea carbonyl become better acceptor than pyridyl N and interacts with both urea NH donors in bifurcated N–H···O motif (Figures 13b, 13c). Pyridyl N forms C–H···N interactions. In the crystal structure of N-(tetrafluoro-*p*-pyridyl)-N'-phenylurea (TFPU),[17] planar conformation is perturbed by *ortho*-fluorine atoms. In twisted conformation electron density on urea carbonyl increases due to loss of both resonance and intramolecular C–H···O interactions and the electron density on pyridyl N is considerably reduced by electron withdrawing fluorine atoms. Therefore the characteristic urea tape is restored (Figure 13d).

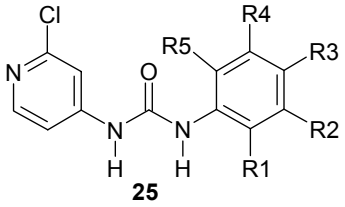

25

25a: R1=R2=R3=R4=R5=H
25b: R1=F;R2=R3=R4=R5=H
25c: R1=R2=F;R3=R4=R5=H
25d: R1=R2=R3=F;R4=R5=H
25e: R1=R2=R3=R4=F;R5=H
25f: R4=F;R1=R2=R3=R5=H
25g: R3=R4=F;R1=R2=R5=H
25h: R1=R5=F;R2=R3=R4=H
25i: R1=R3=R5=F;R2=R4=H
25j: R1=R2=R4=R5=F;R3=H

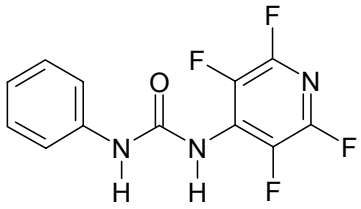

TFPU

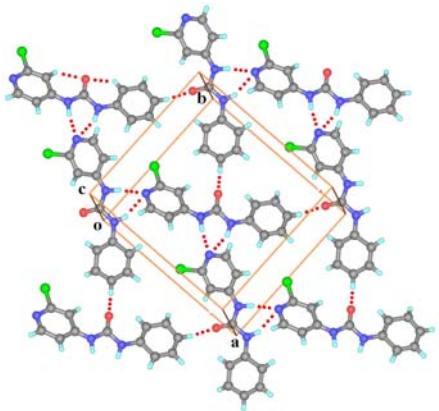

(a)

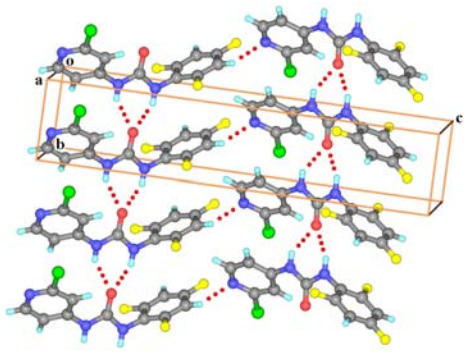

(b)

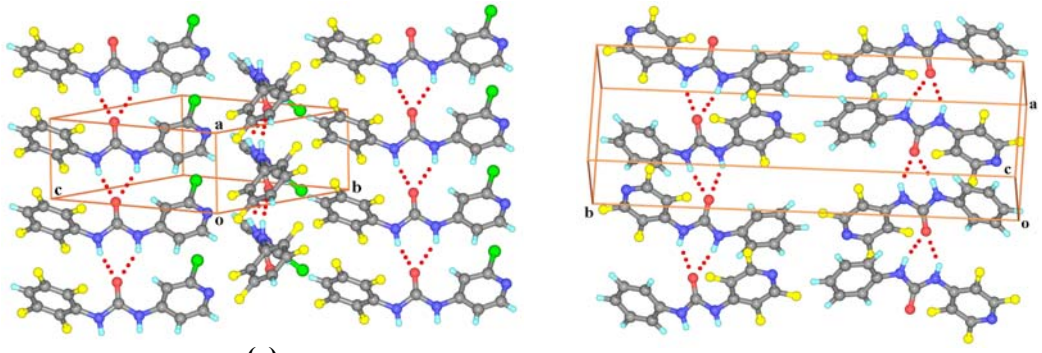

Figure 13. (a) Bifurcated N–H···$N_{pyridyl}$ mediated layered structure of **25a**. (b) N–H···O urea tape in the crystal structure of **25i**. (c) Crystal structure of **25j**. (d) Crystal structure of TFPU (TAPRAD), note that urea tape is restored in (b), (c) and (d).

3.5 Electrostatic potential (ESP) and conformation energy calculations

The strength of urea C=O and pyridyl N acceptors was computed by the negative electrostatic surface potential (ESP) using Spartan (DFT-B3LYP/6-31G*). ESP charges were calculated on the molecular conformation extracted from the crystal structure (single-point energy) and also in the energy minimized conformation. The single point and energy minimized conformations are nearly the same in all structures (Table 3). ESP charges on urea O and pyridyl N acceptors are in good agreement with observed hydrogen bond preferences in pyridylureas. The conformational energy and atomic charge on dipyridylurea **21** were calculated as a function of aryl–N–C=O torsion angle (Figure 14). Analysis of data in Table 3 and Figure 14 leads to the following points. (1) The charge on urea O is sensitive to the aryl–N–C=O torsion angle, it being more electron-rich (better hydrogen bond acceptor) when the aryl group is twisted and less negative (poorer hydrogen bond acceptor) when it is planar. A weakening of the C=O acceptor strength changes hydrogen bonding in the structure from urea α-network to other motifs. The distant pyridyl N is largely unaffected in various conformations, as would be expected if it is the C–H···O interactions that are attenuating the electron density at the C=O acceptor (Figure 14b). (2) ESP charges (Table 3) nicely parallel the observed hydrogen bond acceptor order for urea NH donors in complexes of **3**: COO^- > *N*-oxide > H_2O > pyridyl N > urea O (in planar conformation). All this shows that intramolecular C–H···O interactions of synthon **IV** and planar conformation sufficiently reduce the electron density at the urea O and so it is not available for the strong NH donors in the competitive environment of pyridyl N or water. Remarkably, it is the

planar conformation and weak C–H···O interactions of the electron-withdrawing phenyl rings that control the strong hydrogen bond networks in diarylurea structures.

Table 3: Electrostatic surface potential charge calculated in Spartan[18] (DFT-B3LYP/6-31G*, kcal/mol) on urea O and pyridyl N acceptor atoms.

Compound	Experimental X-ray structure			Energy minimized structure		
	Mol. Conf.[a]	$C{=}O_{urea}$	$N_{pyridyl}$ / $O_{N\text{-}oxide}$	Mol. Conf.[a]	$C{=}O_{urea}$	$N_{pyridyl}$ / $O_{N\text{-}oxide}$
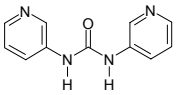	planar	–35.8	–48.0	planar	–36.8	–47.2
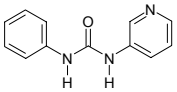	planar	–34.5	–44.2	planar	–34.0	–43.3
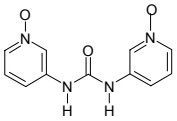	quasi-planar	–34.6	–52.2	planar	–32.9	–49.6
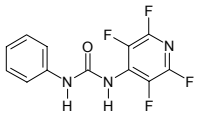	twisted	–41.3	–33.9	quasi-planar	–36.6	–34.0

[a] The molecular conformation is defined as planar when the aryl ring and urea N–C(O)–N group are roughly coplanar (C–C–N–C torsion angle τ = 0–15°) and twisted for τ = 30–45°. The orthogonal conformation (τ = 90°) is the least stable and has the highest ESP charge on urea O.

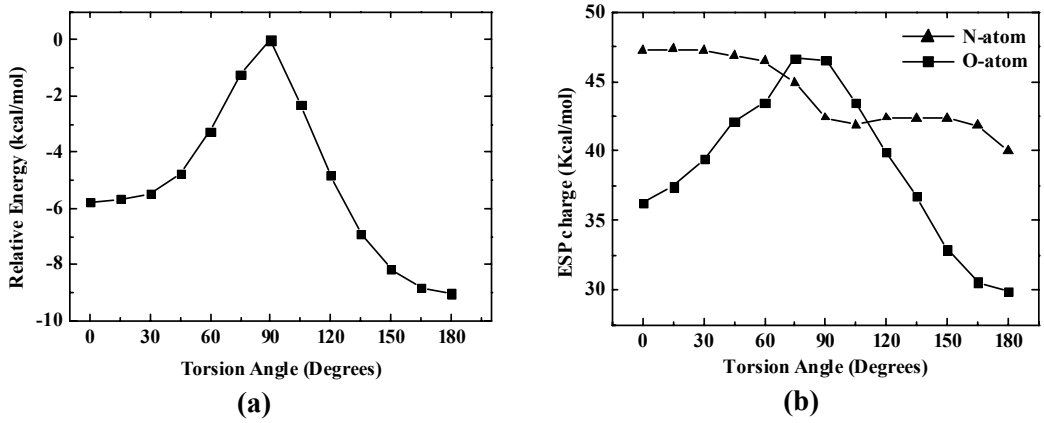

Figure 14. Spartan computations on dipyridylurea **21** as a function of aryl–N–C=O torsion angle. (a) Relative energy is plotted such that the highest energy conformer is fixed at 0. (b) ESP charge on urea O and pyridine N atoms. Note that urea O-atom charge is higher in the twisted conformation and lower when the molecule is planar but the charge on N atom is not so sensitive to conformational changes.

The energy profile in figure 14 shows that the planar *anti–anti* conformation of **21** (τ = 180°) is more stable than the twisted conformation (τ = 90°) by 9.0 kcal/mol. The difference between more stable *anti–anti* conformation to *syn–syn* conformation is about 3 kcal/mol, an energy difference that is in agreement with a recent calculation on **21**.[9] The planar conformation of **21** is more stable because of two additive effects: conjugation of urea N with electron-withdrawing phenyl ring and intramolecular C–H···O interactions. In order to estimate the stabilization from conjugation, energy profile of the methylene analog of diphenylurea, was calculated (Scheme 4). The energy difference between the stable, near planar (τ = 30°) and the high energy, twisted (τ = 90°) conformation is 4.4 kcal/mol, which gives an upper bound for the stabilization due to resonance. The energy difference (9.0 – 4.4 = 4.6 kcal/mol) therefore is the lower bound for the stabilization from the two short C–H···O interactions (H···O ~2.2 Å) of synthon **IV**. The energy of 2.5 kcal/mol per interaction is in the normal range for activated C–H···O hydrogen bonds.[19] The energy of intramolecular C–H···O interaction is higher (4–8 kcal/mol)[20] in the more activated carboranyl group compared to the phenyl ring (pK_a: carborane 27, benzene 43).

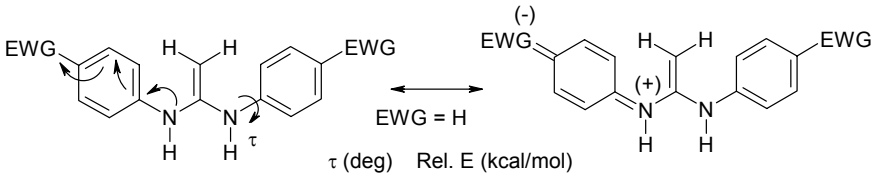

τ (deg)	Rel. E (kcal/mol)
0	–3.20
15	–3.93
30	–4.37
45	–4.34
60	–3.37
75	–1.84
90	0

Scheme 4. Contribution from resonance but no C–H···O interaction in model compound diphenylurea (Spartan, DFT-B3LYP/6-31G*).[18]

3.6 nOe experiment

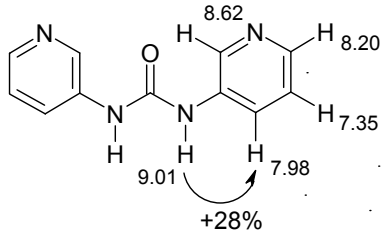

Figure 15. ^{1}H NMR nOe (DMSO-d_6) on dipyridylurea, **21**. Enhancement of the δ 7.98 signal shows that **21** reside in the *syn–syn* conformation in solution.

Intramolecular carboranyl C–H···O interactions have been characterized in solution by NMR spectroscopy[20] and energy of C–H···O hydrogen bonds in peptides is estimated to be 2.0-2.5 kcal/mol.[21] To confirm the conformation of dipiridylurea **21** in solution difference nOe ^{1}H NMR experiments were performed in DMSO-d_6 as discussed in chapter 2. Irradiation of the NH proton of dipyridylurea **21** at δ 9.01 shows enhancement of the *ortho*-H signal at δ 7.98 (28%), implying that the planar *syn–syn* conformation of **21** in the crystal is present in solution (Figure 15). The more activated CH donor proximal to pyridyl N makes C–H···O interactions with urea O in the observed *syn–syn* conformation. The persistence of bifurcated synthon **IV** and planar molecular conformation in solution is consistent with their strength. Variable-temperature (300-200 K) and variable concentration (0.005-0.5 M in MeOH-d_4) NMR experiments show no change in peak position indicates the rigidity of conformation.

3.7 Differential scanning calorimetry (DSC) and thermal gravimetric analysis (TGA) of hydrates

DSC confirms the phase purity of solid adducts and quantifies the energy change associated with guest release and melting point of host compound and TGA measurement gives an independent estimation of host-guest ratio. DSC measurement of **21**·(4/3)H_2O compounds shows two endotherms (Figure 16a). Endotherm at 62 °C indicates the loss of water and the second endotherm at 226 °C shows the melting point of compound **21**. In case of **21**·2H_2O water is lost at about 70 °C (Figure 16b). TGA measurements are in good agreement with crystal stoichiometries (Table 4). TGA and DSC measurement of **22**·H_2O indicate the loss of water at 145 °C and compound **22** decomposes at about 280°C.

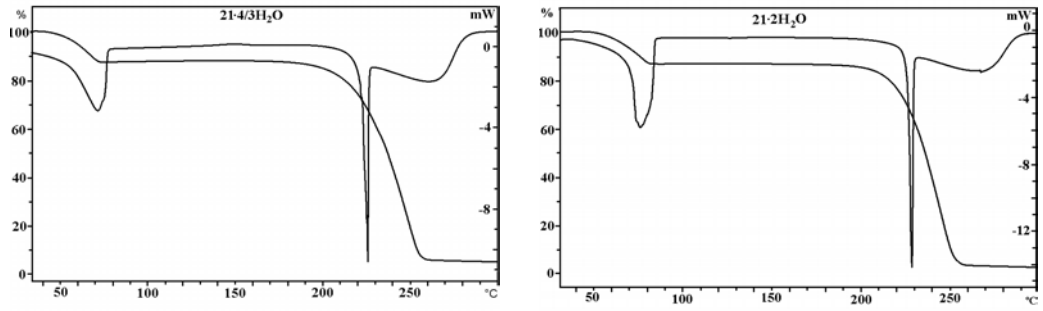

(a) **(b)**

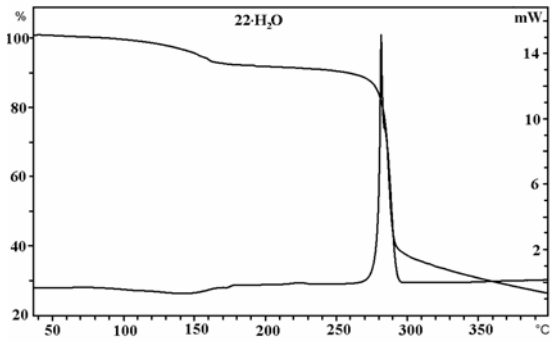

(c)

Figure 16. DSC and TGA thermograms of hydrate compounds **21**·(4/3)H_2O, **21**·2H_2O and **22**·H_2O.

Table 4. Thermal measurements (TGA and DSC) on hydrate crystals.

Compound	Calculated weight loss from X-ray (%)	Observed weight loss in TGA (%)	Guest loss endotherm temp. in DSC (T_{onset}/ °C)	Δ*H* for guest loss (J/g)
21·(4/3)H_2O	10.34	12.11	62.15	–349.40
21·2H_2O	15.52	14.79	70.35	–408.16
22·H_2O	6.82	6.75	145.89	–191.46

3.8 Discussion

The crystal structure of dipyridylurea **21** is stabilized by N–H···$N_{pyridyl}$ and C–H···O_{urea} hydrogen bonds instead of the commonly observed urea α-network. Dipyridylurea **21** also crystallizes as two hydrates, **21**·(4/3)H_2O and **21**·2H_2O, with N–H···O_{water} and O–H···$N_{pyridyl}$ hydrogen bonds but no N–H···O_{urea} tape. Attempts to engage the interfering pyridyl N in molecular complexes of **21** with carboxylic acids (such as fumaric acid and succinic acid) *via* COOH···pyridine heterosynthon did not restore the urea tape. Instead of bonding to urea C=O, the NH donors preferentially interact with the COOH group through N–H···O_{acid} hydrogen bonding. Oxidation of the pyridine ring to bis *N*-oxide **22** resulted in a monohydrate and crystal structure shows N–H···$O_{N\text{-}oxide}$ hydrogen bonding. Bis *N*-methylation of the pyridyl ring gave salt **23** having N–H···I^- interactions with the counter ion. The urea tape synthon is consistently absent in several dipyridylurea structures because of interference from N–H···$N_{pyridyl}$, N–H···O_{water}, N–H···O_{acid}, N–H···O_{oxide} or N–H···I^- interactions. Interestingly, while the strong hydrogen bond motifs change

depending on the presence of competing acceptor groups, a common motif in crystal structures of **21** is planar conformation and synthon **IV** of intramolecular C–H···O_{urea} interactions. Based on structural motifs in this study, as well as previously reported structures in the CSD, it can be generalized that planar conformation and C–H···O synthon **IV** is persistent in pyridylureas because the phenyl donor hydrogens are activated. ^{1}H NMR difference nOe in DMSO-d_6 confirms that the stable planar conformation of dipyridylurea **21** in the solid-state is also present in solution.

The intramolecular C–H···O interactions of synthon **IV** are shorter than the van der Waals sum of H and O (2.7 Å) in all structures. Even though the pyridyl ring could have twisted out of the urea plane, it is always present in a planar conformation, stabilized by the short, intramolecular C–H···O interactions. The persistence of planar conformation and C–H···O synthon **IV** in a variety of crystal structures of dipyridylurea means that it is a structure-directing synthon even though it is a weak interaction in this family of strongly hydrogen bonded pyridylureas. The remaining strong donors and acceptors then form N–H···O/ N–H···N hydrogen bonds to complete the crystal packing. What is significant from hydrogen bond hierarchy rule, namely that the strongest donor will bond to the strongest acceptor, is that even though the urea C=O is traditionally believed to be a strong acceptor group it is not involved in hydrogen bonding with strong NH donors. As a matter of fact, C=O accepts only weak C–H···O interactions in the present family of dipyridylureas except in hydrates, where more number of hydrogen bond donors are available. There is sufficient precedent for the strongest-donor to strongest-acceptor hydrogen bonding in functionalized ureas. The deviation in α-network because of interference from planar conformation and C–H···O synthon **IV** is referred to as non-urea tape structures.

Table 5. Structural summary of diarylureas extracted from the CSD

Entry	Structural Formula	Refcode/reference	Torsion Angle (C–C–N–C)/º	H bond Motif
1	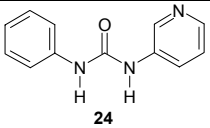 **24**	–	1.9, 15.5	non-urea tape
2	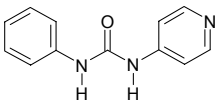	MEPXAG	1.9, 35.8	non-urea tape
3	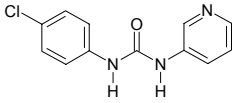	WICBEP	6.6, 7.3	non-urea tape

4	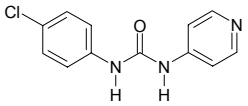	WICBIT	1.6, 10.9	non-urea tape
5	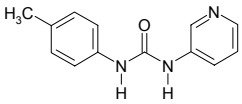 $AgNO_3$·MeOH	EZUKIT	0.4, 1.3, 1.2, 7.5, 3.8, 9.9, 2.9, 30.5, 2.7, 6.8, 8.2, 20.8	non-urea tape
6	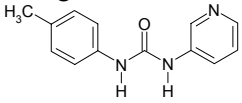 $AgCF_3SO_3·H_2O$	EZUKOZ	4.3, 23.0, 6.8, 36.7, 4.2, 40.7	non-urea tape
7	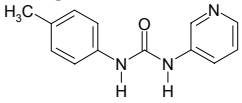 Ag_2SO_4	EZUKUF	16.5, 21.6	non-urea tape
8	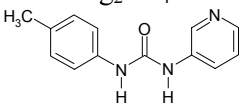 $NiSO_4·H_2O$	EZULEQ	16.0, 25.8	non-urea tape
9	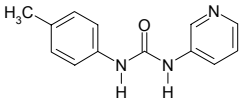 $PdCl_2$·DMF	FANWEX	3.7, 28.4	non-urea tape
10	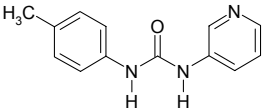 $ZnCl_2$	FANXEY	21.6, 23.9, 36.7, 40.0	non-urea tape
11	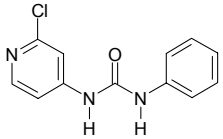	MEPWUZ	7.5, 17.3	non-urea tape
12	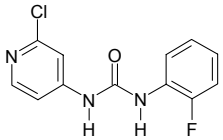	16	3.3, 19.0	non-urea tape
13	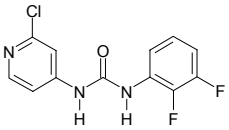	16	4.2, 6.6	non-urea tape
14	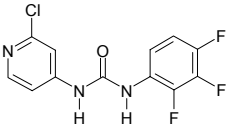	16	5.5, 9.2	non-urea tape
15	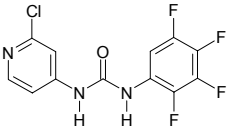	16	6.6, 11.5	non-urea tape

16	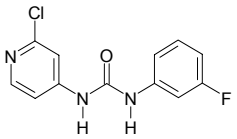	16	6.8, 27.6	non-urea tape
17	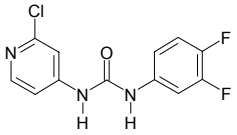	16	16.5, 29.2	non-urea tape
18	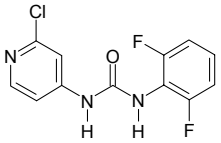	16	16.3, 65.2	non-urea tape
19	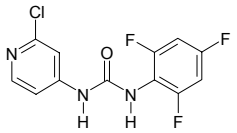	16	39.4, 90.0	urea tape
20	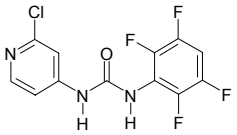	16	24.0, 61.9	urea tape
21	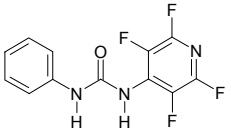	TAPRAD	29.6, 51.7	urea tape
22	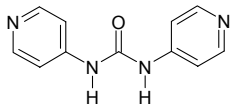 water·ethyleneglycol	GASMUJ	4.2, 10.3	non-urea tape
23	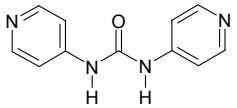 $HCl{\cdot}1.66H_2O$	GASNAQ	1.3, 3.5, 3.0, 9.9	non-urea tape
24	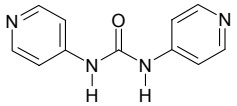 calcium-trifluoromethanesulfonate-methanol	EKJAF	0.9, 5.8	non-urea tape
25	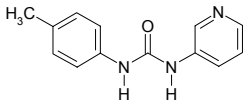 $ZnSO_4.H_2O.EtOH$	9	3.8, 19.4	non-urea tape
26	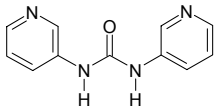 $ZnSO_4.H_2O$	9	2.8, 2.9	non-urea tape

27	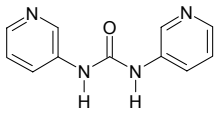 $Cu(NO_3)_2$	9	4.6, 53.8, 15.4, 39.3	non-urea tape
28	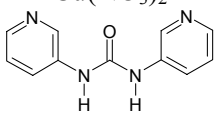 $Cu(CF_3SO_3)_2.H_2O$	9	3.6, 19.4 9.1, 22.9	non-urea tape
29	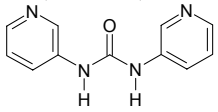 $Zn(ClO_4).H_2O$	9	15.9, 22.2	non-urea tape
30	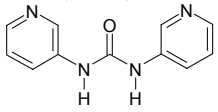 $Zn(ClO_4)_2$	9	34.4, 41.1	urea tape

3.9 Conclusions

Hydrogen-bonding in dipyridylureas, and in general in diarylureas having electron-withdrawing groups, is different from diarylureas with neutral or electron-donating groups. Difference nOe NMR experiments confirm that the planar *syn-syn* conformation of dipyridylurea **21** in its crystal structure is also present in solution. The acceptor strength of urea C=O depends on the molecular conformation and the intramolecular C–H···O interactions: it is a better hydrogen bond acceptor in the twisted conformation than in the planar conformation. Because of the reduced acceptor-strength of C–H···O-bonded C=O in dipyridylurea **21**, the strong NH donors approach other acceptors like pyridyl N, water O atoms. The notion that urea N–H···O tape is the result of strongest-donor to strongest-acceptor matching breaks down in *meta*-pyridylureas because of planar conformation and weak intramolecular C–H···O interactions. Surprisingly, the urea C=O is hardly involved in strong hydrogen bonding in the non-urea tape structures except in hydrate of **21**. When pyridylureas loose both planarity and intramolecular C–H···O interactions due to steric effect of *ortho*-substituents, urea carbonyl becomes better acceptor and the urea tape is restored.

Electrostatic surface potential (ESP) charges on **21** indicate that the acceptor strength of urea C=O is reduced in the planar conformation of synthon **IV** compared to the twisted conformation in which the oxygen has higher electron density. Diarylureas with electron-donating and neutral groups organize as one-dimensional tape in a twisted

conformation. Therefore, the nature of substitution on the phenyl ring dramatically influences the molecular conformation and hydrogen bonding of diarylureas in the solid-state. Results discussed above show that electron-withdrawing functional groups, which are also good to moderate hydrogen-bond acceptors, result in planar conformation with synthon **IV** and non-urea tape structures.

A better understanding of role of molecular conformation and weak hydrogen bonds in controlling strongly hydrogen bonded supramolecular structures is important not only for crystal engineering but also towards our understanding of protein folding. These trends on hydrogen bond donor–acceptor preferences discussed in the context of organic structures should be transferable to metal–ligand bonding modes in coordination polymers and hybrid materials, e.g. metal–pyridine vs. metal–carbonyl bonding for isonicotinamide and dipyridylurea ligand.[21] Drug molecules typically contain several hydrogen bonding groups of the acid, amide, urea and pyridine type (e.g. Piroxicam). Results in this chapter on hydrogen bond preferences in multi-functional dipyridylurea system could serve as a guide for designing pharmaceutical cocrystals and understanding drug polymorphism.[22]

3.10 Experimental Section: All compounds are characterized by IR and NMR. ^{1}H NMR spectra (δ scale in ppm, *J* coupling constant in Hz) were recorded on Bruker Avance at 400 MHz and FT-IR spectra (ν in cm^{-1}) on Jasco 5300 spectrophotometer. Melting points were recorded on Fisher–Johns apparatus.

***N*,*N*'-bis(3-pyridyl)urea 21:**[23] A 2:1 molar solid mixture of 3-aminopyridine and urea (10 mmol, 940 mg; 5 mmol, 300 mg) was heated at 160 °C for 5 h. The reaction mixture was cooled and poured into water. The light-violet colored precipitated was filtered and washed with EtOAc and recrystallized from the same solvent (60%). ^{1}H NMR (DMSO-d_6): δ 9.01 (s, 2H), 8.62 (s, 2H), 8.20 (d, *J* = 5, 2H), 7.98 (d, *J* = 8, 2H), 7.35 (dd, *J* = 8,5, 2H). IR (KBr): 3526, 3256, 1714, 1631, 1485, 1026, 802 cm^{-1}. M. p. 224 °C.

Crystallization of **21** from MeOH at room temperature afforded diffraction quality single crystals of a hydrate, **21**·(4/3)H_2O, and crystallization from EtOH at room temperature afforded the dihydrate, **21**·2H_2O. The release of water from hydrate crystals was confirmed by DSC and TGA.

21·succinic acid: A 1:1 molar mixture of ground dipyridylurea **21** and succinic acid (0.2 mmol, 40 mg; 0.2 mmol, 24 mg) was dissolved in ethanol. Slow evaporation at room temperature afforded single crystals of the molecular complex **21**·SA. ^{1}H NMR (MeOH-d_4):

δ 8.59 (br s, 2H), 8.17 (d, *J* = 5, 2H), 8.00 (d, *J* = 8, 2H), 7.34 (dd, *J* = 8, 5, 2H), 2.45 (s, 4H). M. p. 179-181 °C.

21·fumaric acid·H_2O: A 1:1 molar mixture of ground dipyridylurea **21** and fumaric acid (0.2 mmol, 40 mg; 0.2 mmol, 23 mg) was dissolved in ethanol. Slow evaporation at room temperature afforded single crystals of the hydrate, **21**·FA·H_2O. ^{1}H NMR (DMSO-d_6): δ 9.11 (s, 2H), 8.70 (br s, 2H), 8.38 (s, 1H), 8.28 (br s, 2H), 8.02 (d, *J* = 8, 2H), 7.49 (dd, *J* = 8, 5, 2H), 6.70 (s, 2H). M. p. 134 °C.

***N*,*N*'-bis(3-pyridyl-*N*-oxide)urea, 22:** Oxidation of dipyridylurea **21** (1 mmol, 214 mg) with *m*-CPBA (2 mmol, 340 mg) in EtOAc afforded the product (78%) which was crystallized from methanol to obtain the hydrate, **22**·H_2O. The water content was confirmed by DSC and TGA. ^{1}H NMR (DMSO-d_6): δ 9.04 (s, 2H), 8.59 (s, 2H), 7.80 (d, *J* = 6, 2H), 7.36 (d, *J* = 8, 2H), 7.17 (m, 2H). IR (KBr): 3290, 1716, 1589, 1423, 1153, 790 cm^{-1}. M. p. 280 °C (dec.).

***N*,*N*'-bis(*N*-methyl-3-pyridinium)urea iodide, 23:** To a solution of dipyridylurea **21** (0.7 mmol, 160 mg) in 5 ml of DMSO was added MeI (3.7 mmol, 0.23 ml) at room temperature. The reaction mixture was stirred for 8 h. A yellow colored precipitate was formed on adding EtOAc (10 ml). The precipitate was filtered and dried under vacuum (65%). X-ray quality crystals are obtained from EtOH. ^{1}H NMR (DMSO-d_6): δ 10.20 (br s, 2H), 9.15 (br s, 2H), 8.69 (br s, 2H), 8.46 (br s, 2H), 8.09 (br s, 2H), 4.38 (s, 3H), 3.85 (s, 3H). IR (KBr): 3217, 2978, 1716, 1635, 1597, 1556, 1504, 1469, 1309, 1199, 1037, 951 cm^{-1}. M. p. 256 ºC.

***N*-phenyl-*N*'-(3-pyridyl)urea, 24:** Prepared by the reaction of phenylisocyanate (10 mmol, 0.5 ml) with 3-aminopyridine (10 mmol, 470 mg) in benzene (83%). ^{1}H NMR (DMSO-d_6): δ 8.84 (s, 1H), 8.80 (s, 1H), 8.60 (s, 1H), 8.19 (d, *J* = 4, 1H), 7.95 (d, *J* = 8, 1H), 7.47 (d, *J* = 8, 2H), 7.31 (m, 3H), 7.00 (t, *J* = 7, 1H). IR (KBr): 3364, 3271, 3200, 1711, 1628, 1489, 1024, 802 cm^{-1}. M. p. 165 °C.

X-ray crystallography: X-ray reflections on dipyridylurea, **21**, **21**·(4/3)H_2O and **21**·2H_2O were collected on Enraf-Nonius FAST area detector with rotating anode source, **21**·SA and **21**·FA·H_2O on Enraf-Nonius MACH-3 diffactometer, **21**·2H_2O (100 K), **22**·H_2O, **23** and **24** on SMART APEX CCD diffractometer. All data were collected using Mo-Kα radiation (λ = 0.71073 Å) and crystal structures were solved by direct methods using SHELXS-97 and refined by full matrix least-squares refinement on F^2 with anisotropic displacement

parameters for non-H atoms using SHELXL-97. N–H and O–H hydrogens were refined from difference Fourier maps; aromatic and aliphatic C–H hydrogens were generated by the Riding model in idealized geometries.

DSC/TGA: DSC was recorded on Mettler Toledo DSC 822e module and TG on Mettler Toledo TGA/SDTA 851e module, managed by the integrated STAR software. The stoichiometry of **21**·(4/3)H_2O, **21**·2H_2O and **22**·H_2O determined by X-ray diffraction is consistent with DSC and TGA measurements.

^{1}H–^{1}H NMR difference nOe: Dipyridylurea, **21** (8-10 mg) was dissolved in 0.5 ml of DMSO-d_6 and the sample was degassed with dry N_2 under vacuum. The built-in program for difference nOe spectroscopy in Bruker Avance 400 was used: power 50 db, relaxation delay 6 s, 128 scans. Irradiation of the urea NH signal at δ 9.01 showed positive enhancement of the signal at 7.98 in dipyridylurea **21**. No enhancement was observed at 8.62. The percentage enhancement was calculated as the ratio of enhanced signal to the irradiated peak. Proton nOe enhancements of 20-30% are in agreement with proximal H atoms in constrained systems.[24]

3.11 References

1. (a) A. Nangia, *CrystEngComm,* **2002**, *4*, 93. (b) G. R. Desiraju, *J. Mol. Struct.,* **2003**, *656*, 5. (c) D. Braga, L. Brammer and N.R. Champness, *CrystEngComm,* **2005**, *7*, 1.
2. (a) P.L. Magueres and L. Ouahab, *Acta Crystallogr.* **1994**, *C50*, 1507. (b) P. Yonova, E. Guleva, E. Zozikova and E. Kotseva, *Bulg. J. Plant Physiol.,* **1997**, *23*, 49; (c) K. Yabuuchi, E. Marfo-Owusu and T. Kato, *Org. Biomol. Chem.,* **2003**, *1*, 3464; (d) C.-K. Lam and T. C. W. Mak, *Chem. Commun.,* **2001**, 1568. (e) C.-H. Chien, M.-K. Leung, J.-K. Su, G.-H. Li, Y.-H. Liu and Y. Wang, *J. Org. Chem*., **2004**, *69*, 1866.
3. S. George and A. Nangia, *Acta Crystallogr.,* **2001**, E*57*, o719.
4. S. Kashino and M. Haisa, *Acta Crystallogr.,* **1977**, *B33*, 855.
5. V. Velikova, O. Angelova and K. Kossev, *Acta Cryst.,* **1997**, C*53*, 1273.
6. (a) G.R. Desiraju, *J. Chem. Soc., Chem. Commun.,* **1991**, 426. (b) A.L. Gillon, N. Feeder, R.J. Davey and R. Storey, *Cryst. Growth Des.,* **2003**, *3*, 663. (c) L. Infantes, J. Chisholm and S. Motherwell, *CrystEngComm,* **2003**, *5*, 480.
7. (a) P. Vishweshwar, A. Nangia and V.M. Lynch, *J. Org. Chem.,* **2002**, *67*, 556. (b) B.R. Bhogala, P. Vishweshwar and A. Nangia, *Cryst. Growth Des.,* **2002**, *2*, 325. (c) B.R. Bhogala and A. Nangia, *Cryst. Growth Des.,* **2003**, *3*, 547.

8. (a) T.L. Nguyen, F.W. Fowler and J.W. Lauher, *J. Am. Chem. Soc*. **2001**, *123*, 11057.
9. R. Custelcean, B.A. Moyer, V.S. Bryantsev and B.P. Hay, *Cryst. Grouth Des.*, **2006**, *6*, 555.
10. (a) P. Grosshans, A. Jouaiti, V. Bulach, J.M. Planeix, M.W. Hosseini and J.-F. Nicoud, *Chem. Commun*., **2003**, 1336. (b) Y. Cui and W. Lin, *Chem. Commun*., **2003**, 1388. (c) S. Hanessian, A. Gomtsyan, M. Simard and S. Roelens, *J. Am. Chem. Soc*., **1994**, *116*, 4495. (d) P. Dapporto, P. Paoli and S. Roelens, *J. Org. Chem*., **2001**, *66*, 4930.
11. (a) S.J. Brooks, P.A. Gale and M.E. Light, *CrystEngComm,* **2005**, *7*, 586. (b) S.J. Brooks, P.A. Gale and M.E. Light, *Chem. Commun.*, **2005**, 4696.
12. D.K. Kumar, D.A. Jose, A. Das and P. Dastidar, *Chem.Commun.*, **2005**, 4059.
13. M. Barboiu and A.van der Lee, *Acta Crystallogr.*, **2003**, *C59*, 366.
14. K. Yamaguchi and K. Shudo, *J. Agric. Food. Chem.,* **1991**, *39*, 793.
15. (a) F. H. Allen and R. Taylor, *Chem. Soc. Rev.,* **2004**, *33*, 463. b) Cambridge Structural Database, ConQuest 1.8, January 2006 update. www.ccdc.cam.ac.uk.
16. A. Abad, C. Agulló, A.C. Cuñat, C. Vilanova and M.C. Ramírez de Arellano, *Cryst. Growth Des*., **2006**, *6*, 46.
17. K.Yamaguchi, G.Matsumura, N.Haga and K.Shudo, *Acta Crystallogr.*, **1992**, *C48*, 559.
18. Spartan '04, Wave Function Inc. www.wavefun.com.
19. G. A. Jeffrey, *An Introduction to Hydrogen Bonding*, Oxford University Press, New York, **1997**.
20. (a) A. Donati, S. Ristori, C. Bonechi, L. Panza, G. Martini and C. Rossi, *J. Am. Chem. Soc.,* **2002**, *124*, 8778. (b) A. Cappelli, G. Giorgi, M. Anzini, S. Vomero, S. Ristori, C. Rossi and A. Donati, *Chem. Eur. J.,* **2004**, *10*, 3177.
21. (a) S. Scheiner, T. Kar and Y. Gu, *J. Biol. Chem.,* **2001**, *276*, 9832. (b) P. W. Baures, A. M. Beatty, M. Dhanasekaran, B.A. Helfrich, W. Pérez-Segarra and J. Desper, *J. Am. Chem. Soc.,* **2002**, *124*, 11315.
22. (a) B. R. Bhogala, P. K. Thallapally and A. Nangia, *Cryst. Growth Des.,* **2004**, *4*, 215.
23. (a) A.R. Sheth, S. Bates, F.X. Muller and D.J.W. Grant, *Cryst. Growth Des.,* **2004**, *4*, 1091. (b) S. Datta and D.J.W. Grant, *Nature Reviews*, **2004**, *3*, 42.
24. H. Friebolin, *Basic One- and Two-Dimensional NMR Spectroscopy*, 2nd ed., VCH, Weinheim, **1993**, pp. 275-286.

CHAPTER 4

PHENYL–PERFLUOROPHENYL STACKING AND SUPRAMOLECULAR REACTIVITY IN MULTI-COMPONENT COCRYSTALS

4.1 Introduction

Arene–arene (π–π) interactions are significant in many areas of chemistry, biochemistry and materials science and recently highlighted for their significance in drug design.[1] An important class among arene–arene contacts is the interaction between arenes and perfluoroarenes. The first complex of this type was obtained serendipitously by Patrick and Prosser[2] in 1960 from liquid hexafluorobenzene (melting point 5.0 °C) and benzene (melting point 5.4 °C) as a solid of melting point 23.7 °C. Due to its complicated polymorphism elucidation of its crystal structure was delayed until 1992 from high resolution neutron and synchrotron powder diffraction data.[3] Meanwhile, complexes of hexafluorobenzene with methyl-substituted arenes were studied crystallographically by Dahl.[4] Crystal structure of benzene and hexafluorobenzene shows that the complex is composed of infinite stacks of alternating benzene and hexafluorobenzene molecules (Ph–Ph^F synthon, Scheme 3) in contrast to the crystal structures of the pure component molecules which are arranged in a herringbone fashion.[5] 1:1 molecular complex of hexamethylbenzene and hexafluorobenzene exits in two temperature dependant polymorphs.[6] Crystals were found to be trigonal at room temperature and transformed to triclinic modification when cooled below 0 °C. Marder *et al.* have shown that hexafluorobenzene forms 1:1 complexes with a variety of fused-ring polyaromatic molecules.[7]

It was initially thought that arene–perfluoroarene complexes are stabilized by charge transfer interaction. But most of the arene–perfluoroarene complexes do not exhibit charge transfer bands except the 1:1 complex of hexafluorobenzene with bis(benzene)chromium.[8] The stacking arrangement of aryl–perfluoroaryl rings is due to the minimization of electrostatic repulsions and maximization of electrostatic attractions between the molecules. Benzene and hexafluorobenzene have large quadrupole moments, which are of similar magnitude but opposite in sign.[9] This leads to the stacking motif dictated by electrostatic quadrupole–quadrupole interactions. A schematic diagram of how

the quadrupole moments direct the packing of 1:1 molecular complex of benzene and hexafluorobenzene (Figure 1). Other perfluoroarene compounds such as octafluoronaphthalene (OFN) also form complexes with electron rich arenes. OFN forms a 1:1 complex with naphthalene stabilized by quadrupole–quadrupole interactions.[10] It has been shown that OFN can also form 1:1 complexes with a variety of fused-ring polyaromatic molecules,[11] as well as with diphenylacetylene, 1,8 diaminonaphthalene, and acenaphthene.[12] OFN has also been shown to form a 3:2 complex with ferrocene,[13] and a variety of complexes with both acyclic and heterocyclic sulfur-nitrogen containing molecules.[14]

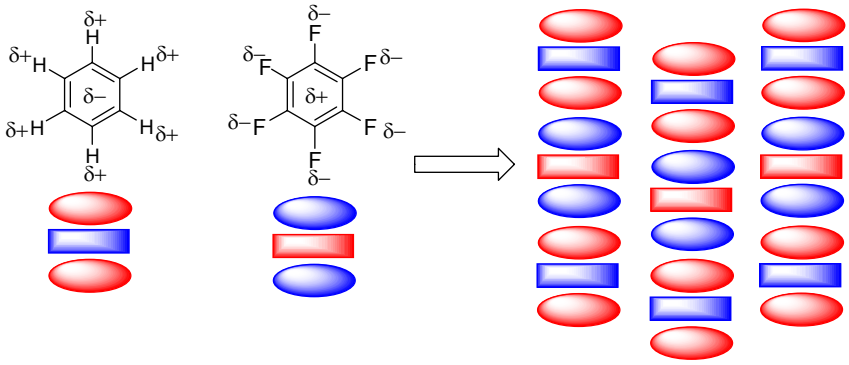

Figure 1. Schematic representation of quadrupole–quadrupole interactions in 1:1 molecular complex of benzene and hexafluorobenzene.

4.2 Role of Ph–Ph^F synthon in crystal engineering

Alternating stacks of π-rich and π-poor aromatic systems offer a design principle for the formation of extended linear columns. This approach is successfully used in catenane and rotaxane systems where self-assembly is directed by the overlap of π-electron-deficient bipyridinium or aromatic diimide cores with π-electron-rich aromatic diethers.[15] OFN is used to form aggregates with polyethyleneglycols containing pyrene end-groups, which form hydrogels upon addition of water.[16] Nangia *et al.*[17] examined the role of Ph–Ph^F stacking synthon in a family of azine compounds by gradually increasing the extent of fluorination in molecules. The crystal structure of unsymmetrical AZINE2, contains planar molecules stacked in a head-to-tail fashion such that the phenyl ring of one molecule is π-stacked on the perfluorophenyl group of another at a centre-to-centre distance of 3.78, 3.73 Å; the distance between centroid and ring plane of adjacent phenyl rings is 3.38, 3.45 Å (Figure 2a). The structure of 1:1 cocrystal of symmetrical azines AZINE1 and AZINE3 is very similar to AZINE2 and dominated by the Ph–Ph^F stacking synthon (Figure 2b).

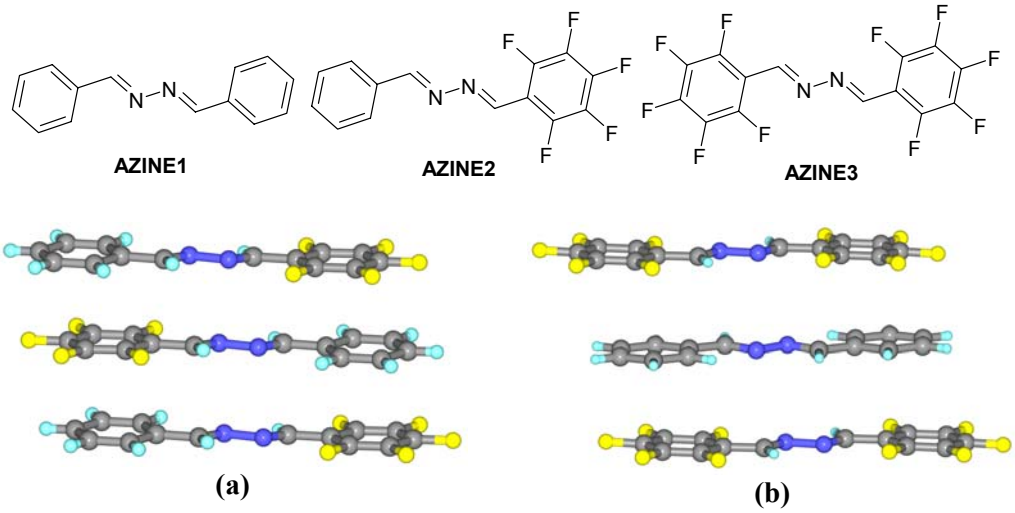

Figure 2. (a) Ph–Ph^F stacking in unsymmetrical AZINE2 (EGAVUD). (b) Ph–Ph^F stacking in cocrystal of symmetrical AZINE1 and AZINE3 (EGAWEO).

Grubbs and coworkers successfully achieved the desired arrangement of molecules by using Ph–Ph^F synthon for the solid-state UV-initiated topological synthesis of stereoregular polymers.[18] It is well established that a prerequisite for an efficient topochemical polymerization of 1,3-butadiynes is the tilted stacking of the monomers, with a distance '*d*' between the diyne centers of about 4.7–5.2 Å and the angle 'ϕ' between molecular and stacking axes of about 45° (scheme 1). Generally polymerization of diyne through 1,4-addition process produces a conjugated enyne polymer with *trans* configuration. But synthesis of *cis*-polymer is very difficult because butadiyne monomers have to stack without much offset (ϕ~90°) and the distance between diyne centers must be about 3.4 Å (scheme 1). Phenyl–perfluorophenyl stacking in fluorinated diphenyldiacetylenes (scheme 2) brings the monomers to pack in the required geometry for a *cis*-specific polymerization (Figure 3). Photochemically-induced polymerization occurs in 1:1 cocrystal of 1,4-diphenylbutadiyne (DPB) and 1,4-bis(pentafluorophenyl)-butadiyne (BPFPB) as well as in 1-pentafluorophenyl-4-phenylbutadiyne (PFPB).

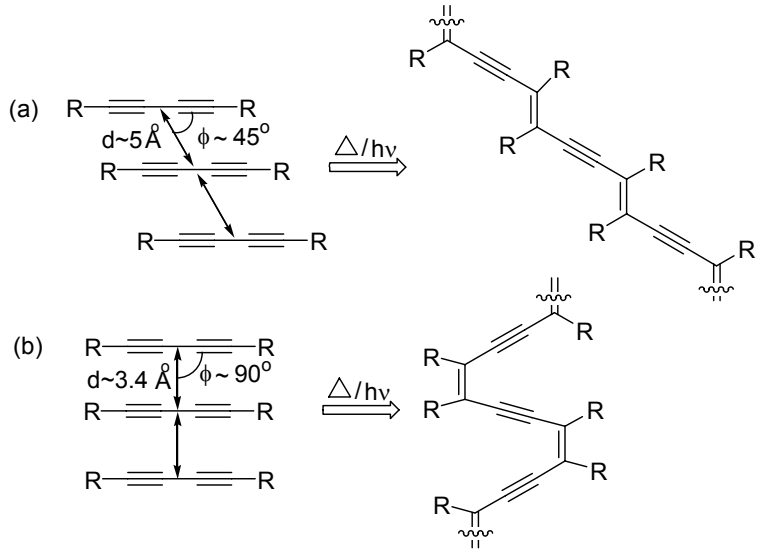

Scheme 1. (a) Commonly observed diyne polymerization to yield *trans*-polybutadiyne. (b) Unprecedented synthesis of a *cis*-polybutadiyne

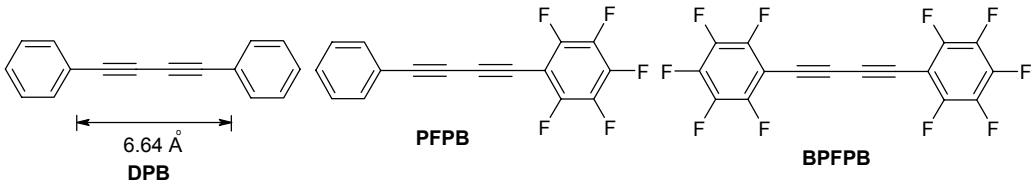

Scheme 2. Butadiyne derivatives used to synthesize *cis*-specific polymer.

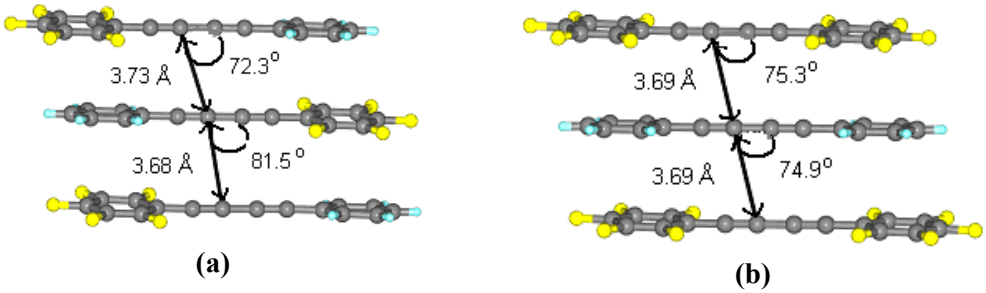

Figure 3. Geometrical requirement of diyne monomers for *cis*-specific photochemical reactions in the crystal structures of (a) PFPB and (b) 1:1 cocrystal of DPB and BPFPB.

Ph–Ph^{F} synthon also been successfully used in the solution phase synthesis of macrocycles,[19] molecular electronics and photonics[20] and stabilization of liquid crystalline mesophases.[21] The hexafluorobenzene solvate of hexamelamine shows anticancer activity.[22] It also offers new possibilities for the modification of biologically important structures including peptides and oligonucleotides.[23]

4.3 Results

In earlier studies Ph–Ph^F synthon was tested and exploited only in the absence of strong hydrogen bonding functionalities. We are interested to evaluate its robustness in multi-functional molecules *via* cocrystallization experiment.[24] Carboxylic acids and carboxamides are reliable functional groups in crystal engineering because they form robust aggregates as dimers and catemers (**I**–**IV**) *via* strong O–H···O and N–H···O hydrogen bonds (8-10 kcal mol^{-1}). The energy of C_6H_6–C_6F_6 dimer in the eclipsed face-to-face arrangement is 4–5 kcal mol^{-1} (r = 3.6–3.7 Å) by *ab initio*, semiempirical, and DFT calculations.[25] Furthermore, the hetero dimer is calculated to be more stable than the homo dimer in all cases. Given that the energy of Ph–Ph^F synthon is about half that of a strong O–H···O or N–H···O hydrogen bond, cocrystallization of aryl and perfluoroaryl carboxylic acids and amides is attempted. Crystallographic data of compounds studied in this chapter is given in appendix.

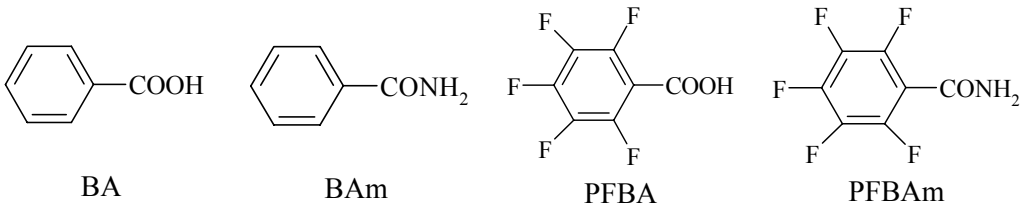

BA·PFBA, **26**

BAm·PFBAm, **27**

BAm·PFBA, **28**

BA·PFBAm, **29**

BA·BAm, **30**

PFBA·PFBAm, **31**

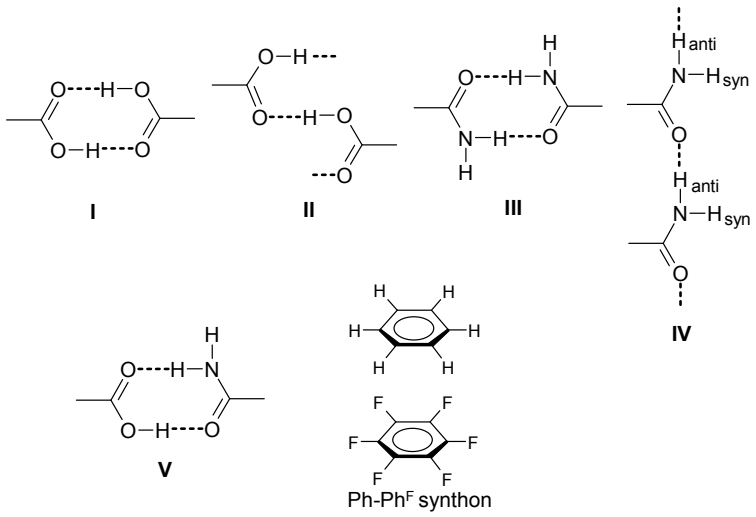

Scheme 3. Synthons discussed in this chapter.

Table 1. Geometrical parameters of hydrogen bonds[a]

Cocrystal	Number	Hydrogen bond	*d*/Å	*D*/Å	*θ*/°
26	i	O–H···O	1.67	2.647(3)	169.4
	ii	O–H···O	1.68	2.653(3)	168.7
	iii	O–H···O	1.63	2.605(3)	171.2
	iv	O–H···O	1.65	2.624(3)	170.2
		C–H···O	2.50	3.437(4)	143.7
		C–H···O	2.68	3.479(4)	130.6
		C–H···O	2.56	3.503(4)	144.7
		C–H···O	2.46	3.318(4)	135.2
		C–H···F	2.49	3.220(5)	123.7
27	i	N–H···O	2.16	3.118(3)	159.0
	ii	N–H···O	2.15	3.088(3)	152.9
	iii	N–H···O	2.03	2.997(3)	159.5
	iv	N–H···O	1.94	2.936(3)	169.7
		C–H···O	2.35	3.415(3)	167.7
28	i	O–H···O	1.51 (1.39)[b]	2.487(2)	170.8
	ii	N–H···O	2.02	3.003(2)	164.4
	iii	N–H···O	2.02	2.983(2)	157.3
		C–H···O	2.37	3.429(2)	164.1
31	i	O–H···O	1.65	2.617(3)	167.0
	ii	N–H···O	1.90	2.895(3)	166.0
	iii	N–H···O	1.93	2.915(3)	164.9

[a] O–H, N–H, C–H bonds are neutron normalized. [b]Experimental X-ray distance in very short hydrogen bond.

Table 2. Selected torsion angles

Cocrystal	Torsion	*θ*/°
26	C2-C1-C7-O2	32.6
	C9-C8-C14-O4	27.2
	C16-C15-C21-O5	11.3
	C27-C22-C28-O8	5.0
27	C2-C1-C7-O8	42.9
	C6A-C1A-C7A-O8A	21.6
28	C2-C1-C7-O1	22.8
	C9-C8-C14-O3	22.5
31	C3-C2-C1-O2	24.8
	C10-C9-C8-O3	44.4

4.3.1 Crystal structure of BA·PFBA, 26

BA·PFBA, **26** crystallizes in the monoclinic space group *Cc* with two residues of each component in the asymmetric unit. The molecules adopt different conformations about

the C_{aryl}-C_{COOH} bond (Table 2), twisted conformation (designated **A**) and near-planar conformation **B**. BA and PFBA of both **A** and **B** type aggregates engage in symmetry-independent dimer with homosynthon **I** (Figure 4a). The O–H···O hydrogen bond from PFBA to BA is shorter (iii, 1.63 Å, 171.2°, electron-deficient donor to electron-rich acceptor) than the other hydrogen bond in **I** from BA to PFBA (iv, 1.65 Å, 170.2°, electron-rich donor to electron-deficient acceptor) for **B** dimer aggregate, but the difference is not significant for **A** dimer aggregate. The hydrogen bonds in synthon **I** of twisted **A** molecules are longer (i, ii, 1.67, 169.4, 1.68 Å, 168.7°) than iii and iv because conjugation between phenyl ring and carboxylic acid group in planar **B** molecules strengthens hydrogen bonding. Such dimers are connected *via* C–H···O interactions listed in table 1 and shown in figure 4b. The structure has an overall van der Waals close packing such that the phenyl and perfluorophenyl groups are in proximity. The phenyl and perfluorophenyl rings of dimer aggregates **A** and **B** have excellent π-stacking with little offset at an intercentroid distance (*d*) of 3.81, 3.84, 3.95, 3.97 Å (Figure 4c&4d) and an interplanar distance (*r*) of ca. 3.5 Å. (3.53, 3.49, 3.47, 3.55 Å). The crystal structure of binary component **25** may be compared with the structure of PFPB (Scheme 3) in which molecules are stacked in a head-to-tail fashion at interlayer distance (*r*) of *ca.* 3.7 Å (Figure 3a).[18a]

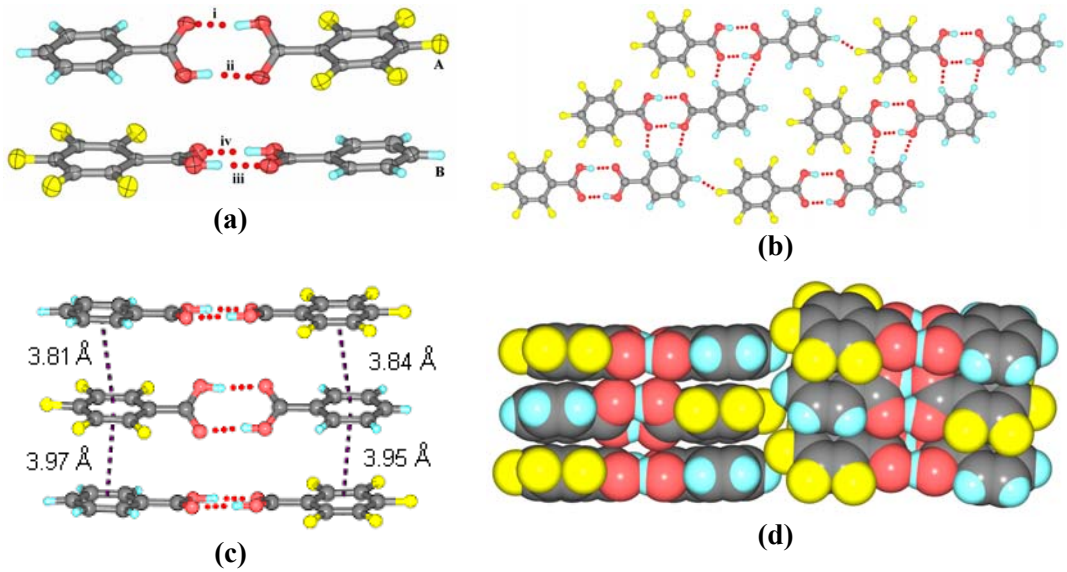

Figure 4. (a) Symmetry-independent carboxylic acid dimers are labeled **A** and **B**. (b) Corrugated tapes are connected by C–H···F to form layered structure in **26**. (c) Ph–Ph^F stacking along the *b*-axis. (d) CPK model along the *b*-axis shows how two stacked columns are related.

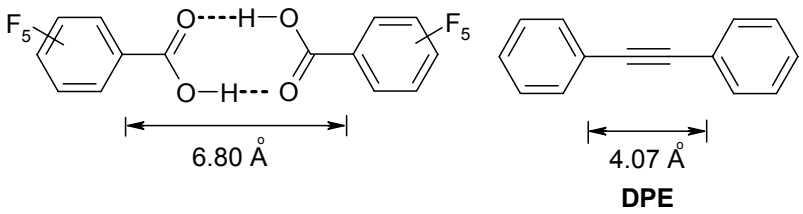

In an independent study Gdaniec and coworkers[26] also studied crystal structure of **26** along with 1:1 cocrystal of PFBA and 2,4,6-trimethylbenzoic acid. Interestingly hydrogen bonded assembly and stacking is similar to that of **26** (Figure 5a). They also reported the crystal structure of 1:1 cocrystal of PFBA and DPB (Scheme 2). Crystal structure reveals that the dimers of synthon **I** is sandwiched between the molecules of the DPB which leads to formation of regular columns (Figure 5b). The covalent diyne spacer in DPB and hydrogen bond synthon **I** in PFBA are interchangeable, and, moreover, the C_{aryl}–C_{aryl} distance between pentafluorophenyl rings is very similar in the two structures (6.64 Å in DPB, 6.80 Å in PFBA). Due to distance mismatch in the crystal structure of 1:1 cocrystal of diphenylacetylene (DPE) and PFBA, two phenyl rings of DPE interact with the two different perfluorophenyl rings of PFBA dimer (Figure 5c). Nangia *et al.* previously noted the equivalence between molecular and supramolecular connectors in a family of wheel-and-axle host-guest structures.[27]

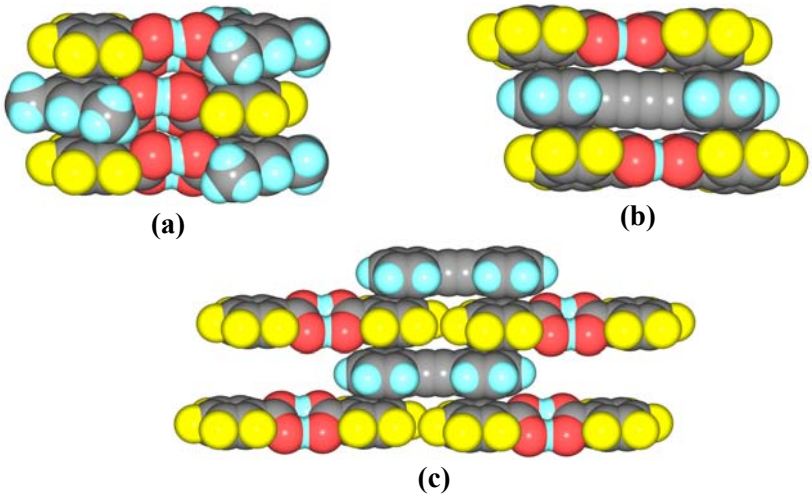

Figure 5. (a) Crystal structure of 1:1 cocrystal of PFBA and 2,4,6-trimethylbenzoic acid (UKOKOU). (b) 1:1 cocrystal of PFBA and DPB (UKOKUA). (c) 1:1 cocrystal of PFBA and DPE (UKOLIP). Note that the presence of Ph–Ph^F stacking synthon in all structures.

The assignment of *Cc* space group is fraught with the possibility that there might be true higher symmetry that is overlooked,[28] and this error is even more likely when there are

two or more symmetry-independent molecules (Z' > 2) as in **26**. We have verified that the assignment of *Cc* space group is correct in this case. There is an approximate, noncrystallographic inversion center at 0.4, 0.25, 0.2, which explains the centrosymmetric intensity statistics observed in data collection. However, from examination of the molecular conformations of BA and PFBA and the two hydrogen-bonded dimers **I** it is obvious that they are different. A check of the cif file in platon for MISSYM also agrees with our assignment and the higher symmetry *C*2/*c* space group is ruled out for **26**.

4.3.2 Crystal structure of BAm·PFBAm, 27

BAm·PFBAm, **27** crystallizes in the polar space group $P2_1$ with one molecule of each residue in the asymmetric unit. The $CONH_2$ group in PFBAm is twisted with respect to the aromatic ring when compared with BAm (Table 2). PFBAm and BAm are connected *via* $N–H_{anti}\cdots O$ hydrogen bonds as catemer **IV** that run parallel to [110] and [1-10] directions. The $N–H_{anti}\cdots O$ hydrogen bond iv from PFBAm to BAm is significantly shorter than the bond from BAm to PFBAm (Figure 6a, iv 1.94 Å, 169.7°; ii 2.15 Å, 152.9°). The syn NH groups form a twisted noncentrosymmetric dimer **III** (i, iii, 2.16, 159.0, 2.03 Å, 159.5°) with N–C–O–N torsion angles of 47.9°and 44.9° (Table 2). Hydrogen bond iv is shorter than the other three N–H···O bonds in the same structure because the donor and acceptor groups are activated and it is simultaneously stabilized by the attractive $Ph–Ph^F$ synthon (Figure 6b, 6c, d = 3.66 Å). The π-cloud of phenyl and pentafluorophenyl rings have excellent quadrupole–quadrupole interactions because they stack with little offset. The shortness of $N_{anti}–H\cdots O$ compared to $N_{syn}–H\cdots O$ is significant because *syn* NH is generally assumed to be the stronger hydrogen bond donor than *anti* NH in primary amide.[29] Weak C–H···O, C–H···F, and F···F interactions are present in the crystal. Crystal structure of *N*-(tetrafluoro-*p*-pyridyl)-*N*′-phenylurea (TFPU) can be compared with the crystal structure of complex **27** in terms of chain propagation and mode of stacking. In the crystal structure glide related TFPU molecules interact *via* bifurcated N–H···O hydrogen bonds and the stacking occurs not between the molecules forming urea tape but between different molecules (Figure 6d).

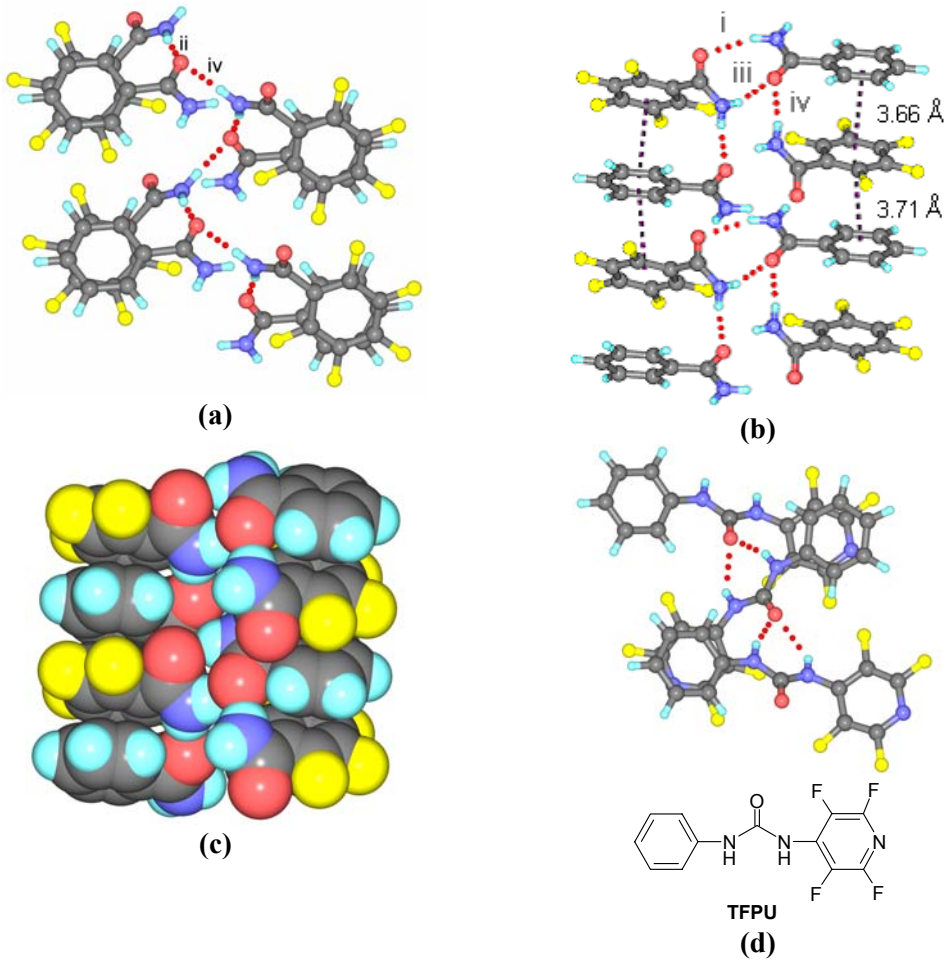

Figure 6. (a) N–H···O catemer and Ph–Ph^F synthons in the crystal structure of **27**. (b) Ph–Ph^F stacking, N–H···O dimer and N_{anti}–H···O bond iv along the *a*-axis. (c) CPK model along *a*-axis. (d) Ph–Ph^F stacking and N–H···O urea tape in the crystal structure of TFPU. Note the similarities in the stacking and hydrogen bonding with (a).

4.3.3 Crystal structure of BAm·PFBA, 28

Crystals of 1:1 complex **28** were obtained from EtOAc/hexane at ambient temperature that solved in the $P2_1/n$ space group. The twist in molecular conformation of acid and amide molecules is listed in table 2. The crystal structure is stabilized by acid···amide heterosynthon **V** (Figure 7a, O–H···O, i, 1.51 Å, 170.8°; N–H···O, ii, 2.02 Å, 164.4°). O–H···O bond i is in the range of a very short (strong) hydrogen bond (O···O 2.487 Å) with an H···O distance of 1.39 Å (X-ray). The shortness of O–H···O is due to the very strong donor (PFBA) and highly basic acceptor group (BAm). Short O–H···O hydrogen bonds have been noted in acid-amide cocrystals, e.g., oxalic acid, *trans*-cinamamide (O···O

2.489 Å, O–H···O 174.3°). The heterodimers are connected to the COOH group of a glide-related aggregate by N–H···O bond (iii, 2.02 Å, 157.3°), and such inversion-related dimers are connected by C–H···O interaction (2.37 Å, 164.1°). Weak C–H···F and F···F interactions can also be identified in the structure. Ph–Ph^F stacking in **28** is weaker because of lateral offset (d = 3.93 Å, r = 3.47 Å, Figure 7b&7c).

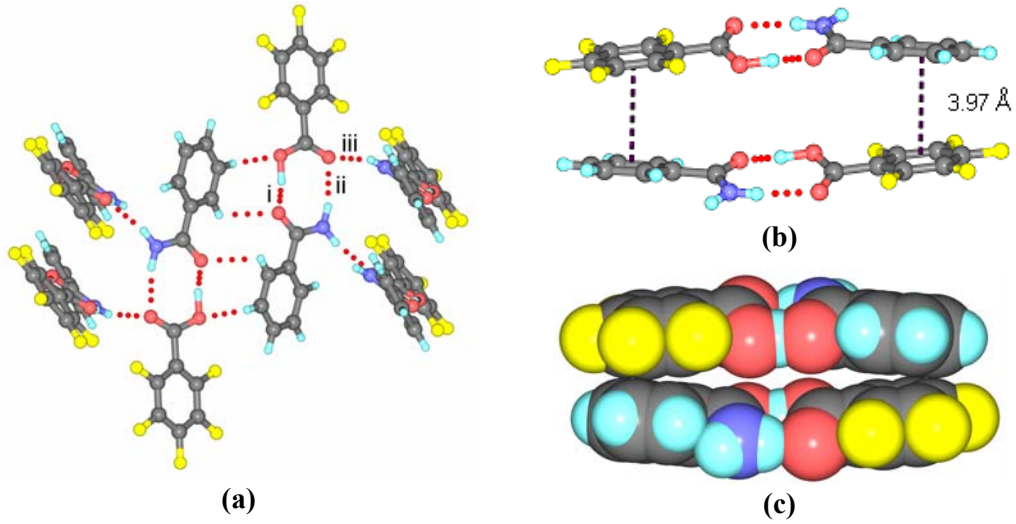

Figure 7. (a) N_{anti}–H···O bond and C–H···O interaction with PFBA of glide- and inversion related aggregate. (b) Offset Ph–Ph^F stacking along the *a*-axis. (c) CPK model along *a*-axis.

4.4 Literature structures

Cambridge structural database (CSD version 5.27, January 2006 update) was searched for compounds containing phenyl and perfluorophenyl rings along with strong hydrogen bonding functionalities like carboxy, carbamido, amine and hydroxy groups resulted in 30 hits. There are 8 cocrystals (refcodes: DOCRIW, IJOCOZ, OCUJUR, PASOFP, QEGKAO, UKOKUA, UKOLIP, UKOKOU) other than three cocrystals discussed in this chapter. In cocrystals of triphenylphosphine oxide and triphenylarsinic oxide with pentafluorophenol (DOCRIW, PASOFP) Ph–Ph^F stacking is not observed because of awkward conformation of oxide compounds whereas in other structures the Ph–Ph^F stacking synthon is present. In the crystal structure of 1:1 complex of BAm and *N*-(pentafluorophenyl)urea, **32**[30] along with bifurcated urea N–H···O motif and amide dimer the Ph–Ph^F stacking synthon (3.67 Å) is also observed. The stacking pattern is similar to the cocrystal **27** (Figure 8a). In 1:1 cocrystal of diphenylmethanol and

bis(pentafluorophenyl)methanol, **33**[31] hydroxy groups form a O–H···O tetramer in such a way that phenyl and perfluorophenyl rings come close about 3.62 and 3.78 Å (Figure 8b).

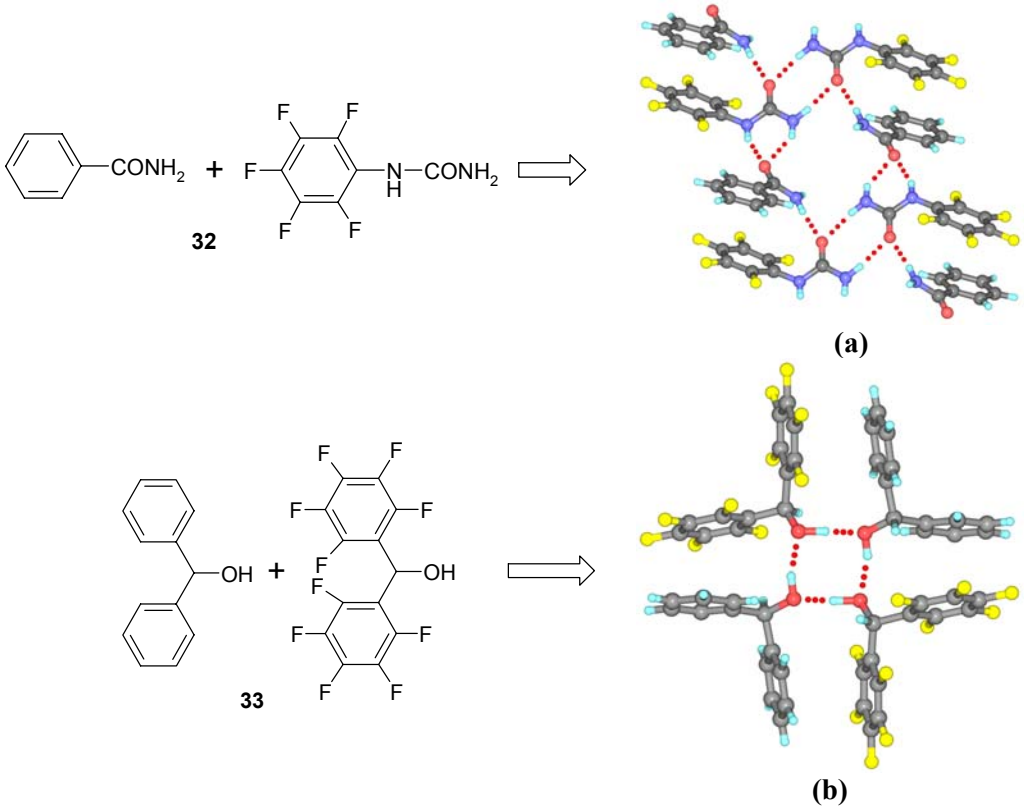

Figure 8. Ph–Ph^F stacking synthon is retained in the presence of strong hydrogen bonding functionalities like urea, primary amide (**a**, QEGKAO) in **32** and hydroxy in **33**(**b**, OCUJUR).

4.5 Discussion

While the Ph–Ph^F stacking stabilizes structures **26** and **27**, the interaction is weaker in **28** *via* lateral offset (d = 3.93 Å, r = 3.47 Å). Phenyl perfluorophenyl mediation during cocrystallization of **28** is weaker because acid···amide heterosynthon **V** is stronger than homosynthons **I** and **III**. It appears that the role of the Ph–Ph^F synthon toward cocrystallization is based on need, akin to anchimeric assistance in S_N2 displacement reaction.[32] The higher strength of acid···amide heterosynthon **V** compared to acid···acid and amide···amide homosynthons **I** and **III** is explained by the best hydrogen bond donor (COOH) approaching the best acceptor (amide C=O) and the second-best donor (CONH) bonding with the next best acceptor (acid C=O) in COOH···$CONH_2$. Another reason for the formation of heterosynthon is to avoid lone pair repulsion between hydroxyl and carbonyl O atoms that occurs in hydrogen-bonded chains built from homosynthons and connected *via*

N–H···O hydrogen bonds. In the heterosynthon arrangement, the distance between neighboring NH groups hydrogen bonded to the same O atom increases and so the lone-pair repulsion is minimized.[33] Despite these factors, several attempts to cocrystallize pentafluorobenzamide and benzoic acid did not yield any adduct crystal PFBAm·BA, **29** presumably because both the COOH donor and the amide C=O acceptor are weaker hydrogen bonding groups compared to **28**. Although the reasons are not fully clear, melting point of cocrystals **26**, **27** and **28** is significantly lower than the pure acids and amides whereas in many of the other phenylperfluorophenyl adduct crystals, it is generally higher than the pure components. Thus, despite the attractive Ph–Ph^F synthon and the stronger hydrogen bonding in these cocrystals there are possibly other factors contributing to crystal lattice forces that are not additive. Apart from enthalpy, entropy is very important in explaining melting point lowering, though the latter property is much more difficult to quantify and rationalize. Factors such as the different number of residues, symmetry independent molecules, and their conformation in the component and adduct crystals are likely to complicate a lattice energy-based approach to calculate enthalpy for correlation with melting point.

4.6 Mechanochemistry and solid-state reactivity and of carboxylic acids and carboxamides

A common method of recrystallization is slow evaporation of solvent, because it is an effective means of purification and it can yield large, well-defined single crystals. However there are several drawbacks to the solution-based approach in cocrystal synthesis. The solubility of the starting components is one of the problems; one has to identify a suitable solvent or solvent mixture for all components involved in the cocrystallization experiment. Unexpected solvate formation may hamper the rational cocrystal design, because the solvent employed in the cocrystallization may have the ability to interact with individual components and thus may be incorporated into the crystal lattice. There are some reports where solvent promote the crystallization of meta-stable polymorphs.[34] An alternative to the solution-based approach to prepare cocrystals is solid-state grinding of components in defined stoichiometries is known as mechanochemistry and can be regarded as an attractive and eco-friendly alternative route to avoid the use of large amounts of solvent.[35] Typical mechanochemical reactions, which are activated by co-grinding the individual components, are usually carried out by either manually in an agate mortar or electromechanically by ball mill grinding. In the solid-state grinding relative solubility of

individual components is not a concern and there is no possibility of forming undesired solvates. While it is not yet fully understood, there are instances in which certain cocrystals are obtained only *via* solid state grinding. For example cocrystal **34** could not be obtained by solvent crystallization method whereas by solid-state grinding it was formed but took about 48 hours to form the cocrystal.[36] Etter *et al.*[37] reported two polymorphs of cocrystal **35**, both crystallised from solution, but only one was obtainable from solid-state grinding. The 1:2 salt of **36** form two polymorphs depending on the preparation technique and crystallization speed. Form I is obtained by solid-state co-grinding or by rapid crystallization, whereas Form II is obtained by slow crystallization.[38] Cocrystallisation by simple grinding is not always successful. Grinding with small amount of solvent (known as kneading) some times increase the reaction kinetics significantly and desired product is obtained quickly. For example the cocrystal of cyclohexane-1,3*cis*,5*cis*-tricarboxylic acid (CTA) and 4,4'-bipyridine (BP) is obtained from MeOH solution. When an equimolar mixture of CTA and BP is ground for 1 hour only partial reaction occurs, while the grinding is carried out with addition of approximately 0.05 ml of MeOH the cocrystallization is found to be significantly accelerated and complete conversion is achieved within 20 minutes.[39]

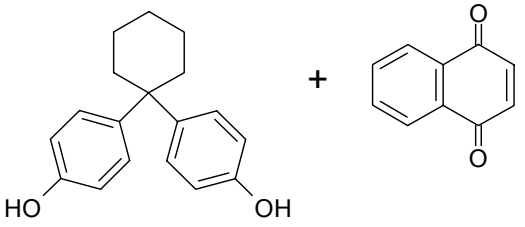

34

35 **36**

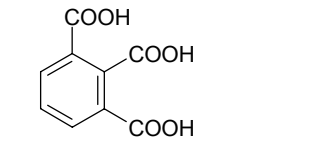

1,2,3-Benzene-tricarboxylic acid (**BTA**)

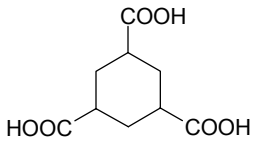

1,3,5-Cyclohexane-tricarboxylic acid (**CTA**)

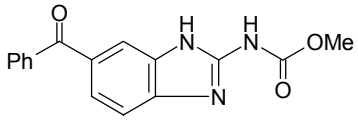

Mebendazole

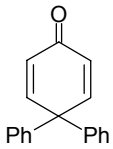

4,4-diphenyl-2,5-cyclo-hexadienone

Powder X-ray diffraction (PXRD) has become a very important technique in solid-state chemistry and crystal engineering because PXRD pattern of a compound or polymorph can be considered as finger print pattern for identification. In the pharmaceutical industry, the identification of the crystalline components of bulk materials is essential to understand the nature of crystalline materials and whether the API is a single phase or not. There have been significant advances in recent years for carrying out complete structure determination of molecular solids directly from powder X-ray diffraction data.[40] For example 1,2,3-benzenetricarboxylic acid (BTA) is known to form dihydrate, solvates with several different alcohols and other solvent molecules.[41] But its unsolvated crystal structure is not reported, because it does not crystallize without solvent. Recently Harris *et al.*[42] determined the crystal structure from powder diffraction data using the direct-space genetic algorithm technique for structure solution, followed by Rietveld refinement. They also determined the crystal structure of **26** from powder diffraction data.[43] Similarly crystal structure of unsolvated CTA was determined by Jones *et. al*.[44] from powder diffraction data.

Cocrystal formation and solid-state reactions can be monitored by powder X-ray diffraction as the pattern of the complex is quite different from those of the precursors. Furthermore if no solid state reaction occurs the pattern is a simple summation of the patterns of the precursors. If crystal structure of the cocrystal and precursors are available the calculated powder patterns can be compared to identify complex formation. Variable temperature powder X-ray diffraction (VT-PXRD) may contribute towards understanding the thermal behaviour of compounds since the formation, disappearance and conversion of crystalline phases will result in changes of powder profiles. For example Mebendazole drug used in the treatment of ascariasis, uncinarisis etc. exits in three polymorphic forms, A, B and C. By using VT-PXRD it was concluded that polymorph C is stable between room

temperature and about 180 °C and is converted to polymorph A at higher temperatures (205-220 °C).[45] Very recently Nangia and Kruger have studied polymorph inter-conversion and stability of four polymorphs (A, B, C and D) of 4,4-diphenyl-2,5-cyclohexadionone[46] by using VT-PXRD along with *ab initio* calculations and showed that form A is the thermodynamic polymorph and B is the kinetic form of the enantiotropic system A–D.[47]

4.7 Solid-state reactivity of acids and amides

4.7.1 BA/PFBA, 26

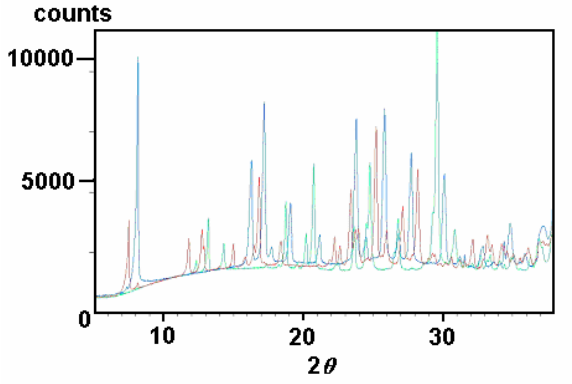

Figure 9a. Comparison of the measured powder patterns. BA (blue), PFBA (green) and product **26** (pink).

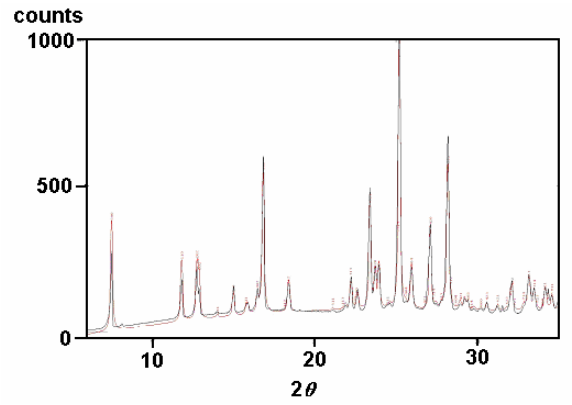

Figure 9b. Comparison of simulated (red) and experimental (black) powder patterns of **26**.

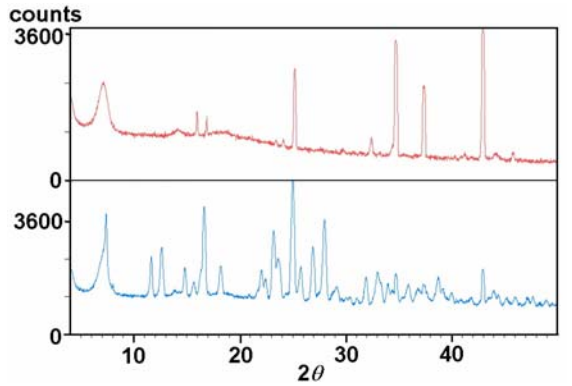

Figure 9c. Comparison of experimental powder patterns at room temperature (bottom) and after heating to 90 °C (top).

Benzoic acid and pentafluorobenzoic acid in 1:1 ratio was taken in mortar and grounded for 10 minutes without adding any solvent. Powder XRD pattern is recorded to check whether supramolecular reaction occurs between BA and PFBA. Satisfyingly there are no peaks corresponding to individual components, indicating the chemical change (Figure 9a). The powder patterns in figure 9a show that the peaks corresponding to the product do not belong to any of the two individual precursors. The peaks in the mixture (pink curve) at 2θ position 7.51, 11.81, 12.75, 15.01, 16.48 and 16.85° are new peaks. As X-ray single crystal structure of cocrystal is available, comparison of simulated powder pattern from the crystal structure and that of experimental powder pattern shows a nice fit and overlay (Figure 9b). It indicates 100% complex formation by simple grinding at room temperature. VT-PXRD shows after melt, only peaks corresponding to sample holder (alumina) are remained (Figure 9c). The powder diffraction pattern of cocrystal **26** is matching with the pattern reported by Harris *et al.,* where they determined the crystal structure from powder diffraction.[48]

4.7.2 BAm/PFBAm, 27

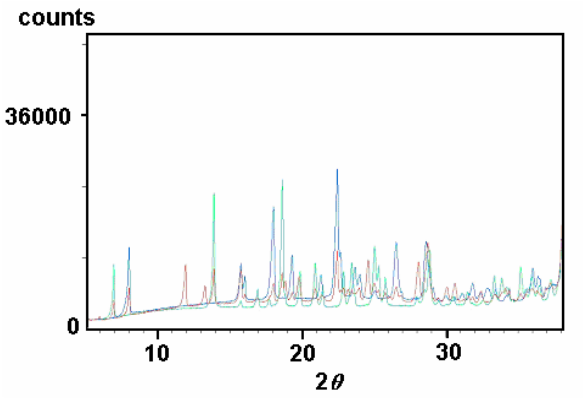

Figure 10a. Comparison of the measured powder patterns BAm (blue), PFBAm (green) and product **27** (pink).

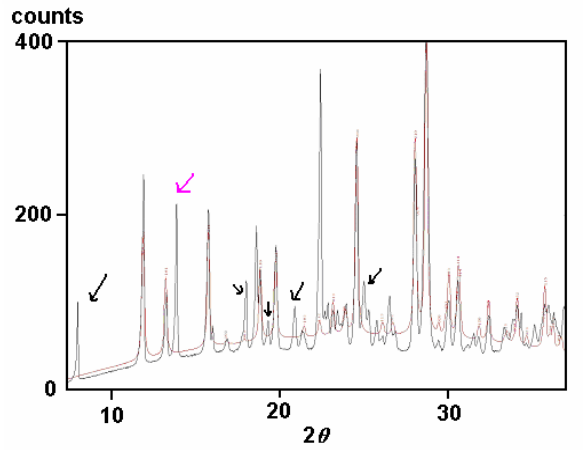

Figure 10b. Simulated (red) and experimental (black) powder patterns of **27** at room temperature.

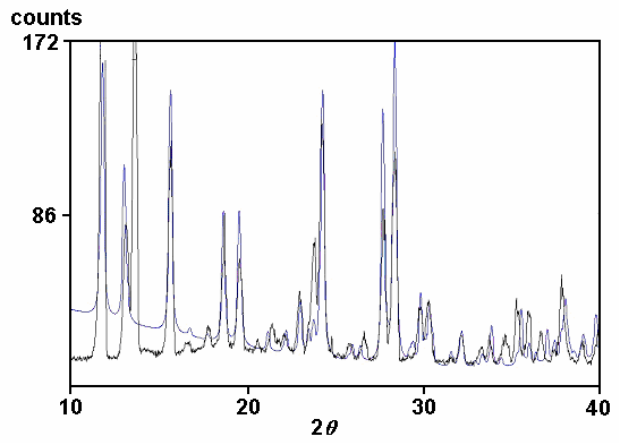

Figure 10c. Simulated (blue) and experimental (black) powder patterns of **27** at 100 °C temperature.

The overlay of powder patterns of BAm, PFBAm and grounded mixture of **27** (Figure 10a) shows that some of the peaks corresponding to the product, **27** do not belong to individual precursors. For example peaks at 2θ position 11.99, 13.31, 18.90, and 18.05° are new peaks (pink plot). At the same time peaks at 6.95, 8.02, 13.91, 15.79, 16.06 and 18.66° belong to individual precursors. Comparison of simulated powder pattern from the crystal structure of cocrystal and the experimental powder pattern at room temperature shows that there is an incomplete molecular complex formation (Figure 10b). Peaks indicated with arrows correspond to BAm and PFBAm. As the mixture is heated to 100 °C, the reaction proceeds to completion. Figure 10c shows that the simulated and experimental powder patterns at high temperature have a good overlay and fit. As the sample mixture is heated the complex sublimes or melts as powder lines of the sample holder are only observed. An intense peak at 14.32° in the experimental powder XRD pattern (indicated with pink arrow in Figure 10b), is not matching with any of product **27** or individual precursors. This may be due to the preferred orientation of a small crystal or a bunch of crystals.

4.7.3 BAm/PFBA, 28

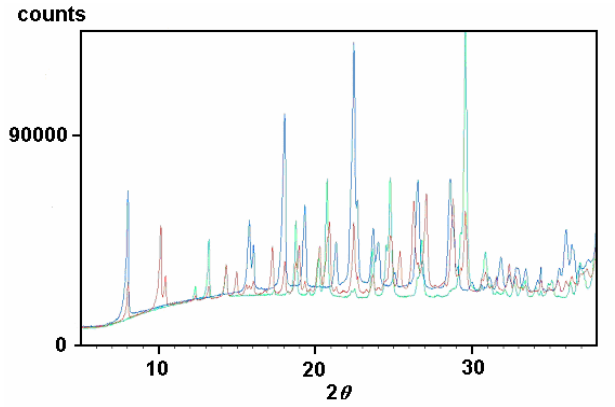

Figure 11a. Ovelay of measured powder patterns of BAm (blue), PFBA (green) and product **28** (pink).

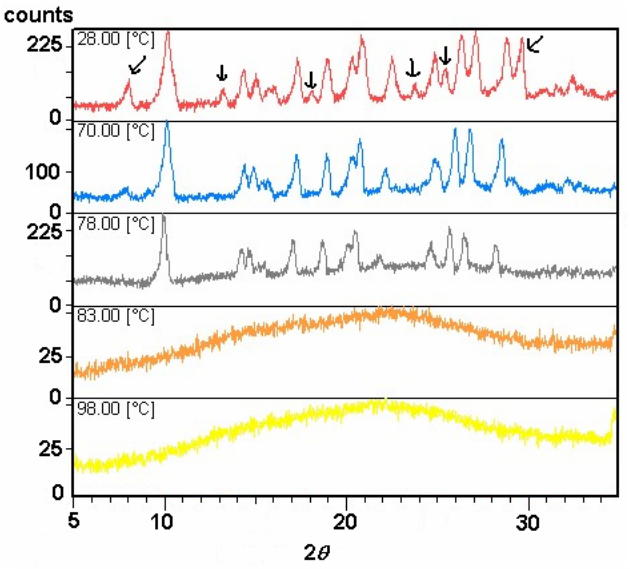

Figure 11b. VT-PXRD of the mixture, **28**. Note the changes in PXRD profile as temperature increases.

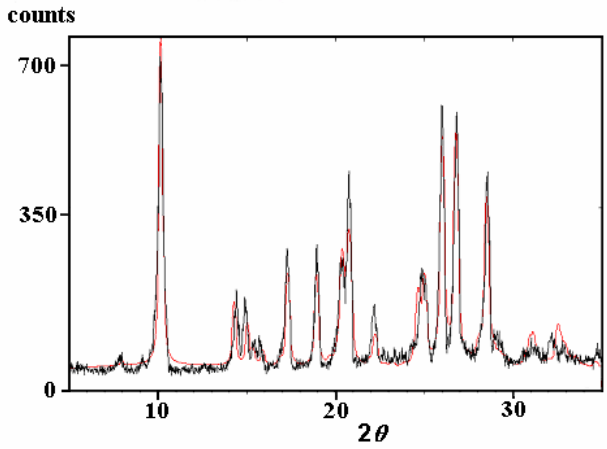

Figure 11c. Overlay of simulated (red) and experimental (black) powder patterns at 78 °C.

Figure 11a shows the comparison of PXRD patterns of BAm, PFBA and the grounded mixture of **28**, indicating there are some new peaks (pink plot). The peak at 2θ position 8.03° is not present in BAm or PFBA. Similarly peaks at 10.11, 10.41, 12.33, 13.18, 14.30, 15.00 and 17.26° are new peaks. At the same time there are some peaks which arise from the respective precursors indicating that complex formation is incomplete. In VT-PXRD (Figure 11b) experiment there is a change in PXRD pattern at 78 °C, some of the peaks indicated with arrows disappear. Comparison of simulated and experimental powder patterns at high temperature (Figure 11c) shows a nice fit and overlay indicating that the completion of supramolecular reaction at 78 °C. Further heating results in melting of complex.

4.7.4 BA/PFBAm, 29

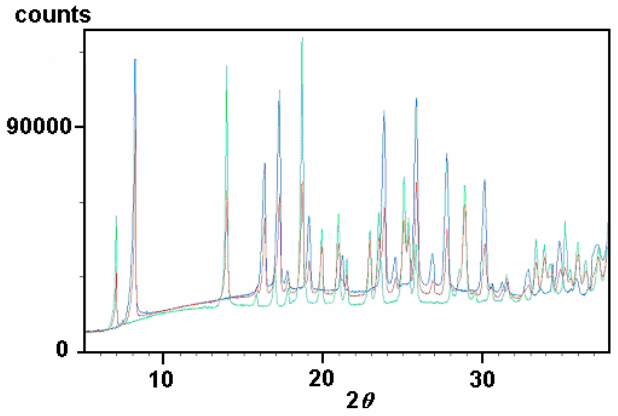

Figure 12a. Overlay of measured powder patterns of BA (blue), PFBAm (green) and mixture **29** (pink).

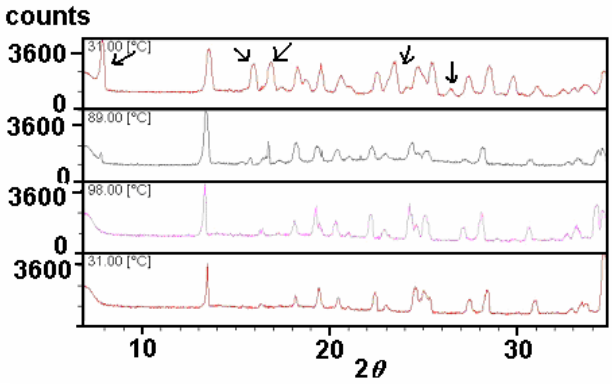

Figure 12b. VT-PXRD of the mixture, **29**. Note that the peaks indicated with arrows are disappearing at 98 °C.

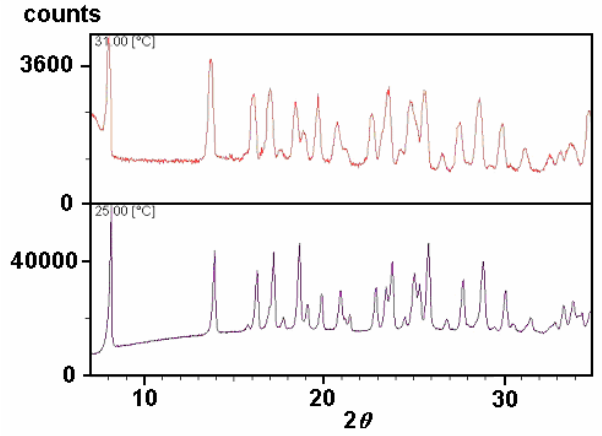

Figure 12c. Comparison of powder patterns of the **29** after heating with that of the powder pattern of PFBAm.

Comparison of powder patterns of BA, PFBAm and grounded mixture of **29** shows that the peaks corresponding to the product look like just summation of two individual precursors (Figure 12a). The nice fit in overlay of experimental powder pattern of the product and the individual precursors indicates that there is no complex formation at room temperature. VT-PXRD (Figure 12b) indicates that at about 80 °C the peaks corresponding to BA start to get smaller and by 98 °C disappeared completely and only the peaks

corresponding to PFBAm (Figure 12c). At no stage in heating and cooling process change in powder pattern is observed.

4.7.5 BA/BAm, 30

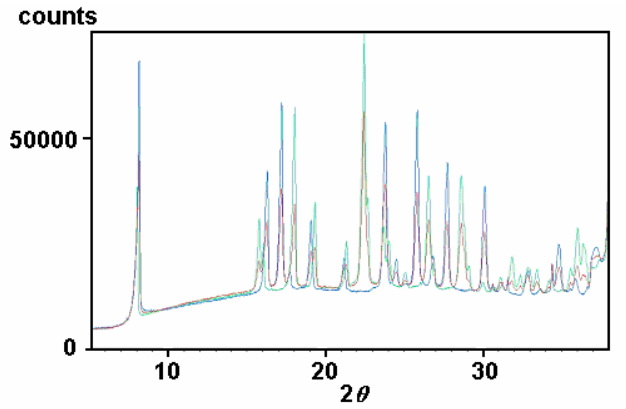

Figure 13a. Overlay of measured powder patterns of BA (blue), BAm (green) and product **30** (pink).

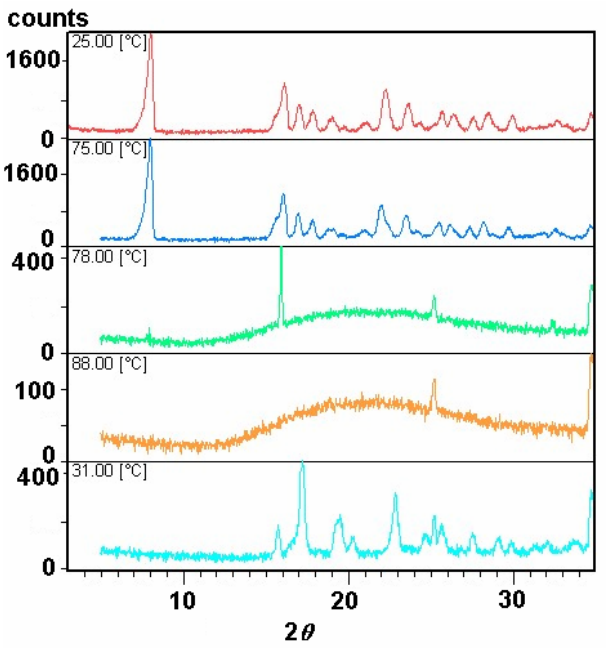

Figure 13b. VTPXRD pattern of mixture, **30**. Note the new powder pattern after melting.

Figure 13a shows a nice fit of the experimental powder patterns of BA, BAm and the grounded mixture of **30** indicating that there is no complex formation at room temperature. VT-PXRD (Figure 13b) shows that there is no change in the diffraction profile from 25 °C to 75 °C. Around 78 °C most of the peaks disappear indicating the melting process has possibly started. On cooling to room temperature it crystallises again and gives different pattern indicating a new molecular complex or decomposition of the product. We have to do further experiments on this system.

4.7.6 PFBA/PFBAm, 31

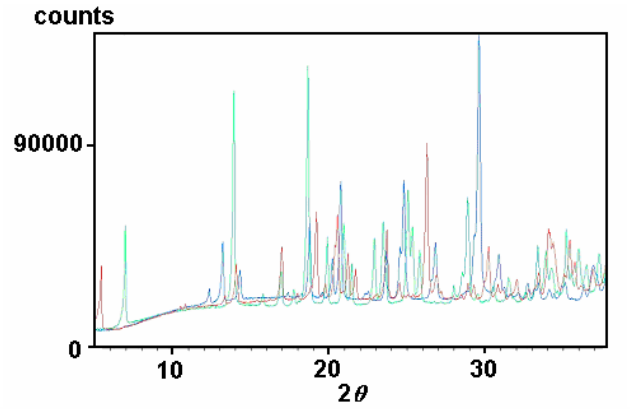

Figure 14a. Overlay of measured powder patterns of PFBA (blue), PFBAm (green) and **31** (pink).

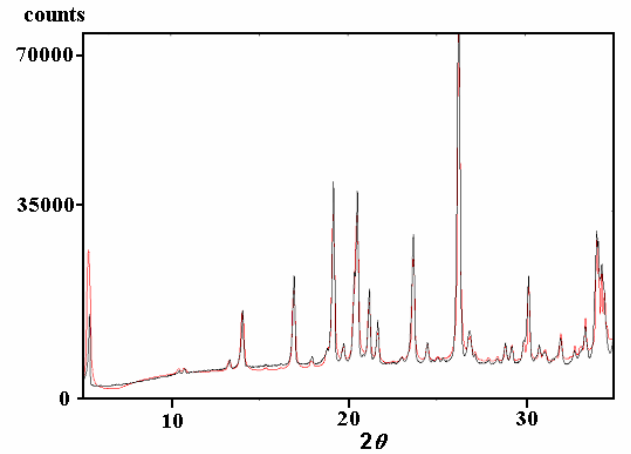

Figure 14b. Simulated (black) and experimental (red) patterns of **31** at room temperature.

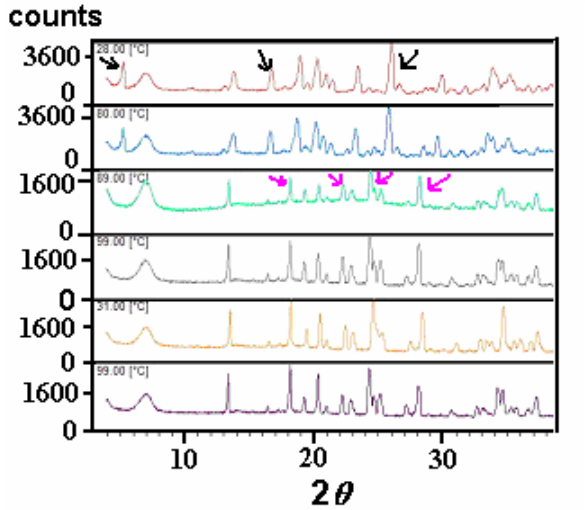

Figure 14c. VT-PXTD pattern of mixture, **31**.

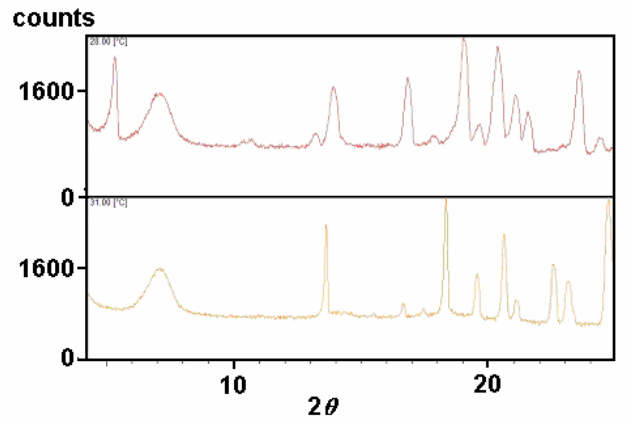

Figure 14d. Powder peaks of the molecular complex **31** before (red) and after (orange) heating to 89 °C.

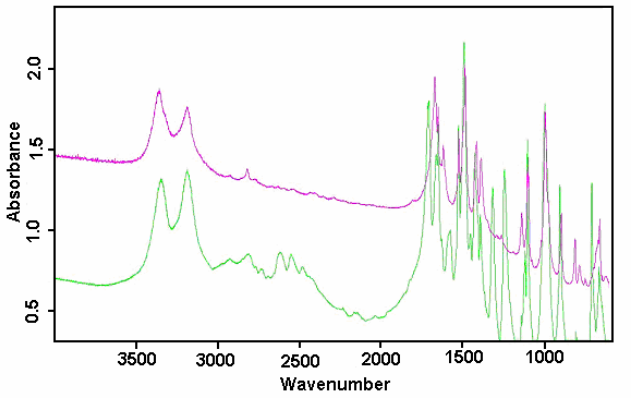

Figure 14e. IR pattern of **31** before heating (green) and after heating (pink).

Comparison of experimental powder patterns of PFBA, PFBAm and their 1:1 grounded mixture shows that the peaks corresponding to the product do not belong to individual precursor (Figure 14a, pink plot). For example, the peak at 2θ = 5.42° is not observed in PFBA and PFBAm. Similarly peaks at 14.08, 16.98 and 19.20° are also new, indicating the formation of new compound which could be the molecular complex. At this stage cocrystallization of 1:1 mixture of PFBA and PFBAm was attempted. Diffraction quality single crystals were obtained by slow evaporation of dioxane solvent at room temperature. Simulated PXRD pattern of cocrystal structure perfectly matches with the experimental powder pattern cocrystal at room temperature (Figure 14b). VT-PXRD (Figure 14c) experiment on mixture of **31** shows another new pattern that appears at high temperature. Peaks indicated with black arrows disappeared at about 90 °C and at the same time new peaks indicated by pink arrows appeared. Two reasons can be ascribed for the appearance of new pattern at high temperature: (i) This new powder pattern could be a high temperature polymorph which is stable at room temperature, (ii) At the high temperature the two components may react with each other to form a new compound and as a result the

powder pattern changes. The IR spectra of room temperature mixture and high temperature mixture are similar, indicating the possibility of a high temperature polymorph (Figure 14e).

Cocrystal **31** crystallizes in orthorhombic *Pbca* space group with one molecule each of PFBA and PFBAm in the asymmetric unit. Carboxylic acid and amide functionalities are twisted out of the aromatic plane (Table 2) due to steric hindrance. *Syn* NH donor of amide interacts with strong acid carbonyl acceptor *via* N–H···O (ii, 1.90 Å, 166°) and forms hetero dimer. These heterodimers are connected by N–H_{anti}···O (iii, 1.93 Å, 164.9°) and form corrugated one dimensional tape structure (Figure 17).

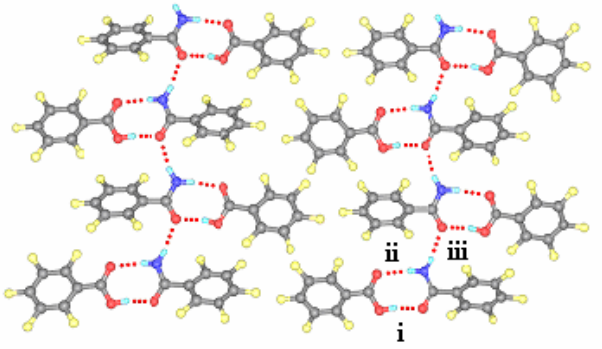

Figure 17. Acid···amide heterodimers and N–H_{anti}···O hydrogen bonds in **31**.

4.8 Conclusions

Earlier studies on the Ph–Ph^F synthon have dealt with molecules in which strong hydrogen bonding groups were generally absent. We demonstrate that the phenyl–perfluorophenyl stacking synthon is a viable recognition motif in the cocrystallization of strong hydrogen bonding carboxylic acids and carboxamides. However there are other favorable considerations in exploiting the Ph–Ph^F synthon to mediate cocrystallization. The pentafluorophenyl group activates the COOH and $CONH_2$ donor groups for hydrogen bonding because of the high electronegativity of fluorine (F 4.0, H 2.1, C 2.5; Pauling scale), while the similar van der Waals radius of H and F (1.20 Å, 1.47 Å) means that the aryl/perfluoroaryl rings are nearly isosteric. Furthermore, organic fluorine has little hydrogen-bond acceptor ability,[49] and hence phenyl perfluorophenyl stacking was expected to prevail in the presence of other strong hydrogen bonding groups, e.g., COOH, $CONH_2$.

From the room temperature and variable temperature powder diffraction data it can be concluded that cocrystals **26** and **31** are formed by simple mechanical grinding at room temperature whereas in case of cocrystals **27** and **28** cocrystal formation is incomplete at room temperature. As temperature increases the supramolecular reaction of cocrystal

assembly proceeds to completion at about 100 °C in case of cocrystal **27** at 78 °C for cocrystal **28**. Molecular complexes are not formed with **29** and **30** even at high temperatures. Molecular complex **31** goes through a phase change on heating to form a stable new phase that does not change on cooling and substantial reheating. These results show that when more activated and acidic donors are involved, supramolecular recognition is fast and leads to complete conversion of mixture to molecular complex at room temperature by simple grinding. Because in complexes **26** and **31**, BA, PFBA and PFBAm are involved, which have acidic and activated donors, therefore cocrystallization reaction is rapid and facile. In molecular complexes **27** and **28**, although activated PFBA and PFBAm are involved the other partner is BAm, which is not so reactive for hydrogen bonding and so the supramolecular reaction is incomplete at room temperature. For the complete cocrystallization of **27** and **28** heating is necessary. In case of **29** both the COOH donor and the amide C=O acceptor are weaker hydrogen bonding groups compared to **28** whereas in **30**, BA and BAm are not activated and Ph–Ph^F synthon is also absent, therefore no complex formation is observed.

4.9 Experimental Section

In all cocrystallization experiments, the components were finely ground using mortar-and-pestle. Single crystals of **26**, **27** and **28** obtained by slow evaporation of solvent (EtOAc/hexane, 1:1) at room temperature and complex **31** from dioxane. The molecular complexes were characterized by its difference in melting point from the pure components and the structure confirmed by X-ray diffraction and variable temperature PXRD. Melting point is determined on Fisher-Johns apparatus (visual inspection). Melting point of benzoic acid is 122 °C, benzamide is 129 °C, pentafluorobenzoicacid is 101 °C, and pentafluorobenzamide is 145 °C.

Cocrystallization

(Benzoic Acid)·(Pentafluorobenzoic Acid), 26: A 1:1 mixture of benzoic acid (0.030 g, 0.25 mmol) and pentafluorobenzoicacid (0.053 g, 0.25 mmol) was dissolved in hot EtOAc/hexane (1:1). Plate-shaped colorless crystals were obtained after few days at room temperature. M. p. 85-87 °C.

(Benzamide)·(Pentafluorobenzamide), 27: A 1:1 mixture of benzamide (0.030 g, 0.25 mmol) and pentafluorobenzamide (0.052 g, 0.25 mmol) was dissolved in hot EtOAc/ hexane (1:1).Needle-shaped colorless crystals were obtained after few days at room temperature. M. p. 103-105 °C.

(Benzamide)·(Pentafluorobenzoic Acid), 28: A 1:1 mixture of benzamide (0.030 g, 0.25 mmol) and pentafluorobenzoicacid (0.053 g, 0.25 mmol) was dissolved in hot EtOAc/ hexane(1:1). Needle-shaped colorless crystals were obtained after few days at room temperature. M. p. 85 °C.

Cocrystallization of benzoic acid and pentafluorobenzamide using the above conditions did not afford the expected molecular complex **29**. Crystals of benzoic acid precipitated after a few days.

(Pentafluorobenzoic Acid)·(Pentafluorobenzamide), 31: A 1:1 mixture of benzoic pentafluorobenzoicacid (0.053 g, 0.25 mmol) and pentafluorobenzamide (0.052 g, 0.25 mmol) was dissolved in dioxane. Needle-shaped colorless crystals were obtained after few days at room temperature. M. p. 91°C.

X-Ray diffraction: Reflections were collected on Nonius Kappa and Smart Apex CCD diffractometers using incident X-ray radiation Mo-Kα (0.71073 Å). Crystals were cooled with an Oxford Cryosystem device attached to a CCD machine. Data reductions were performed using DENZO-SMN.11 Structures were solved by direct methods using SHELXS-97 and refined by full matrix least-squares refinement on F^2 with anisotropic displacement parameters for non-H atoms using SHELXL-97. In complex **26** H1A, H6A, and H3A atoms are fixed. Geometrical analysis was carried out in PLATON.

Method of powder XRD sample preparation: All the molecular complexes under study have been prepared by grinding the 1:1 mixture of their precursors in a mortar using pestle for 10–15 min. Samples were loaded in to a 10-millimetre aluminium sample holder.

Powder X-Ray diffraction: Powder data were collected on a Panalytical X'Pert Plus automated X-ray powder diffractometer with Cu Kα radiation. The computer programs Powder Cell 2.3 and X'Pert Plus was used for the calculation of X-ray powder patterns and the program X'Pert HighScore was used for the comparison of the powder patterns.

4.10 References

1. E.A. Meyer, R.K. Castellano and F. Diederich, *Angew. Chem., Int. Ed.,* **2003**, *42*, 1210.
2. C.R. Patrick and G.S. Prosser, *Nature,* **1960**, *187*, 1021.
3. J.H. Williams, J.K. Cockcroft and A.N. Fitch, *Angew. Chem., Int. Ed. Engl*., **1992**, *31*, 1655.
4. (a) T. Dahl, *Acta Chem. Scand*., **1971**, *25*, 1031. (b) T. Dahl, *Acta Chem. Scand*., **1972**, *26*, 1569. (c) T. Dahl, *Acta Chem. Scand.*, **1975**, *A29*, 170. (d) T. Dahl, *Acta Chem. Scand*., **1975**, *A29*, 699.

5. (a) G.R. Desiraju and A. Gavezzotti, *Acta Crystallogr.*, **1989**, *B45*, 473. (b) N. Boden, P.P. Davis, C.H. Stam and G.A. Wesselink, *Mol. Phys.*, **1973**, *25*, 81.
6. T. Dahl, *Acta Chem. Scand.*, **1973**, *27*, 995.
7. J.C. Collings, K.P. Roscoe, E.G. Robins, A.S. Batsanov, L.M. Stimson, J.A.K. Howard, S.J. Clarke and T.B. Marder, *New J. Chem.*, **2002**, *26*, 1740.
8. C.J. Aspley, C. Boxwell, M.L. Buil, C.L. Higgitt, C. Long and R.N. Perutz, *Chem. Commun.*, **1999**, 1027.
9. M.R. Battaglia, A.D. Buckingham and J.H. Williams, *Chem. Phys. Lett.*, **1981**, *78*, 421.
10. J. Potenza and D. Mastropaolo, *Acta Crystallogr.*, **1975**, *B31*, 2527.
11. J.C. Collings, K.P. Roscoe, R.L. Thomas, A.S. Batsanov, L.M. Stimson, J.A.K. Howard and T.B. Marder, *New J. Chem.*, **2001**, *25*, 1410.
12. (a) J.C. Collings, A.S. Batsanov, J.A.K. Howard and T.B. Marder, *Acta Crystallogr.*, 2001, *C57*, 870. (b) A.S. Batsanov, J.C. Collings, J.A.K. Howard, T.B. Marder and D.F. Perepichka, *Acta Crystallogr.*, **2001**, *C57*, 1306. (c) A.S. Batsanov, J.C. Collings, J.A.K. Howard and T.B. Marder, *Acta Crystallogr.*, **2001**, *E57*, o950. (d) J.C. Collings, A.S. Batsanov, J.A.K. Howard and T.B. Marder, *Cryst. Eng.*, **2002**, *5*, 37.
13. J.A.C. Clyburne, T. Hamilton and H.A. Jenkins, *Cryst. Eng.*, **2001**, *4*, 1.
14. I.Y. Bagryanskaya, Y.V. Gatilov, E. Lork, R. Mews, M.M. Shakirov, P.G. Watson and A.V. Zibarev, *J. Fluorine Chem.*, **2002**, *116*, 149.
15. (a) D.B. Amabilino and J.F. Stoddart, *Chem. Rev.,* **1995**, *95*, 2725. (b) L. Raehm, D.G. Hamilton and J.K.M. Sanders, *Synlett.,* **2002**, 1743.
16. A.F.M. Kilbinger and R.H. Grubbs, *Angew. Chem. Int. Ed.*, **2002**, *41*, 1563.
17. V.R. Vangala, A. Nangia and V.M. Lynch, *Chem. Commun.,* **2002**, 1304.
18. (a) G.W. Coates, A.R. Dunn, L.M. Henling, D.A. Dougherty and R.H. Grubbs, *Angew. Chem., Int. Ed. Engl.*, **1997**, *36*, 248. (b) G.W. Coates, A.R. Dunn, L.M. Henling, J.W. Ziller, E.B. Lobkovsky and R.H. Grubbs, *J. Am. Chem. Soc.*, **1998**, *120*, 3641.
19. M.J. Marsala, Z.-Q. Wang, R.J. Reid and K. Yoon, *Org. Lett.*, **2001**, *3*, 885.
20. (a) M.L. Renak, G.P. Bartholomeu, S. Wang, P.J. Ricatto, R.J. Lachicotte and G.C. Bazan, *J. Am. Chem. Soc*., **1999**, *121*, 7787. (b) W.J. Feast, P.W. Lovenlich, H. Puschmann and C. Taliani, *Chem. Commun*., **2001**, 505.

21. (a) C. Dai, P. Nguyen, T.B. Marder, A.J. Scott, W. Clegg and C. Viney, *Chem. Commun.*, **1999**, 2493. (b) M. Weck, A.R. Dunn, K. Matsumoto, G.W. Coates, E.B. Lobkovsky and R.H. Grubbs, *Angew. Chem., Int. Ed*., **1999**, *38*, 2741.
22. M.J. Aroney, T.W. Hambley, E. Patsalides, R.K. Pierens, H.-K. Chan and I. Gonda, *J. Chem. Soc., Perkin Trans. 2*, **1987**, 1747.
23. (a) S. Butterfield, P.R. Patel and M.L.Waters, *J. Am. Chem. Soc.*, **2002**, *124*, 9751. (b) G. Mathis and J. Hunziker, *Angew. Chem. Int. Ed*., **2002**, *41*, 3203. (c) K.A. Frey and S.A. Woski, *Chem. Commun.,* **2002**, 2206.
24. (a) B.R. Bhogala, P. Vishweshwar and A. Nangia, *Cryst.Growth Des.,* **2002**, *2*, 325. (b) V.S.S. Kumar, A. Nangia, A.K. Katz and H.L. Carrell, *Cryst. Growth Des.,* **2002**, *2*, 313. (c) V.S.S. Kumar, A. Nangia, M.T. Kirchner and R. Boese, *New J. Chem.,* **2003**, *27*, 224. (d) P. Vishweshwar, A. Nangia and V.M. Lynch, *Cryst. Growth Des.,* **2003**, *3*, 783. (e) C.B. Aakeröy, A.M. Beatty and B.A. Helfrich, *J. Am. Chem. Soc.,* **2002**, *124*, 14425.
25. A.P. West, Jr., S. Mecozzi and D.A. Dougherty, *J. Phys. Org.Chem.,* **1997**, *10*, 347. (b) J. Hernández-Trujillo, F. Colmenares, G. Cuevas and M. Costas, *Chem. Phys. Lett.,* **1997**, *265*, 503.(c) O.R. Lozman, R.J. Bushby and J.G. Vinter, *J. Chem. Soc., Perkin Trans. 2,* **2001**, 1446.
26. M.Gdaniec, W. Jankowski, M.J. Milewska and T. Połoński, *Angew. Chem. Int. Ed.*, **2003**, *42*, 3903.
27. R.K.R. Jetti, F. Xue T.C.W. Mak and A. Nangia, *J. Chem.Soc., Perkin Trans. 2,* **2000**, 1223.
28. W.H. Baur and D. Kassner, *Acta Crystallogr.* **1992**, *B48*, 356.
29. K. Kobayashi, A. Sato, S. Sakamoto and K. Yamaguchi, *J. Am.Chem. Soc.,* **2003**, *125*, 3035.
30. T.D. Petrova, V.E. Platonov, I.V. Kolesnikova, T.V. Ribalova, I.Yu. Bagryanskaya and Yu.V. Gatilov, *J. Fluorine Chem.*, **2000**, *103*, 63.
31. M.W. Day, A.J. Matzger and R.H. Grubbs, *Private Communication*, **2001**, CCDC No. 133768.
32. J. March, *Advanced Organic Chemistry. Reactions, Mechanisms and Structure*, 3rd ed.; Wiley: New York, **1985**, pp268-286.
33. L. Leiserowitz and A.T. Hagler, *Proc. R. Soc. London,* **1983**, *A388*, 133.

34. I. Weissbuch, V.Y. Torbeev, L. Leiserowitz and M. Lahav, *Angew. Chem. Int. Ed*., **2005**, *44*, 2.

35. (a) M.C. Etter and G.M. Frankenbach, *Chem. Mater.*, **1989**, *1*, 10. (b) F. Toda and H. Miyamoto, *Chem. Lett.*, **1995**, 861. (c) F. Toda, *Acc. Chem. Res.*, **1995**, *28*, 480. (d) V.R. Pedireddi, W. Jones, A.P. Chorlton and R. Docherty, *Chem. Commun.*, **1996**, 987. (e) K. Tanaka and F. Toda, *Chem. Rev.*, **2000**, *100*, 1025.

36. F. Toda, K. Tanaka and A. Sekikawa, *J. Chem. Soc., Chem. Commun.*, **1987**, 279.

37. M.C. Etter and D.A. Adsmond, *Chem. Commun*., **1990**, 589.

38. D. Braga and L. Maini, *Chem. Commun*., **2004**, 976.

39. N. Shan, F. Toda and W. Jones, *Chem. Commun*., **2002**, 2372.

40. (a) K.D.M. Harris, M. Tremayne, P. Lightfoot and P.G. Bruce, *J. Am. Chem. Soc.,* **1994**, *116*, 3543. (b) K.D.M. Harris, M. Tremayne and B.M. Kariuki, *Angew. Chem.*, *Int. Ed.,* **2001**, *40*, 1626. (c) K.D.M. Harris and E.Y. Cheung, *Chem. Soc. Rev.,* **2004**, *33*, 526. (d) C. Baerlocher and L.B. McCusker, *Z. Kristallogr.,* **2004**, *216,* 782.

41. (a) F. Takusagawa and A. Shimada, *Bull. Chem. Soc. Jpn.,* **1973**, *46*, 2998. (b) F. Mo and E. Adman, *Acta Crystallogr.,* **1975**, *B31*, 192. (c) S.H. Dale, M.R.J. Elsegood and A.E.L. Coombs, *CrystEngComm,* **2004**, *6*, 328.

42. F. Guo and K.D.M. Harris, *J. Am. Chem. Soc.*, **2005**, *127*, 7314.

43. D. Albesa-Jové, B.M. Kariuki, S. J. Kitchin, L. Grice, E. Y. Cheung and K.D.M. Harris, *ChemPhysChem*, **2004**, *5*, 414.

44. H. Nowell, N. Shan, J.P. Attfield, W. Jones and W.D.S. Motherwell, *Cryst. Eng*., **2003**, *6*, 57.

45. M.M. de Villiers, R.J. Terblanche, W. Liebenberg, E. Swanepoel, T.G. Dekker and M. Song, *J. Pharmaceut. Biomed. Anal.,* **2005**, *38*, 435.

46. V.S.S. Kumar, A. Addlagatta, A. Nangia, W.T. Robinson, C.K. Broder, R. Mondal, I.R. Evans, J.A.K. Howard and F.H. Allen, *Angew. Chem. Int. Ed.,* **2002**, *41*, 3848.

47. S. Roy, R. Banergee, A. Nagia and G.J. Kruger, *Chem. Eur. J.*, **2006**, (DOI: 10.1002/chem.200501417).

48. D. Albesa-Jové, B.M. Kariuki, S.J. Kitchin, L. Grice, E.Y. Cheung and K.D.M. Harris, *ChemPhysChem*, **2004**, *5*, 414.

49. (a) J.D. Dunitz and R. Taylor, *Chem. Eur. J.,* **1997**, *3*, 89. (b) J.A.K. Howard, V.J. Hoy, D. O'Hagan and G.T. Smith, *Tetrahedron,* **1996**, *52*, 12613.

CHAPTER 5

PHENAZINE AND ACRIDINE STACKS IN COCRYSTALS WITH MULTI-FUNCTIONAL MOLECULES

5.1 Introduction

Aryl-aryl interactions between aromatic moieties are particularly useful in crystal engineering and supramolecular chemistry and can be used to manipulate the organization of molecular components in the crystalline state.[1] Arene rings interact *via* edge-to-face geometry or herringbone T-motif, parallel-displaced geometry with lateral offset, and face-to-face or π-stacked sandwich geometry (Figure 1a). Unperturbed phenyl rings generally adopt the herringbone motif with major stabilization to the T-geometry arising from dipole-quadrupole interaction between the positively polarized hydrogen and the negatively charged π-cloud of the benzene ring. However, stacked structures become increasingly favorable with increasing arene size.[2] For example larger systems such as pyrene and coronene show an offset π-stacking with the hydrogens roughly over ring centers.[3] Molecular mechanics calculations on co-facial porphyrin dimers consistently predicted a perfectly stacked arrangement of the porphyrin rings, whereas experimental studies show an offset arrangement. In 1990, Hunter and Sanders proposed a simple model to describe the nature of π–π stacking geometry in porphyrins.[4] In this model the aromatic ring described as a positively charged σ-framework sandwiched between two regions of negatively charged π-electron density. The electrostatic interaction between such systems as a function of orientation is summarized in figure 1b. The offset stacked arrangement minimizes π-electron repulsion and maximizes the attraction between the σ-framework of one porphyrin with the π-electrons of the ring immediately below it. This model predicts that face-to-face π-stacked interactions will be disfavoured due to the dominance of π–π repulsion. However the offset π-stacked and edge-on or T-shaped geometries are favourable due to π–σ attractions.

Although π–π interactions are accepted as weak, they play an important role in peptide folding[5] and thermal stability of proteins.[6] DNA base stacking is important in determining structure and function,[7] aromatic interactions are widely used in template directed and asymmetric synthesis[8] and the properties of many crystalline solids are controlled by aromatic interactions that dictate the molecular organization.[9] There are

several examples of systems that form supramolecular arrays in solution by self association *via* π–π stacking interactions alone.[10] Kol and coworkers proved that planarity is not an obligatory requirement for achieving strong π-stacking, as long as complementarity between the stacking moieties can be achieved.[11] Many crystal structures of protein complexes with small molecules reveals aromatic interactions involving aromatic amino acid side chains of the receptor and/or aromatic and heteroaromatic rings of the ligands. For example Sussman *et al.*[12] developed a complex of the enzyme acetylcholinesterase (AChE) with the drug E2020 (Aricept) to treat Alzheimer's disease is stabilized by π–π stacking, O–H$\cdots\pi$ and cation$\cdots\pi$ interactions (Figure 2).

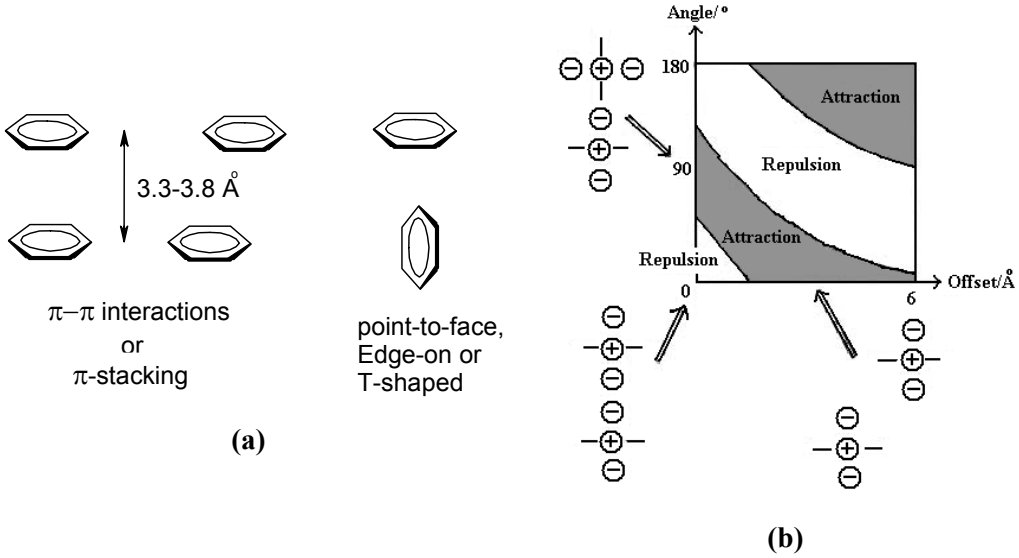

Figure 1. (a) Possible orientations of aryl-aryl interactions. (b) Electrostatic interactions between π-charge distributions as a function of orientation

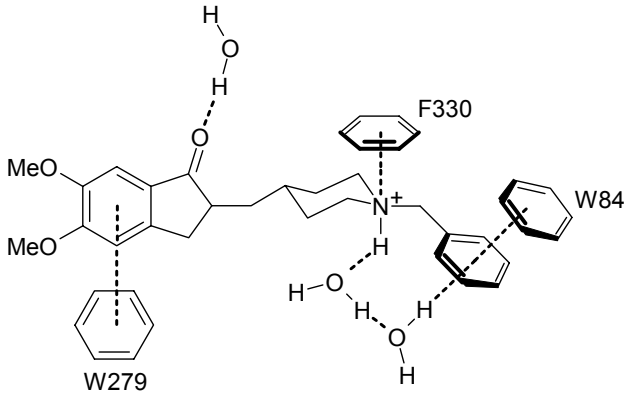

Figure 2. Binding mode of the anti-Alzheimer drug E2020 within the active site of acetylcholinesterase.

5.2 Aryl-aryl interactions in heterocyclic compounds

The polarization of aromatic systems, through the introduction of heteroatoms, electron-withdrawing groups or electron-donating groups, alters the nature of π–π interactions. Electron-donating substituent (e.g. NMe_2) increases the electron density associated with the ring, thereby increasing the π-electron repulsion. An electron-withdrawing substituent (e.g. NO_2) has the opposite effect (Figure 3). According to Hunter and Sanders model electron-deficient aromatic rings prefer stacking interactions over electron rich aromatic rings.[4] From aromatic hydrocarbon structures it is well known that π–π stacking becomes increasingly favorable with the number of connected arene rings.[13] Electrostatic attraction between atoms with positive or negative partial charges and the alignment of molecular dipoles become important in determining how two or more heterocyclic π systems interact. Christoph Janiak[14] did a Cambridge Structural Database (CSD) search on the geometry of π–π stacking interactions in metal complexes with aromatic nitrogen-containing ligands. He observed that perfect face-to-face π–π alignment is a rare phenomenon. The usual π interaction is an offset or slipped stacking, *i.e.* the rings are parallel displaced. Such a parallel displaced structure also has a contribution from π–σ attraction. He also concluded that the stability order of the stacking interaction in polarized aromatic π-system is π-deficient–π-deficient > π-deficient–π-rich > π-rich–π-rich.

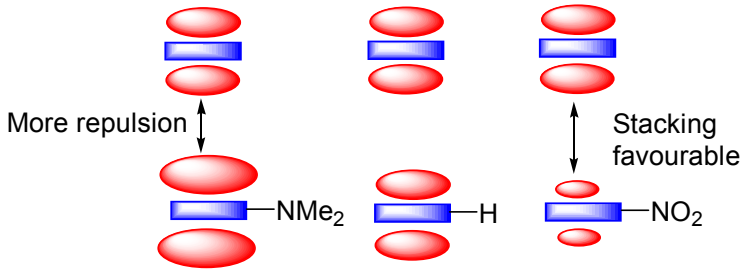

Figure 3. Schematic representation of the effect of substituents on stacking interaction.

5.3 Aryl-aryl stacking in multi-component systems

Stacking plays a significant role in crystal structures of heterocyclic compounds, aromatic compounds with larger rings and in the stabilization of multi-component strong hydrogen bonded systems. For example, Diederich and coworkers[15] have studied the complexation between a series of Rebek imides and 9-ethyladenine (Figure 4). They proposed that the host·guest complexes formed by receptors with amide linkers to the aromatic platform are generally more stable than those formed by receptors with ester

linkers. Lehn *et al*.[16] have studied the host-guest chemistry of 9,10-bis(2-aminopyrimidin-5-yl)anthracene (APA) and phenazine. Crystal structure reveals that APA molecules form a two dimensional 'pigeon-hole' lattice with channel size of about 7 Å *via* N–H···N hydrogen bonds involving amino-pyrimidine groups and phenazine is inserted between two anthracene units by stacking (Figure 5).

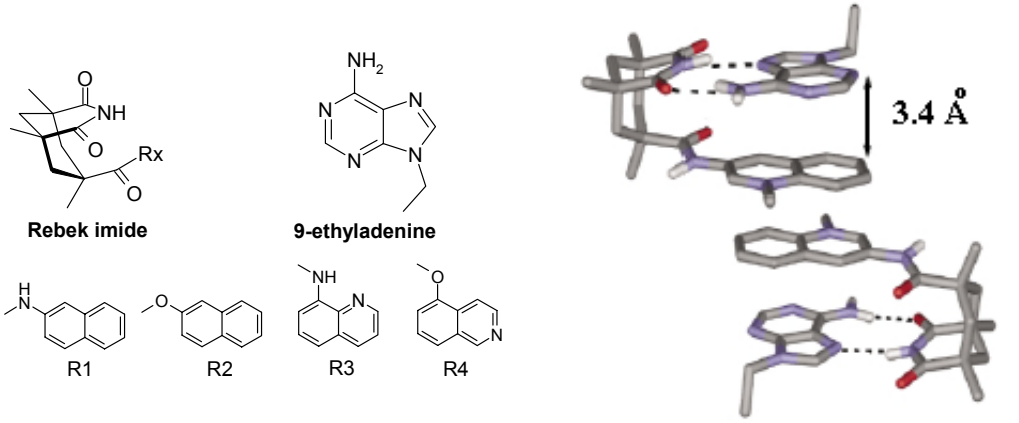

Figure 4. Crystal structure of cocrystal formed between 9-ethyladenine and Rebek imide with R4. Non-hydrogen bonding H-atoms are removed for clarity. Note the heterocyclic π–π stacking interactions (CSD refcode: ATEXOM).

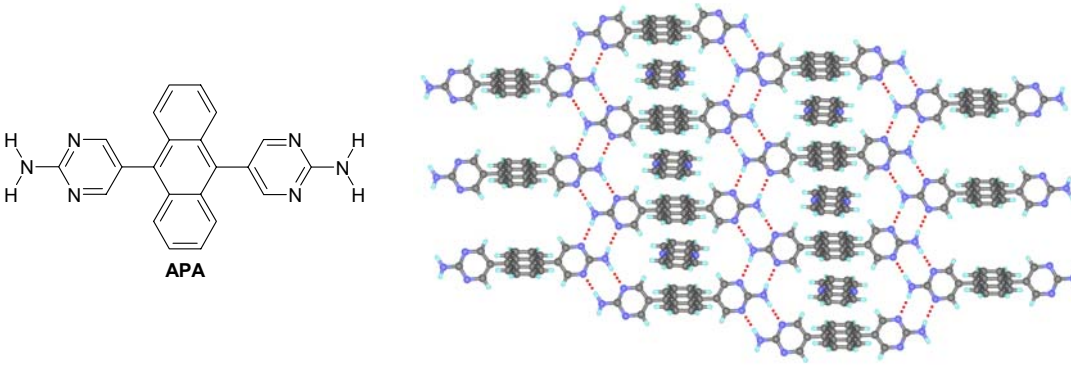

Figure 5. Two dimensional host-guest structure of **APA** and phenazine (CSD refcode: VIJVAL).

Resnati *et. al*.[17] used aryl-aryl stacking and halogen bonding together as a template to make stereoselective cyclobutane derivatives. Template (pentaerytritol derivative) adopts a conformation where couples of tetrafluorophenyl rings lie on the same side and are paired in a quasi-parallel fashion due to face-to-face π–π stacking interactions. Stacking brings the iodine atoms in the periphery of template to a distance of about 4 Å. Halogen bonding and

π–π stacking thus bring the olefin double bonds of *trans*-1,2-bis-(4-pyridyl)ethylene into close proximity, which is prerequisite for photochemical reaction. Irradiation of the cocrystal of template and olefin yields the *rctt* isomer of tetrakis(4-pyridyl)cyclobutane in quantitative yields (Figure 6).

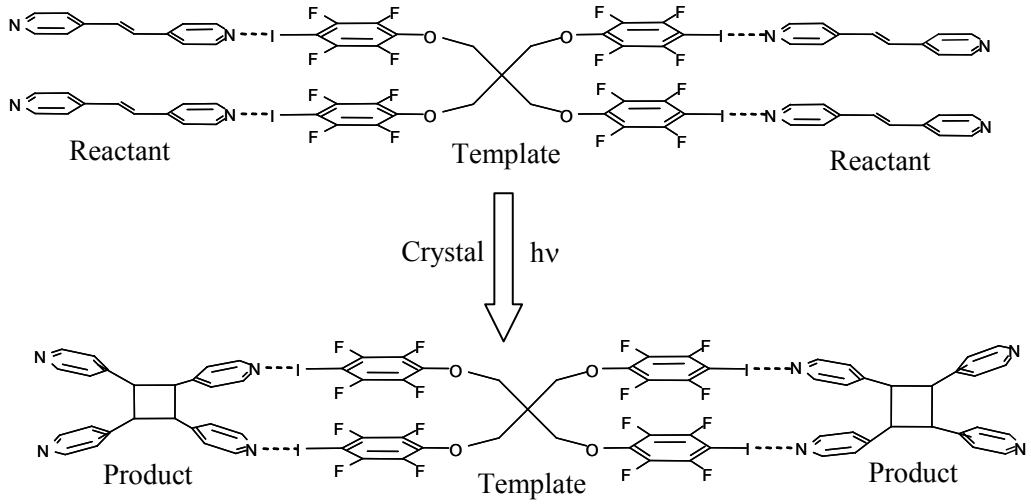

Figure 6. π–π stacking and halogen bonding mediated photochemical synthesis of tetrakis(4-pyridyl)cyclobutane.

5.4 Cocrystals of phenazine and acridine in literature

Phenazine and acridine are employed in many cocrystallization experiments, because of their ability to interact with cocrystal formers *via* stacking, hydrogen bonding and halogen bonding. Phenazine has been used in the design of charge-transfer complexes[18] and hydrogen bonded assemblies.[19] Phenazine based hydrogen bonded cocrystals are used in photochromic applications.[20] Recently Horiuchi *et al.* have developed new ferroelectric low molecular weight organic solids with cocrystals of phenazine with chloranilic acid or bromanilic acid, in which intermolecular O–H···N hydrogen bonds and stacking form supramolecular structure (Figure 7a).[21] Phenazine and chloranilic acid cocrystal has higher Curie temperature (*T*c = 253 K) and shows significant spontaneous polarization at low temperature as well as high dielectric constant (100 at room temperature). Phenazine is used as template to determine the crystal structure of tetrabromobutatriene because it does not readily form X-ray quality single crystals alone. In these cocrystals, each phenazine nitrogen atom involves in halogen bonding with bromine (3.05 Å, Figure 7b).[22] Boese *et al.*[23] synthesized a ternary cocrystal based on isomorphous replacement of phenazine with acridine. Phenazine forms 3:2 cocrystal with 2,2'-dihydroxybiphenyl instead of expected 1:1

cocrystal. In the crystal structure five molecular [3(phenazine):2(2,2'-dihyrdoxybiphenyl)] discrete aggregates were formed *via* O–H···N hydrogen bonds. Interestingly end phenazine molecules accept only one hydrogen bond although it has two N acceptors as shown in figure 7c. Based on this structure a 1:2:2 (phenazine: 2,2'-dihyrdoxybiphenyl:acridine) ternary cocrystal was designed where the terminal phenazine moieties were successfully replaced with acridine (Figure 7d).

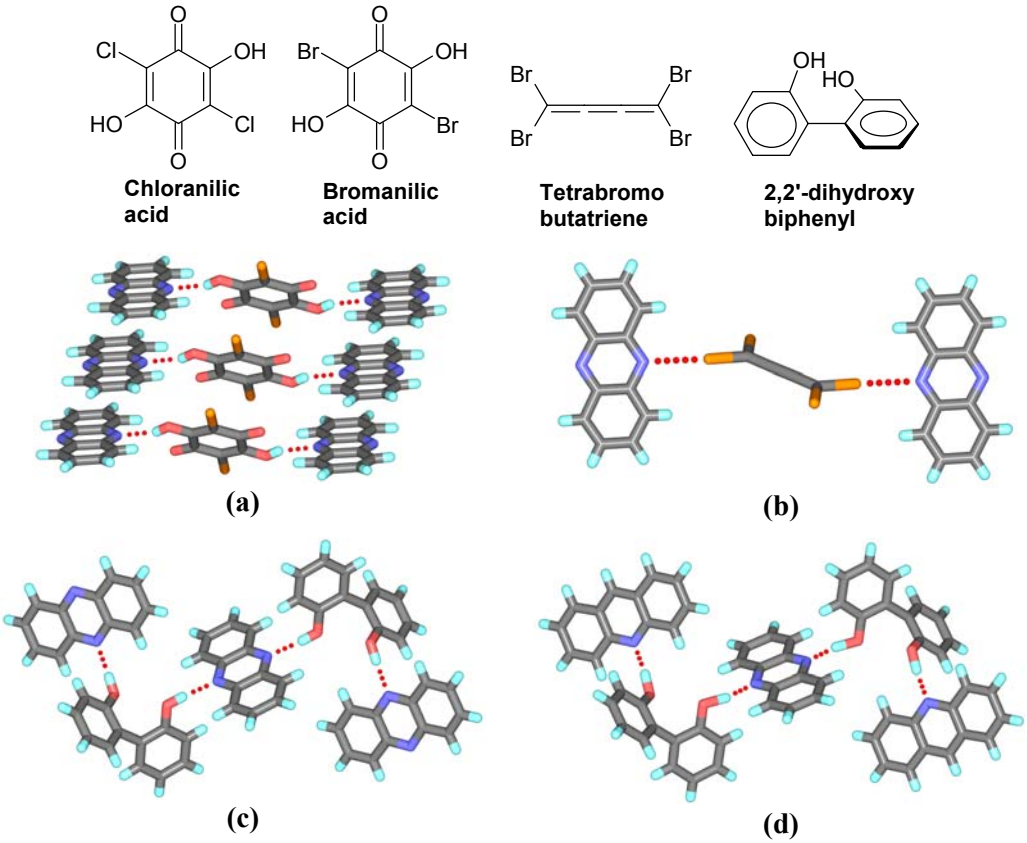

Figure 7. (a) O–H···N hydrogen bonds and stacking in 1:1 cocrystal of phenazine and broranilic acid (WIVDVA). (b) Halogen bond mediated cocrystallization of tetrabromobutatriene (FIHSOF). (c) O–H···N hydrogen bonds in 3:2 cocrystal of phenazine and 2,2'-dihyrdoxybiphenyl (MEFJAI). (d) Isomorphous replacement of end phenazine molecules with acridine in 1:2:2 ternary cocrystal (MEFJEM).

5.5 Results

With the background of chapter 4, where we have studied the robustness and reliability of Ph–Ph^F stacking synthon in presence of strong hydrogen functionalities like carboxylic acids and amides, and the applications of phenazine and acridine based cocrystals, cocrystallization of phenazine and acridine was attempted with multi-functional

molecules such as phloroglucinol (PG) and 3,5-dihydroxybenzoic acid (DHBA, Scheme 1). Crystallographic data of compounds studied in this chapter is given in appendix.

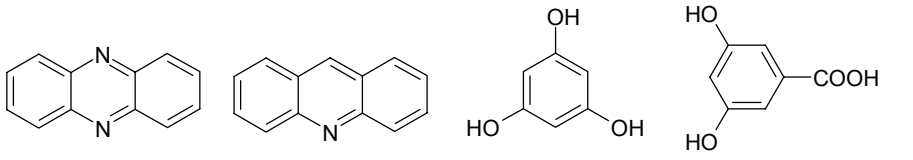

37 = 1:1.5 (PG:PHE)
38 = 2:3.5 (PG:PHE)
39 = 1:2:1 (PG:PHE:water)
40 = 0.5:1 (PG:PHE)
41 = 1:2 (PG:ACR)
42 = 1:1.5 (DHBA:PHE)
43 = 2:2:1 (DHBA:ACR:water)
44 = 1:3:1 (DHBA:ACR:acetonitrile)
45 = 1:3:1 (DHBA:ACR:ethanol)

Scheme 1. Cocrystals discussed in this chapter.

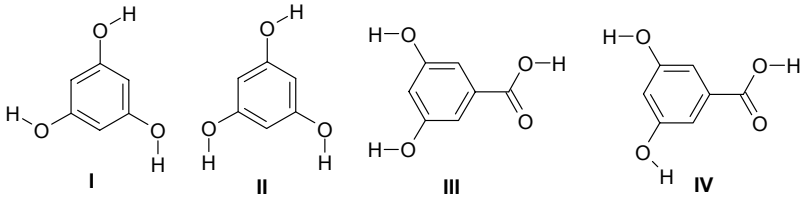

Scheme 2. Conformations of phloroglucinol and 3,5-dihydroxybenzoic acid.

Table 1. Hydrogen bond parameters of Cocrystals studied in this chapter.

Compound	Interaction[a]	*d* /(Å)	*D* /(Å)	*θ* /(°)
37	O1–H1···N2	1.81	2.785(2)	172.7
	O2–H2···N1	1.85	1.834(2)	177.0
	O3–H3···N3	1.89	2.873(2)	175.3
	C16–H16···O3	2.56	3.625(3)	167.6
38	O1–H1···N4	1.84	2.815(3)	173.7
	O2–H2···N1	1.82	2.801(3)	172.5
	O3–H3···N2	1.89	2.865(4)	169.3
	O4–H4···N5	1.84	2.778(4)	157.3
	O5–H5···N7	1.79	2.768(4)	174.7
	C7–H7···O1	2.35	3.291(4)	143.8
	C9–H9···N3	2.42	3.451(5)	159.0
	C11–H11···N6	2.62	3.591(6)	149.2
	C28–H28···O4	2.67	3.745(5)	174.4
	C33–H33···O3	2.57	3.594(4)	157.7
	C45–H45···O1	2.50	3.563(4)	167.1
	C46–H46···O5	2.67	3.690(5)	156.1
39	O1–H1···N3	1.97	2.949(4)	173.4
	O2–H2···N2	1.83	2.765(4)	158.3
	O3–H3···N4	1.86	2.842(4)	173.0
	O4–H4A···O2	1.92	2.893(4)	170.0

	O4–H4B···N1	1.95	2.934(4)	175.2
	C2–H2A···O4	2.50	3.562(4)	167.9
	C9–H9···O2	2.89	3.950(5)	164.9
	C15–H15···O4	2.51	3.513(5)	154.3
	C16–H16···O1	2.54	3.622(5)	174.2
	C27–H27···O1	2.56	3.533(5)	148.6
	C28–H28···O4	2.36	3.404(5)	160.6
40	O1–H1···N2	2.18	2.938(3)	132.6
	O2–H2···N1	1.79	2.769(3)	171.3
	C7–H7···O2	2.46	3.449(4)	151.5
	C8–H8···O2	2.43	3.468(4)	160.0
41	O1–H1···O2	1.75	2.726(5)	169.7
	O2–H2···N2	1.65	2.624(4)	169.9
	O3–H3···N1	1.74	2.703(5)	163.9
	C9–H9···O2	2.65	3.642(6)	151.8
	C15–H15···O3	2.70	3.707(5)	153.4
	C19–H19···O3	2.25	3.199(5)	144.9
	C29–H29···O2	2.66	3.680(5)	156.4
	C32–H32···O1	2.57	3.613(5)	161.1
42	O1–H1···N2	1.77	2.738(2)	169.6
	O3–H3···N1	1.84	2.818(2)	173.8
	O4–H4···N3	1.84	2.810(2)	169.2
	C3–H3···O3	2.34	3.408(2)	168.5
	C12–H12···O2	2.68	3.489(2)	131.0
	C16–H16···O2	2.43	3.507(2)	170.2
	C21–H21···O2	2.33	3.295(2)	147.9
43	O1–H7···O7	1.60	2.580(2)	171.3
	O5–H2A···N1	1.69	2.660(2)	166.4
	O9–H3A···O5	1.74	2.723(2)	174.2
	N2–H4···O7	1.73	2.723(2)	168.0
	O4–H5A···O9	1.65	2.630(2)	176.9
	O3–H6A···O6	1.76	2.710(2)	162.2
	O6–H7A···O8	1.62	2.604(2)	176.4
	O9–H8A···O3	1.84	2.769(2)	155.6
	C13–H13···O3	2.46	3.529(3)	168.8
	C15–H15···O9	2.54	3.609(3)	167.7
	C23–H23···O4	2.40	3.408(3)	154.1
	C26–H2···O8	2.60	3.577(3)	150.4
	C27–H27···O5	2.78	3.783(3)	154.1
44	O1–H1···N1	1.61	2.586(4)	172.9
	O3–H2···N3	1.85	2.837(4)	177.0
	O4–H4···N2	1.77	2.745(4)	169.3
	N4–H48A···N2	3.06	3.59(3)	113.4
	C7–H7···O4	2.89	3.858(4)	149.1
	C14–H14···O2	2.60	3.566(4)	147.5
	C17–H17···O4	2.66	3.741(5)	177.1
	C23–H23···O2	2.65	3.681(5)	159.7
	C23–H23···O2	2.63	3.625(5)	153.1
45	O1–H1···N2	1.59	2.5652(16)	172.9

O5–H5AA···O4	1.72	2.623(3)	150.3
O4–H2···N3	1.81	2.7851(19)	172.7
O3–H3···N1	1.72	2.6934(16)	171.7
C5–H5A···N3	2.82	3.8284(19)	154.2
C17–H17···O2	2.52	3.4569(19)	144.4
C25–H25···O3	2.56	3.593(2)	159.8
C31–H31···O3	2.55	3.5973(17)	161.3

5.6 Different stoichiometric cocrystals of phenazine and phloroglucinol, 37, 38, 39 and 40.

Cocrystals **37** and **38** are obtained concomitantly from the same conical flask (Figure 8), when 2:3 mixture of phloglucinol and phenazine was crystallized from ethylacetate at room temperature. Crystals were filtered and mother liquor was kept for crystallization again, cocrystal **39** was formed after complete evaporation of solvent. Cocrystallization experiment was repeated without filtering the crystals from mother liquor and allowed to complete evaporation of solvent resulted in only cocrystals **37** and **38**. When 1:1 PG and phenazine cocrystallization was attempted, corcystal **40** was resulted (Scheme 1). In all these cocrystals, PG molecule adopts the conformation where two hydroxy groups are pointing towards same side (Scheme 2, **II**) unlike its native structure and hence it has lost its trigonal molecular symmetry in the crystal lattice.

Cocrystal **37** crystallizes in monoclinic $P2_1/c$ space group with one molecule of PG and 1.5 molecules of phenazine in the asymmetric unit. One of the phenazine molecules is sitting on a special position, the inversion center. Three OH donors of PG interact with phenazine N acceptor *via* hydroxy···pyridine heterosynthon. Each PG molecule is linked to three phenazine molecules through O–H···N (1.80, 172.7, 1.85, 177.0, 1.89 Å, 175.3°) hydrogen bonds leading to a kind of tape structure parallel to (-102) plane (Figure 9a). In this tape phenazine molecules form a discrete three molecular stack (interplanar distance/centroid···centroid 3.55/4.19 Å) in ABA fashion (A and B are symmetry independent phenazine molecules) and these discrete stacks form continuous offset stacks. Phenazine rings interdigitate in the third dimension to achieve close packed structure *via* C–H···π (2.82 Å) interaction (Figure 9b). The overall crystal structure of cocrystal **38** (space group, *P*-1) is very similar to cocrystal **37** except small differences in the mode of hydrogen bonding and stacking. Because there is imbalance in number of strong hydrogen bond donors and acceptors one of the phenazine N acceptor forms weak C–H···N (2.41 Å, 159.0°) hydrogen bond. Phenazine molecules form two types of stacking as shown in figure 9c. One

is continuous stacked column, formed by two symmetry independent phenazine molecules (interplanar distance/centroid···centroid: A, B, 3.46/3.74 Å, 3.31/3.78Å) and the other is a two molecule discrete stack between symmetrically equivalent molecules (C, 3.36/3.74 Å). These discrete stacks are connected by another symmetry independent phenazine (D) molecule by herringbone interactions.

Cocrystal **39** solved and refined in triclinic *P*-1 space group with one molecule of PG, two molecules of phenazine and one water molecule in the asymmetric unit. PG accepts $O–H_w\cdots O_{PG}$ (1.92 Å, 170.0°) hydrogen bond and acts as tetrahydroxy benzene. Three OH groups of PG and water interacts with phenazine molecules *via* O–H···N (1.97, 173.4, 1.83, 158.3, 1.86, 173.0, 1.95 Å, 175.2°) hydrogen bonds leading to a tape like structure parallel to (0-12) plane. Adjacent tapes are connected by stacking between phenazine and weak C–H···O (2.56 Å, 148.6°) interaction to form the 2D layer (Figure 10a). Two symmetry independent phenazine molecules form different stacked columns (for A: 3.64/3.68 Å, 3.48/ 3.80 Å; for B: 3.45/3.79 Å, 3.43/3.98 Å) within a layer. Cocrystal **40** crystallizes in monoclinic space group *C*2/*c* with 0.5 molecule of PG, one molecules of phenazine in the asymmetric unit. PG molecule is sitting on 2-fold axis. One of the phenolic-H atoms is disordered over two positions. The one-, two- and three dimensional structures are very similar to **39** (Figure 10b). One dimensional adjacent tapes are connected through stacking between phenazine molecules along *c*-axis (3.46/3.63, 3.68/3.80) to form 2D layers. These layers interdigitate and form a close packed structure along *a*-axis.

An interesting feature of these crystal structures discussed above is that the three different kinds of interactions play an important role in the stabilization of one-, two- and three dimensional crystal lattices. As shown in figure 9a, hydrogen bonding in one direction, stacking in the perpendicular direction and the herringbone interactions (Figure 9b) in the third dimension stabilizes the crystal structure. Similar kind of situation is observed in the crystal structure of 9-(5-pyrimidinyl)anthracene·$Cd(NO_3)_2$·$2(CH_3OH)$, where metal coordination, hydrogen bonding and aromatic stacking interactions dominate in the formation of one-, two- and three-dimensional networks.[24]

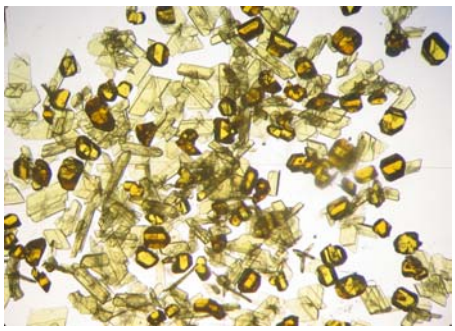

Figure 8. Concomitant cocrystals of **37** (dark yellow prisms) and **38** (pale yellow plates).

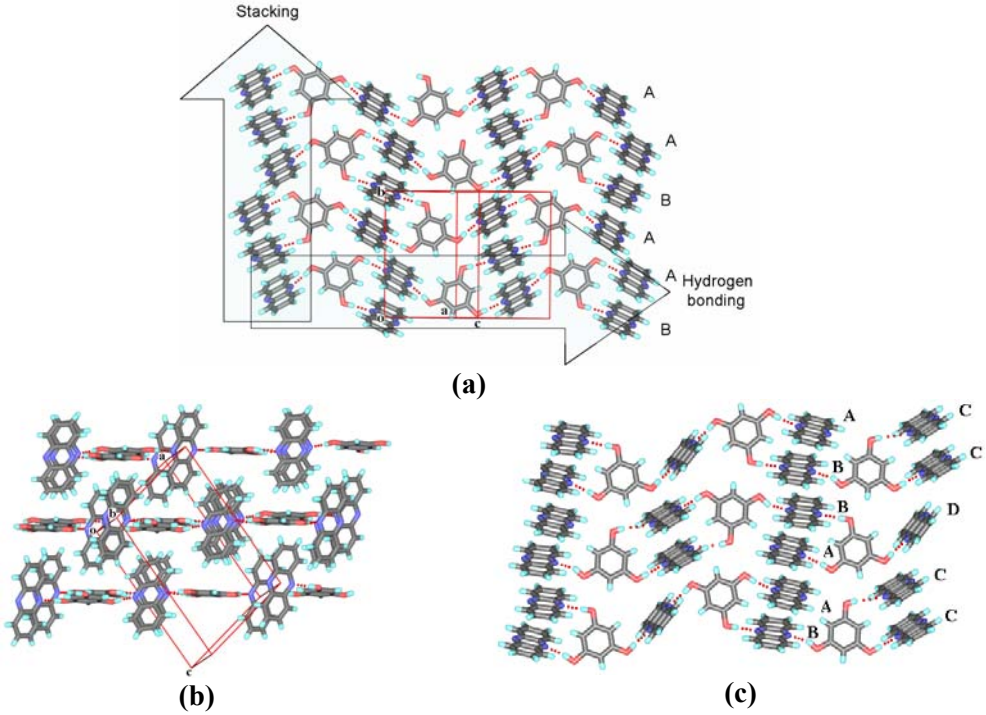

Figure 9. (a) O–H···N hydrogen bonds in layered like two dimensional structure parallel to (-102) plane of **37.** (b) View down *b*-axis. (c) Crystal structure of **38**, O–H···N layer like two dimensional structure in (112) plane.

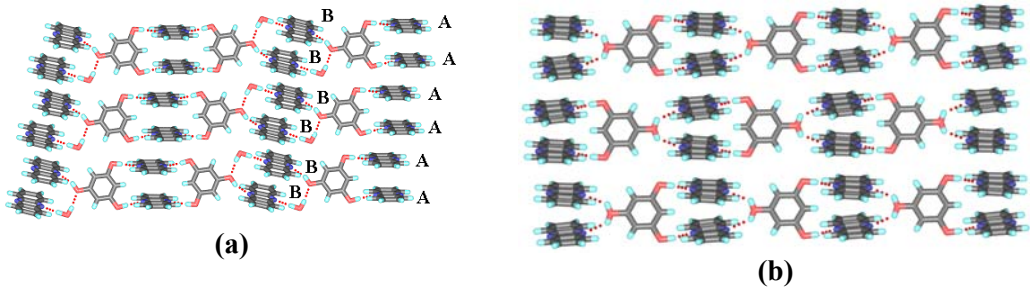

Figure 10. (a) O–H···N, O_w–H···N and O_w–H···O hydrogen bonds mediated layer like two dimensional structure in (0-12) plane in **39**. (b) O–H···N and stacking mediated layered structure along *bc*-plane in **40.**

All these crystal structure of can be compared with cocrystals of phenazine with hydroquinone, 4,4'-dihydroxybiphenyl and 1,5-dihydroxynaphthalene in terms of hydrogen bonding and stacking. Phenazine forms 2:1 cocrystals with hydroquinone and 1,5-dihydroxynaphthalene and 3:1 cocrystals with 4,4'-dihydroxybiphenyl instead of expected 1:1 cocrystals.[25] In these crystals structures also, like structures discussed above three different interactions dominate in three dimensions of crystal lattice. For example in 2:1 cocrystal of phenazine and hydroquinone, both O–H···N and weak C–H···N hydrogen bonds dominate along *a*-axis leading to a tape like structure and these tapes are connected by stacking of phenazine moieties in the perpendicular direction (Figure 11a). Herringbone interactions stabilize the third dimension of the crystal structure (Figure 11b).

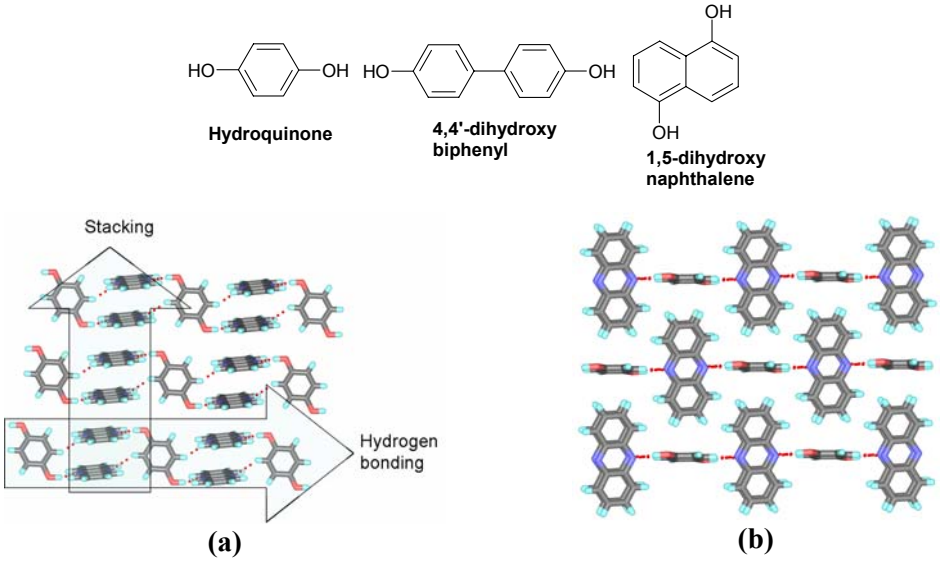

Figure 11. (a) O–H···N, C–H···N hydrogen bonds along *a*-axis and stacking interactions in perpendicular direction in 2:1 cocrystal of phenazine and hydroquinone (FOQHEY). (b) View down *a*-axis, Note that only herringbone interactions in the third dimension.

5.7 Crystal structure of 1:2 cocrystal of phloroglucinol and acridine, 41

Cocrystals of 1:2 (PG:ACR) were formed, when the cocrystallization was set up1:3 ratio of components. It crystallizes in orthorhombic $Pca2_1$ space group with one molecule of PG and two molecules of acridine in the asymmetric unit. PG adopts the conformation similar to that observed in cocrystals of phenazine. One of three phenolic–OH protons is fixed. Two of three –OH groups of PG act as O–H···N (1.65, 169.9, 1.74 Å, 163.9°) hydrogen bond donors and the other form O–H···O (1.75 Å, 169.7°) along *c*-axis leading to one dimensional tapes (Figure 12a). Adjacent tapes are connected by stacking acridine

molecules (3.60/3.83 Å, 3.37/3.76Å) to form layered structure. In this cocrystal both hydrogen bonded tapes and stacking columns are in the same direction unlike PG and phenazine complexes. Adjacent layers are interdigitated along *b*-axis to achieve close packing (Figure 12b).

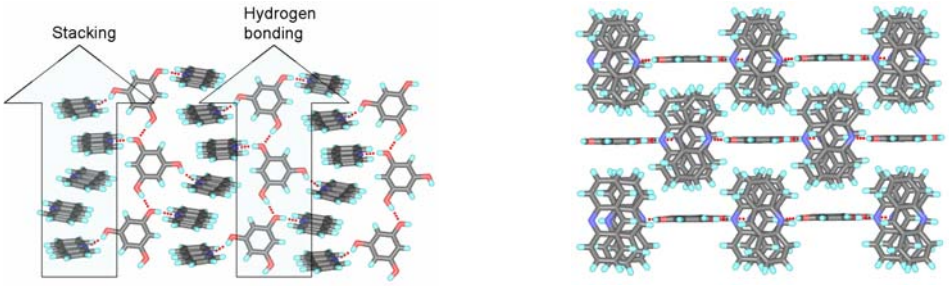

Figure 12. (a) O–H···N, O–H···O and stacking interactions along *c*-axis. (b) View down *b*-axis, Notice the stacking and interdigitated acridine molecules in the third dimension.

5.8 Crystal structure of 1:1.5 cocrystal of 3,5-dihydroxybenzoic acid and phenazine, 42

It crystallizes in monoclinic space group *C*2/*c* with one molecule of 3,5-dihydoxybenzoic acid and 1.5 molecules of phenazine in the asymmetric unit. The phenolic-OH groups of DHBA are projecting on the same side (scheme 2, **III**). Two hydroxy groups and acid group act as O–H···N (1.76, 169.6, 1.84, 173.8, 1.84 Å, 169.2°) hydrogen bond donors and two N atoms in phenazine act as an O–H···N acceptors to form tape structure. Adjacent tapes are connected *via* stacking of phenazine molecules (3.55/3.86 Å, 3.56/3.86 Å) to form 2D layers (Figure 13a) in *ac*-plane and these layers are interdigitated to form 3D close packed structure (Figure 13b). Interestingly the strong acid carbonyl acceptor is not involved in any kind of hydrogen bonding. In this structure, like in cocrystals **37**, **38**, **39** and **40**, hydrogen bonding, stacking and herringbone interactions dominate in one-, two- and three dimensional networks.

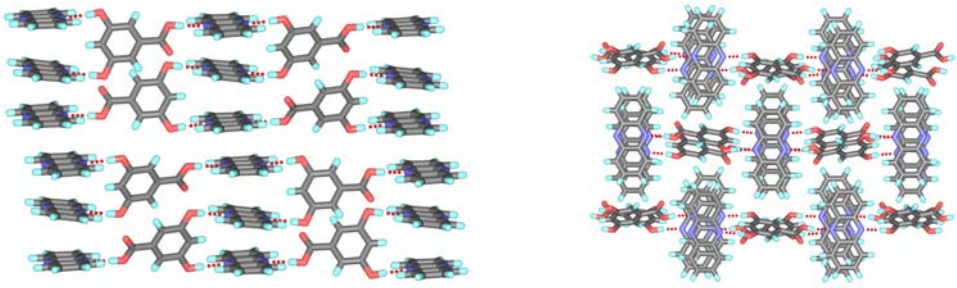

Figure 13. (a) O–H···N and stacking layers along a*c*-plane (b) View down *a*-axis, Notice the stacking and interdigitated phenazine molecules in the third dimension.

5.9 Stacking and host-guest chemistry in cocrystals of acridine and 3,5-dihydroxybenzoic acid

5.9.1 Crystal structure of 2:2:1 (ACR:DHBA:H_2O) cocrystal, 43

It crystallizes in non-centrosymmetric space group $Pna2_1$ with two molecules each of 3,5-dihydroxybenzoic acid and acridine moieties and one water molecule. One of the acids transfers its proton to acridine N atom. Carboxylate, carboxylic acid and water together form a three dimensional hexagonal channel network *via* strong O–H···O^- and O–H···O hydrogen bonds with channel internal dimensions of 10 × 14 $Å^2$ (Figure 14a). These hexagonal channels are filled by protonated and unprotonated acridine infinite stacked columns (3.48/3.68 Å, 3.45/3.81 Å) as guest (Figures 14b, 14c). Phenolic-OH groups of both 3,5-dihydroxybenzoic acid and cabroxylate molecules are projecting towards different sides (Scheme 2, **IV**). The opposite walls of hexagonal channel are formed by carboxylic acid-water and carboxylate-water hydrogen bonding. One of the phenolic –OH of carboxylate form O_{phe}–H···O^- (1.62 Å, 176.2°) with another screw axis related carboxylate, while the other OH donor form O_{phe}–H···N (1.69 Å, 166.6°) with acridine acceptor. The carboxylate group also accepts O_{acid}–H···O^-, O_w–H···O_{phe} and N^+–H···O^- (1.60, 171.3, 1.74, 174.2, 1.72 Å, 168.0°) hydrogen bonds. Neutral carboxylic acid participates in O_{phe}–H···O_w, O_{phe}–H···O_{phe} and O_w–H···O_{phe} (1.65, 176.9, 1.76, 162.2, 1.84 Å, 155.6°) hydrogen bonds. Similar structures of nitrilotri(methylphoshponic acid) with 1,7-phenanthroline, 1,10-phenanthroline and acridine were reported by Clearfield and coworkers.[26] In the crystal structure of **46** one of the acridine molecules is protonated. Nitrilotri(methylphoshponic acid) forms a three dimensional hexagonal lattice *via* very strong O–H···O^- hydrogen bonds with internal dimension of the hexagon 8.3 × 12.3 $Å^2$. Neutral acridine molecules stack with protonated acridines in such a way that every third molecule in the stacked column is a neutral acridine and these stacked columns fill the hexagonal channels as guest (Figure 14d).

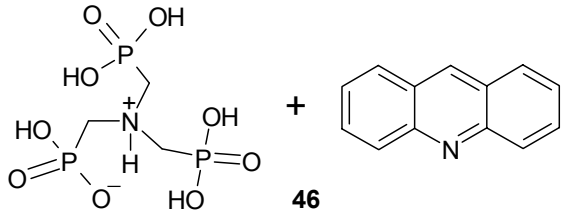

46

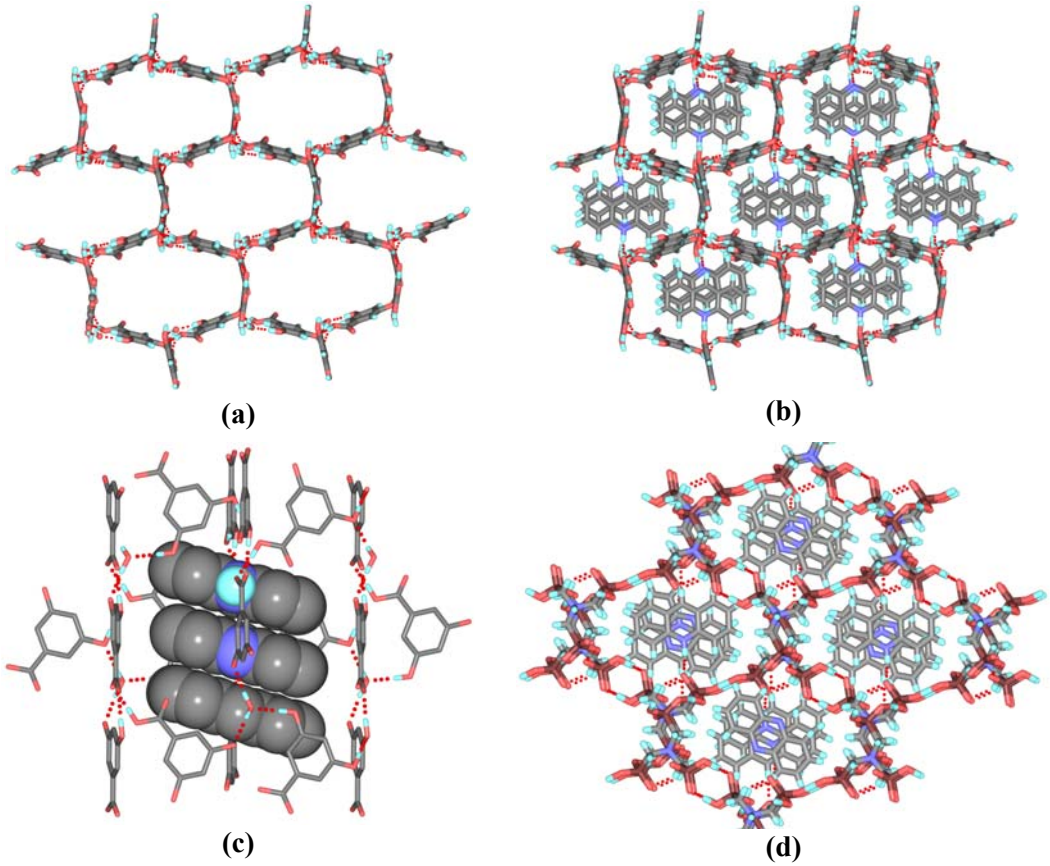

Figure 14. (a) Hexagonal channel formed by carboxylic acid and water molecules down the *a*-axis. (b) Acridine stacked columns fill the hexagonal channels as guest. (c) Acridine stacked column along *a*-axis non-hydrogen bonding hydrogen atoms are removed for clarity. (d) Hexagonal channels formed by phosphonic acid moieties are filled by acridine stacked columns in **46** (GUMKAA). Note that one of the acridine nitrogen atoms is disordered over two positions and looks like phenazine in the figure.

5.9.2 1:3 Cocrystals of 3,5-dihydroxybenzoic acid and acridine, 44 and 45

When 1:3 mixture of acridine and 3,5-dihydroxybenzoic acid was crystallized from the mixture acetonitrile and methanol (1:1) solvents, within two hours crystals of **44** were precipitated. Ethanol was included in the crystal lattice when above mixture was recrystallized from ethanol (cocrystal **45**). All three structures have the similar host network.

In cocrystal **44** (space group $P2_1/c$), 3:1 acridine and DHBA crystallizes with disordered acetonitrile solvent sitting on special position. Both acidic and phenolic-OH donors interact with three acridine molecules *via* acid···pyridine and hydroxy···pyridine heterostnthons (1.61, 172.9, 1.85, 177.0, 1.77 Å, 169.3°) to form a four molecular discrete trigonal motif (Figure 15a). These trigonal motifs interact *via* stacking and herringbone interactions of acridine molecules to form two dimensional layered structure, which

generates cavities of 7 × 9 $Å^2$ between two trigonal motifs (Figure 15b). These cavities are filled by disordered acetonitrile solvent with C–H···π interaction (Figure 15c). Cocrystals **45** also form similar two dimensional host network as described above but guest interact with O–H···O hydrogen bonds instead of C–H···π interaction in **44** (Figure 15d).

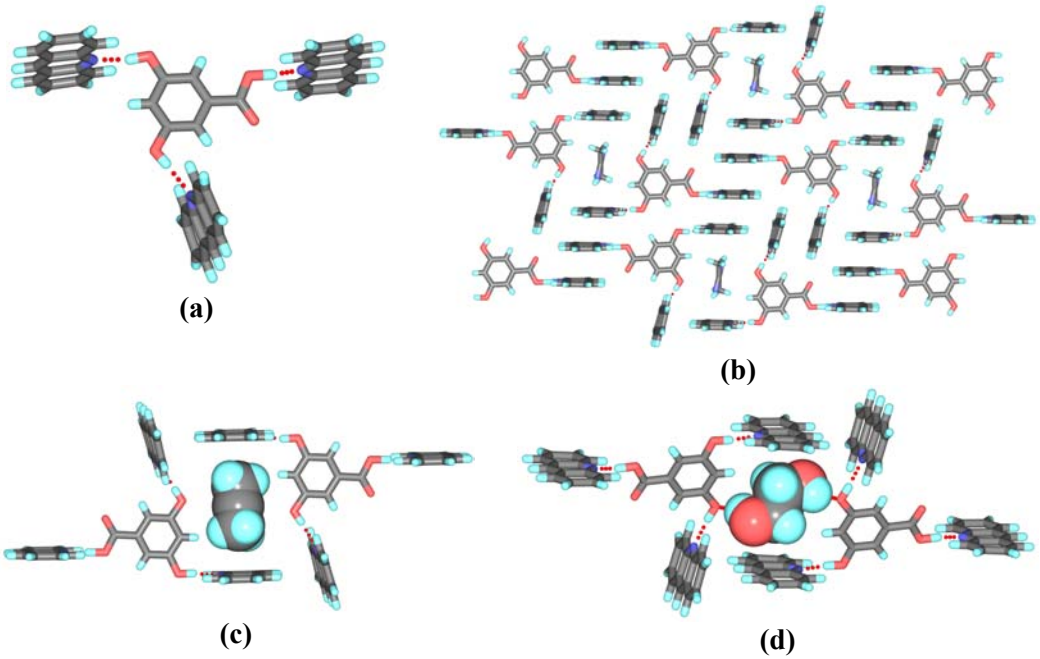

Figure 15. (a) Four molecular trigonal motif formed by acid···pyridine and hydroxy···pyridine synthons in 3:1 cocrystals. (b) 2D layered host-quest structure of acetonitrile solvate, **44**. (c) Disordered acetonitrile in the cavity of **44**. (d) Disordered ethanol solvent in the cavity of **45**.

5.10 Conclusions

From all structures studied above following conclusions can be drawn. (i) Crystal structures **37-40** and **42** show a remarkable cooperation of hydrogen bonding, aromatic stacking and herringbone interactions in the formation of one-, two- and three-dimensional network crystal structures. Similar interactions and packing is present in other phenazine cocrystals with dihydroxy aryl compounds indicate the crystal structure is robust. (ii) PG adopts –OH group conformation **II** unlike in its native structure indicates that stacking may be driving the conformation of PG molecule in all these crystal structures, because conformation **II** is favourable for stacking interactions. (iii) Melting points of all four phenzine and PG cocrystals are in the same range, which is indication of similar one-, two and three-dimensional crystal structure. (iv) Although there are significant variations in hydrogen bonding donors and molecular shape the consistent formation of phenazine and

acridine stacking suggests that these stacks can be used in the reliable assembly of desired structures.

5.11 Experimental Section:

Cocrystallization: All cocrystallization experiments were carried out by slow evaporation of solvent at room temperature. Melting points were recorded onset temperature of differential scanning calorimetry (DSC).

Cocrystals 37, 38 and 39: Grounded mixture of phloroglucinol (58.5 mg, 0.36 mmol) and phenazine (97 mg, 0.54 mmol) was crystallized from ethylacetate at room temperature. Cocrystals **37** and **38** are obtained concomitantly from same conical flask within two days. Crystals were filtered and mother liquor was kept for crystallization again, cocrystal **39** was formed after complete evaporation of solvent. Melting points of **37**, **38** and **39** are 241, 240, 241 °C respectively.

Cocrystal 40: When 1:1 grounded mixture of phloroglucinol (58.5 mg, 0.36 mmol) and phenazine (64.8 mg, 0.36 mmol) was crystallized from ethylacetate at room temperature, cocrystals of **40** resulted. M. p. 237 °C.

Cocrystal 41: Mixture of phloroglucinol (29.2 mg, 0.18 mmol) and acridine (96 mg, 0.54 mmol) was recrystallized from methanol, but 1:2 cocrystals **41** formed at room temperature. M. p. 222 °C.

Cocrystal 42: Grounded mixture of phenazine (97.2mg, 0.54 mmol) and 3,5-dihydroxybenzoic acid (56 mg, 0.36 mmol) was dissolved in methanol and allowed to evaporate at room temperature, yellow blocks were formed in about 5 days. M. p. 238 °C.

Cocrystal 43: Acridine (64 mg, 0.36 mmol) and 3,5-dihydroxybenzoic acid (56 mg, 0.36 mmol) was crystallized from methanol. M. p. 222 °C.

Cocrystals 44 and 45: When grounded mixture of acridine (96 mg, 0.54 mmol) and 3,5-dihydroxybenzoic acid (28 mg, 0.18 mmol) was crystallized from the mixture acetonitrile and methanol (1:1) solvents, within two hours crystals of **44** were precipitated. Cocrystals **45** formed when above mixture was crystallized from ethanol.

5.12 References

1. C. A. Hunter, K. R. Lawson, J. Perkins and C. J. Urch, *J. Chem. Soc., Perkin Trans. 2*, **2001**, 651.
2. R. Goddard, M. W. Haenel, W. C. Herndon, C. Krüger and M. Zander, *J. Am. Chem. Soc.*, **1995**, *117*, 30.

3. (a) G.R. Desiraju and A. Gavezzotti, *J. Chem. Soc.*, *Chem. Commun.*, **1989**, 621. (b) A. Gavezzotti and G.R. Desiraju, *Acta Crystallogr.*, **1988**, *A44*, 427.
4. C.A. Hunter and J.K.M. Sanders, *J. Am. Chem. Soc*., **1990**, *112*, 5525.
5. R. Bhattacharyya, U. Samanta and P. Chakrabarti, *Protein Eng*., **2002**, *15*, 91.
6. N. Kannan and S. Vishveshwara, *Protein Eng.*, **2000**, *13*, 753.
7. (a) W. Saenger, *Principles of Nucleic Acid Structure*; Springer-Verlag: New York, **1988**. (b) C.A. Hunter, *J. Mol. Biol.,* **1993**, *230*, 1025. (c) R.L. Eoof, T.L. Spurling and K.D. Raney, *Biochemistry* **2005**, *44*, 666.
8. (a) D.B. Amabilino and J.F. Stoddart, *Chem. Rev.,* **1995**, *95*, 2725. (b) H.C. Kolb, P.G. Andersson and K.B. Sharpless, *J. Am. Chem. Soc.,* **1994**, *116*, 1278.
9. M. Weck, A.R. Dunn, K. Matsumoto, G.W. Coates, E.B. Lobkovsky and R.H. Grubbs, *Angew. Chem., Int. Ed.,* **1999**, *38*, 2741.
10. (a) A.S. Shetty, J. Zhang and J.S. Moore, *J. Am. Chem. Soc.*, **1996**, *118*, 1019. (*b*) E. Ishow, A. Gourdon and J.-P. Launay, *Chem. Commun.*, **1998**, 1909. (c) E. Ishow, A. Gourdon, J.-P. Launay, C. Chiorboli and F. Scandola, *Inorg. Chem.*, **1999**, *38*, 1504. (d) K. R. Koch, C. Sacht and C. Lawrence, *J. Chem. Soc., Dalton Trans.*, **1998**, 689. (e) K. Nakamura, H. Okubo and M. Yamaguchi, *Org. Lett.*, **2001**, *3*, 1097.
11. S.D. Bergman, D. Reshef, S. Groysman, I. Goldberg and M. Kol, *Chem. Commun*., **2002**, 2374.
12. (a) G. Kryger, I. Silman and J.L. Sussman, *J. Physiol.,* **1998**, *92*, 191. (b) G. Kryger, I. Silman and J.L. Sussman, *Structure,* **1999**, *7*, 297.
13. R. Goddard, M. W. Haenel, W. C. Herndon, C. Krüger and M. Zander, *J. Am. Chem. Soc.*, **1995**, *117*, 30.
14. C. Janiak, *J. Chem. Soc*., *Dalton Trans*., **2000**, 3885.
15. R. Faraoni, R.K. Castellano, V. Gramlich and F. Diederich, *Chem. Commun*., **2004**, 370.
16. M.J. Krische, J.-M. Lehn, N. Kyritsakas, J. Fischer, E.K. Wegelius and K. Rissanen, *Tetrahedron*, **2000**, *56*, 6701.
17. T. Caronna, R. Liantonio, T.A. Logothetis, P. Metrangolo, T. Pilati, G. Resnati, *J. Am. Chem. Soc*., **2004**, *126*, 4500.
18. (a) N. Karl, W. Ketterer and J.J. Stezowski, *Acta Crystallogr.,* **1982**, *B38*, 2917. (b) C.V.K. Sharma and R. D. Rogers, *Cryst. Eng.*, **1998**, *1*, 139.

19. (a) V.R. Pedireddi, W. Jones, A.P. Chorlton and R. Docherty, *Chem. Commun.*, **1996**, 997. (b) E. Batchelor, J. Klinowski and W. Jones, *J. Mater. Chem.*, **2000**, *10*, 839.
20. (a) T. Smolka, R. Sustmann and R. Boese, *J. Prakt. Chem.*, **1999**, *341*, 378.
21. S. Horiuchi, F. Ishii, R. Kumai, Y. Okimoto, H. Tachibana, N. Nagaosa and Y. Tokura, *Nat. Mater.,* **2005**, *4*, 163.
22. P.-H. Liu, L. Li, J.A. Webb, Y. Zhang and N.S. Goroff, *Org. Lett*., **2004**, *6*, 2081.
23. T. Smolka, R. Boese and R. Sustmann, *Struct. Chem.*, **1999**, *10*, 429.
24. T. Ezuhara, K. Endo, O. Hayashida and Y. Aoyama, *New J. Chem*., **1998**, 183.
25. V.R. Thalladi, T. Smolka, R. Boese and R. Sustmann, *CrystEngComm*, **2000**, 17.
26. C.V.K. Sarma and A. Clearfield, *J. Am. Chem. Soc*., **2000**, *122*, 4349.

CHAPTER 6

CARBOXAMIDE···*N*-OXIDE HETEROSYNTHON AND ITS APPLICATION IN COCRYSTAL DESIGN

6.1 Introduction

Currently there is an intense interest in the systematic engineering of crystalline organic solids, in which careful control of the packing arrangements of the individual components leads to desirable macroscopic properties. The successful construction of a particular supramolecular motif is not an easy goal and requires a complete understanding of the nature and strength of intermolecular interactions. The key requirement in the development of crystal engineering strategies is the availability of reliable supramolecular synthons, which in turn is judged from the frequency of occurrence of the recognition pattern in the Cambridge Structural Database (CSD).[1] As discussed in chapter 1, supramolecular synthons are classified as homosynthons and heterosynthons based on the interacting complementary functional groups being the same or different. Heterosynthons are generally more robust than homosynthons. Robustness is defined as the ability of synthon to withstand changes in molecular shape, substituent groups, competition from other intermolecular interactions and solvents. For example, Steiner[2] studied the formation of hydrogen bonds by carboxylic acid and other functional groups and found that only 33% of all carboxylic acid groups in crystals form the acid dimer and 2.8% form catemer. The remaining 64% form hydrogen bonds with a variety of acceptors such as oxygen and nitrogen atoms. The success rate of strongest acceptors like COO^-, P=O, pyridyl N and F^- for carboxylic acid donor was found to be over 90%. Water is also a very strong competitor with a success rate of 84%. These studies indicate that carboxylic acid dimer can be engineered only in the absence of successful competitors. For example, when pyridyl N atom is present as a competitor, it is much more likely that a carboxylic acid···pyridine heterosynthon is formed (91%) than a carboxylic acid dimer or catemer. CSD study of supramolecular synthons involving primary amides by Zaworotko and cowokers have shown that 84% form amide···amide dimers and 14% form catemers in the absence of competing hydrogen bond donors/acceptors. When there are competing groups such as carboxylic acid, secondary amide, aminopyridine, pyridine, water, alcohol, amines, carbonyl, ether, ester, cyano, nitro, chloride ion and bromide ion, the formation of

amide···amide dimer and catemer is 35% and 18% respectively.[3] When only carboxylic acid and primary amide functionalities are present in the system formation of acid···amide heterosynthon (47%) is favoured over acid···acid (6%) and amide···amide (44%) homosynthons.

6.2 Heterosynthons in crystal engineering

Heterosynthons are well exploited in crystal engineering because of their strength and probability of formation. Acid···pyridine, phenol···pyridine, phenol···amine and acid···amide recognitions are some of the strong hydrogen bonded heterosynthons recently used in the construction of novel network structures, high yielding supramolecular reactions, synthesis of laderanes and API cocrystals. Zaworotko and coworkers[4] have identified a new 2-aminopyridine···carboxylic acid supramolecular heterosynthon and exploited in cocrystallization of 2-aminopyridine and 2-amino-5-methylpyridine with different carboxylic acids. They also performed a CSD search and found that 2-aminopyridine···carboxylic acid heterosynthon has 77% probability of formation of compounds containing both 2-aminopyridine and carboxylic acid moieties and the occurrence of heterosynthon increases to 97% in the absence of other competing functionalities.

6.3 Heterosynthons in pharmaceutical cocrystals

There is a considerable interest in recent years on pharmaceutical cocrystallization because API cocrystals may be a possible alternative to polymorphs, salts and solvates in the modification of an active pharmaceutical ingredient (API) in dosage forms.[5] Solvates or hydrates are less stable forms because of high mobility and vapour pressure of solvents when compared to cocrystals. Desolvation or dehydration may lead to amorphous compounds, which are less chemically stable and can crystallize into less soluble forms. In contrast, most cocrystal formers are unlikely to evaporate from solid dosage forms, making phase separation and other physical changes less likely. The other problem of great importance in pharmaceutical industry is polymorphism of drugs. Cocrystals are less prone to be polymorphic because of strong hydrogen bond recognition between components involved in cocrystallization. Pharmaceutical cocrystals are defined as hydrogen-bonded complexes between an API and a benign solid component. The novel crystalline phases are being developed for superior efficacy, solubility and stability in drug formulation.[6] Traditionally, cocrystallization has involved robust supramolecular synthons with strong interactions. Application of crystal engineering approach to make pharmaceutical cocrystals

can be traced from the work of Whitesides *et al.* on substituted barbituric acid and melamine derivatives to generate supramolecular linear tape, crinkled tape and rosette motifs sustained by robust three-point N–H···O and N–H···N hydrogen bonds (Figure 1).[7] But the focus of those cocrystals was not the physical properties but the supramolecular complementarity of barbitals with melamine.

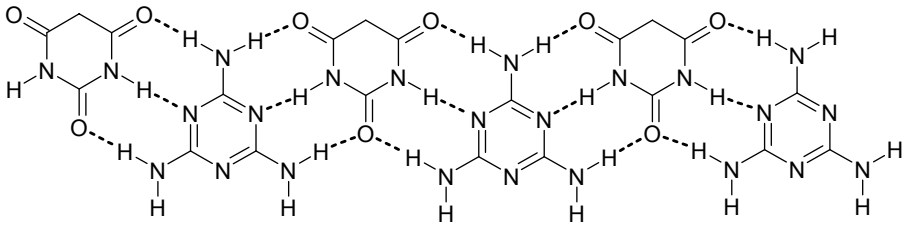

Figure 1. N–H···O and N–H···N hydrogen bonds in 1:1 cocrystal of barbituric acid and melamine.

Robust acid···pyridine heterosynthon (Scheme 1) is successfully used in the synthesis of model API cocrystals.[6a] Remenar and coworker[8] have used acid···pyridine heterosynthon in the cocrystallization of itraconazole, an antifungal drug with pharmaceutically acceptable dicarboxylic acids. Hydrogen-bonded trimers of two molecules of *cis*-itraconazole and one molecule of a 1,4-dicarboxylic acid are formed *via* acid···pyridine heterosynthon (Figure 2a). The extended succinic acid molecule fills a pocket, bridging the triazole groups. The strength of acid···amide heterosynthon over acid···acid and amide···amide homosynthons is exploited in the cocrystallization of piracetam with other drug molecules such as *p*-hydroxy benzoic acid and gentisic acid by Zaworotko and coworkers.[9] These 1:1 cocrystals are formed *via* acid···amide heterosynthon (Figures 2b, 2c). Piracetam,[10] *p*-hydroxy benzoic acid[11] and gentisic acid[12] are polymorphic in their own right but their cocrystals do not show any kind of polymorphism.[9]

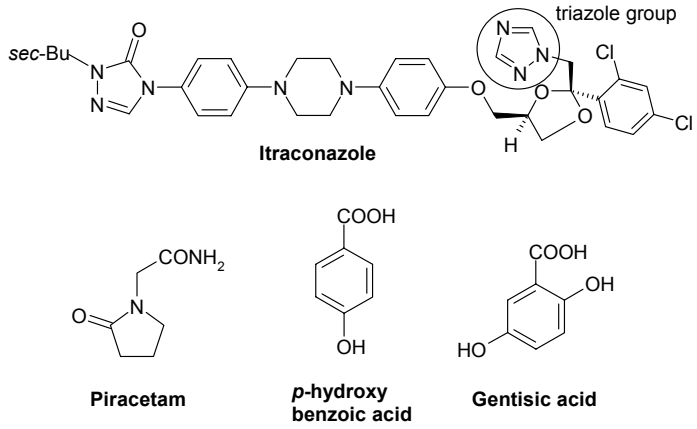

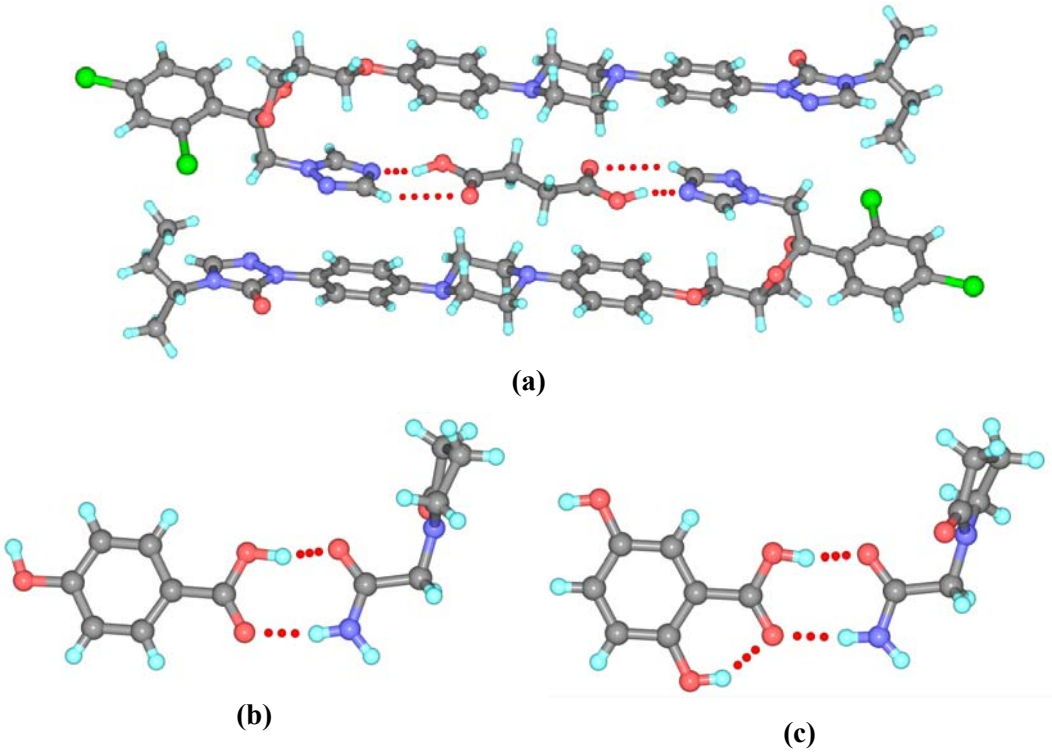

Figure 2. (a) Acid···pyridine heterosynthon in 2:1 cocrystal of itraconazole and succinic acid. (b) Acid···amide heterosynthon in 1:1 cocrystal of piracetam and 4-hydroxybenzoic acid. (c) Acid···amide heterosynthon in piracetam and gentisic acid cocrystal.

6.4 Results

As discussed earlier when there is competition between acid···acid homosynthon and acid···pyridine heterosynthon, the possibility of the latter is 91%. However, out of 84 crystal structures containing primary amide and pyridine functionalities in CSD, only 4 structures have amide···pyridine heterosynthon. The less probability of formation of amide···pyridine heterosynthon appeared unsuited because hydrogen bond acceptor strength of pyridine N is slightly less than amide C=O and weakness of N–H···N hydrogen bond. By taking advantage of the greater acceptor strength of *N*-oxide and strength of N–H···O^- hydrogen bond, carboxamide···*N*-oxide heterosynthon is designed and exploited in model API cocrystals of barbiturate drugs. All compounds discussed here were synthesized by the oxidation of corresponding pyridylamides with either *m*-CPBA or H_2O_2/AcOH (Scheme 2). After characterizing by satisfactory NMR and IR spectra their crystal structures were determined by X-ray diffraction and crystallographic data of compounds studied in this chapter is given in appendix.

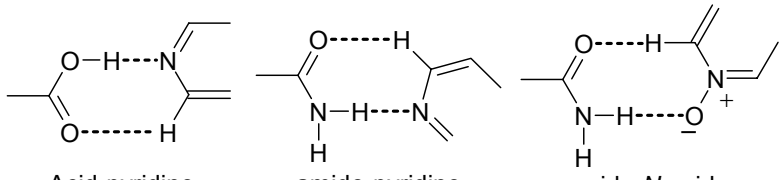

Scheme 1. Some heterosynthons discussed in this chapter.

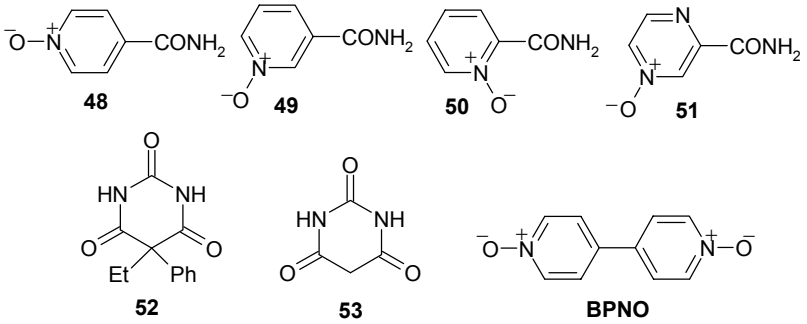

Scheme 2. Compounds studied in this chapter.

Table 1. Hydrogen bond geometry in crystal structures.[a]

Compound	Interaction	*d* /(Å)	*D* /(Å)	*θ* /(°)
48	N2–H2A···O1(*syn*)[b]	1.89	2.883(5)	168.4
	C1–H1···O2	2.25	3.272(6)	156.8
	N2–H2B···O1(*anti*)[b]	1.95	2.927(5)	161.9
	C2–H2···O1	2.28	3.349(6)	167.0
	C5–H5···O2	2.27	3.035(6)	125.5
49	N2–H2A···O1(*syn*)	1.93	2.915(2)	164.9
	C5–H5···O2	2.43	3.286(2)	134.5
	N2–H2B···O1(*anti*)	1.88	2.852(2)	159.8
	C1–H1···O1	2.31	3.356(2)	161.1
	C4–H4···O2	2.47	3.175(2)	121.3
50	N2–H2A···O2(*syn*)	1.95	2.956(2)	173.2
	N2–H2B···O1(*anti*, intra)	1.73	2.594(2)	141.2
	C4–H4···O2	2.35	3.199(3)	133.7
	C3–H3···O1	2.28	3.365(3)	174.2
	C5–H5···O1	2.31	3.379(3)	169.7
51	N2–H2A···O4(*syn*)	1.93	2.921(3)	168.3
	C9–H9···O2	2.28	3.334(3)	162.8
	N6–H6A···O1(*syn*)	1.91	2.907(3)	168.2
	C4–H4···O3	2.28	3.339(3)	164.0
	N2–H2B···O4(*anti*)	2.14	2.916(3)	132.2
	N6–H6B···O1(*anti*)	2.27	2.921(3)	121.3
	N2–H2B···N3(*anti*, intra)	2.24	2.729(3)	107.9
	N6–H6B···N5(*anti*, intra)	2.16	2.725(3)	113.8
	C3–H3···O3	2.25	3.300(4)	161.4

	C8–H8···O2	2.20	3.237(3)	159.3
52·(BPNO)$_{0.5}$	N2–H2···O1	1.78	2.782(2)	173.3
	C13–H13···O3	2.28	3.271(2)	151.0
	N3–H3···O1	1.81	2.785(2)	162.5
	C10–H10···O3	2.43	3.330(2)	139.6
	C6–H6C···O3	2.49	3.484(2)	151.5
	C9–H9···O4	2.43	3.358(3)	142.8
	C17–H17···O1	2.18	3.201(2)	155.9
53·BPNO·H$_2$O	N3–H3···O6	1.73	2.743(2)	178.5
	C8–H8···O3	2.67	3.643(2)	149.2
	O6–H6A···O1	1.72	2.690(2)	169.3
	O6–H6B···O1	1.74	2.721(2)	173.4
	N4–H4···O2	1.76	2.749(2)	164.7
	C1–H1···O3	2.23	3.171(2)	143.8
	C2–H2···O6	2.32	3.253(3)	143.1
	C9–H9···O2	2.13	3.190(3)	163.7

[a] N–H, O–H and C–H distances are neutron normalized to 1.009, 0.983 and 1.083 respectively. [b] *Syn* and *anti* refer to primary amide N–H donors.

Table 2. Torsion angle (O–N–O$^-$–C, # atoms) in amide–*N*-oxide heterosynthon.

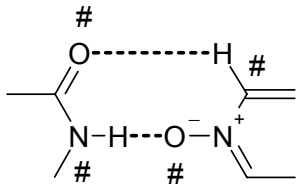

Compound	Torsion angle (º)
Isonicotinamide *N*-oxide **48**	12.5
Nicotinamide *N*-oxide **49**	25.1
Picolinamide *N*-oxide **50**	absent
Pyrazinamide-4-*N*-oxide **51**	10.1, 14.3
Phenobarbital·(BPNO)$_{0.5}$	21.0
Barbituric acid·BPNO·H$_2$O	40.3

Table 3. IR stretching frequency (KBr, cm^{-1}) of the N–H group in pyridine *N*-oxides and corresponding pyridyl-amides.

Pyridine amide	Pyridine *N*-oxide amide
Isonicotinamide 3368, 3184	Isonicotinamide *N*-oxide, **48**, 3350, 3153
Nicotinamide 3368, 3159	Nicotinamide *N*-oxide, **49**, 3298, 3144
Picolinamide 3435, 3171	Picolinamide *N*-oxide, **50**, 3250, 3103
Pyrazinamide 3416, 3290	Pyrazinamide-4-*N*-oxide, **51**, 3381, 3194
Phenobarbital 3306	**52**·(BPNO)$_{0.5}$ 3186
Barbituric acid 3182, 3096	**53**·BPNO·H$_2$O 3101, 3007

6.4.1 Crystal structure of isonicotinamide *N*-oxide, 48

Compound **48** crystallizes in the orthorhombic chiral space group $Pna2_1$ with one molecule in the asymmetric unit. Amide functionality is almost co-planar with pyridine ring (torsion angle is 3.61º). The carboxamide *syn* NH hydrogen bonds to pyridine *N*-oxide *via* N–H···O^- interaction (1.89 Å, 168.4º) to form 1D zig-zag tapes (Figure 3a). The auxiliary C–H···O (2.25 Å, 156.8º) interaction is also important because the heterosynthon is planar (Table 2). The *anti*-NH of amide is donated to *N*-oxide moiety (forming a bifurcated interaction) of the next layer and this repeats in the whole crystal to generate helical interactions of amide and *N*-oxide functional groups (Figure 3b). If both *syn* and *anti* N–H···O_{oxide} (Table 1) are considered it forms a triple helix architecture (Figure 3c), which is a sought after network because of its potential application in non-linear optics.[13] Its non-centrosymmetric packing is consistent with a two-fold higher SHG response compared to urea (Nd^{+3}-YAG laser at 1064 nm).

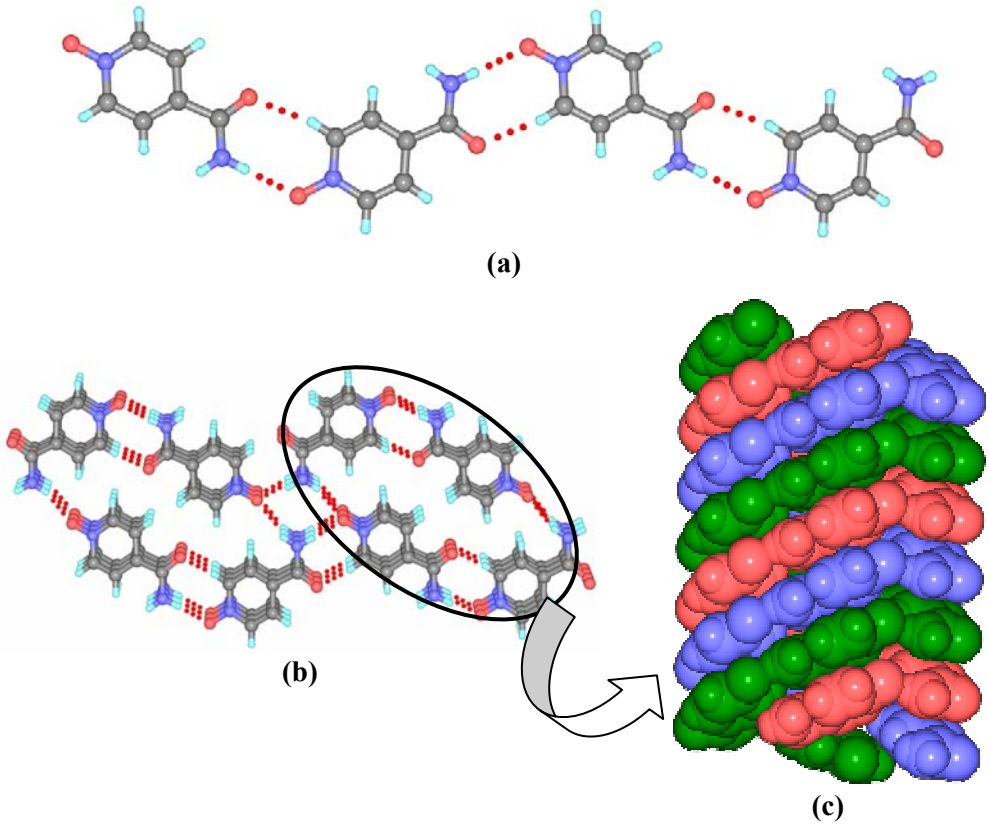

Figure 3. (a) N–H···O^- and C–H···O interaction in amide···*N*-oxide heterosynthon. (b) View down the *c*-axis of triple stranded helices and their interconnection. (c) Triple helices in the non-centrosymmetric structure of **48** along c-axis. Each strand is made up of alternating *syn* and *anti* NH donors bonding to the *N*-oxide acceptor.

6.4.2 Crystal structure of nicotinamide *N*-oxide, 49

Compound **49** is solved and refined in space group $P2_1/n$ with one molecule in the asymmetric unit. Amide functional group twists out of the pyridine ring plane (torsion angle is 31.39º). Glide related molecules are connected *via* heterosynthon between an amide and *N*-oxide (1.93 Å, 164.9º; 2.43 Å, 134.5º) to form linear tapes (Figure 4a). These linear tapes are connected *via anti* N–H···O^- (1.88 Å, 159.8º) to produce inversion-related helices (Figure 4b). Because the hydrogen bond ring closes between two molecules, when compared to four molecules in **48** there is no triple helical architecture.

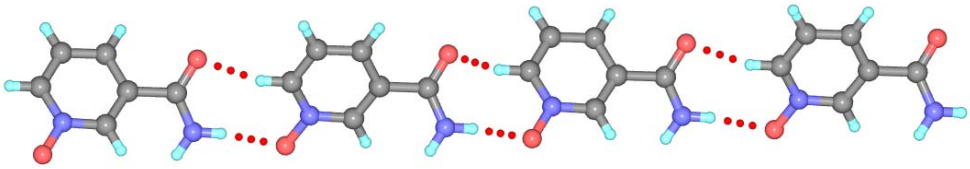

(a)

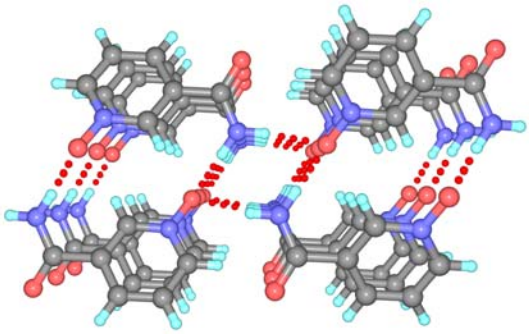

(b)

Figure 4. (a) 1D tapes formed by heterosynthon in the crystal structure of **49**. (b) Helical interactions formed between the amide and *N*-oxide.

6.4.3 Crystal structure of pyridine-2-carboxamide *N*-oxide, 50

Compound **50** crystallizes in *Pbca* space group with one molecule in the asymmetric unit. Amide group is co-planar with the pyridine ring (torsion angle is 0.51º), due to strong intramolecular N–H_{anti}···O_{oxide} hydrogen bond (1.73 Å, 141.2º). Thus the acceptor strength of *N*-oxide decreases and it forms intermolecular N–H···O (1.95 Å, 173.2º) hydrogen bonded homodimers. These homodimers are connected by C–H···O_{oxide} (Table 1) dimer to form one dimensional tapes (Figure 5a) and these tapes are in turn connected by C–H···$O_{carbonyl}$ interactions to form two dimensional corrugated layers (Figure 5b). These corrugated layers are stacked in the third dimension to achieve close packing (Figure 5c).

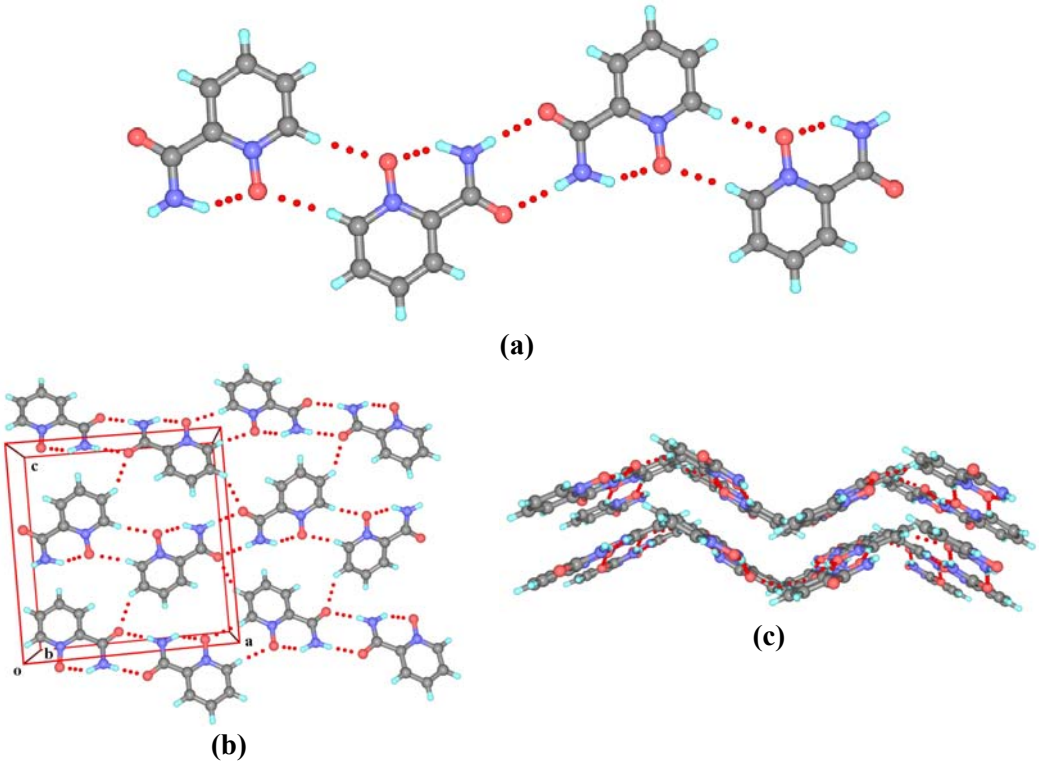

Figure 5. (a) 1D Zig-zag tapes formed by amide···amide homodimer and C–H···O dimer. (b) 2D-sheets *via* weak C–H···O interactions between the carbonyl oxygen of the amide and aromatic pyridine ring protons. (c) Corrugated tapes in the third dimension.

6.4.4 Crystal structure of pyrazinamide-4-*N*-oxide, 51

Oxidation of the sterically exposed and more reactive pyridyl group with H_2O_2/AcOH afforded pyrazinamide-4-*N*-oxide, **51**. It crystallizes in the space group *P*-1 with two symmetry independent molecules in the asymmetric unit. Amide groups in both molecules are nearly co-planar with the pyridine ring (torsion angles are 3.56º and 5.80º). Symmetry independent molecules are connected by heterosynthon formed between amide and the *N*-oxide functional groups leading to one-dimensional tapes structure (Figure 6a). These tapes are connected by N–H···O_{oxide} (bifurcated), weak C–H···$O_{carbonyl}$ and C–H···N (Table 1) interactions to form two dimensional layers (Figure 6b) and these 2D layers are stacked in third direction (Figure 6c).

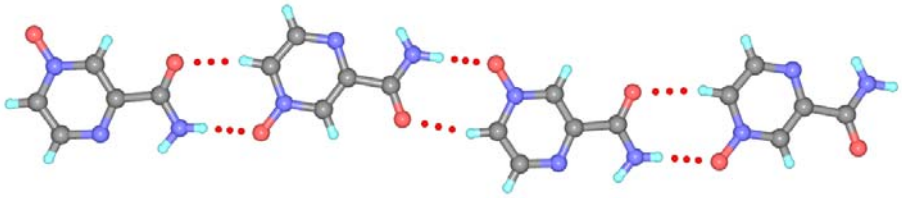

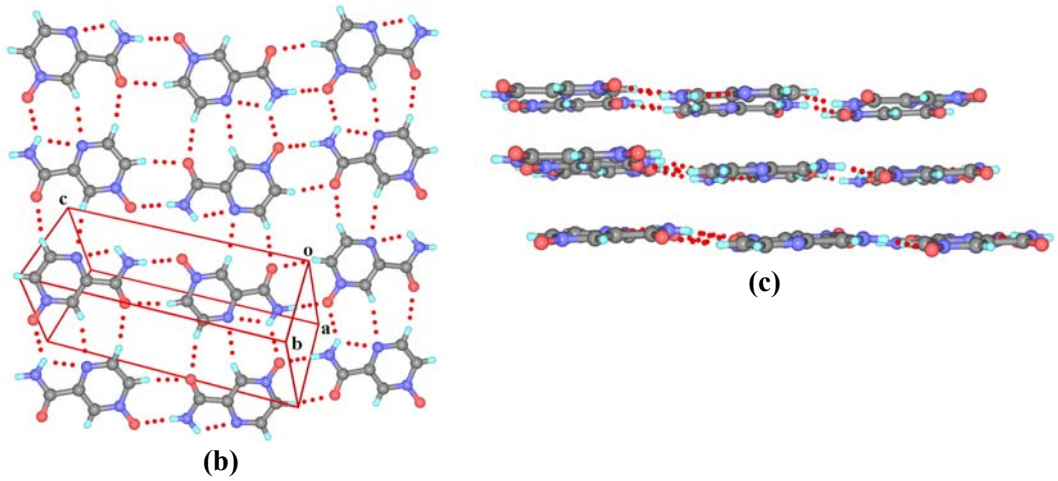

Figure 6. (a) 1D tape in **51** assembled *via* amide···*N*-oxide heterosynthon between symmetry independent molecules. (b) 2D layer formed by N–H···O_{oxide}, weak C–H···$O_{carbonyl}$ and C–H···N interactions (c) Stacked layers in the third dimension.

6.5 Application of amide···*N*-oxide heterosynthon in model API cocrystallization

After successfully evaluating the robustness of amide···*N*-oxide heterosynthon in multi-functional molecules, cocrystallization of two different components with carboxamide and pyridine *N*-oxide functional groups was attempted. The amide···*N*-oxide heterosynthon was tested in barbiturate drugs because (i) barbiturates are known to be polymorphic[14] (ii) polymorphic compounds with several hydrogen bond donor/acceptor groups (e.g. isonicotinamide, pyrazinamde) tend to cocrystallize readily,[15] and (3) cocrystals offer a practical solution to controlling polymorphism in pharmaceuticals.[9]

6.5.1 Crystal structure of 52·$(BPNO)_{0.5}$

Cocrystal 1:0.5 is formed when phenobarbital **52** and 4,4'-bipyridine-*N,N'*-dioxide (BPNO) were cocrystallized in 1:1 ratio from MeOH. It crystallizes in the space group $P2_1/c$ with one molecule of phenobarbitone and half molecule of BPNO in the asymmetric unit, BPNO residing on inversion center. Phenobarbital and BPNO interact *via* N–H···O_{oxide} and C–H···O (1.81, 162.5º, 2.28 Å, 151.0º) heterosynthon to form a discrete tape (Figure 7a). These discrete tapes are connected through N–H···O_{oxide}(1.78 Å, 173.3º, bifurcated) to form a helical motif (Figure 7b). These helical motifs are dovetailed to complete the close packing (Figure 7c).

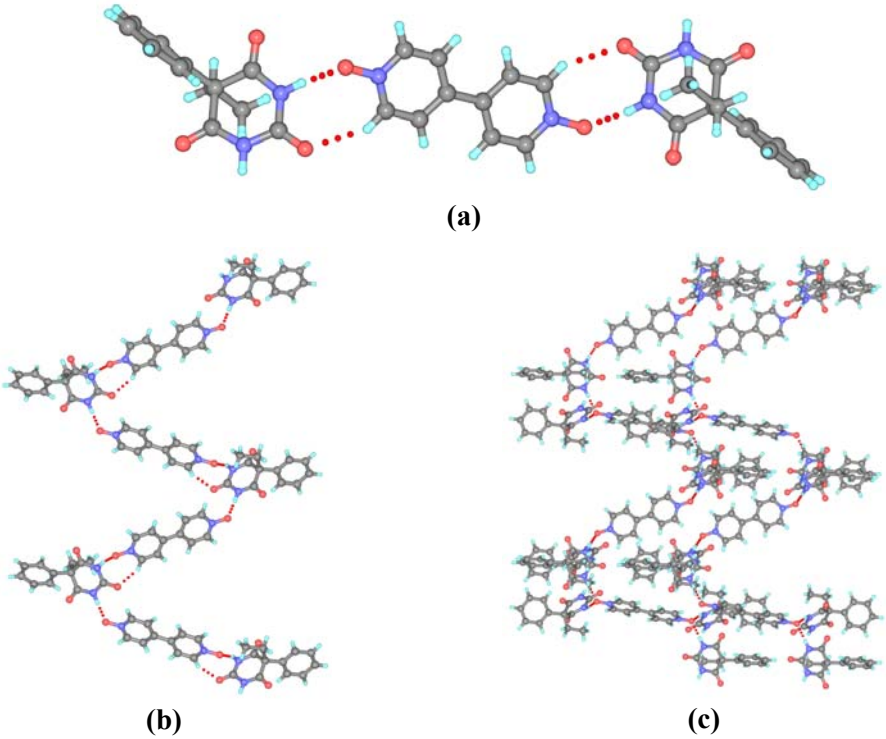

(a) **(b)** **(c)**

Figure 7. (a) Binary aggregate of phenobarbital **52** and BPNO. (b) Helical array of molecules in the cocrystal, **52·BPNO**. Note that phenobarbital interacting with bifurcated N–H···O_{oxide} is removed for clarity. (c) Dovetailed helices.

6.5.2 Crystal structure of 53·BPNO·H_2O

Complex crystallizes in the space group *Pbca* with one molecule of each barbituric acid, BPNO and water in the asymmetric unit. Out of the two *N*-oxide moieties in BPNO, one forms a heterosynthon *via* N–H···O_{oxide} and C–H···O interactions with barbituric acid and other *N*-oxide also forms heterosynthon excepting that the water replaces the acceptor site of the barbituric acid by acting as a spacer between the barbituric acid and *N*-oxide groups (Figure 8a). These interactions repeat within the crystal to form one dimensional corrugated tapes and these tapes are connected by weak C–H···O interactions to form two dimensional layers (Figure 8b). These two dimensional layers further extend into third dimension *via* O_w–H···O_{oxide} hydrogen bonds.

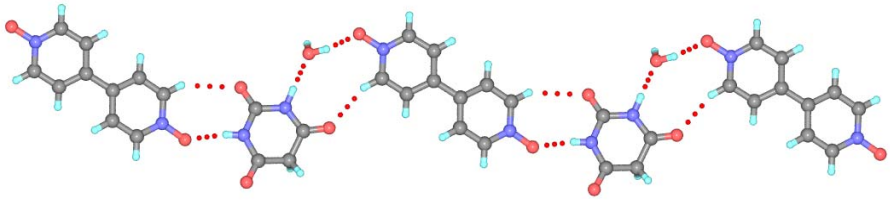

(a)

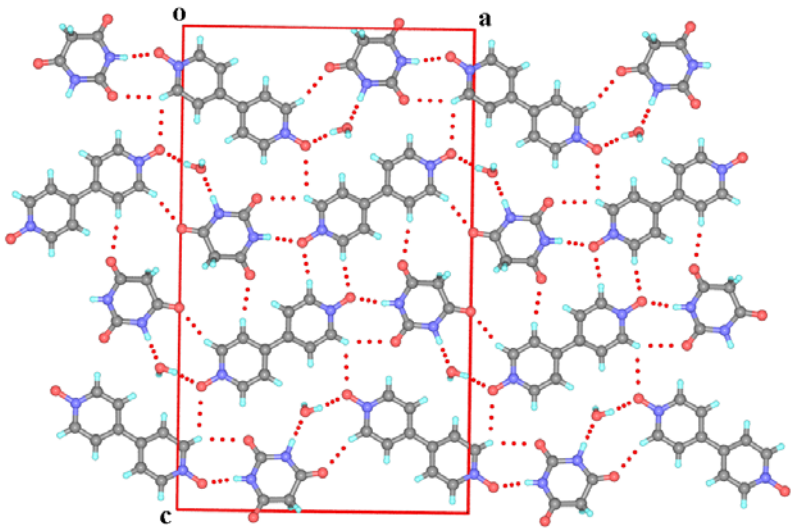

(b)

Figure 8. (a) **53·BPNO·H_2O** has both amide···*N*-oxide and its hydrate motif. (b) Two dimensional layered structure along *c*-axis.

6.6 Hydrogen bond energies: *Ab initio* calculations

Hydrogen bond synthon energies were calculated in *Spartan* using RHF/6-31G** basis set on model compounds acetamide, pyridine *N*-oxide and isonicotinamide *N*-oxide. $E_{synthon}$ is the energy of hydrogen bond synthon and $\Delta E_{synthon}$ is the energy difference between the heterosynthon and the constituent homosynthons. The amide···*N*-oxide heterosynthon is stabilized by ~0.5 kcal/mol compared to homosynthons, amide and pyridine *N*-oxide dimers, when the *syn* NH of the amide group is considered (Scheme 3). The difference is 0.39 kcal/mol when calculations are performed on isonicotinamide *N*-oxide. In addition the *anti* NH engages in N–H···O^- bond with *N*-oxide compared to N–H···O in the amide tape. The energy of a single N–H···O^- is estimated as: heterosynthon = –11.62 kcal/mol = N–H···O^- + C–H···O hydrogen bonds. If the sp^2 hybridized C–H···O interaction is ~2 kcal/mol, the N–H···O^- bond = –9.62 kcal/mol. The energy of a single neutral N–H···O in amide dimer = 13.11 ÷ 2 = –6.55 kcal/mol. So the enthalpic advantage in the heterosynthon compared to competing homosynthons, designated as ΔE_{HB}, is ~3.0 kcal/mol. This energy difference looks chemically reasonable because both N–H donors form stronger N–H···O^- hydrogen bonds in amide *N*-oxide structures whereas pyridyl amides have neutral N–H···O/N–H···N hydrogen bonds.

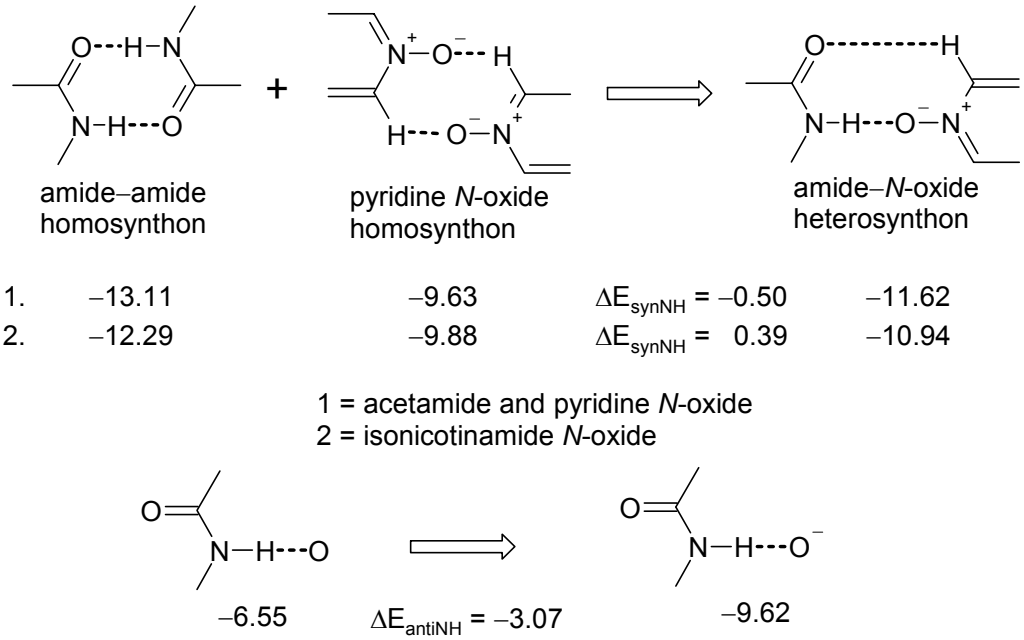

Scheme 3. Hydrogen bond energy calculation in model compounds.

The above enthalpy calculation is also valid in the cocrystal of phenobarbital and BPNO, **52**·(BPNO)$_{0.5}$, because CONH of two different molecules hydrogen bond with a pyridine *N*-oxide moiety such that there is one amide···*N*-oxide synthon and one N–H···O$^-$ hydrogen bond. In effect, two secondary amide groups in the cocrystal play the role of *syn* and *anti* NH donors in isonicotinamide *N*-oxide **48** (Figure 9).

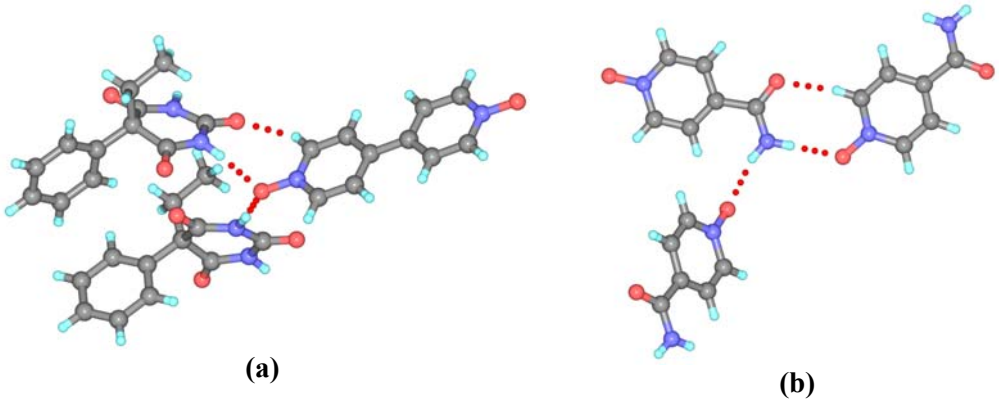

Figure 9. (b) Portion of the crystal structure of **52**·(BPNO)$_{0.5}$ to show the bifurcated O$^-$ as part of amide···*N*-oxide synthon and N–H···O$^-$ interaction. BPNO resides on the inversion center. (b) Identical bifurcated hydrogen bond motif in isonicotinamide *N*-oxide **48**.

6.7 Discussion

Ab initio calculations reveals that the two-point amide···*N*-oxide heterosynthon is worth 11-12 kcal/mol with an enthalpic advantage, ΔE_{HB}, of ~3.0 kcal/mol over homosynthon aggregation, a value that is comparable to the energy gain in acid···pyridine and amide···acid heterosynthons (ΔE_{HB} 2.0-4.0 kcal/mol).[16] We argue that formation of amide···*N*-oxide heterosynthon is kinetically preferred because the strongest hydrogen bond donor (amide NH) will readily approach the strongest acceptor (pyridine *N*-oxide),[17] a hypothesis that is in agreement with the frequency of acid···pyridine and amide···acid heterosynthons in the CSD (91% and 47%). The hydrogen bond formation constant pK_{HB} of pyridine N and amide carbonyl are 1.86 and 1.96 respectively. Furthermore the difference in electrostatic surface potential (ESP) on pyridyl N (–43.7 kcal/mol) and amidecarbonyl O (–47.4 kcal/mol) of isonicotinamide is only –3.4 kcal/mol, whereas the difference is –10.2 kcal/mol (*N*-oxide O^-, –53.3, amidecarbonyl O, –43.1 kcal/mol) in isonicotinamide *N*-oxide. More negative charge indicates a better hydrogen bond acceptor. Therefore amide···*N*-oxide heterosynthon is favoured over amide···amide homosynthon and amide···pyridine heterosynthon. When kinetically formed synthons are also thermodynamically favored, polymorphism is hardly likely under normal P/T conditions because the global free energy minimum structure will be much lower in energy than other possible metastable polymorphs.[18] Of course, here we are analyzing only the hydrogen bond contribution to the lattice energy and polymorphism could well be possible through different arrangements of the same heterosynthon, or through differences in close packing of layers/hydrophobic groups or different molecular conformations but the same heterosynthon. Formation of strong N–H···O_{oxide} hydrogen bond in the heterosynthon can be observed in solid-state IR spectra, where the N–H stretching frequency of *N*-oxide compounds is systematically shifted to lower ν_s values by 50-100 cm^{-1} compared to that in amides (Table 3).

Why the ratio of barbituric acid to BPNO is 2:1 with **52** but 1:1 with **53** is difficult to say, however different stoichiometries have been noted in barbiturate–aza-heteterocycle cocrystals.[19] The formation of binary bulk phases was found to be about 50% complete after 30 min of ball mill grinding by powder X-ray diffraction.

6.8 Conclusions

A novel carboxamide···pyridine *N*-oxide heterosynthon is designed by exploiting the better acceptor strength of anionic oxygen and shown to result in helical motifs, a sought after architecture in crystal design. Notably, the amide···*N*-oxide heterosynthon dominates over amide dimer homosynthon and should have a high probability of occurrence in crystal structures, except when it is in competition with intramolecular H bonding. Hydrogen bond preferences and synthon energy calculations suggest that amide *N*-oxides should be less prone to polymorphism compared to amide pyridines. Polymorphism in isonicotinamide[15a] and pyrazinamide[20] may be understood from different occurrences of N–H···O and N–H···N hydrogen bond synthons, perhaps due to the comparable acceptor strength of amide C=O and pyridine N groups. On the other hand, the strong N–H···O^- H bond controls crystallization in amide···*N*-oxides, therefore synthon based polymorphism is less likely.

6.9 Experimental section: All compounds discussed in this chapter were synthesized by the oxidation of corresponding pyridylamides with either *m*-CPBA or H_2O_2/AcOH. All compounds are characterized by IR and NMR. ^{1}H NMR spectra (δ scale in ppm, *J* coupling constant in Hz) were recorded on Bruker Avance at 400 MHz and FT-IR spectra (ν in cm^{-1}) on Jasco 5300 spectrophotometer. Melting points were recorded on Fisher–Johns apparatus.

Synthesis of the isonicotinamide *N*-oxide: 1.9 g (15.5 mmol) of the isonicotinamide was dissolved in 100 ml of hot EtOAc. To this hot solution, 3.8 g of 70 % of (15.5 mmol) *m*-CPBA dissolved in 10 ml of EtoAc was added at once and the solution was allowed to stand at room temperature for 10 minutes, a white compound precipitated from the solution. The precipitate was filtered and washed with 2 x 50 ml of EtOAc, dried and weighed. Yield: 70 %. ^{1}H NMR (DMSO-d_6): δ 8.28 (d, *J* = 7, 2H), 8.14 (s, 1H), 7.82 (d, *J* = 7, 2H), 7.63 (s, 1H). IR (KBr): 3350, 3153, 1936, 1685, 1630, 1547, 1496, 1446, 1396, 1313, 1242, 1195, 1151, 1120, 1032 cm^{-1}. M. p. Above 250 ºC.

Synthesis of the nicotinamide *N*-oxide: 1.9 g (15.5 mmol) of the nicotinamide was dissolved in 100-120 ml of hot EtOAc. To this hot solution, 3.8 g of 70 % of (15.5 mmol) *m*-CPBA dissolved in 10-15 ml of EtOAc is added at once and the solution was allowed to come to room temperature. After 10 minutes, a white compound precipitated from the solution. Precipitated compound was filtered and washed with 2 x 50 ml of EtoAc. Yield: 70 %. ^{1}H NMR (DMSO-d_6): δ 8.64 (s, 1H), 8.23 (d, *J* = 6, 1H), 8.15 (s, 1H), 7.72 (d, *J* = 8,

2H), 7.59 (s, 1H), 7.40 (t, *J* = 6, 1H). IR (KBr): 3375, 3140, 1687, 1631, 1568, 1485, 1439, 1396, 1236, 1165, 1113, 1020 cm^{-1}. M. p. Above 250 ºC.

Synthesis of the pyridine-2-carboxamide *N*-oxide: 500 mg (4.0mmol) of the pyridine-2-carboxamide was dissolved in the 5 ml of 30 % H_2O_2 and 2 ml of glacial AcOH. The solution was stirred at 60 ºC for 24 hrs. The reaction mixture was cooled to room temperature and solvent was removed under vacuum. A white solid was separated and recrystallized from hot EtoAc. Yield: 86%. ^{1}H NMR ($CDCl_3$): δ 10.79 (s, 1H), 8.41 (dd, *J* = 8, 8, 1H), 8.28 (d, *J* = 5, 1H), 7.72 (d, *J* = 7, 1H), 7.69 (dd, *J* = 9, 7, 1H), 6.26 (s, 1H). IR (KBr): 3250, 3103, 1684, 1437, 1377, 1277, 1230, 1151 cm^{-1}. M. p. 151 ºC.

Synthesis of the Pyrazinamide-4-N-oxide: 500 mg (4.0 mmol) of the pyrazinamide was dissolved in the 5 ml of 30 % H_2O_2 and 2 ml of glacial AcOH. The solution was stirred at 60 ºC for 36 hrs. At the end of the reaction, a white solid precipitated. This compound was further recrystallized from the pure glacial acetic acid to obtain good quality crystals.

Yield: 78%. ^{1}H NMR (DMSO-d_6): δ 8.58 (d, *J* = 4, 1H), 8.54 (s, 1H), 8.49 (d, *J* = 5, 1H), 8.29 (s, 1H), 8.00 (s, 1H). IR (KBr): 3381, 3194, 1793, 1685, 1595, 1508, 1444, 1394, 1307, 1269, 1126, 1084, 1005 cm^{-1}. M. p. Above 250 ºC.

Synthesis of cocrystals:

52·BPNO: Dissolution of an equimolar mixture of phenobarbital (0.21 mmol, 50 mg) and BPNO (0.21 mmol, 33.6 mg) in MeOH by warming and cooling to room temperature afforded single crystals of the binary aggregate **52**·$(BPNO)_{0.5}$ suitable for X-ray diffraction at room temperature. M. p. Above 250 ºC.

53·BPNO·H_2O: An equimolar mixture of barbituric acid (0.39 mmol, 50 mg) and BPNO (0.39 mmol, 66 mg) in MeOH was dissolved in methanol and allowed to evaporate at room temperature. The monohydrate of **53**·BPNO (1:1) was formed. M. p. Above 250 ºC.

6.10 References

1. F.H. Allen, W.D.S. Motherwell, P.R. Raithby, G.P. Shields and R. Taylor, *New J. Chem.*, **1999**, *23*, 25.
2. T. Steiner, *Acta Crystallogr.*, *Sect. B*, **2001**, *57*, 103.
3. (a) J.A. McMahon, J.A. Bis, P. Vishweshwar, T.R. Shattock, O.L. McLaughlin and M. J. Zaworotko, *Z. Kristallogr.*, **2005**, *220*, 340. (b) S.G. Fleischman, S.S. Kuduva, J.A. McMahon, B. Moulton, R.D.B. Walsh, N. Rodríguez-Hornendo and M.J. Zaworotko, *Cryst. Growth Des.*, **2003**, *3*, 909.

4. J.A. Bis and M. Zaworotko, *Cryst. Growth Des.*, **2005**, *5*, 1169.
5. S.L. Morissette, Ö. Almarsson, M.L. Peterson, J.F. Remenar, M.J. Read, A.V. Lemmo, S. Ellis, M.J. Cima, C.R. Gardner, *Adv. Drug Del. Rev.*, **2004**, 56, 275.
6. (a) R.D.B. Walsh, M.W. Bradner, S.G. Fleischman, L.A. Morales, B. Moulton, N. Rodríguez-Hornendo and M.J. Zaworotko, *Chem. Commun.*, **2003**, 186. (b) Ö. Almarsson and M.J. Zaworotko, *Chem. Commun.*, **2004**, 1889.
7. (a) J.A. Zerkowski, J.C. MacDonald and G.M. Whitesides, *Chem. Mat.*, **1997**, *9*, 1933. (b) J.A. Zerkowski, C.T. Seto, D.A. Wierda and G.M. Whitesides, *J. Am. Chem. Soc*., **1990**, *112*, 9025. (c) J.A. Zerkowski, C.T. Seto, and G.M. Whitesides, *J. Am. Chem. Soc*., **1992**, *114*, 5473. (d) J.A. Zerkowski and G.M. Whitesides, *J. Am. Chem. Soc.*, **1994**, *116*, 4298. (e) J.A. Zerkowski, J.C. MacDonald, C.T. Seto, D.A. Wierda and G.M. Whitesides, *J. Am. Chem. Soc*., **1994**, *116*, 2382. (f) J.A. Zerkowski, J.P. Mathias and G.M. Whitesides, *J. Am. Chem. Soc*., **1994**, *116*, 4305.
8. J.F. Remenar, S.L. Morissette, M.L. Peterson, B. Moulton, M. MacPhee, H. Guzmán, Ö. Almarsson, *J. Am. Chem. Soc*., **2003**, *125*, 8456.
9. P. Vishweshwar, J.A. McMahon, M.L. Peterson, M.B. Hickey, T.R. Shattock and M.J. Zaworotko, *Chem. Commun.*, **2005**, 4601.
10. (a) C. Giurgea, F.E. Moeyersoons and A.C. Evraerd, *Arch. Int. Pharmacodyn.*, **1967**, *166*, 238. (b) G. Admiraal, J.C. Eikelenboom and A. Vos, *Acta Crystallogr.*, **1982**, *B38*, 2600. (c) D. Louder, M. Louder, V.A. Dzyabchenko, V. Agafonov and R. Ceolin, *Acta Crystallogr.*, **1995**, *B51*, 182. (d) F.P.A. Fabbiania, D.R. Allan, S. Parsons and C.R. Pulham, *CrystEngComm*, **2005**, *7*, 179.
11. B.M. Kariuki, C.L. Bauer, K.D.M. Harris and S.J. Teat, *Angew. Chem. Int. Ed.*, **2000**, *39*, 4485.
12. (a) E. Ginoulhiac, F. Semenza and L. Mainardi, *Boll. Soc. Ital. Biol. Sper.*, **1950**, *26*, 583. (b) A. Pavlova, K. Konstantinova, H. Daskalov and A. Georgiev, *Pharmazie*, **1983**, *38*, 634.
13. P. Grosshans, A. Jouaiti, V. Bulach, J.M. Planeix, M.W. Hosseini, and J.-F. Nicoud, *Chem. Commun*., **2003**, 1336. (b) Y. Cui and W. Lin, *Chem. Commun*., **2003**, 1388. (c) G.O. Lloyd, J.L. Atwood and L.J. Barbour, *Chem. Commun*., **2005**, 1845.
14. T.C. Lewis, A. Tocher and S.L. Price, *Cryst. Growth Des.*, **2004**, *4*, 979. (b) C. Platteau, J. Lefebvre, S. Hemon, C. Baehtz, F. Danede and D. Prevost, *Acta Crystallogr.*, **2005**, *B61*, 80.

15. (a) C.B. Aakeröy, A.M. Beatty, B.A. Helfrich and M. Nieuwenhuyzen, *Cryst. Growth Des.*, **2003**, *3*, 159. (b) C.B. Aakeröy, J. Desper, B.A. Helfrich, *CrystEngComm*, **2004**, *6*, 19.
16. (a) P. Vishweshwar, A. Nangia and V.M. Lynch, *J. Org. Chem.*, **2002**, *67*, 556. (b) P. Vishweshwar, A. Nangia and V.M. Lynch, *Cryst. Growth Des.*, **2003**, *3*, 783.
17. M.C. Etter, *J. Phys. Chem.*, **1991**, *95*, 4601.
18. G. R. Desiraju, *Nat. Mater.*, **2002**, *1*, 77.
19. P. Vishweshwar, R. Thaimattam, M. Jaskólski and G.R. Desiraju, *Chem. Commun.,*, **2002**, 1830.
20. A. Nangia and G.R. Desiraju, *Top. Curr. Chem.*, **1998**, *198*, 57.

CHAPTER 7

POLYMORPHISM IN 6-AMINO-2-PHENYLSULFONYLIMINO-1,2-DIHYDROPYRIDINE AND DERIVATIVES

7.1 Introduction

Polymorphism, the phenomenon that molecule can crystallize in more than one solid-state form, is a major challenge in our fundamental understanding of crystallization and is of immense practical importance in molecular materials, e. g. pharmaceuticals. According to McCrone "*the number of forms known for a given compound is proportional to the time and money spent in research on that compound*".[1] However, there are differences of opinion as to the frequency of polymorphism under normally accessible conditions of crystallization. Although some investigators believe that polymorphism is extremely common, the Cambridge Structural Database (CSD) contains only 4-5% organic compounds, 5.5% organometallics and 2.1% of coordination compounds have more than one crystalline form.[2] Desiraju and Sarma[3] showed that the frequency of occurrence of polymorphic modifications is not necessarily uniform in all categories of substances and the phenomenon is probably more common with molecules that have conformational flexibility and/or multiple groups capable of forming hydrogen bonding. Polymorphism can be synthon based or conformational based polymorphism.[4] Synthon based polymorphism arises due to the difference in hydrogen bonding pattern whereas conformational polymorphism arises due to differences in conformation of molecules in different structures.

The way molecules are packed in a crystal influences the properties of many practical materials, such as pigments, pharmaceuticals, explosives and nonlinear optical (NLO) properties. For example, a molecule with high NLO coefficient will only produce an active material if it crystallizes in a non-centrosymmetric space group. Therefore, the ability to predict the crystal packing for an unknown compound would be desirable.[5] Crystal structure prediction (CSP) is closely connected to polymorphism,[6] the occurrence of alternative structures in a narrow energy range. Different packing arrangements of organic molecules result in different physical properties such as melting point, solubility, hardness, and density. Therefore controlled crystallization of the correct polymorph is crucial. When a novel pharmaceutical compound has been developed, it is a regulatory requirement[7] that all reasonable experiments are performed in order to identify and characterize the maximum

possible number of crystalline polymorphs. This is often done by recrystallizing the compound from various solvents (a "solvent screen"). Despite current application of high throughput methodologies to such screens,[8] there is no guarantee that all possible polymorphs will be isolated; hence, the ability to predict the possible polymorphs for new molecules would be invaluable. Recognizing the importance of CSP, blind tests were conducted by the Cambridge Crystallographic Data Centre (CCDC) in 1999, 2001 and 2004 to test how well currently available methods of crystal structure prediction perform.[9] The molecules of three CSP tests are listed in scheme 1.

Most methods of CSP are based on a search for the crystal structure that corresponds to the global minimum in the lattice energy. The basic problem with lattice energy based methods is that many structures are found within a few kcal/mol of the global minimum and take only the thermodynamic (enthalpic) factors in to account. Matters concerning kinetics and entropy are not taken into account. But crystallization is governed by both thermodynamic and kinetic factors and the latter is more important in polymorphic systems.

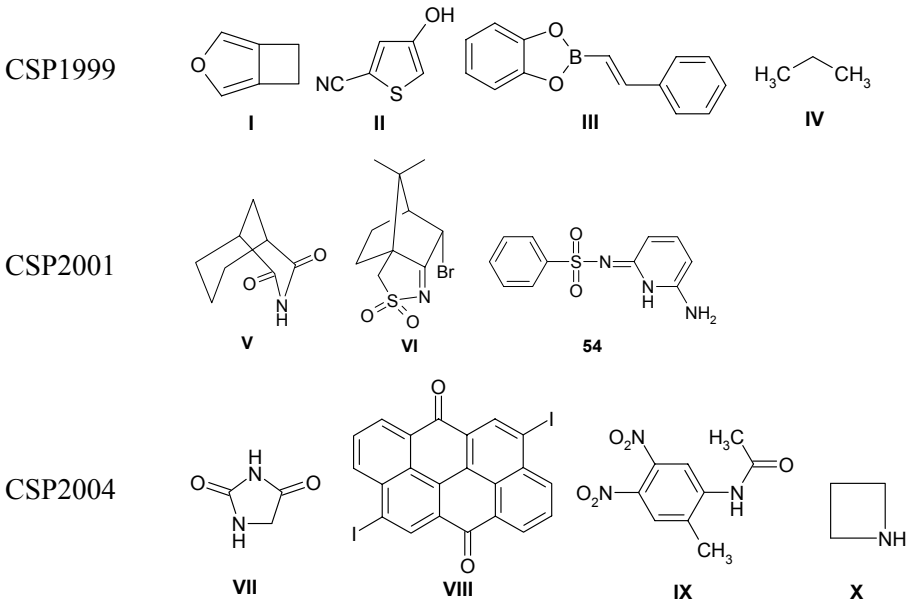

Scheme 1. Compounds given in blind tests conducted by CCDC.

7.2 Results

Synthon based polymorphism is quite common in sufonamide molecules.[10] 6-Amino-2-phenylsulfonylimino-1,2-dihydropyridine, **54**, is a conformationally flexible molecule with two degrees of acyclic torsional freedom, is one of the three molecules supplied in CSP2001. My project was to find polymorphs of compound **54** as well as its

derivatives experimentally. All compounds discussed here were synthesized according to the literature procedure[11] given for 2-(aminobenzenesulfonylamino)-6-aminopyridine by taking the corresponding sulfonyl chloride with 2,6-diaminopyridine. After characterizing by NMR and IR spectra their crystal structures were determined by X-ray diffraction. Crystallographic data of compounds studied in this chapter is given in appendix.

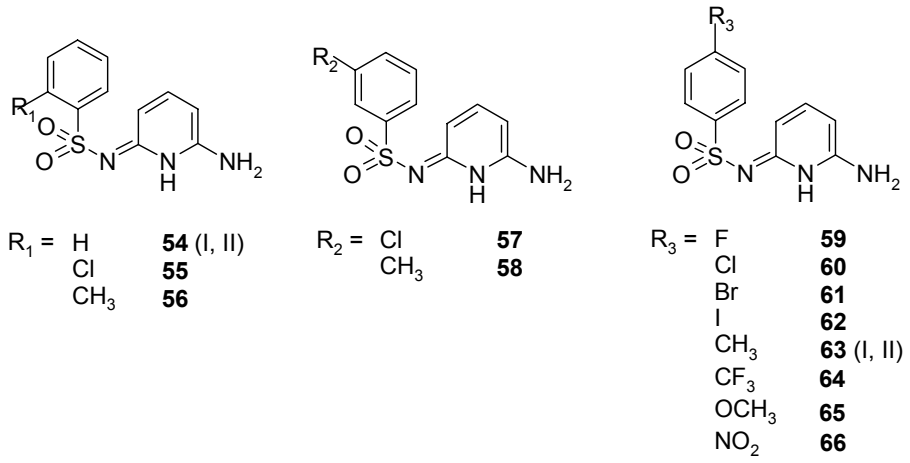

Scheme 2. Compounds studied in this chapter.

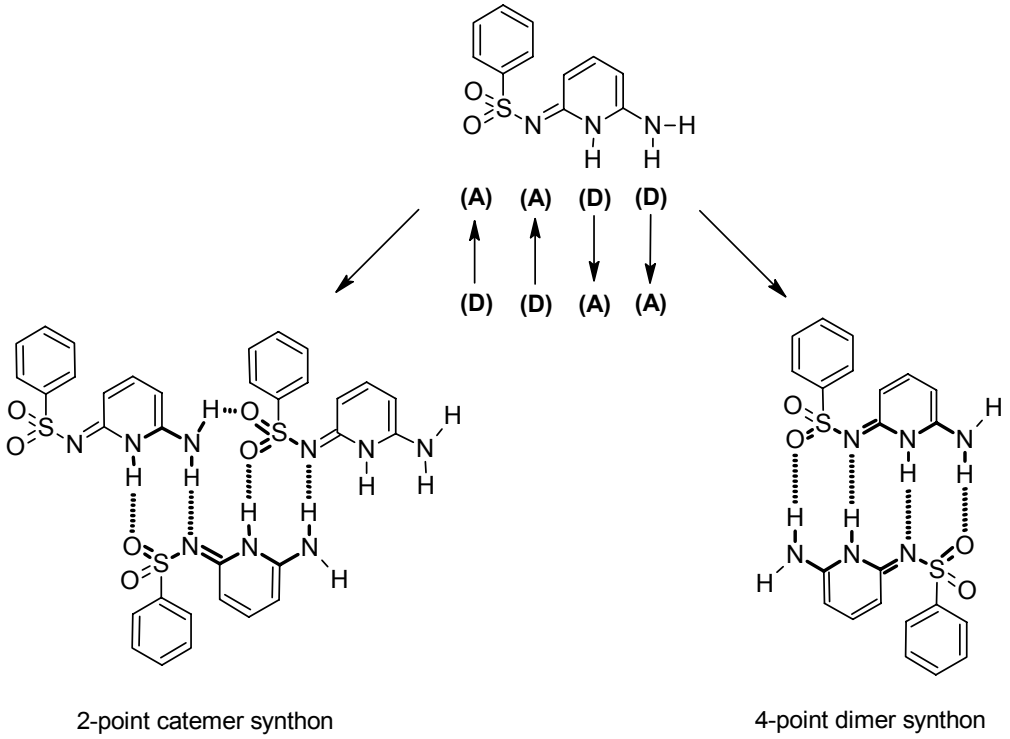

Scheme 3. Two possible synthons in this family of compounds (A = hydrogen bond acceptor, D = hydrogen bond donor).

Table 1. Hydrogen bonding parameters of compounds studied in this chapter.

Compound	Interaction	*d*/ Å	*D*/Å	θ/(º)
54 (Form I)	N1–H1···O2	1.78	2.772(2)	165.4
	N7–H7a···N8	2.24	3.250(2)	176.9
	N7–H7b···O1	2.18	3.116(2)	153.6
54 (Form II)	N17–H17b···O3	1.84	2.821(3)	163.3
	N11–H11···N28	1.95	2.951(3)	170.1
	N21–H21···N18	2.06	3.050(3)	164.8
	N27–H27a···O2	1.80	2.795(4)	168.5
	N17–H17a···O1	2.02	3.025(3)	174.3
	N27–H27b···O4	2.07	3.061(3)	165.0
55	N1–H1···O2	1.83	2.825(3)	166.1
	N7–H7a···N8	2.12	3.122(4)	174.5
	N7–H7b···O1	2.36	3.275(4)	150.5
56	N1–H1···O2	1.82	2.805(2)	165.0
	N7–H7a···N8	2.08	3.086(3)	175.7
	N7–H7b···O1	2.27	3.205(2)	152.6
58	N1–H1···O2	1.74	2.736(3)	166.1
	N7–H7b···N8	2.14	3.135(3)	169.0
	N7–H7a···O1	2.07	3.027(3)	156.5
59	N1–H1···O1	1.87	2.815(9)	154.1
	N7–H7b···N8	2.10	3.053(2)	156.7
	N7–H7a···O2	2.33	3.083(9)	130.1
60	N7–H7a···O1	1.90	2.806(4)	147.0
	N1–H1···N8	2.01	3.018(4)	173.5
	N7–H7b···O2	1.97	2.968(4)	168.0
61	N22–H22a···O7	1.75	2.761(5)	174.3
	N16–H16···N53	2.25	3.257(5)	171.9
	N46–H46···N23	2.22	3.200(5)	162.4
	N52–H52a···O3	2.02	2.765(6)	128.4
	N7–H7a···O5	1.81	2.716(5)	147.9
	N1–H1···N38	2.14	3.139(5)	169.4
	N31–H31···N8	2.10	3.099(5)	169.9
	N37–H37a···O2	1.98	2.744(5)	130.2
	N52–H52b···O6	1.99	2.900(5)	147.7
	N7–H7b···O4	1.92	2.942(5)	168.8
	N22–H22b···O1	1.89	2.885(5)	167.7
	N37–H37b···O8	2.04	2.927(4)	145.0
62	N7–H7a···O3	1.72	2.713(9)	167.2
	N1–H1···N23	2.23	3.194(9)	159.8
	N16–H16···N8	2.20	3.134(8)	153.0
	N22–H22a···O1	1.75	2.729(9)	163.6
	N7–H7b···O2	2.04	2.876(8)	138.5
	N22–H22b···O4	2.14	2.934(8)	133.6
63 (Form I)	N7–H7a···O4	1.79	2.782(3)	164.9
	N1–H1···N24	2.09	3.075(3)	162.1
	N17–H17···N8	1.99	2.997(3)	175.4
	N23–H23b···O2	1.88	2.823(3)	153.7
	N7–H7b···O1	2.09	3.098(3)	172.4

	N23–H23a···O3	2.02	3.017(3)	167.9
63 (Form II)	N23–H23a···O6	1.95	2.791(9)	139.4
	N17–H17···N40	2.02	3.028(9)	175.4
	N33–H33···N24	2.08	3.083(9)	171.4
	N39–H39a···O4	1.87	2.767(8)	145.9
	N7–H7a···O8	1.83	2.775(8)	154.0
	N1–H1···N56	2.10	3.105(9)	170.4
	N49–H49···N8	1.98	2.987(9)	175.9
	N55–H55a···O2	1.95	2.783(9)	137.6
	N23–H23b···O7	2.08	3.083(9)	171.4
	N7–H7b···O5	2.12	3.030(9)	149.2
	N39–H39b···O1	2.15	3.055(9)	148.8
	N55–H55b···O3	2.04	2.962(9)	151.3
64	N7–H7b···O3	1.75	2.755(3)	173.6
	N1–H2···N24	2.23	3.238(3)	175.8
	N17–H6···N8	2.20	3.174(3)	160.4
	N23–H23a···O1	1.88	2.784(3)	147.3
	N7–H7a···O2	1.91	2.910(3)	172.1
	N23–H23b···O4	2.03	2.980(3)	156.4
65	N7–H7b···O4	1.81	2.780(8)	159.7
	N1–H1···N25	2.13	3.121(7)	167.2
	N18–H18···N8	2.17	3.174(6)	170.3
	N24–H24a···O1	1.70	2.705(8)	172.1
	N7–H7a···O2	2.01	2.921(7)	149.2
	N24–H24b···O3	1.90	2.893(8)	167.2
66	N1–H1···O5	1.90	2.890(7)	165.3
	N7–H7a···O2	2.06	3.009(7)	155.5
	N7–H7b···O5	2.05	3.025(8)	160.3
	O5–H5b···O1	1.90	2.858(7)	163.6

7.3 Polymorphism in 6-amino-2-phenylsulfonylimino-1,2-dihydropyridine, 54

Polymorphism and pseudopolymorphism in sulfa drugs is well documented in literature, with polymorphs occurring in about 50% of the cases.[3,12] In compound **54**, geometrical isomerism about the C=N bond and the conformational polymorphism[13] around the C–S bond is possible. The presence of several distinct hydrogen-bond donors and acceptors of comparable strengths indicates that structural (or synthon based) polymorphism is also likely. Considering that polymorphism is likely in compound **54,**[14] several crystallization conditions were tried.

Single crystals of Form I of **54** obtained from methanol by slow evaporation of solvent at room temperature. It crystallizes in monoclinic $P2_1/c$ space group with one molecule in the asymmetric unit. In the crystal structure, screw axis related molecules are connected by the 2-point catemer synthon (Scheme 3) with N–H···N hydrogen bonds (Table 1) between a primary amine H–atom and an imine N–atom, and N–H···O hydrogen bonds

(Table 1) between a secondary amine H–atom and a sulfonyl O–atom. The two molecules to which a reference molecule forms such synthons are in themselves related by a translation along [010] and an additional N–H···O bond (Figure 1a). These one-dimensional motifs are in turn connected by herringbone interactions (Figure 1b). The conformation of molecule **54** is quite unusual, with an almost never previously observed eclipsing of the phenyl ring and the S–N bond, **a** rather than the expected conformations **b** through **e**, commonly found in sulfonimides (Scheme 4). The C–C–S–N torsion in **54** is 23.6º whereas generally observed conformation of aryl sulfonimides with C–C–S–N torsion is 40–90º (Figure 2).

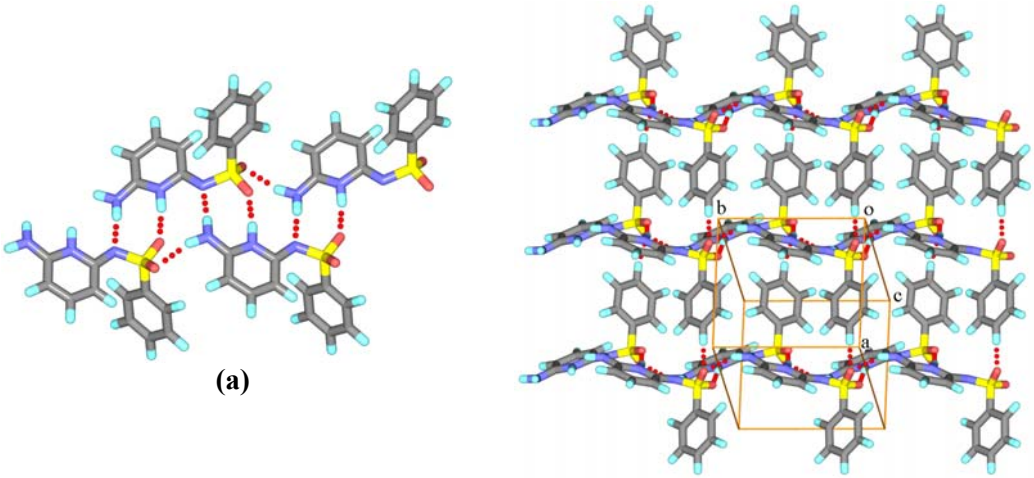

Figure 1. Crystal structure of **54**, (a) One dimensional 2-point catemer chain in Form I. (b) Two catemer chains are connected by C–H···O hydrogen bonds.

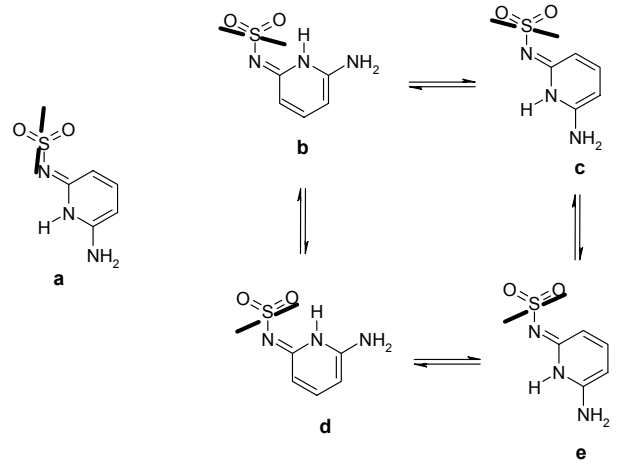

Scheme 4. Possible conformations of compound **54.**

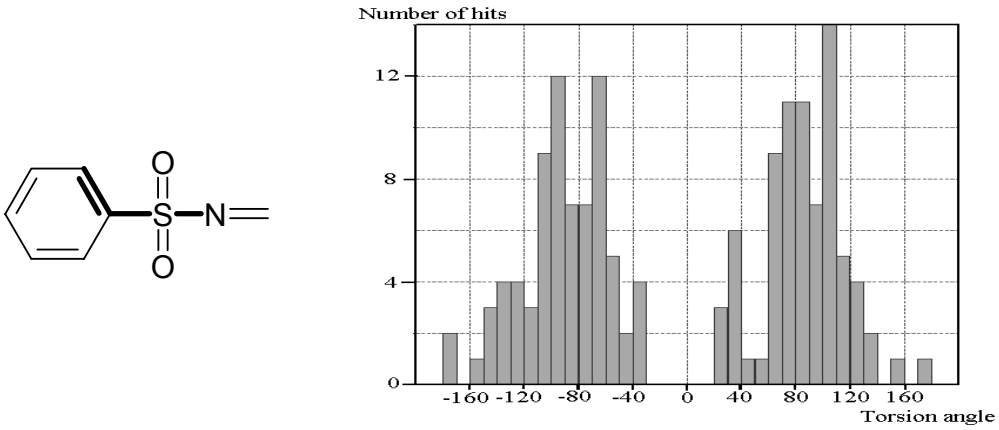

Figure 2. Histogram of The C–C–S–N (bold in fragment shown left side) torsion angle in CSD.

Since polymorphism is very likely in compound **54**, recrystallizations were carried out from a variety of solvents like benzene, toluene, xylene, dichloromethane, chloroform, acetone, acetonitrile, ethyl acetate, methanol, ethanol, 1-propanol, 2-propanol, DMF and DMSO. Solvent combinations; e.g. MeOH–MeCN and benzene–MeCN were also tried. Invariably crystals of Form I or powders were obtained. Other attempts to obtain crystals included slow cooling of saturated solutions under pressure and slow or rapid cooling of supersaturated solutions. In these experiments, we obtained either powders or ill-defined crystals. Sublimation produced flakes with a different appearance (shape). Subsequent trials from various solvents gave Form I crystals. In all, approximately 80 single crystals from different crystallization experiments were selected for cell measurements. While the crystals very often had different morphologies, all of them turned out to be Form I or twinned crystals of the same form. Powder diffraction gave varying patterns due to texture effects, but selected single crystals always confirmed Form I. When compound **54** was recrystallized from nitromethane, the first batch contained only twinned crystals. The second crop was slightly better but the very thin crystals gave only a few weak reflections. However, very good crystals were obtained from the third batch. These crystals were found to be different from those obtained previously and correspond to a new polymorph, namely Form II. This protocol of successive crystallizations from a nitromethane solution was repeated many times and on every occasion, the same behaviour was observed.

The new polymorph also crystallizes in the space group $P2_1/c$, but with two molecules in the asymmetric unit with different molecular conformations. The most important and distinctive structural feature of Form II is the 4-point hydrogen bonded

dimersynthon (Scheme 3) that connects symmetry independent molecules by two N–H···O hydrogen bonds involving one of the O–atoms of the sulfonyl group and a primary amine H-atom of the other molecule. The two N–H···N hydrogen bonds in the middle are formed between the secondary amine H–atoms and imine N–atoms. Both molecules involved in such dimer formation interact with six other dimers with N–H···O and C–H···O hydrogen bonds to form a layer and all phenyl rings project from the same side of the layered structure (Figure 3a). The double layer is constituted with interdigitated aryl rings forming a herringbone motif (Figure 3b). Molecular conformation of two symmetry independent molecules in Form II is different from that observed in Form I (Figure 4). The differences have to do not only with the C–C–S–N torsion but also with the S–N–C–N torsion angle.

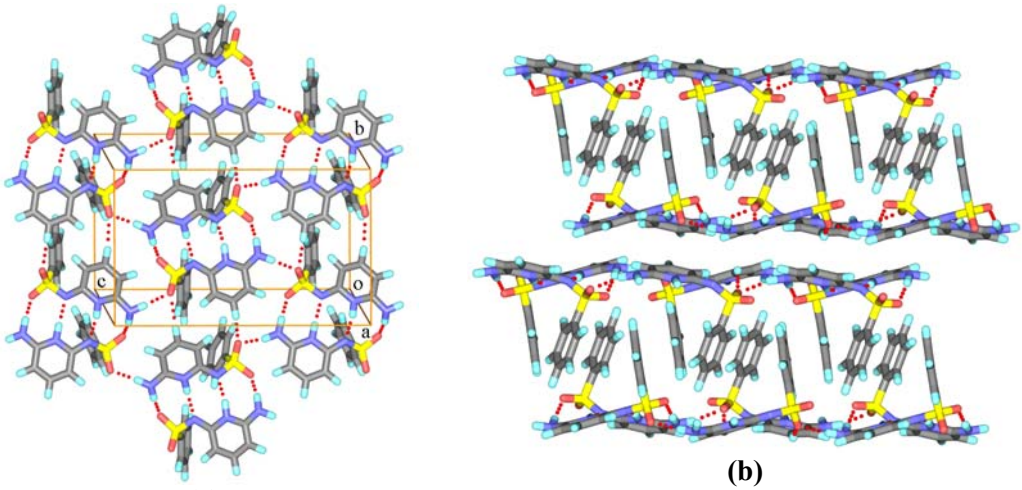

Figure 3. (a) N–H···O, N–H···N and C–H···O hydrogen bonds mediated two-dimensional layered structure of Form II of **54**. (b) Double layered network down the *b*-axis.

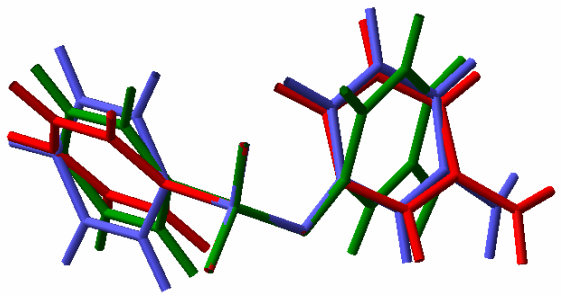

Figure 4. Overlay of molecule **54** in both Form I (red) and Form II (green and blue) indicating the conformational flexibility in the two forms.

7.4 Structural variations and polymorphism in derivatives of 54

To study the effect of subtitution on polymorphism and the structural chemistry, several derivatives of molecule **54** (Scheme 2) were prepared by systematically substituting the H-atoms on the *ortho*-, *meta*- and *para*- positions of the phenyl ring.

The packing of the parent molecule **54** and its derivatives is dominated by an AADD (acceptor–acceptor–donor–donor) hydrogen bond functionality with the sulfonylimino O–atom and N–atom acting as acceptors respectively to the hydropyridine and amino donors (Scheme 3).[15] The second H-atom of the amino group and the second O-atom of the sulfonyl group provide a third strong donor-acceptor pair which flanks the AADD fragment on both sides of the extended hydropyridine system. The three distinct hydrogen bonds so formed (N–H···O, N–H···N, N–H···O) are present in all 14 structures studied in this chapter. Variations in the arrangement of the molecules and hydrogen bond pattern in 11 of the crystal structures can be classified into two distinct families, termed as catemer and dimer, while the three others can possibly be visualised as intermediate between the catemer and dimer families.

7.4.1 Catemer family

Form I of the parent molecule **54** heads the first family followed by *o*-chloro, **55**, *o*-methyl, **56** and *p*-fluoro, **59** derivatives. All these crystals are characterised by a 2-point catemer arrangement. The chain is of the ···AADD···AADD···AADD type as shown in figure 5a for *p*-fluoro derivative, **59**. All these compounds basically have the same structure as demonstrated by the comparable cell parameters all within space group $P2_1/c$. The *a*-axis of **59**, along which the C–F bond is aligned, is ~0.45 Å longer than in Form I of **54**. This increase of the *a*-axis is owing to the steric constraints of fitting the F-atom into the previously occupied position of the H-atom. This is a close fit, as indicated by a short intermolecular F···S distance D = 3.222 Å, which is a short, linear fluorine···sulfonyl contact below the sum of the van der Waals radii (Figure 5b). Due to conformational difference, the phenyl substituents in **55** and **56** are perpendicular to the direction of the chain and do not form a herringbone motif with the neighbouring chain as in **54** and **59**, rather they are π-stacked (Figures 5c, 5d).

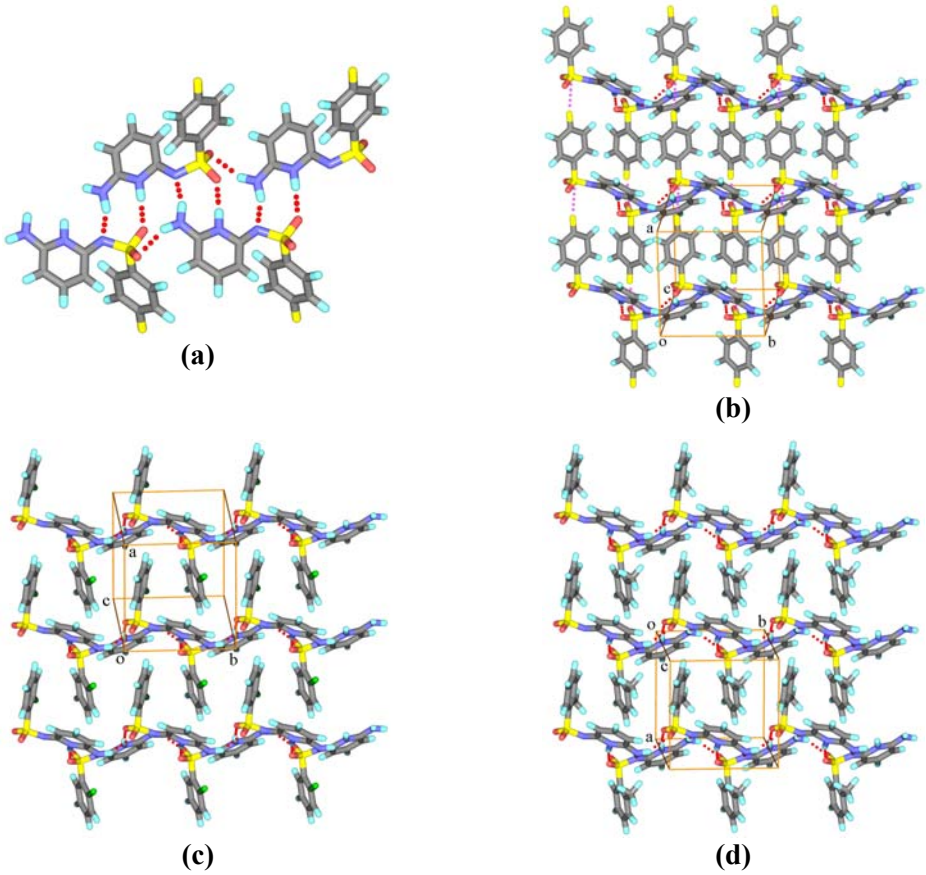

Figure 5. (a) Catemer chain of the *p*-fluoro derivative, **59**. (b) View down *c*-axis showing two catemer chains with a herringbone pattern between phenyl rings. The F-atom points towards an S-atom of an adjacent chain (F···S, 3.222 Å; C–F···S, 173°). (c) *o*-chloro derivative, **55** and (d) *o*-methyl derivative, **56**. Note the change in the packing of phenyl rings from a herringbone to a π-stacking motif.

7.4.2 Dimer family

Form II of the parent molecule **54** is the prototype of the dimer family. The two polymorphs of the *p*-methyl, **63**, *p*-bromo, **61**, *p*-iodo, **62**, *p*-trifluoromethyl, **64** and *p*-methoxy, **65** derivatives fall into this family. Two symmetry-independent molecules form an AADD···DDAA dimer synthon with N–H···O and N–H···N hydrogen bonds. Each dimer is linked to six others with N–H···O and C–H···O interactions (Figure 6a) to form a layer and all phenyl or tolyl substituents project same side of the layer. The double layer is constituted with interdigitated aryl rings forming a herringbone motif (Figure 6b). The structures in the dimer family are characterised by this hydrogen bond network forming a double layer.

Both polymorphs of the methyl derivative **63** are very similar to Form II of the parent molecule **54**. Unlike in **54** where the dimorphs are structurally very distinct, the

polymorphs of **63** are mere variants. Form I of **63** crystallizes in space group $P2_1/n$ with two molecules in the asymmetric unit (Z' = 2). The two-dimensional hydrogen bond network is relatively flat and the distance between the double layers is 3.40 Å and 9.89 Å within a double layer. For the parent compound **54** (Form II) the corresponding values are 3.37 Å and 8.64 Å. The increase of 1.25 Å represents the change from a C–H spatial requirement of 2.3 Å to a C–CH_3 requirement of 3.3–3.8 Å. It should be noted that the density of crystalline Form I of **63** is only 1.367 g cm^{-3} (1.379 g cm^{-3} for Form II) compared to 1.463 g cm^{-3} in Form II of **54**. Form II of **63** adopts space group $P2_1/c$ with Z' = 4. The two dimers in the asymmetric unit are related by pseudosymmetry and can be fitted to a dimer of Form I plus its *c*-glide related equivalent with an rms deviation of less than 0.1 Å. In effect, the geometry of the hydrogen bonded networks and of the layers themselves are homomorphic. The next four derivatives **61**, **62**, **64** and **65** in the dimer family may be grouped into a subfamily since they show a common deviation from the methyl derivatives and the parent Form II of **54** packing. The general arrangement and hydrogen bond pattern stays the same (Figure 7a) but the dimer orientation is different in that the pyridine rings are slanted with respect to the hydrogen bond network. In this way, the previously planar two-dimensional hydrogen bond network becomes more corrugated, enabling weak C–H···O hydrogen bonds between these networks (Figure 7b). Compounds **62**, **64** and **65** share the same space group *Pbca* with Z' =2, and have similar unit cell parameters. The unit cell of bromo compound **61** ($P2_1/c$, $\beta = 94.33°$, Z' = 4) is very similar to Form II of **63**.

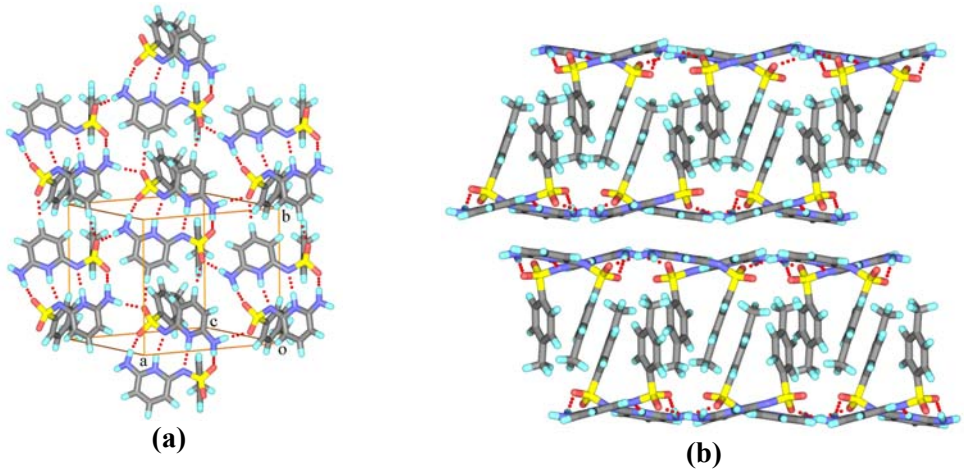

(a) **(b)**

Figure 6. (a) Form I of *p*-methyl derivative, **63**, dimers are connected by four strong hydrogen bonds. Each dimer is surrounded by six others to which it is linked by N–H···O and C–H···O hydrogen bonds. All *p*-tolyl substituents are on the far side of the resulting two-dimensional hydrogen bonded layer. (b) View down *b*-axis, hydrogen bonded networks interdigitate with the phenyl substituents to form double layers.

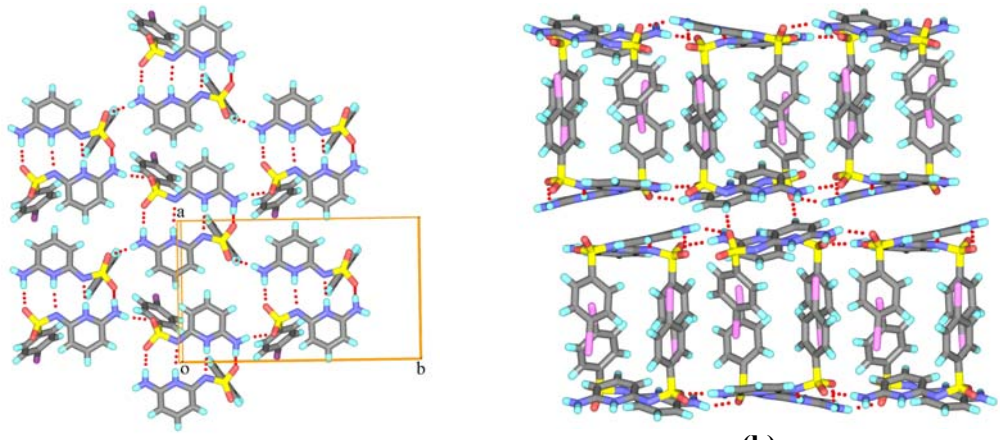

(a) **(b)**

Figure 7. (a) Two dimensional layered strcuture of *p*-Iodo derivative **62**. (b) View down *a*-axis, the slant of both pyridine ring systems can be seen, while the general features of double layer formation are kept. Notice C–H···O hydrogen bonds between double layers.

The intermolecular geometry of the dimer changes in going from the planar to the slanted subfamilies. The mean N–H···O bond length shortens from D ≈ 2.8 Å in the planar dimer to D ≈ 2.75 Å in the slanted dimer while the neighbouring N–H···N bond lengthens on average from D ≈ 3.0 Å to D ≈ 3.15 Å (Figure 8). As expected from the relative strengths of the typical N–H···O and N–H···N hydrogen bonds, the distance change is less for the stronger N–H···O hydrogen bond. Apparently, this lengthening and shortening is mutually compensative; the overall stabilisation of the four-point synthon seems to be unaffected. A calculation at the RHF/6-31G* level of both dimer geometries in Form I of **63** and **65** results in an energy difference of only 1.34 kcal/mol. A possibly alternative DADA type of dimer geometry of other possible tautomer is neither found in any of the crystal structures nor observed in DMSO solution by NMR. These results confirm the observations of Meijer that a prevalence of AADD over DADA is expected because of additional H–atom repulsion in alternating hydrogen bonds.[16] A superposition of the AADD dimers in this study is shown in figure 9. A change of general orientation might be noted within the dimer family as is clearly seen by the gap between overlaid dimers. The structures of Form II of **63** (blue) and **61** (green), which have similar space group ($P2_1/c$) and unit cell parameters ($Z' = 4$) share a common dimer arrangement. This might be seen as transitional packing between the two subfamilies.

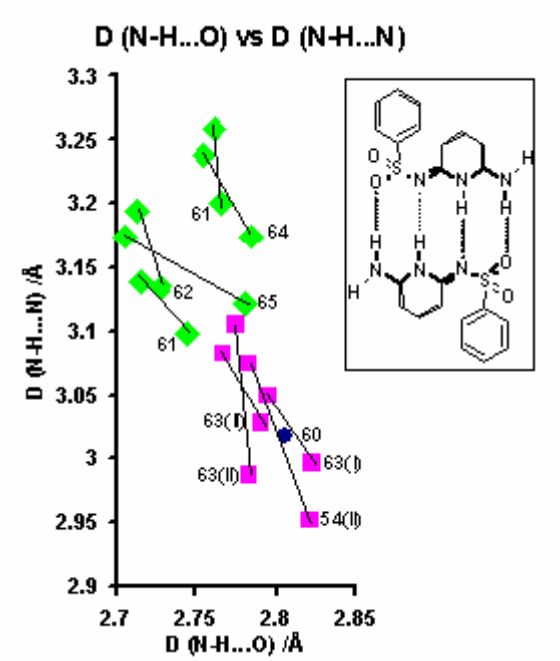

Figure 8. Scatter plot of D (N···O) distances vs neighbouring D (N···N) distances in the dimers. Lines connect D/D pairs within one dimer. The planar subfamily structures have shorter hydrogen bonds to the N-atom acceptor (lower right area, pink squares) while the slanted subfamily structures have shorter hydrogen bonds to the O-atom acceptor (upper left area, green squares). A blue circle is used for the chloro derivative **60**.

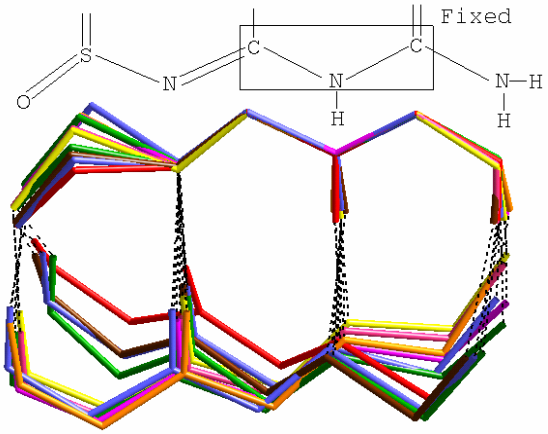

Figure 9. Overlay of AADD fragments in the dimers so that both C–atoms and the pyridine N–atom coincide. red–Form II of **54**, orange–**60**, green–**61**, pink–**62**, brown–Form I of **63**, blue–Form II of **63**, yellow–**64** and magenta–**65**. Note the differences in the dimer geometry.

7.4.3 Intermediate structures

Crystal structrues of *m*-methyl, **58**, *p*-chloro, **60** and the monohydrate of *p*-nitro **66** derivatives come under this family. The crystal strucuture of **58** is charecterised by 2-point catemer chain and additional N–H···O hydrogen bonds (D = 3.028 Å) are formed along the

chain. But the *para* H–atom of the pyridine ring is oriented towards the second sulfonyl O–atom, forming a C–H···O hydrogen bond (d = 2.492 Å) interconnecting these chains leads to a two-dimensional hydrogen bond network (Figure 10a). This network is very comparable to the two-dimensional hydrogen bonded network in the dimer family and it too forms a double layer with interdigitated phenyl residues to form double layered structure (Figure 10b) which is charecteristic of dimer family. Becuase **58** forms 2-point catemer synthon and double layered structure, it can be clasified as an intermediate structure between the catemer and the dimer families. Only, the dimers are shifted relative to each other to form catemer chains. This is possible because the chain is formed not with screw axes as in the other structures of the catemer family but with a glide plane, putting the substituents on the same side, which is crucial for the interdigitation of the double layer.

Para-chloro derivative **60** crystallizes in *C*2/*c* space group with one molecule in the asymmetric unit. Molecules related by a twofold axis form 4-point dimer synthon. This is in contrast to the dimer family described above in which symmetry independent molecules form dimers. The third N–H···O (D = 2.962 Å) hydrogen bond is between stacked dimers threading them into chains running along [110] and [1-10] (Figure 11a). Eventually, a layer in (001) is formed containing all the dimers and with the chlorophenyl substituents sticking out. The general arrangement of stacked phenyl substituents and their arrangement into a chain is more reminiscent of the catemer family (Figures 11b, 11c). In this way, **60** may be regarded as an intermediate between the catemer and the dimer families. Incidentally, it should be noted that the density of **60** is only 1.479 g cm^{-3} while that of the isomeric **55** is 1.527 g cm^{-3}. This is unusual and polymorphs of **60** were searched exhaustively but without success. However, **60** is the most likely candidate for polymorphism in this series of compounds.

The hydrate of the *p*-nitro derivative **66** is a clear exception to the rule that molecules bind to each other *via* the AADD fragment. Here, water accepts a N–H···O hydrogen bond from the hydropyridine (D = 2.890 Å), while the catemer chain is still formed, it incorporates only the flanking sulfonylimino O–atom and the amine N–atom (Figure 12).

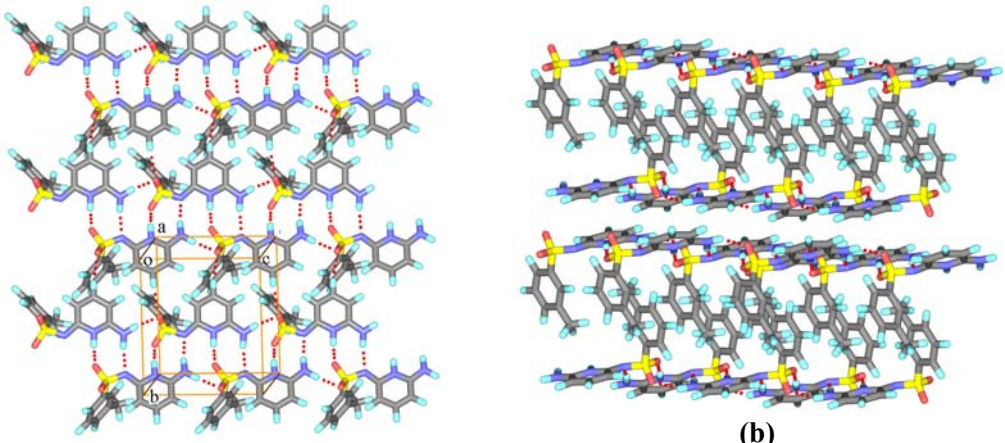

Figure 10. (a) Two-dimensional N–H···O and C–H···O hydrogen bond network with a catemer motif in *m*-methyl derivative, **58**. (b) Double layer network of **58**. Note that the double layer network charecteristic of dimer family.

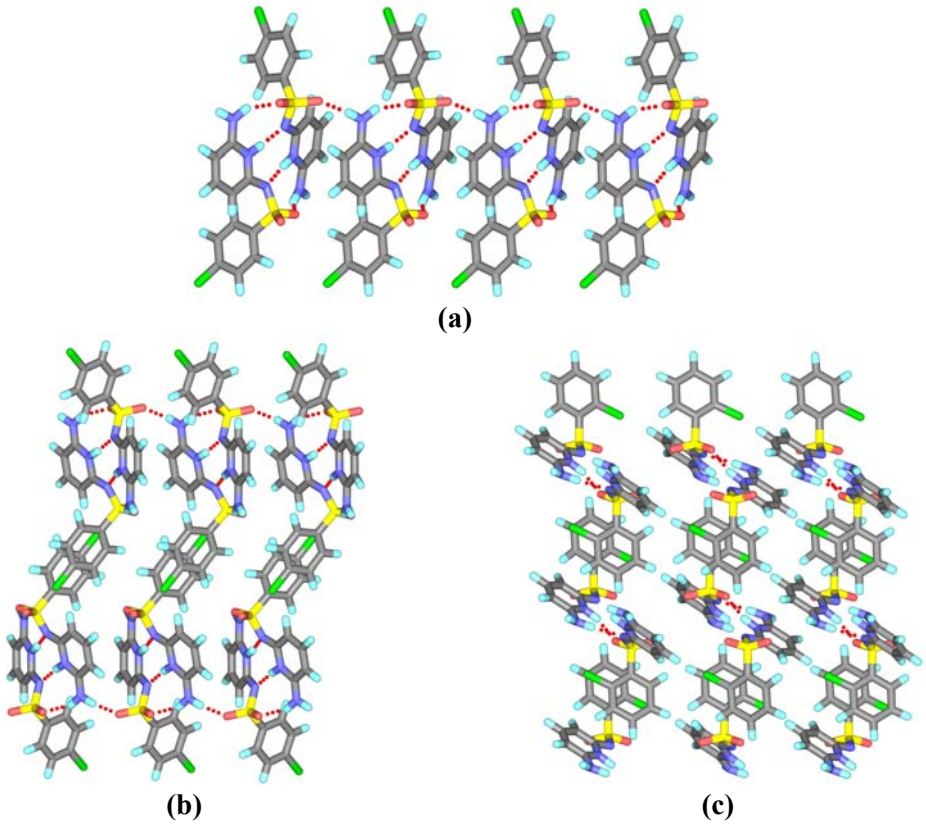

Figure 11. (a) 4-Point dimer synthon in *p*-chloro derivative, **60** to show stacked dimers. (b) View down [-110] showing the stacking of chlorophenyl rings and chain motif of dimers in *p*-chloro derivative, **60**. (c) *o*-chloro derivative, **55**. View down [010] showing the stacking of chlorophenyl rings in **55**. Note the general similarities in stacking between the two structures.

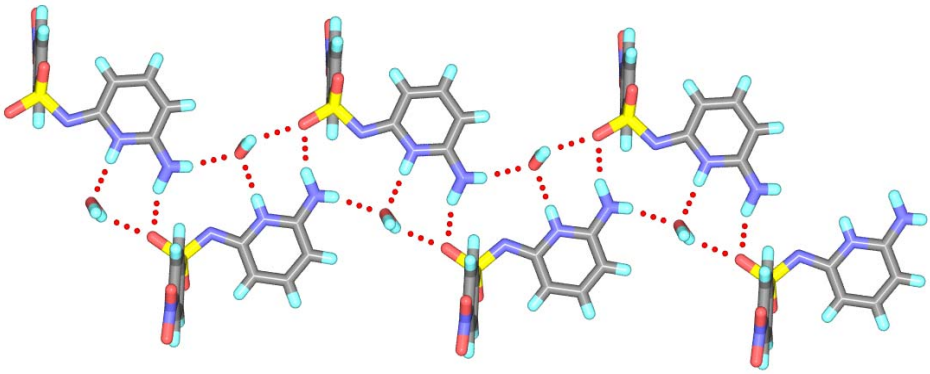

Figure 12. Catemer like hydrogen bonded motif in *p*-nitro derivative, **66**. Notice imine N and nitro group not participating in hydrogen bonding.

7.5 Stability of polymorphs of 54

Lattice energies of both polymorphs of **54** are calculated to evaluate the stability. The packing potential energies involving both intra and intermolecular components are –28.96 kcal/molecule/mol for Form I and –29.82 kcal/molecule/mol for Form II.[17] This shows that Form II is the thermodynamic form. Notwithstanding this, the fact that Form II was seldom observed indicates the importance of kinetic and entropic factors during crystallization, in other words the relevance of cluster propagation. 2-point catemer synthon leads to one-dimensional propagation *via* 2–point recognition but 4-point dimer synthon is of lower dimensionality and propagation is correspondingly less facile.[18] The fact that the one-dimensional patterns in Form I are extended into higher dimensions with weaker C–H···O hydrogen bonds also indicates that this form could be entropically favoured. In order to evaluate the relative strengths of the hydrogen bonds in the two structures, a representative cluster of three molecules in each polymorph considered (Figure 13).

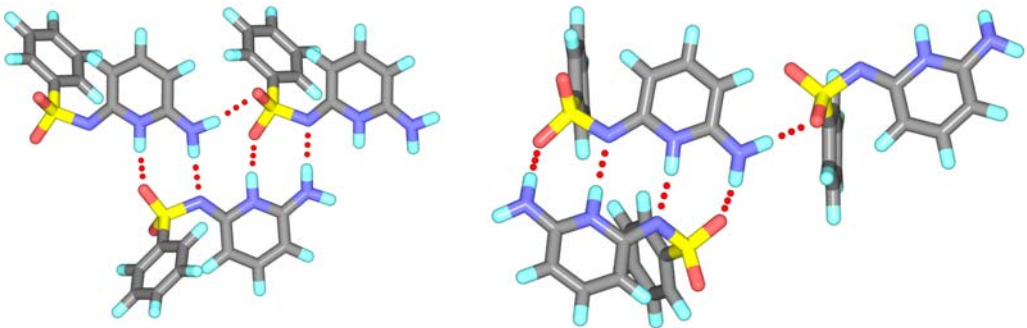

Figure 13. Three molecular clusters of Form I and Form II of **54** taken for hydrogen bond energy calculation. Note the same number of hydrogen bonds and molecules.

The energies of the three molecular cluster in Form I is 22.25 kcal/mol while it is 22.36 kcal/mol in Form II.[19] These values contain components of both intra and intermolecular energies. While, the energy difference of only 0.11 kcal/mol between the two cases could be indicative of the likelihood of polymorphism, the fact that the Form I cluster is slightly more stable hints that this is the kinetic form. However, when the intramolecular components are separated out, 4-point synthon is seen to be stable by as much as 4.83 kcal/mol confirming that the hydrogen bonds in Form II are better than in Form I. All this confirms that while Form I is kinetically favoured, Form II is the thermodynamic crystal.

7.6 Polymorph prediction: Recent Examples

Although there have been cases where the crystal structure of a molecule was genuinely predicted just from the chemical diagram, it is certainly not yet possible to predict the crystal structures of any organic molecule by *ab initio* calculations. Price *et al.* compiled a useful 'atlas' of organic molecules which have been used in crystal structure prediction studies carried out by lattice energy calculations.[20] Jones and coworkers summarized crystal structure prediction of a diverse set of 50 organic rigid molecules by lattice energy minimization and showed about half of all molecules can be found among the five lowest energy predicted structures, or within 1 kJ/mol of the global minimum in lattice energy.[21] Price *et al.*[22] used a combination of both single-crystal and X-ray powder diffraction techniques and crystal structure prediction and characterized three polymorphs of chlorothalonil (2,4,5,6-tetrachloro-1,3-benzenedicarbonitrile, Scheme 5). Recently a new thermodynamically stable polymorph of 5-fluorouracil is reported after 30 years from search inspired by computational prediction.[23] Similarly Jones and coworkers have reported a new polymorph of maleic acid after 124 years of the first polymorph reported which was formed during cocrystallization experiment with caffeine. After obtaining the second form they have performed polymorph prediction computationally and found that the new form is global minimum in lattice energy.[24] Zaworotko and coworkers[25] reported X-ray crystal structure of Form II of aspirin a comformationally flexible molecule, which was computationally predicted by Ouvrard and Price.[6d] Some success is been achieved in recent years by synthon based approach to *ab initio* calculations. Desiraju *et al.* predicted crystal structures of isomeric methylaminophenols (Scheme 5) using synthon based approach and concluded that polymorphism is not so common in this family of compounds because the energy difference between lowest energy packing and second lowest is higher.[26]

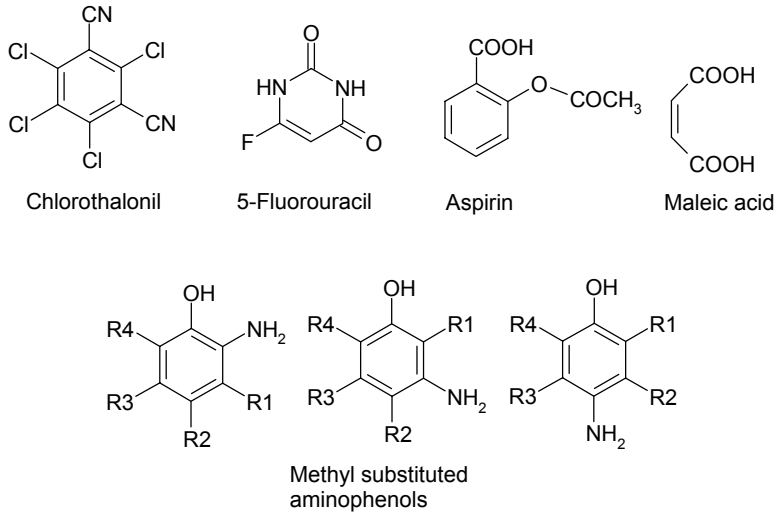

Scheme 5. Compounds whose crystal structures were predicted computationally in recent literature.

7.7 Discussion

A large number of derivatives of **54**, 12 in all, were prepared and each compound was crystallised around six to ten times employing different conditions. None except **54** and **63** was found to be polymorphic. However, polymorphism was not found in a general sense and yet the crystal structures of the compounds in this study may be divided into two families. Lattice energy and cluster energy calculations shows From I (2-point catemer synthon) of parent compound **54** is kinetically driven struture whereas Form II (4-point dimer synthon) is thermodynamically favoured. The catemer family has a one-dimensional hydrogen bond structure that closely resembles the kinetic form of the reference compound **54**. The dimer family has a zero-dimensional structure that resembles the thermodynamic polymorph of **54**. While **63** is technically dimorphic, both forms belong to the same (dimer) family. Derivatives **58**, **61** and **66** crystallise in crystal structures that might be seen as intermediates between the catemer and the dimer families. X-ray quality single crystals of **57** were not obtained. The packing of the catemer family can accommodate small substituents (like F) in the *para*-position and larger substituents (like Cl and Me) in the *ortho*-position.

What is more notable is that none of the derivatives studied in this chapter have structures in both the catemer and dimer families. It is difficult to genaralize why polymorphism is not observed in derivatives but it is possible that polymorphism might still be found in the chloro derivative **60**, since this compound has an intermediate packing pattern and an anomalously low density. However, there is another way of considering the

present results. If the possible structural variations for any given molecule might be said to constitute a 'packing landscape'[27] the landscapes for all the derivatives studied in this chapter might be said to be broadly similar. Variation of experimental conditions of crystallisation is one way of sampling a particular landscape and when one arrives at a local minimum, a new polymorph is found. This study shows that substitutional variation is a good way of sampling different regions of different landscapes. But these different landscapes are generally similar within a chemical family. Therefore, structural variations that are found for differently substituted derivatives (although not yet formally polymorphic) represent putative polymorphic structures that might still be found for any one particular compound if the experimental conditions are made more exotic, or very possibly be identified computationally with programs that generate large number of polymorph structures.

7.8 Conclusions

Following conclusions can be drawn from the above study. (i) Polymorphism can be predicted computationally but experimental realization of the computationally predicted polymorphs is challenging. (ii) Even in a closely related family of compounds like the derivatives of **54**, it is very dificult to obtain polymorphs. There is clearly a unique combination of molecular features that lead to polymorphism; the question is what are they? (iii) The effect of substitution on hydrogen bonding is less when molecules engage in strong multi-point hydrogen bond recognition.

7.9 Experimental Section

Synthesis: All compounds discussed here were synthesized according to the literature procedure given for 2-(aminobenzenesulfonylamino)-6-aminopyridine by taking the corresponding sulfonyl chloride with 2,6-diaminopyridine. All compounds were characterized by IR and NMR. ^{1}H NMR (δ scale in ppm, *J* coupling constant in Hz) spectra were recorded at 200 MHz on a Bruker ACF instrument and IR (ν in cm^{-1}) spectra were recorded on a Jasco 5300 spectrophotometer. Melting points were recorded on Fisher-Johns apparatus.

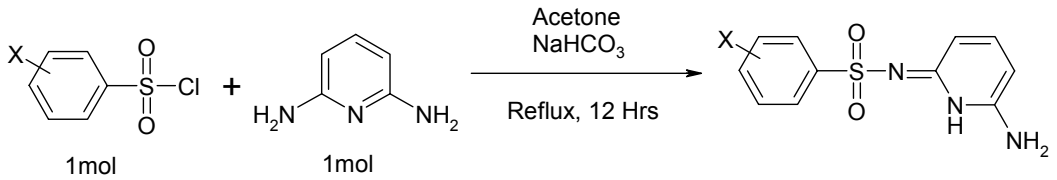

6-Amino-2-phenylsulfonylimino-1,2-dihydropyridine, 54: Yield 72%. ^{1}H NMR (DMSO-*d6*): δ 11.24 (b, NH), 7.82 (d, *J* = 6, 2H), 7.49 (m, 3H), 7.27 (t, *J* = 6, 1H), 6.15 (b, NH2),

6.15 (d, *J* = 6, 1H), 5.91 (d, *J* = 6, 1H). IR (KBr): 3373, 3327, 3200, 1371, 1130 cm^{-1}. M. p. 235 °C.

6-Amino-2-(2-chlorophenylsulfonylimino)-1,2-dihydropyridine, 55: Yield 60%. ^{1}H NMR (DMSO-*d6*): δ 11.86 (b, NH), 7.82 (d, *J* = 6, 1H), 7.49 (m, 3H), 7.27 (t, *J* = 5, 1H), 6.42 (b, NH_2), 6.10 (d, *J* = 6, 1H), 5.85 (d, *J* = 6, 1H). IR (KBr): 3365, 3329, 3204, 1365, 1134 cm^{-1}. M. p. 222-225 °C.

6-Amino-2-(2-methylphenylsulfonylimino)-1,2-dihydropyridine, 56: Yield 65%. ^{1}H NMR (DMSO-*d6*): δ 11.20 (b, NH), 7.94 (d, *J* = 6, 1H), 7.40 (m, 3H), 7.22 (t, *J* = 6, 1H), 6.23 (b, NH_2), 6.10 (d, *J* = 6, 1H), 5.86 (d, *J* = 6, 1H), 2.59 (s, 3H). IR (KBr): 3357, 3337, 1373, 1114 cm^{-1}. M. p. 210-211 °C.

6-Amino-2-(3-chlorophenylsulfonylimino)-1,2-dihydropyridine, 57: Yield 56%. ^{1}H NMR (DMSO-*d6*): δ 11.72 (b, NH), 8.32 (s, 1H), 7.92 (d, *J* = 6, 1H), 7.42 (d, *J* = 6, 1H), 7.35 (t, *J* = 6, 1H), 7.23 (t, *J* = 6, 1H), 6.22 (b, NH2), 6.10 (d, *J* = 6, 1H), 5.87 (d, *J* = 6, 1H). IR (KBr): 3355, 3187, 1352, 1123 cm^{-1}. M. p. 225-227 °C.

6-Amino-2-(3-methylphenylsulfonylimino)-1,2-dihydropyridine, 58: Yield 73%. ^{1}H NMR (DMSO-*d6*): δ 11.14 (b, NH), 7.67 (s, 1H), 7.65 (s, 1H), 7.42 (d, *J* = 6, 1H), 7.30 (t, *J* = 6, 1H), 7.23 (t, *J* = 5, 1H), 6.16 (b, NH2), 6.16 (d, *J* = 6, 1H), 5.89 (d, *J* = 6, 1H), 2.35 (s, 3H). IR (KBr): 3375, 3335, 3200, 1362, 1134 cm^{-1}. M. p. 235-236 °C.

6-Amino-2-(4-fluorophenylsulfonylimino)-1,2-dihydropyridine, 59: Yield 79%. ^{1}H NMR (DMSO-*d6*): δ 11.40 (b, NH), 7.94 (d, *J* = 6, 2H), 7.35 (d, *J* = 6, 2H), 7.29 (t, *J* = 5, 1H), 6.28 (b, NH2), 6.18 (d, *J* = 6, 1H), 5.89 (d, *J* = 6, 1H). IR (KBr): 3305, 3292, 3223, 1340, 1128 cm^{-1}. M. p. 182-185 °C.

6-Amino-2-(4-chlorophenylsulfonylimino)-1,2-dihydropyridine, 60: Yield 58%. ^{1}H NMR (DMSO-*d6*): δ 11.52 (b, NH), 7.84 (d, *J* = 6, 2H), 7.35 (d, *J* = 6, 2H), 7.27 (t, *J* = 6, 1H), 6.34 (b, NH2), 6.16 (d, *J* = 6, 1H), 5.89 (d, *J* = 6, 1H). IR (KBr): 3393, 3203, 1375, 1134 cm^{-1}. M. p. 192 °C.

6-Amino-2-(4-bromophenylsulfonylimino)-1,2-dihydropyridine, 61: Yield 62%. ^{1}H NMR (DMSO-*d6*): δ 11.54 (b, NH), 7.78 (d, *J* = 6, 2H), 7.67 (d, *J* = 6, 2H), 7.27 (t, *J* = 5, 1H), 6.31 (b, NH2), 6.13 (d, *J* = 6, 1H), 5.89 (d, *J* = 6, 1H). IR (KBr): 3423, 3327, 3275, 1369, 1126 cm^{-1}. M. p. 215 °C.

6-Amino-2-(4-iodophenylsulfonylimino)-1,2-dihydropyridine, 62: Yield 60%. ^{1}H NMR (DMSO-*d6*): δ 11.40 (b, NH), 7.89 (d, *J* = 6, 2H), 7.60 (d, *J* = 6, 2H), 7.26 (t, *J* = 6, 1H),

6.32 (b, NH2), 6.12 (d, *J* = 6, 1H), 5.89 (d, *J* = 6, 1H). IR (KBr): 3435, 3362, 1350, 1125 cm^{-1}. M. p. 240-242 °C.

6-Amino-2-(4-methylphenylsulfonylimino)-1,2-dihydropyridine, 63. Yield 79%. ^{1}H NMR (DMSO-d_6): δ 11.40 (b, NH), 7.77 (d, *J* = 6, 2H), 7.33 (d, *J* = 6, 2H), 7.25 (t, *J* = 6, 1H), 6.17 (b, NH2), 6.12 (d, *J* = 6, 1H), 5.92 (d, *J* = 6, 1H), 2.34 (s, 3H). IR (KBr): 3377, 3198, 1371, 1132 cm^{-1}. M. p. 205-207 °C.

6-Amino-2-[4-(trifluoromethyl)phenylsulfonylimino]-1,2-dihydropyridine, 64: Yield 79%. ^{1}H NMR (DMSO-d_6): δ 11.72 (b, NH), 8.02 (d, *J* = 6, 2H), 7.87 (d, *J* = 6, 2H), 7.30 (t, *J* = 5, 1H), 6.40 (b, NH2), 6.16 (d, *J* = 6, 1H), 5.89 (d, *J* = 6, 1H). IR (KBr): 3387, 3318, 3214, 1365, 1138 cm^{-1}. M. p. 220-223 °C.

6-Amino-2-(4-methoxyphenylsulfonylimino)-1,2-dihydropyridine, 65: Yield 68%. ^{1}H NMR (DMSO-d_6): δ 10.84 (b, NH), 7.79 (d, *J* = 6, 2H), 7.24 (t, *J* = 6, 1H), 6.90 (d, *J* = 6, 2H), 6.15 (d, *J* = 6, 1H), 5.95 (b, NH2), 5.73 (d, *J* = 6, 1H), 3.70 (s, 3H). IR (KBr): 3467, 3372, 1356, 1130 cm^{-1}. M. p. 160 °C.

6-Amino-2-(4-nitrophenylsulfonylimino)-1,2-dihydropyridine, 66 : Yield 80%. ^{1}H NMR (DMSO-d_6): δ 10.00 (b, NH), 8.30 (d, *J* = 6, 2H), 8.02 (d, *J* = 6, 2H), 7.36 (t, *J* = 5, 1H), 6.50 (b, NH2), 6.16 (d, *J* = 6, 1H), 5.90 (d, *J* = 6, 1H). IR (KBr): 3355, 3282, 3243, 1480, 1345, 1132 cm^{-1}. M. p. 213-215 °C.

Recrystallisation experiments: Because of possibility of polymorphism, crystals of **54** were grown from acetone, acetonitrile, chloroform, dichloromethane, DMF, DMSO, dioxane, ethanol, ethyl acetate, methanol, nitromethane, tetrachloromethane and THF for all derivatives. For **59**–**63** additionally benzene, n-butanol, ether, and toluene were tried. Upto five crystals from each batch, and around 250 crystals in all, were checked for their cell parameters. Only for compound **63** were two polymorphs found. Crystallisation from nitromethane which successfully yielded the thermodynamic form of **54**, was not successful in generating polymorphs of derivates **56**, **58**, **59**–**63**, **65** and **66**. **57** did not yield crystals and **66** crystallised as a hydrate.

X-ray Data Collection and Crystal Structure Determinations: X-ray data for **66** were collected on a Bruker P4 diffractometer, while those for **55**, **56**, **58** and **59**–**65** were collected on a SMART diffractometer using Mo-Kα radiation. The structure solution and refinement were carried out using SHELXL programs built in with the SHELXTL (Version 6.12) package. The positions of the H-atoms bound to phenyl groups in **59**–**66** and amino groups in **59**, **61**, **62**, **63** Form II and **64** were generated by a riding model on idealized geometries

with $U_{iso}(H) = 1.2\ U_{eq}(C)$ or $1.2\ U_{eq}(N)$, while the H-atoms of the amino groups in **55**, **56**, **58**, **60**, **63** Form I, **65**, **66** and methyl groups in **63** Form I were located in difference Fourier maps and these H-atoms were also refined as riding, with $U_{iso}(H) = 1.2\ U_{eq}(N)$ or $1.5\ U_{eq}(C)$. The hydrogen atoms of the water molecule in **66** were also taken from Fourier maps and also refined as riding, with $U_{iso}(H) = 1.5\ U_{eq}(O)$. The F-atoms of the CF_3 group in **64** were disordered over two sites with occupancies 0.5 each. In some cases the U-values seem to be a bit too large or too small and this is because of poor crystal quality, especially in **59**. The details of the X-ray data collection, structure solution, and refinement are given in the supporting information.

7.10 References

1. W.C. McCrone, *Polymorphism in Physics and Chemistry of the Organic Solid-State;* ed. D. Fox, M.M. Labes, A. Weisemberg, Interscience, New York, **1965**, 726.
2. J. Van de Streek and S. Motherwell, *Acta Crystallogr.,* **2005**, *B61*, 504.
3. J.A.R.P. Sarma and G.R. Desiraju, Polymorphism and Pseudopolymorphism in Organic Crystals: A Cambridge Structural Database Study. *Crystal Engineering: The Design and Application of Functional Solids*; ed. M.J. Zaworotko, K.R. Seddon, Kluwer: Dordrecht, **1999**, 325.
4. (a) J. Van de Streek and W.D.S. Motherwell, *Acta Crystallogr.,* **2005**, *B61*, 504. (b) D. Braga and F. Grepeoni, *Chem. Soc. Rev.*, **2000**, *29*, 229.
5. G. R. Desiraju, *Nature Materials,* **2002**, *1*, 77.
6. (a) T. Beyer and S.L. Price, *CrystEngComm,* **2000**, *3*, 183. (b) T. Beyer, G.M. Day and S.L. Price, *J. Am. Chem. Soc.,* **2001**, *123*, 5086. (c) E.D.L. Smith, R.B. Hammond, M.J. Jones, K.J. Roberts, J.B.O. Mitchell, S.L. Price, R.K. Harris, D.C. Apperley, J.C. Cherryman and R. Docherty, *J. Phys. Chem.,* **2001**, *B105*, 5818. (d) C. Ouvrard and S.L. Price, *Cryst. Growth Des.,* **2004**, *4*, 1119.
7. S.R. Byrne, R.R. Pfeiffer and J.G. Stowell, *Solid State Chemistry of Drugs*, 2nd ed.; SSCI Inc.: West Lafayette, IN, **1999**; pp 489-498.
8. M.L. Peterson, S.L. Morissette, C. McNulty, A. Goldsweig, P. Shaw, M. LeQuesne, J. Monagle, N. Encina, J. Marchionna, A. Johnson, J. Gonzalez-Zugasti, A.V. Lemmo, S.J. Ellis, M.J. Cima, and O. Almarsson, *J. Am. Chem. Soc.* **2002**, *124*, 10958.
9. (a) J.P.M. Lommerse, W.D.S. Motherwell, H.L. Ammon, J.D. Dunitz, A. Gavezzotti, D.W.M. Hofmann, F.J.J. Leusen, W.T.M. Mooij, S.L. Price, B. Schweizer, M.U. Schmidt, B.P. van Eijck, P. Verwer and D.E. Williams, *Acta Crystallogr.,* **2000**, *B56*, 697. (b) W.D.S. Motherwell, H.L. Ammon, J.D. Dunitz, A. Dzyabchenko, P. Erk, A.

Gavezzotti, D.W.M. Hofmann, F.J.J. Leusen, J.P.M. Lommerse, W.T.M. Mooij, S.L. Price, H. Scheraga, B. Schweizer, M.U. Schmidt, B.P. van Eijck, P. Verwer and D.E. Williams, *Acta Crystallogr.,* **2002**, *B58*, 647. (c) G.M. Day, W.D.S. Motherwell, H.L. Ammon, S.X.M. Boerrigter, R.G. Della Valle, E. Venuti, A. Dzyabchenko, J.D. Dunitz, B. Schweizer, B.P. van Eijck, P. Erk, J.C. Facelli, V.E. Bazterra, M.B. Ferraro, D.W.M. Hofmann, F.J.J. Leusen, C. Liang, C.C. Pantelides, P.G. Karamertzanis, S.L. Price, T.C. Lewis, H. Nowell, A. Torrisi, H.A. Scheraga, Y.A. Arnautova, M.U. Schmidt and P. Verwer, *Acta Crystallogr.,* **2005**, *B61*, 511.

10. N. Blagden, R.J. Davey, H.F. Lieberman, L. Williams, R. Payne, R. Roberts, R. Rowe and R. Docherty, *J. Chem. Soc., Faraday Trans.,* **1998**, *94*, 1035.
11. K. Tuda, Z. Izikawa and D. So, *J. Pharm. Soc. Japan*, **1939**, *59*, 213.
12. (a) D.S. Hughes, M.B. Hursthouse, R.W. Lancaster, S. Tavener and T.L. Threlfall, *Chem. Commun*., **2001**, 603. (b) I. Bar and J. Bernstein, *J. Pharm. Sci.,* **1985**, *74*, 255. (c) S.R. Byrn, *Solid State Chemistry of Drugs*, Academic Press, **1982**, pp. 103–116.
13. (a) J. Bernstein, *Conformational Polymorphism* in *Organic Solid State Chemistry,* ed.. G.R. Desiraju, Elsevier, Amsterdam, **1987**, pp. 471–518. (b) J. Bernstein, *Polymorphism in Molecular Crystals*, Clarendon Press, Oxford, **2002**, pp. 151–187.
14. J.A.R.P. Sarma and G.R. Desiraju, *Cryst. Growth Des*., **2002**, *2*, 93.
15. (a) J. Pranata, S.G. Wierschke and W.L. Jorgensen, *J. Am. Chem. Soc*., **1991**, *113*, 2810. (b) K. Biradha, A. Nangia, G.R. Desiraju, C.J. Carrell and H.L. Carrell, *J. Mater. Chem.,* **1997**, 1111. (c) R.E. Meléndez and A.D. Hamilton, Hydrogen-bonded ribbons, tapes and sheets as motifs for crystal engineering. In: *Design of organic Solids*; ed. E. Weber, Springer: Berlin, **1998**; pp 97-129. (d) G.M. Whitesides, E.E. Simanek, J.P. Mathias, C.T. Seto, D.N. Chin, M. Mammen, and D.M. Gordon, *Acc. Chem. Res.,* **1995**, *28*, 37. (e) G.M. Whitesides, J.P. Mathias and C.T. Seto, *Science,* **1991**, *254*, 1312. (f) C.T. Seto and G.M. Whitesides, *J. Am. Chem. Soc*., **1993**, *115*, 905. (g) J.A. Zerkowski, C.T. Seto and G.M. Whitesides, *J. Am. Chem. Soc*., **1990**, *112*, 9025. (h) A. Ranganathan, V.R. Peddireddi and C.N.R. Rao, *J. Am. Chem. Soc*., **1999**, *121*, 1752.
16. R.P. Sijbesma and E.W. Meijer, *Chem. Commun.*, **2003**, 5.
17. The lattice energy calculations were carried out in the two forms with H–normalised molecules. The Crystal Packer module which is part of the *Cerius*^{2} program environment was used. Similar potentials as defined earlier were used. No minimisation of either cell parameters or molecular positions was carried out.

18. 4-Point dimer and 2-point catemer synthons may be likened to dimer and catemer motifs in the crystal structures of carboxylic acids and amides with the corresponding implications for crystal growth. See also W.T.M. Mooji, B.P. van Eijck, S.L. Price, P. Verwer and J. Kroon, *J. Comput. Chem*., **1998**, *19*, 459.
19. The lattice energy calculations were carried out in the two forms with H–normalised molecules. Energy calculations were carried out using the CVFF95 force field in the *Cerius*^{2} program. *Cerius*^{2}, Accelrys Ltd., 334 Cambridge Science Park, Cambridge CB4 0WN, U. K. www.accelrys.com.
20. T. Beyer, T. Lewis and S.L. Price, *CrystEngComm,* **2001**, *4*, 1.
21. G.M. Day, J. Chisholm, N. Shan, W.D.S. Motherwell and W. Jones, *Cryst. Growth Des.*, **2004**, *4*, 1327.
22. M. Tremayne, L. Grice, J.C. Pyatt, C.C. Seaton, B.M. Kariuki, H.H.Y. Tsui, S.L. Price and J.C. Cherryman, *J. Am. Chem. Soc.,* **2004**, *126*, 7071.
23. A.T. Hulme, S.L. Price, and D.A. Tocher, *J. Am. Chem. Soc.*, **2005**, *127*, 1116.
24. G.M. Day, A.V. Trask, W.D.S. Motherwell and W. Jones, *Chem. Commun.*, **2006**, 54.
25. P. Vishweshwar, J.A. McMahon, M. Oliveira, M.L. Peterson and M.J. Zaworotko, *J. Am. Chem. Soc.*, **2005**, *127*, 16802.
26. A. Dey, M.T. Kirchner, V.R. Vangala, G.R. Desiraju, R. Mondal, and J.A.K. Howard, *J. Am. Chem. Soc.*, **2005**, *127*, 10545.
27. N. Blagden and R.J. Davey, *Cryst. Growth Des.,* **2003**, *3*, 873.

CHAPTER 8

WEAK C–H···N HYDROGEN BOND MEDIATED NETWORK STRUCTURES

8.1 Introduction

The description of crystal structures in terms of networks is one of the most promising of systematic approaches to communicate structural information in a precise fashion. Network structures attract great attention due to their potential applications in materials science as functional solid materials as well as fascinating architectures.[1] One conceptual approach to building networks can be carried out by representing molecules as nodes and the intermolecular interactions connecting the molecules as node connectors.[2] The topology of a given network is represented in terms of the general symbol (n,p), where n is number of nodes in the smallest closed circuits in the net and p is the number of connections to neighboring nodes that radiate from any node. It also can be represented by Schläfli symbols. This method has been applied to understand many complex crystal structures and is very useful in elucidating relationships between different structures.

Design of three-dimensional solid-state structures is a difficult problem since it involves the control and prediction in the third dimension. Inorganic and metal–organic crystal structures have traditionally been compared to two dimensional and three dimensional networks,[3] the depiction of organic structures as nets of different topologies is more recent.[4] The exercise of generating organic network structures by choosing examples of inorganic solids may improve design strategies.[5] In this context, there have been major advances with organic–inorganic hybrid systems.[6] Inorganic solids provide a wealth of information about various network structures. However, much interesting structural chemistry has also emerged from all-organic systems.[7] Generally supramolecular structure of a two connected node may form discrete circles, chains and helices.[8] Three connected nodes can extend into a variety of networks ranging from one-dimensional ladders to complicated three-dimensional network structures.[9] For example, planar trigonal node forms a honeycomb net whereas a pyramidal node forms β-arsenic and black phosphorus nets. Similarly planar three connected node with T-shaped geometry may connects into a variety of nets such as ladder, brick wall and herringbone (parquet). Recently guest induced

supramolecular isomerism of three-connected T-node and H-node is reported from our laboratory, where network topology changes from one-dimensional ladder to two-dimensional brick-wall network based on guest molecule.[10] Other important three-connected three-dimensional networks are $SrSi_2$ and $ThSi_2$ (Figure 1).

Diamondoid network (Figure 1), which is formed by four connected nodes, is more common in organics because of the tetrahedral nature of the sp^3-hybridized carbon molecular framework. There are two kinds of diamondoid networks namely cubic and hexagonal diamondoid nets and these networks are formed due to slight variation in the mode of connectivity of tetrahedral nodes.[9,11] The planar four connected nodes lead to two dimensional square networks and three dimensional $NbO/CdSO_4$ network structures (Figure 1).[12] Other four-connected networks are $SrAl_2$ (**sra**) and PtS type structures. The α-Po net has 6-connected topology while the rutile net has nodes of different connectivity (Figure 1).

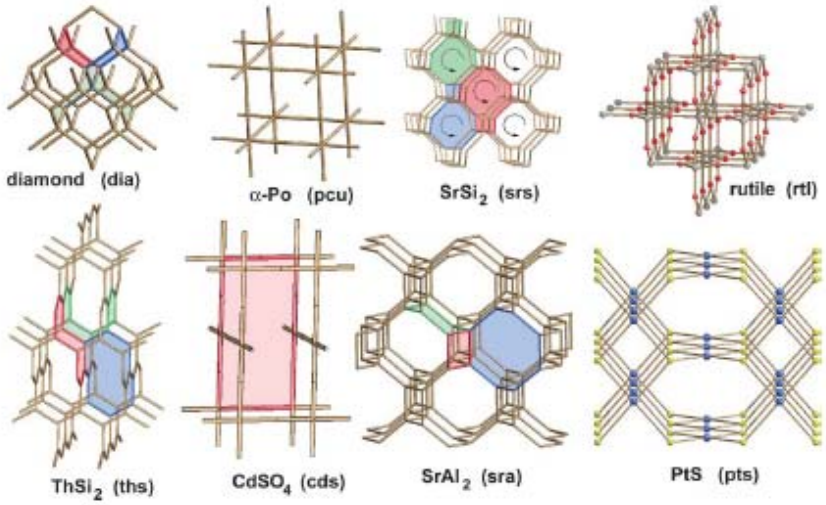

Figure 1. Some network structures formed by three-connected and four-connected nodes. This figure is taken from ref. 25.

8.2 Organic network structures formed by strong and weak hydrogen bonds

Conventional hydrogen bonds like O–H···O and N–H···O have been extensively used to generate three-dimensional network structures because of their strength and directionality.[13] The carboxylic acid dimer synthon was successfully utilized in the construction of a wide range of network structures. For example terephthalic acid, trimesic acid and adamatane-1,3,5,7-tetracarboxylic acid, which can act as two, three and four connected nodes *via* robust acid···acid homosynthon produce supramolecular one-dimensional tape, two-dimensional hexagonal and three-dimensional diamondoid networks

respectively (Scheme 1).[14] Wuest and coworkers utilised the amide dimer in the construction of diamondoid networks.[15] Nangia and coworkers exploited acid···pyridine heterosynthon in the design of a variety of two- and three-dimensional network structures.[16] Some unusual organic network structures topologically equivalent to zeolite narsarsukite ($Na_2TiOSi_4O_{10}$) and carborundum III (polytype SiC), which are formed by amine···phenol heterosython are reported by Desiraju and coworkers.[17] Diamond nets also been successfully assembled *via* weak interactions like C–H···O, π···π, C–H···π, halogen···halogen, iodo···nitro and ethynyl···nitro.[18] Desiraju *et al.*[19] reported weak C–H···N hydrogen bonds mediated triply interpenetrated hexagonal network in the crystal structure of MeCN solvate of tetrakis(4-cyanophenyl)methane (Scheme 1). Six molecules of tetrakis(4-cyanophenyl)methane are connected by two disordered MeCN molecules *via* C–H···N hydrogen bonds involving the *meta* C–H groups of the phenyl rings and the MeCN molecules, generating hexagonal networks in the *ab*-plane. The hexagonal networks close pack with inclined 3-fold interpenetration (Figure 2). The networks are held together by C–H···N (2.633Å, 126.3°) internetwork interactions involving the *meta* C–H groups of the phenyl rings and the MeCN molecules. Robson and coworkers reported a 3-connetcted (10,3)-a net in a family of $[C(NH_2)_3][N(CH_3)_4][XO_4]$ (X=S, Cr, Mo), where network can be constructed *via* strong as well as weak hydrogen bonds.[20]

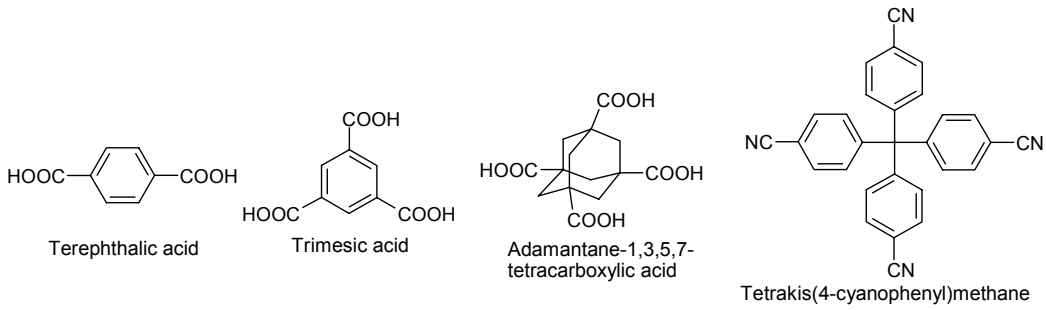

Scheme 1. Compounds form different network structure from literature.

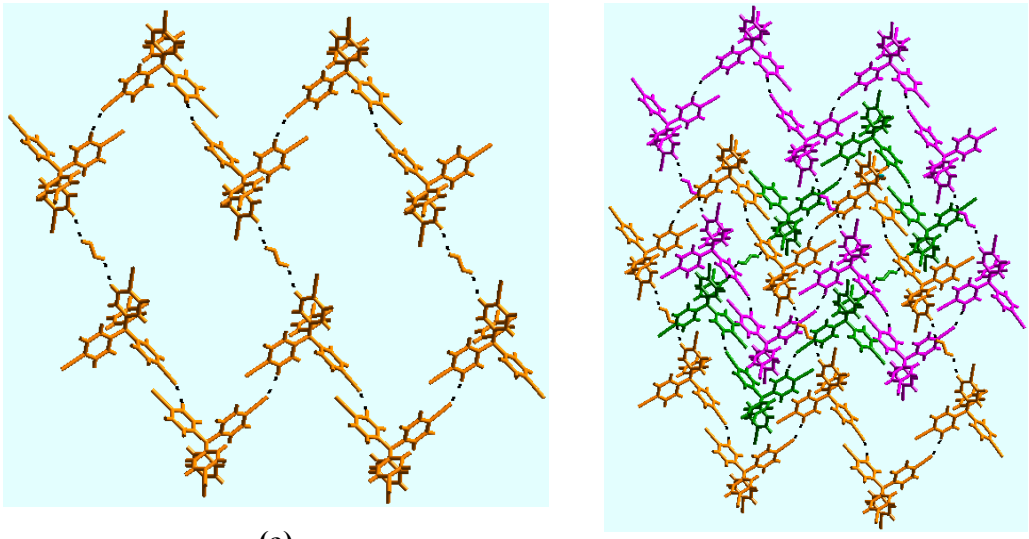

(a) **(b)**

Figure 2. (a) Hexagonal network in crystal structure of MeCN solvate of tetrakis(4-cyanophenyl)methane. (b) 3-fold interpenetration of hexagonal networks. The methyl groups of the disordered MeCN molecules are removed for clarity.

8.3 Results

Compound **68** is prepared by the Heck coupling of 1,3,5-tribromobenzene with 4-vinylpyridine in dry Et_3N under N_2 atmosphere at 100 ºC.[21] The saturated analogue **68** is prepared by hydrogenation of **68** with 10% activated Pd/C in EtOAc. After characterizing by satisfactory NMR and IR spectra their crystal structures were determined by X-ray diffraction. Crystallographic data of compounds studied in this chapter is given in appendix.

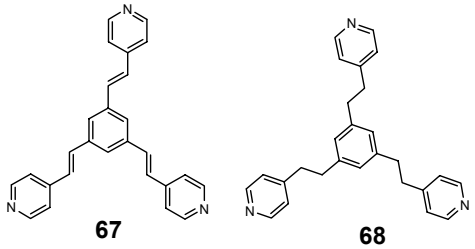

67 **68**

Table 1. Hydrogen bond interactions in **67** and **68**.

Compound	Number	Interaction	*d*/Å	*D*/Å	*θ*/°
67	i	C22–H22···N1	2.60	3.522(1)	164.9
	ii	C4–H4···N1	2.68	3.567(2)	156.2
	iii	C15–H15···N1	2.71	3.526(2)	144.0
	iv	C13–H13···N3	2.73	3.602(2)	152.0
	v	C7–H7···N3	2.69	3.484(2)	141.9
	vi	C10–H10···N2	2.75	3.524(2)	139.5

68	i	C3–H3···N1	2.94	3.650(18)	150.3
	ii	C1–H1···N2	2.73	3.780(16)	172.7
	iii	C5–H5···N3	2.84	3.730(4)	159.5

8.3.1 C–H···N mediated $SrAl_2$ network in 1,3,5-tris[4-pyridyl(ethenyl)]benzene, 67

The crystal structure of **67** was solved and refined in the monoclinic space group *C*2/*c* with one molecule in the asymmetric unit. The molecule does not adopt three-fold orientation of ethenylpyridyl groups in the crystal. Instead, two of the flexible side-arm groups are oriented roughly parallel while the third is related to these groups by approximately 120° rotation. Detailed analysis of the intricate structural packing shows a dense network of C–H···N interactions.

Each molecule of **67** is connected to two glide related molecules via acceptor-trifurcated C–H···N interactions i, ii, iii from phenyl and ethenyl CH donors to pyridyl N along the *c*-axis (2.60 Å, 164.9º; 2.68 Å, 156.2º; 2.71 Å, 144.0º). The donor-rich molecule is further connected via bifurcated, centrosymmetric C–H···N motifs (iv, v: 2.73 Å, 152.0º; 2.69 Å, 141.9º) on one side and by 2-fold rotation related C–H···N interaction vi (2.75 Å, 139.5º) on the other side. The five-molecule supramolecular aggregate is a four connected node (Figure 3a) having six vertex angles in the range 65-156° when the centers of benzene rings are treated as nodes. Propagation of the three-dimensional network (Figure 3b) shows that the structure contains tetragons, hexagons and octagons (Figure 3c) in the ratio 2:3:1. The tetragons have no voids, hexagons are of 13 × 14 Å size, and octagons have voids of 18 × 18 Å. The smaller cavities are filled by the edges of hexagons from two translated nets and the larger voids include two staircase-like tetragonal tapes, thereby generating the three-fold interpenetrated net (Figure 3d). This **sra** network, constructed using C–H···N interactions up to the van der Waals radius sum (<2.8 Å, Table 1), is identical to the idealized $SrAl_2$ net shown in figure 1. There is a long C–H···N interaction (2.98 Å, 125.0°) and weak van der Waals contacts between the networks. Thus, the classification of structure **67** as three-dimensional **sra** net is justified because interactions within a network are stronger (shorter) compared to those between them. Moreover, node connections are either collinear or roughly parallel with intermolecular C–H···N interactions.

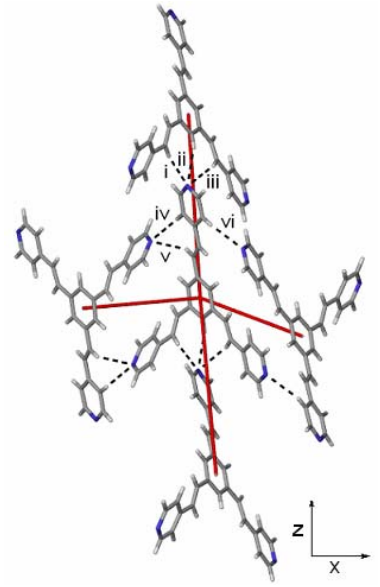

(a)

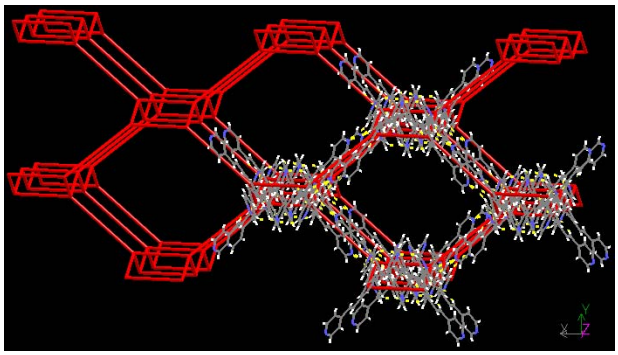

(b)

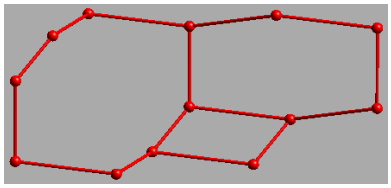

(c)

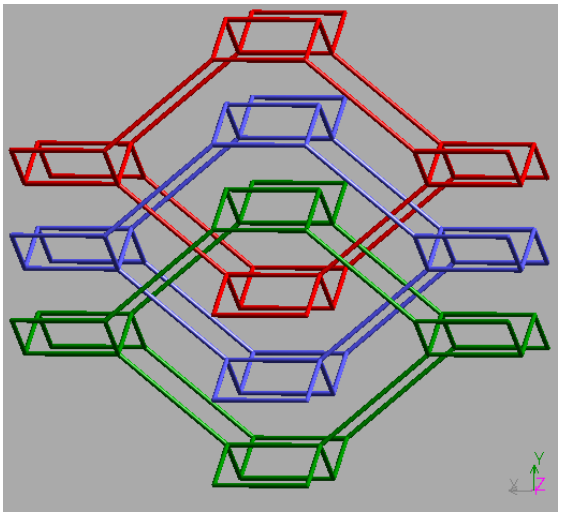

(d)

Figure 3. (a) Self-assembly of molecule **67** *via* C–H···N interactions to generate the 4-connected node. (b) Propagation to the **sra** network (red lines) generates hexagons (along [110]), and tetragons, octagons (down [001]). Part of the network is shown without molecules for clarity. (c) Tetragon, hexagon and octagon in **67**. (d) Schematic representation of 3-fold interpenetrated **sra** nets in **67** along [010].

Recently Nangia and coworkers[22] reported a series of crystal structures where conformationally flexible trigonal dihydrogen-1,3*cis*,5*cis*-cyclohexane tricarboxylate (H_2CTA^-) functions as a tetrahedral tecton in the presence of suitable ammonium cation templates. In the crystal structure of **H_2CTA^- NH_4^+** each molecule of H_2CTA^- is hydrogen

bonded to four others in a tetrahedral array (Figure 4a). Two neutral COOH donors are connected to different oxygen atoms of COO^- *via* short and linear charge-assisted O–H···O^- hydrogen bonds (1.55 Å, 177.8º; 1.57 Å, 164.8º). The supramolecular tetrahedron of five H_2CTA^- anions is the building block for the diamond network (Figure 4b) *via* O–H···O^- H-bonds. NH_4^+ ions sit in the channels and interact with H_2CTA^- anions *via* N–H···O hydrogen bonds.

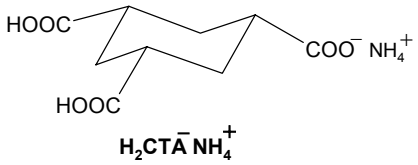

H_2CTA^- NH_4^+

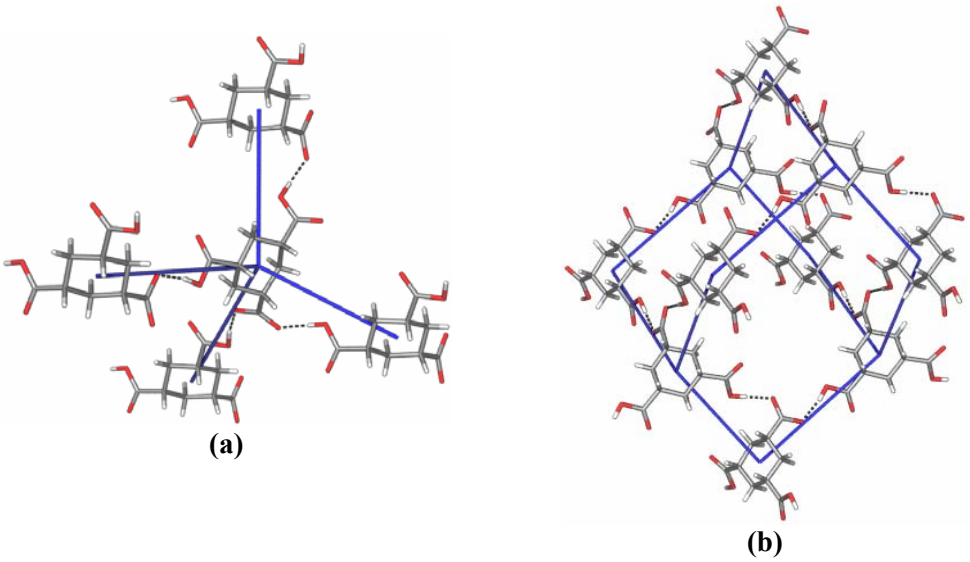

(a) **(b)**

Figure 4. (a) Tetrahedral assembly of five H_2CTA^- molecules connected *via* O–H···O^- hydrogen bonds in **H_2CTA^- NH_4^+**. (b) Diamondoid network formed *via* (solid lines) of O–H···O^- hydrogen bonds in **H_2CTA^- NH_4^+**. NH_4^+ ions are not shown for clarity. Note the similarities of figure 3a and figure 4a.

8.3.2 C–H···N mediated trigonal network in 1,3,5-tris[4-pyridyl(ethyl)]benzene, 68

Structure solution proceeded in the enantiomorphous space group $P6_5$ with one molecule of **68** in asymmetric Each molecule of **68** participates in six mutual C–H···N interactions i, ii and iii that are somewhat longer (H···N 2.7-3.0 Å, Table 1) compared to **67**. If the center of the phenyl ring is viewed as a node and the C–H···N interactions as the node connectors, the result is the chiral, trigonal network (Figures 5a, 5b) a target motif in octupolar NLO materials.[23] A similar polar, trigonal network of C–H···O interactions was

noted previously in tribenzyl isocyanurate (Figure 5c).[24] SHG measurement (Nd^{+3}-YAG laser at 1.064 μm) on a microcrystalline powder of non-centrosymmetric solid **68** did not display a green signal visible to the naked eye, perhaps because the molecule lacks extended conjugation between the aromatic and pyridyl rings.

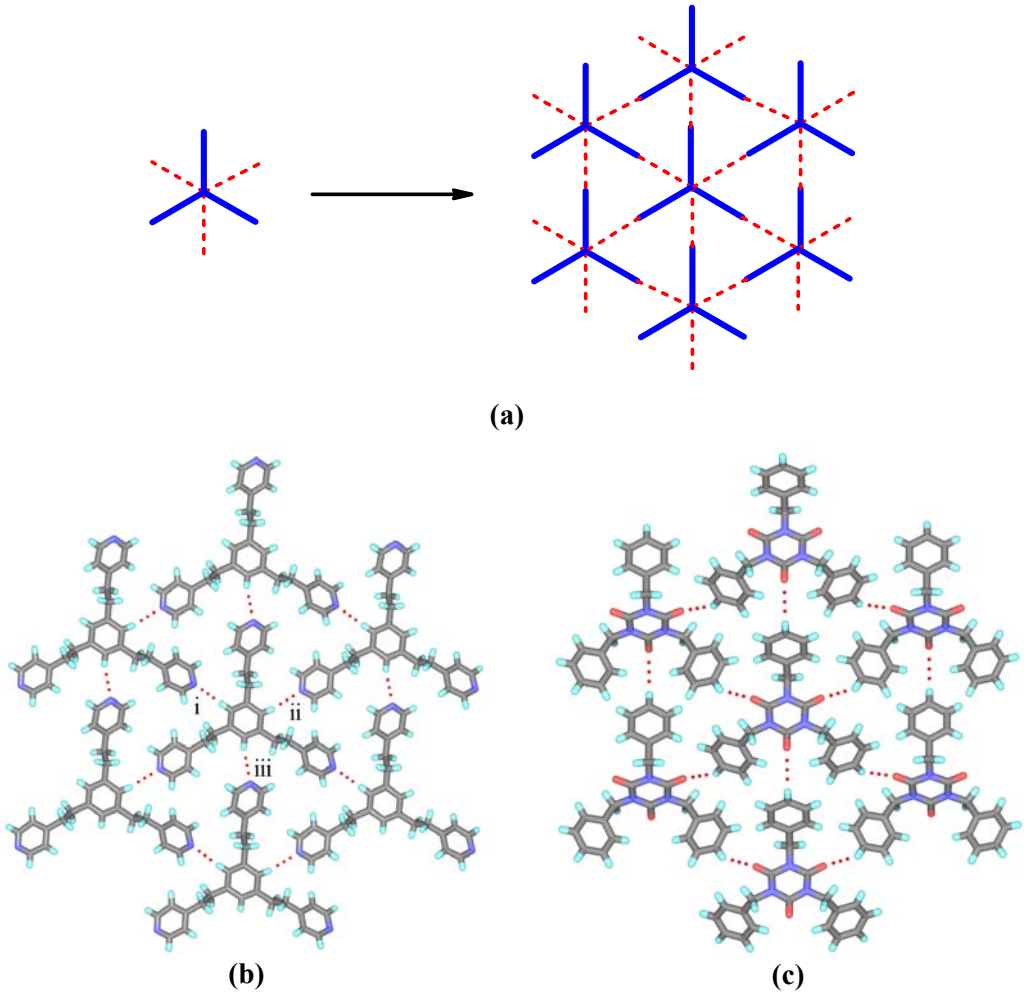

Figure 5. (a) Schematic representation of trigonal network (b) Trigonal 3,6 network of C–H···N interactions in **68**. (c) Trigonal network meadiated by C–H···O interactions in tribenzyl isocyanurate.

8.4 Interpenetrated $SrAl_2$ networks in literature

Proserpio, Ciani and coworkers[25] reported a comprehensive analysis of the CSD and ICSD structural databases for the occurrence of interpenetrating metal-organic and inorganic networks. A list of 301 interpenetrating metal-organic three-dimensional structures was analyzed on the basis of their topologies and distinct classes of interpenetrating nets. It was found that the large majority of inorganic and metal-organic networks are found to exhibit a

limited number of 'common' topologies. The distribution of the 47 different topologies (Figure 6) shows that the most common interpenetrating nets are by far the diamondoid nets (42%, including supertetrahedral nets), followed by the α-polonium nets (17%), but also many uncommon and new topologies are observed within interpenetrating networks. The $SrAl_2$ net (Schläfli symbol $4^2.6^3.8$, described as 4^26^38-*a* net by Wells) is an uncommon topology among 4-connected interpenetrated nets, occurring in only five metal–organic structures. The CSD Refcodes of entangled metal–organic structures having **sra** topologies in literature are IDUDOA, ECIWOC, GEHQAL, GEHQOZ and CNSMAG.

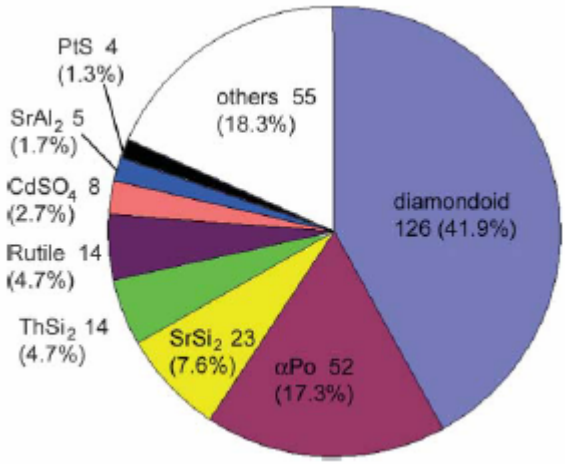

Figure 6. Distribution of different interpenetrating networks reported in ref. 25.

8.5 Differences between diamondoid and $SrAl_2$ networks

Although both diamondoid and $SrAl_2$ networks are formed by four-connected tetrahedral node there are differences in the connectivity of hexagonal super black phosphous sheets in the third dimension. The $SrAl_2$ net may be viewed as growing through node connections between undulated hexagonal sheets of super black phosphorus (Figure 7). The node connectivity shown in figure 7a generates additional tetragons and octagons of the "open" **sra** network whereas only hexagons of the "close-packed" diamond net are produced in figure 7b. Thus, differences in the stacking mode and inter-layer connection of identical two-dimensional sheets generate distinct three-dimensional nets. The self-assembly model suggests that construction of uncommon 4^26^38 nets may be planned from flexible four-connected building blocks that have been used to build diamond nets. This build-up model also perhaps explains why two[26] of the five networks classified as $SrAl_2$ in a recent classification were inadvertently[25] named as diamond nets in their original publications.

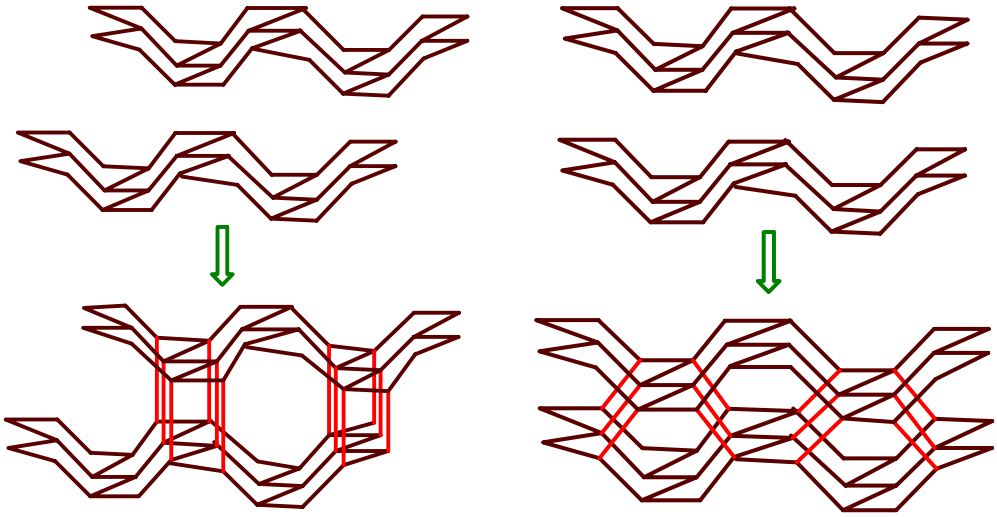

Figure 7. Sheets of super black phosphorus topology (brown lines) are connected (*via* red lines) to generate (a) $SrAl_2$ network, and (b) diamond network through the sliding of layers. Note that the inter-layer connectivity in (a) produces additional tetragons and octagons whereas (b) has all hexagons.

8.6 Discussion

Crystal structures of **67** and **68** were determined as part of ongoing studies on C_3 carboxylic acid–bipyridine cocrystals to find out if these trigonal molecule adopts C_3 (or pseudotrigonal) conformation in the solid state. To our surprise, tritopic molecule **67** functions as a four-connected node in the three-dimensional **sra** net and **68** forms a polar, layer network. These crystal structures are sustained by C–H···N interactions[27] and close-packing of aromatic groups. The striking difference between network structures **67** and **68** may be traced to the activated ethenyl CH donors of **67** that are absent in the ethyl analogue **68**. The C–H···N mediated open framework structure of **67** filling the voids through triple interpenetration and the close-packed layer structure of **68** represent two different ways of achieving optimal packing efficiency (69.3, 62.9%) in organic crystals. The description of these structures as the diamond and graphite prototypes is also reflected in the >200 °C higher melting point of **67** compared to **68**. The **sra** prototype is also related to bimetallic phases like $CeCu_2$ and KHg_2, inorganic salts $(NH_4)LiSO_4$ and $RbAlSO_4$, and synthetic zeolite Li–A(BW).[28] The adoption of non-centrosymmetric 3,6 net for a trigonal molecule is atypical, the more common arrangement being the centrosymmetric, hexagonal motif.[29]

8.7 Conclusions

The following conclusions can be drawn from the study: (i) SrAl2 network in 1,3,5-tris[4-pyridyl(ethenyl)]benzene, **67** is first organic example of its kind. (ii) The relationship in the build-up of **sra** net to the common diamond net is identified. (iii) Supramolecular assemblies based purely on C–H···N interactions are very few even among weakly hydrogen-bonded systems. (iv) Subtle change in molecular conformation leads to two entirely different network structures. Thus, careful analysis of molecular packing and intermolecular interactions and judicious choice of nodes and node connections will lead to new examples of organic network architectures.

8.8 Experimental Section: All compounds are characterized by NMR. 1H NMR spectra (δ scale in ppm, *J* coupling constant in Hz) were recorded on Bruker Avance at 400 MHz. Melting points were recorded on Fisher–Johns apparatus and DSC.

Synthesis of 1,3,5-tris[4-pyridyl(ethenyl)]benzene, 67: Prepared by the Heck coupling of 1,3,5-tribromobenzene with 4-vinylpyridine (ca. 4 equiv.), catalytic $Pd(OAc)_2$ and PPh_3 (10 mol % each) in dry Et_3N under N_2 atmosphere at 100 ºC. Diffraction quality single crystals of **67** appeared during purification by column chromatography from EtOAc/hexane (2:8 ml). ^{1}H NMR ($CDCl_3$): δ 8.63 (d, *J* = 6, 6H), 7.66 (s, 3H), 7.42 (d, *J* = 5, 6H), 7.37 (d, *J* = 5, 3H), 7.14 (d, *J* = 5, 3H). M. p. 322-324 ºC.

Synthesis of 1,3,5-tris[4-pyridylethyl]benzene, 68: Compound **68** was synthesized by the hydrogenation of **68** with 10% activated Pd/C in EtOAc. Crystals of **68** were obtained from EtOAc. ^{1}H NMR ($CDCl_3$): δ 8.49 (d, *J* = 5, 6H), 7.05 (d, *J* = 5, 6H), 6.75 (s, 3H), 2.84 (s, 12H). M. p. 110-112 ºC.

8.9 References

1. (a) M. Eddaoudi, D.B. Moler, H. Li, B. Chen, T.M. Reineke, M. O'keffe and O.M. Yaghi, *Acc. Chem. Res*., **2001**, *34*, 319. (b) B. Moulton and M.J. Zaworotko, *Chem. Rev*., **2001**, *101*, 1629. (c) S.R. Batten, *CrystEngComm*, **2001**, *18*, 1. (d) S.R. Batten and R. Robson, *Angew. Chem., Int. Ed. Engl*., **1998**, *37*, 1460.
2. (a) G.R. Desiraju, *Chem. Commun*., **1997**, 1475. (b) M.J. Zaworotko, *Chem. Commun*., **2001**, 1.
3. (a) A.F. Wells, *Structural Inorganic Chemistry*, Oxford University Press, Oxford, 5th edn., **1984**. (b) A.F. Wells, *Three-dimensional Nets and Polyhedra*, Wiley, New York, **1977**.

4. (a) G.R. Desiraju, *Chem. Commun.*, **1997**, 1475 (b) O. Ermer and A. Eling, *J. Chem. Soc., Perkin Trans. 2*, **1994**, 925.
5. (a) W. Lin, L. Ma and O.R. Evans, *Chem. Commun*., **2000**, 2263. (b) H. Gudbjarston, K. Biradha, K.M. Poirier and M.J. Zaworotko, *J. Am. Chem. Soc*., **1999**, *121*, 2599. (c) B.F. Abrahams, P.A. Jackson and R. Robson, *Angew. Chem., Int, Ed.,* **1998**, *37*, 2656. (d) L. Carlucci, G. Ciani, P. Macchi and D.M. Proserpio*., Chem. Commun*., **1998**, 1837. (e) A.J. Blake, N.R. Champness, S.S. Chung, W.-S. Li and M. Schröder, *Chem. Commun*., **1997**, 1005. (e) O.R. Evans, R.-G. Xiong, Z. Wang, G.K. Wong and W. Lin, *Angew. Chem., Int, Ed*., **1999**, *38*, 536.
6. (a) S.-I. Noro, S. Kitagawa, M. Kondo and K. Seki, *Angew. Chem. Int. Ed*., **2000**, *39*, 2082. (b) C.N.R. Rao, S. Natarajan, A. Choudhary, S. Neeraj and A.A. Ayi, *Acc. Chem. Res*., **2001**, *34*, 80. (c) J. Kim, B. Chen, T.M. Reineke, H. Li, M. Eddaoudi, D.B. Moler, M. O'Keeffe and O.M. Yaghi, *J. Am. Chem. Soc*., **2001**, *123*, 8239. (d) O.R. Evans and W. Lin, *Acc. Chem. Res*., **2002**, *35*, 511. (e) S. Ferlay, S. Koenig, M.W. Hosseini, J. Pansanel, A.D. Cian and N. Kyritsakas, *Chem. Commun.,* **2002**, 218.
7. (a) K.C. Pich, R. Bishop, D.C. Craig, I.G. Dance, A.D. Rae and M.L. Scudder, *Struct. Chem*., **1993**, *4*, 41. (b) L.R. MacGillivray, J.L. Reid and J.A. Ripmeester, *Chem. Commun*., **2001**, 1034. (c) B.Q. Ma and P. Coppens, *Chem. Commun*., **2003**, 412.
8. (a) M. Bailey and C.J. Brown, *Acta Crystallogr.*, **1967**, *22*, 387. (b) R. Alcala and S. Martinez-Carrera, *Acta Crystallogr.,* **1972**, *B28*, 1671. (c) J.A. McMahon, M.J. Zaworotko and J.F. Remenar, *Chem. Commun.*, **2004**, 278.
9. S.R. Batten and R. Robson, *Angew. Chem., Int, Ed.,* **1998**, *37*, 1460.
10. (a) S. Aitipamula and A. Nangia, *Chem. Eur. J.*, **2005**, *11*, 6727. (b) S. Aitipamula and A. Nangia, *Supramol. Chem.*, **2005**, *17*, 17.
11. O. Ermer and A. Eling, *J. Chem. Soc., Perkin Trans. 2*, **1994**, 925.
12. (a) S.R. Batten, A.R. Harris, K.S. Murray and J.P. Smith, *Cryst. Growth Des.*, **2002**, *2*, 87. (b) S.S. Kuduva, D.C. Craig, A. Nangia and G.R. Desiraju, *J. Am. Chem. Soc.*, **1999**, *121*, 1936. (c) N.R. Brooks, A.J. Blake, N.R. Champness, J.W. Cunningham, P. Hubberstey, S.J. Teat, C. Wilson and M. Schröder, *J. Chem. Soc., Dalton Trans.,* **2001**, 2530. (d) M. Eddaoudi, J. Kim, D. Vodak, A. Sudik, J. Wachter, M. O'Keeffe and O.M. Yaghi, *Proc. Natl. Acad. Sci. U.S.A.,* **2002**, *99*, 4900. (e) B. Moulton, H. Abourahma, M.W. Bradner, J. Lu, G.J. McManus and M.J. Zaworotko, *Chem. Commun.,* **2003**,

1342. (f) B.R. Bhogala, P.K. Thallapally and A. Nangia, *Cryst. Growth Des*., **2004**, *4*, 215.

13. (a) B.-Q. Ma, P. Coppens, *Chem. Commun.*, **2003**, 2290. (b) D.S. Reddy, T. Dewa, K. Endo and Y. Aoyama, *Angew. Chem. Int. Ed.*, 2000, **39**, 4266. (c) J.-H. Fournier, T. Maris, J.D. Wuest, W. Guo and E. Galoppini, *J. Am. Chem. Soc.,* **2003**, *125*, 1002.
14. (a) D.D. MacNicol, F. Toda, and R. Bishop (Eds.) *Comprehensive Supramolecular Chemistry, Volume 6, Solid-State Supramolecular Chemistry: Crystal Engineering*; Pergamon: Oxford, **1996**. (b) O. Ermer, *J. Am. Chem. Soc.,* **1988**, *110*, 3747. (c) O. Ermer and L. Lindenberg, *Helv. Chim. Acta.,* **1991**, *113*, 14696.
15. (a) X. Wang, M. Simard, J.D. Wuest, *J. Am. Chem. Soc.,* **1994**, *116*, 12119. (b) X. Wang, M. Simard, J.D. Wuest, *J. Am. Chem. Soc.,* **1991**, *113*, 825.
16. (a) B.R. Bhogala, P. Vishweshwar and A. Nangia, *Cryst. Growth Des*., **2002**, *2*, 325. (b) B.R. Bhogala and A. Nangia*, Cryst. Growth Des*., **2003**, *3*, 547. (c) B.R. Bhogala, S. Basavoju and A. Nangia, *Cryst. Growth Des*., **2005**, *5*, 1683.
17. (a) B.R. Bhogala, V.R. Vangala, P.S. Smith, J.A.K. Howard and G.R. Desiraju, *Cryst. Growth. Des.*, **2004**, *4*, 647; (b) A. Dey, G.R. Desiraju, R. Mondal and J.A.K. Howard, *Chem. Commun.*, **2004**, 2528.
18. (a) R. Thaimattam, F. Xue, J.A.R.P. Sarma, T.C.W. Mak and G.R. Desiraju, *J. Am. Chem. Soc.*, **2001**, *123*, 4432. (b) W. Guo, E. Galoppini, R. Gilardi, G.I. Rydja and Y.-H. Chen, *Cryst. Growth Des.*, **2001**, *1*, 231. (c) S.V. Lindemann, J. Hecht and J.K. Kochi, *J. Am. Chem. Soc.*, **2003**, *125*, 11599.
19. S. Basavoju, S. Aitipamula and G.R. Desiraju, *CrystEngComm*, **2004**, *6*, 120.
20. B.F. Abrahams, M.G. Haywood, T.A. Hudson and R. Robson, *Angew. Chem. Int. Ed.*, **2004**, *43*, 6157.
21. A.J. Amorso, J.P. Maher, J.A. McCleverty amd M.D. Ward, *J. Chem. Soc., Chem. Commun.*, **1994**, 1273.
22. B.R. Bhogala, P. Vishweshwar, and A. Nangia, *Cryst. Growth Des*., **2004**, *4*, 647.
23. (a) C. Dhenaut, I. Ledoux, I.D.W. Samuel, J. Zyss, M Bourgault and H.L. Bozec, *Nature*, **1995**, *374*, 339. (b) G. Alcaraz, L. Euzenat, O. Mongin, C. Katan, I. Ledoux, J. Zyss, M. Blanchard-Desce and M. Vaultier, *Chem. Commun.*, **2003**, 2766.
24. V. R. Thalladi, S. Brasselet, D. Bläser, R. Boese, J. Zyss, A. Nangia and G. R. Desiraju, *Chem. Commun.*, **1997**, 1841.
25. V. A. Blatov, L. Carlucci, G. Ciani and D. M. Proserpio, *CrystEngComm*, **2004**, *4*, 377.

26. (a) O. R. Evans and W. Lin, *Chem. Mater.*, **2001**, *13*, 2705. (b) S. Ferlay, S. Koenig, M. W. Hosseini, J. Pansanel, A. de Cian and N. Kyritsakas, *Chem. Commun.*, **2002**, 218.
27. M. Mascal, *Chem. Commun.*, **1998**, 303.
28. L Carlucci, G. Ciani, P. Macchi, D.M. Proserpio and S. Rizzato, *Chem. Eur. J.*, **1999**, *5*, 237.
29. (a) B.K. Saha, R.K.R. Jetti, L.S. Reddy. S. Aitipamula and A. Nangia, *Cryst. Growth Des.*, **2005**, *5*, 887. (b) A. Nangia, *Curr. Opin. Solid State Mater. Sci.*, **2001**, *5*, 115.

CHAPTER 9

CONCLUSIONS

9.1 Hydrogen bonding in substituted diarylureas and dipyridylureas

A particular class of organic compounds will have a characteristic hydrogen bond pattern. N–H···O hydrogen bond mediated α-network is a robust synthon in unsubstituted arylureas with twisted conformation. But hydrogen-bonding in diarylureas with electron-withdrawing groups is different from that of diarylureas with neutral or electron-donating groups. As described for a family of *para*-nitro substituted diarylureas in chapter 2, the N–H group of urea preferentially form N–H···O hydrogen bonds with the nitro oxygen rather than the carbonyl in compounds **1**–**6**, thus preventing the formation of the α-network. DMF and DMSO solvents disrupt α-network in crystal structures **7**–**15**. Whenever interfering nitro group is engaged with complimentary interactions like iodo···nitro, ethynyl···nitro and *N,N*-dimethylamine···nitro, even if they are weak, the characteristic α-network is restored in crystal structures **16**–**19**. In a series of dipyridylureas and phenyl-pyridylureas (Chapter 3, **21**-**24**) also the urea tape synthon is consistently absent because of interference from N–H···$N_{pyridyl}$, N–H···O_{oxide} and N–H···I^- interactions. Urea tape is observed only when the molecule is twisted from planar conformation due to steric hindrance.

We hypothesize that the planar conformation and two intramolecular C–H···O interactions are a persistent motif in these structures. They weaken the urea oxygen acceptor because the electropositive H atoms share the electron density of oxygen lone-pairs. An electron-deficient aryl ring with potential hydrogen bond acceptor groups, e.g. as in pyridyl or -NO_2, simultaneously activates the proximal CH donors that stabilize C–H···O interactions. As the urea O gets weakened, pyridyl N and O atoms of solvent/ water molecules become stronger acceptors for urea NHs. This leads to the observed non-urea tape motifs in electron-withdrawing substituted arylureas. Therefore, other stronger acceptors like pyridyl N, solvent O, or nitro O form aggregates with urea NH donors. On the other hand, when urea O is the only acceptor group, e.g. as in diphenylurea, the molecule twists to the metastable conformation to form stronger hydrogen bonds and also better close-packing of aryl rings along the 4.7 Å urea tape. A spot-check and manual analysis of about 50 diarylurea and pyridylurea crystal structures in the CSD as well as our results on nitro-

substituted diarylureas and pyridylureas are in agreement with the hydrogen bonding model of Scheme 1.

The planar conformation of dipyridylurea with tweezer-like donor groups could be exploited for designing anion sensors[1] (Scheme 2). Recently, it has been shown that a hydrogen-bonding donor can be used as a general acid catalyst for various types of reactions in organic chemistry.[2] By keeping in mind that electron-withdrawing group substituted diarylureas acts as only hydrogen bond donors in planar conformation, Nagasawa and coworkers[3] investigated the urea-catalyzed hetero-Michael reaction of α,β-unsaturated carbonyl compounds (Scheme 3). The reaction of pyrrolidine with γ-crotonolactone was carried out in the presence of electron-withdrawing group substituted ureas as catalysts. There is more than 24-fold rate acceleration in the catalyzed reaction.

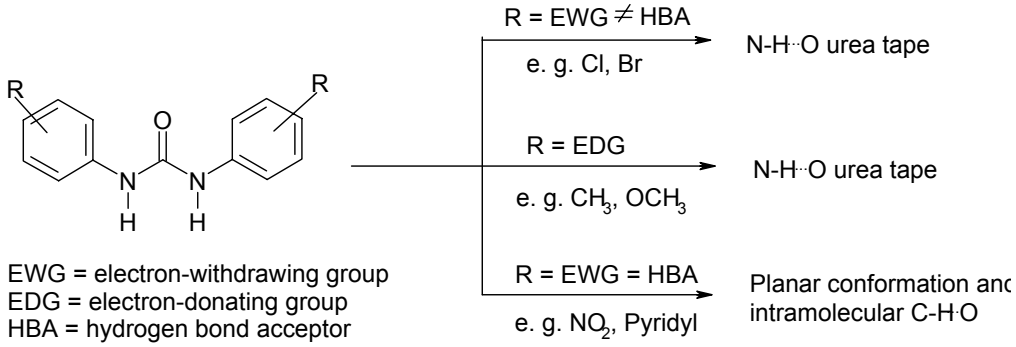

Scheme 1. Correlation between substitution and hydrogen bond pattern in diarylureas.

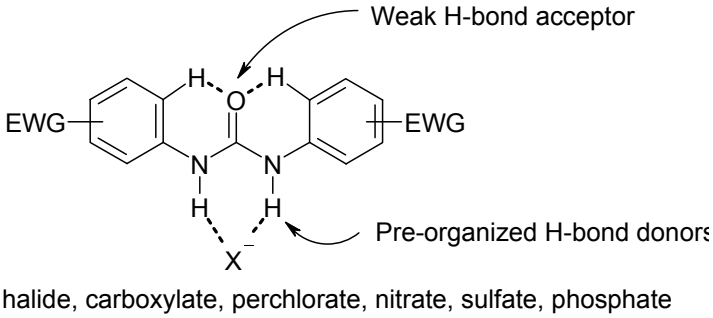

Scheme 2. Potential development of electron-withdrawing substituted diarylureas as selective anion receptor.

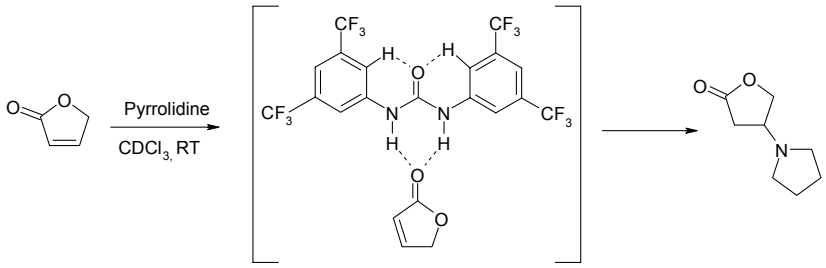

Scheme 3. Hetero-Michael reaction of pyrrolidine to γ-crotanolactone, where planar EWG urea used as catalyst.

9.2 Role of weak interactions in the presence of strong hydrogen bonding functionalities

Weak interactions play an important role in crystal structure stabilization and assembly when strong interactions are absent. On the other hand there are seminal reports where weak interactions play major role in directing the strong interactions. Hence understanding the role of weak interactions in the presence of strong hydrogen bonds is crucial in crystal structure prediction and the design of novel materials.

Earlier studies on the Ph–Ph^F synthon have dealt with molecules in which strong hydrogen bonding groups were generally absent. We demonstrate that the phenyl–perfluorophenyl stacking synthon is a viable recognition motif in the cocrystallization of strong hydrogen bonding carboxylic acids and carboxamides. The Ph–Ph^F stacking stabilizes structures **26** (Figure 1a) and **27**, the interaction is weaker in **28** *via* lateral offset. Phenyl perfluorophenyl mediation during cocrystallization of **28** is weaker because acid···amide heterosynthon is stronger that homosynthons (Chapter 4). Although there are significant variations in hydrogen bonding donors and molecular shape (phloroglucinol, 3,5-dihydroxybenzoic acid) the consistent formation of phenazine and acridine stacking suggests that these stacks can be used in the reliable assembly of desired structures. Crystal structures **37**–**40** and **42** also show a remarkable cooperation of hydrogen bonding, aromatic stacking and herringbone interactions in the formation of one-, two- and three-dimensional network structures (Figure 1b, Chapter 5).

Face-to-face stacking of aromatics in the solid state is an important topic in the field of semiconductor materials.[4] Many reports have underscored the importance of maximizing π-orbital overlap to achieve efficient charge transport properties of such solids. Efforts to promote face-to-face stacking of semiconductor molecules in the solid state have focused on

the use of functional groups expected to direct the assembly process to the prerequisite packing.[5] Very recently MacGillivray and coworkers[6] have described a new approach to control the organization of the aromatic rings of semiconductor molecules in the solid state that enforces face-to-face π-stacking using the strength and directionality of hydrogen bonds. In the pure crystal structure of 9,10-bis(4-pyridylethynyl)anthracene, the pyridyl and anthracene groups participate in alternating face-to-face π-stacked arrays. But the adjacent arrays are held together *via* $C–H_{pyridine}\cdots\pi_{pyridine}$, $C–H_{pyridine}\cdots\pi_{anthracene}$ and $\pi_{pyridine}\cdots\pi_{anthracene}$ interactions. As a consequence of these interactions, extended face-to-face stacking is not observed. When 9,10-bis(4-pyridylethynyl)anthracene is cocrystallized with resorcinol derivatives the components of each solid have assembled to form four-component molecular assemblies held together by four O–H···N hydrogen bonds (Scheme 4) as a result the face-to-face stacking is extended.

Cocrystal formation and solid-state reactions can be monitored by powder X-ray diffraction (PXRD) and variable temperature powder X-ray diffraction (VT-PXRD) as the pattern of the complex is quite different from those of the precursors. As studied in chapter 4, cocrystals **26** and **31** are formed by simple mechanical grinding at room temperature whereas in case of cocrystals **27** and **28** the cocrystal formation is incomplete at room temperature. As temperature increases the supramolecular reaction of cocrystal assembly proceeds to completion about 100 °C in case of cocrystal **27** and 78 °C in cocrystal **28**. Molecular complexes are not formed in **29** and **30** even at high temperatures. Molecular complex **31** goes through a phase change on heating to form a stable new phase that does not change on cooling and substantial reheating. These results indicate that when more activated and acidic donors are involved, the supramolecular reaction is fast and complete conversion of mixture to molecular complex at room temperature by simple grinding.

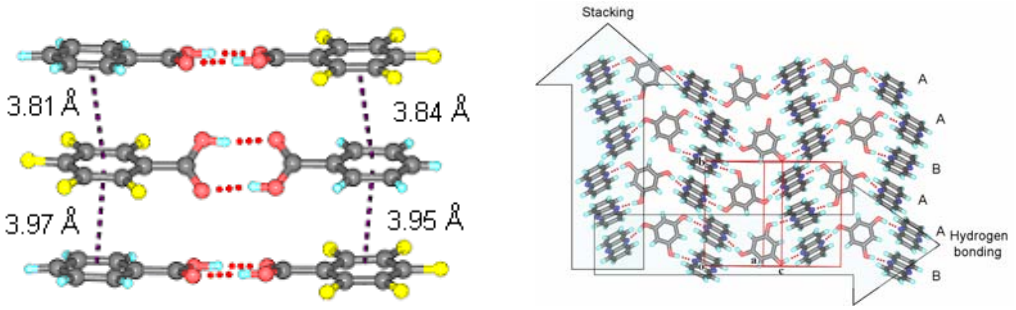

(a) **(b)**

Figure 1. (a) Ph-PhF stacking synthons in 1:1 cocrystal of benzoic acid and pentafluorobenzoic acid. (b) Stacking and hydrogen bonding in 1:1.5 cocrystal of phloroglucinol and phenazine.

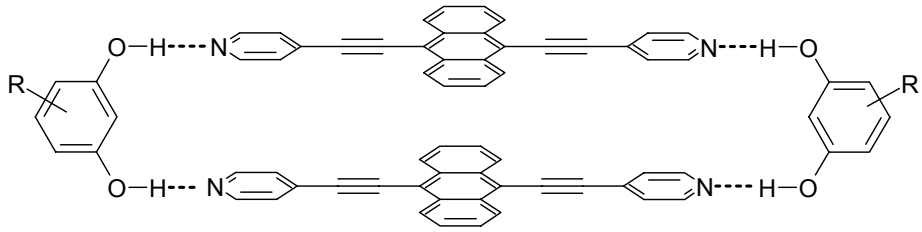

Scheme 4. Template promoted enforced face-to-face π-stacking of anthracene.

9.3 Role of strong hydrogen bonds in cocrystal design

Design of materials with specific properties and controlling polymorphism require a knowledge of the dominant synthons, because these synthons are primarily responsible for the arrangement of molecules in the crystal lattice. A novel carboxamide···pyridine *N*-oxide heterosynthon is designed by exploiting the better acceptor strength of anionic oxygen and shown to result in helical motifs, a sought after architecture in crystal design. Notably, the amide···*N*-oxide heterosynthon dominates over amide dimer homosynthon and should have a high probability of occurrence in crystal structures, except when it is in competition with intramolecular hydrogen bonding (Chapter 6).

Heterosynthons considerably reduce the possibility of alternative hydrogen bond patterns, and hence control polymorphism. Hydrogen bond preferences and synthon energy calculations suggest that amide *N*-oxides should be less prone to polymorphism compared to amide pyridines. For example, due to the comparable acceptor strength of amide C=O and pyridine N groups, isonicotinamide exists in two polymorphs. In form I, amide functionality involves in centro-symmetric amide dimer (Figure 2a) formation whereas in form II, it involves in amide···pyridine heterosynthon (Figure 2b). On the other hand, the strong N–H···O^- hydrogen bond controls crystallization isonicotinamide *N*-oxide *via* amide···*N*-oxide (Figure 2c), therefore synthon based polymorphism is less likely.

The amide···*N*-oxide heterosynthon is successfully tested in model pharmaceutical cocrystals of barbiturate drugs with BPNO. The disadvantage with these cocrystals is BPNO not a GRAS (generally recognised as safe) substance. Moreover there are no *N*-oxide compounds in GRAS list. However, there are some *N*-oxide drugs[7] (Scheme 5), where this heterosynthon can be exploited in cocrystallization with pharmaceutically acceptable carboxamides (Scheme 6).[8] Recently two drug substances are cocrystallized using the

robust acid···amide heterosynthon. Similarly *N*-oxide drugs can be cocrystallized with amide containing drugs such as carbamazepene and piracetam.

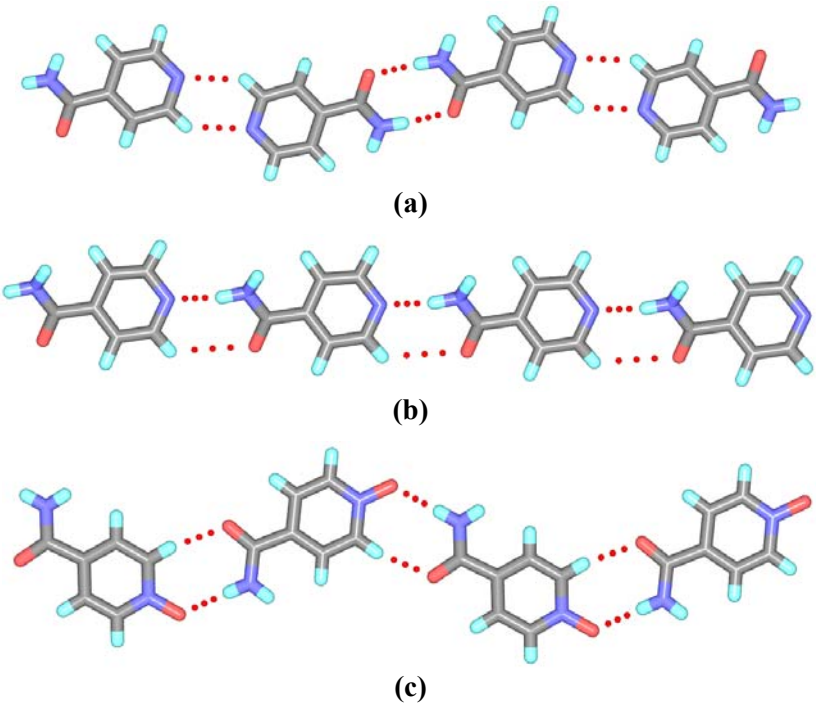

Figure 2. (a) Crystal structure of Form I of isonicotinamide with amide···amide homosynthon. (b) Form II of isonicotanamide dominated amide···pyridine heterosynthon. (c) Amide···*N*-oxide heterosynthon in isonicotinamide *N*-oxide.

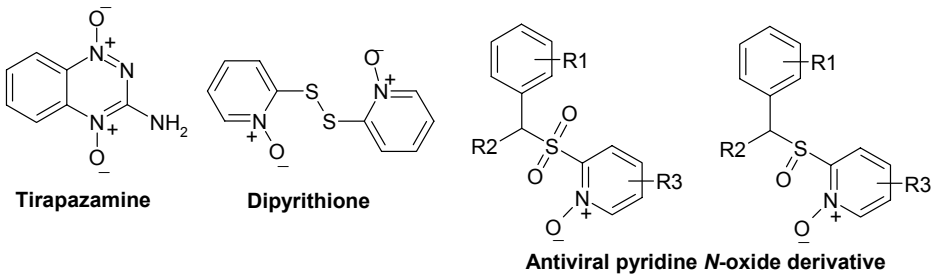

Scheme 5. Some *N*-oxide drugs in literature.

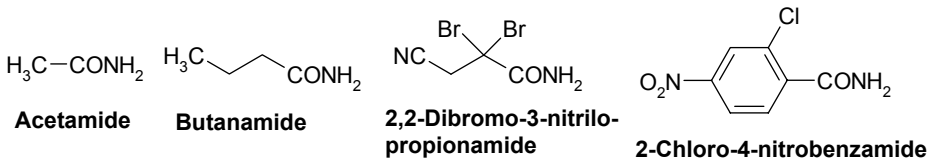

Scheme 6. Some pharmaceutically acceptable carboxamides.

9.4 Polymorphism: Difficulties

Polymorphism is a major hurdle in crystal engineering and is a not fully understood phenomenon at a fundamental level. A better understanding of this phenomenon will certainly improve crystal engineering design strategies. Moreover prediction of polymorphism is far from reality. As studied in chapter 7, compound **54** exhibits synthon based polymorphism. Kinetic Form I is characterized by 2-point catemer synthon whereas thermodynamic Form II is characterized by 4-point dimer synthon (Scheme 7). But in derivatives of **54**, polymorphism was not found in a general sense except in *p*-methyl derivative. Thermodynamic Form II is isolated with much difficulty and crystallizes only from nitromethane. The difficulty in obtaining polymorphs is evident from some of the polymorphs reported recently. Davey and coworkers[9] reported the metastable form of benzamide after 173 years of stable form reported.[10] 1,3,5-trinitrobenzene (TNB) has been known for 120 years as an explosive and in the formation of crystalline π-π donor–acceptor complexes and the known form is a metastable centrosymmetric orthorhombic form. Desiraju and coworkers[11] successfully utilized trisindane as an additive to obtain two novel stable polymorphs of TNB. Jones *et al.* have reported a new polymorph of maleic acid after 124 years of the first polymorph reported which was formed during cocrystallization experiment with caffeine and Form II of aspirin is also reported recently by Zaworotko and coworkers. All this indicates that McCrone's dictum on polymorphism may hold provided several crystallization conditions are tried.

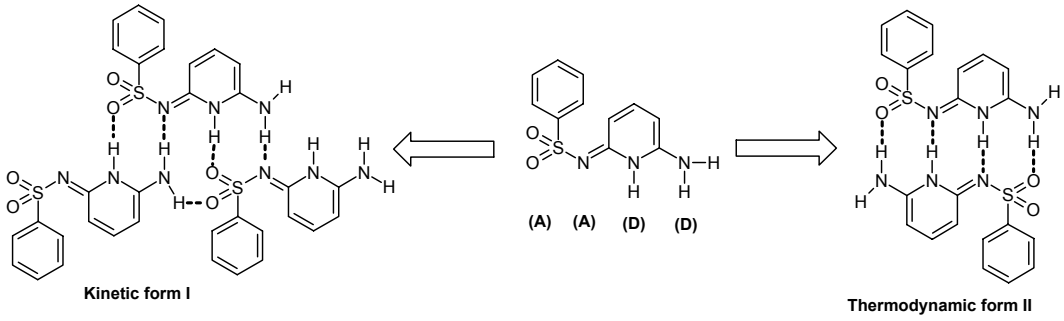

Scheme 7. Two multi-point synthons observed in polymorphs of **54**.

9.5 References

1. D. Curiel, A. Cowley and P.D. Beer, *Chem. Commun.,* **2005**, 236.
2. Y. Takemoto, *Org. Biomol. Chem.*, **2005**, *3*, 4299.
3. Y. Sohtome, A. Tanatani, Y. Hashimoto and K. Nagasawa, *Chem. Pharm. Bull.*, **2004**, *52*, 477.
4. (a) M. Bendikov, F. Wudl and D.F. Perepichka, *Chem. Rev.,* 2004, *104*, 4891. (b) A. Facchetti, M.-H. Yoon, C.L. Stern, G.R. Hutchison, M.A. Ratner and T.J. Marks, *J. Am. Chem. Soc*., 2004, *126*, 13480. (c) G.R. Hutchison, M.A. Ratner and T.J. Marks, *J. Am. Chem. Soc.,* 2005, *127*, 16866.
5. (a) H. Moon, R. Zeis, E.-J. Borkent, C. Besnard, A.J. Lovinger, T. Siegrist, C. Kloc and Z. Bao, *J. Am. Chem. Soc.,* 2004, *126*, 15322. (c) H. Meng, M. Bendikov, G. Mitchell, R. Holgeson, F. Wudl, Z. Bao, T. Siegrist, C. Kloc and C.-H. Chen, *Adv. Mater.,* 2003, *15*, 1090.
6. A.N. Sokolov, T. Friščić and L.R. MacGillivray, *J. Am. Chem. Soc.*, **2006**, ASAP.
7. (a) R.F. Anderson, S.S. Shinde, M.P. Hay and W.A. Denny, *J. Am. Chem. Soc.*, **2006**, *128*, 245. (b) R.F. Anderson, S.S. Shinde, M.P. Hay, S.A. Gamage and W.A. Denny, *J. Am. Chem. Soc.*, **2003**, *125*, 748. (c) S.S. Shinde, R.F. Anderson, M.P. Hay, S.A. Gamage and W.A. Denny, *J. Am. Chem. Soc.*, **2004**, *126*, 7865. (d) J. Balzarini, M. Stevens, E.D. Clercq, D. Schols and C. Pannecouque, *J. Antimicrobial Chemotherapy*, **2005**, *55*, 135.
8. Updated list of GRAS chemicals may be downloaded from www.cfsan.fda.gov/~dms/eafus.html.
9. (a) W.I.F. David, K. Shankland, C.R. Pulham, N. Blagden, R.J. Davey and M. Song, *Angew. Chem. Int. Ed.,* **2005**, *43*, 7032. (b) N. Blagden, R. Davey, G. Dent, M. Song, W.I.F. David, C.R. Pulham and K. Shankland, *Cryst. Growth Des.,* **2005**, *5*, 2218.
10. F. Wöhler and J. Liebig, *Annal. Pharm.,* **1832**, *3*, 249.
11. P.K. Thallapally, R.K.R. Jetti, A.K. Katz, H.L. Carrell, K. Singh, K. Lahiri, S. Kotha, R. Boese and G.R. Desiraju, *Angew. Chem. Int. Ed.,* **2004**, *43*, 1149.

APPENDIX

Table 1. Crystallographic data for structures discussed in this thesis.

	1	**2**	**3**
Emp. formula	C13H10FN3O3	C13H10ClN3O3	C13H10BrN3O3
Formula wt.	275.24	291.69	336.14
Crystal system	Monoclinic	Monoclinic	Monoclinic
Space group	$P2_1/n$	$P2_1/n$	$P2_1/n$
a [Å]	8.1241(8)	8.0360(5)	7.9974(8)
b [Å]	12.9932(12)	13.3397(8)	13.4826(13)
c [Å]	11.6524(11)	11.8513(7)	12.0227(12)
α [deg]	90.00	90.00	90.00
β [deg]	94.967(2)	94.8820(10)	94.671(2)
γ [deg]	90.00	90.00	90.00
Z	4	4	4
Volume [Å^3]	1225.4(2)	1265.82(13)	1292.1(2)
T [K]	293	293	293
D_{calc} [g/cm^3]	1.492	1.531	1.728
N-total	8210	8434	8669
N-independent	2958	3067	3120
N-observed	1740	2200	1919
R_1 [I>2σ(I)]	0.0521	0.0468	0.0491
wR_2	0.1731	0.1515	0.1489
GOF	1.10	1.06	0.96

4	**5**	**6**	**7**
C14H10N4O3	C13H10IN3O3	C13H10BrN3O3	C16H17N4O4
282.26	383.14	336.15	330.34
Monoclinic	Monoclinic	Monoclinic	Monoclinic
$P2_1/n$	$P2_1/n$	$P2_1/n$	$P2_1/c$
7.919(4)	8.4419(17)	8.407899)	9.4442(19)
13.692(6)	12.987(3)	12.7289(13)	7.3883(15)
11.777(6)	12.399(3)	12.3376(13)	23.863(5)
90.00	90.00	90.00	90.00
94.517(10)	96.59(3)	97.552(2)	97.73(3)
90.00	90.00	90.00	90.00
4	4	4	4
1273.0(11)	1350.4(5)	1308.9(2)	1649.9(6)
293	293(2)	293	293
1.473	1.885	1.706	1.330
5981	5931	6248	4014
3037	3075	2580	3789
1606	1825	1444	1467
0.0501	0.0647	0.0481	0.0783
0.1527	0.1775	0.1137	0.2408
0.97	0.91	0.97	1.09

8	**9**	**10**	**11**
C17H17N5O4	C17H19N5O5	C30H32I2N6O8S2	C16H18N4O5S
355.36	373.37	922.54	378.40
Triclinic	Triclinic	Triclinic	Triclinic
P–1	*P*–1	*P*–1	*P*–1
7.9488(7)	7.4728(10)	10.184(2)	8.4835(13)
10.4797(9)	10.2624(14)	13.346(3)	9.5690(14)
11.9563(10)	12.5410(17)	15.502(3)	11.8457(18)
114.671(1)	105.841(2)	66.82(3)	105.069(3)
95.441(2)	104.695(3)	88.22(3)	103.506(3)
101.200(1)	95.110(3)	68.75(3)	98.203(3)
2	2	2	2
870.37(13)	881.9(2)	1789.8(9)	881.4(2)
293	293	293	293
1.356	1.406	1.660	1.426
9150	7382	8625	6195
3437	3479	8168	3482
1998	2245	3868	1893
0.0619	0.0632	0.0768	0.0626
0.1810	0.1740	0.2286	0.1368
1.02	1.03	1.01	0.97

12	**13**	**14**	**15**
C16H19N3O4S	C17H19N3O5S	C15H17F2N3O4S	C13H13N3O5
349.40	377.42	371.36	291.26
Monoclinic	Triclinic	Triclinic	Triclinic
$P2_1/n$	*P*–1	*P*–1	*P*–1
16.0665(10)	6.0509(6)	9.1958(10)	6.7307(10)
5.7448(4)	12.4575(12)	9.5491(10)	10.2019(15)
39.100(3)	12.5937(11)	10.5716(11)	10.2840915)
90	78.120(2)	69.9990(10)	77.995(3)
100.115(2)	82.891(2)	79.3480(10)	84.110(3)
90	80.105(2)	69.5910(10)	75.686(3)
8	2	2	2
3552.8(4)	911.30(15)	815.29(15)	668.30
293	293	100	293
1.306	1.375	1.513	1.447
23182	5415	7443	6219
8599	4087	3201	2644
3157	2105	2940	1708
0.0664	0.0531	0.0365	0.0502
0.1950	0.1559	0.0979	0.1280
0.86	0.89	1.05	1.00

16	**17**	**18**	**19**
C13H10IN3O3	C15H11N3O3	C15H16N4O3	C19H14IN3O3
383.14	281.00	300.32	459.23
Monoclinic	Monoclinic	Triclinic	Monoclinic
Cc	*Cc*	*P*–1	$P2_1/c$
13.552(3)	13.422(3)	6.0710(12)	14.3837(15)
4.6722(9)	4.6511(9)	7.5613(15)	9.3167(10)
21.377(6)	21.261(4)	31.715(6)	13.3889(14)
90	90	89.95(3)	90.00
90.40(3)	94.97(3)	87.01(3)	104.847(2)
90	90	85.23(5)	90.00
4	4	2	4
1353.5(5)	1322.3(5)	1448.8(5)	1734.3(3)
298	298	293	293
1.880	1.413	1.377	1.759
4355	3017	5543	11780
2212	3017	5055	3445
2036	1912	2331	1977
0.0288	0.0475	0.0749	0.0518
0.0739	0.1232	0.2719	0.1143
1.005	1.067	1.02	0.96

21	**21·(4/3)H_2O**	**21·2H_2O**(293 K)	**21·2H_2O** (100 K)
C11H10N4O	C33H38N12O7	C11H14N4O3	C11H14N4O3
214.23	714.75	250.26	250.26
Orthorhombic	Monoclinic	Monoclinic	Monoclinic
*Aba*2	*C*2/*c*	$P2_1/c$	$P2_1/c$
13.707(3)	*12.941(3)*	6.8138(5)	6.7982(8)
7.014(1)	11.789(2)	19.586(11)	19.560(2)
10.006(2)	*22.401(5)*	9.292(4)	9.2746(11)
90	90	90	90
90	101.37(3)	101.24(3)	101.26(2)
90	*90*	90	90
4	4	4	4
962.0(3)	3350.5(13)	1216.3(9)	1208.7(2)
293	120	293	100
1.479	1.417	1.367	1.375
575	3834	2402	5789
575	3834	2402	2386
518	3171	1675	1651
0.0431	0.0449	0.0522	0.0499
0.0999	0.1307	0.1409	0.1097
1.13	1.10	1.04	1.03

21·SA	**21·FA·H_2O**	**22·H_2O**	**23**
C15H16N4O5	C15H16N4O6	C11H12N4O4	C13H16I2N4O
332.32	348.32	264.25	498.10
Monoclinic	Triclinic	Monoclinic	Triclinic
*C*2/*c*	*P*-1	*C*2/*c*	*P*-1
38.093(8)	7.404(2)	7.9686(7)	7.7439(15)
5.282(1)	8.068(4)	12.224(1)	10.464(2)
16.428(3)	13.562(3)	24.538(2)	10.683(2)
90	104.55(3)	90.0	101.42(3)
109.35(3)	98.02(2)	90.650(2)	100.55(3)
90	95.52(3)	90.0	99.28(3)
8	2	8	2
3118.7(2)	769.2(5)	2390.1(4)	816.5(3)
298	298	298	100
1.416	1.504	1.469	2.026
3606	3799	17207	10526
3565	3522	2349	3216
2369	1743	1994	3119
0.0676	0.0651	0.0462	0.0194
0.1546	0.1682	0.1097	0.0490
1.12	1.12	1.12	1.104

24	**26**	**27**	**28**
C12H11N3O	C14H7F5O4	C14H9F5N2O2	C14H8F5NO3
213.24	334.20	332.23	333.21
Orthorhombic	Monoclinic	Monoclinic	Monoclinic
Pbca	*Cc*	$P2_1$	$P2_1/n$
11.779(1)	24.7320(4)	7.3546(3)	11.290(2)
9.461(1)	7.7420(1)	6.0207(2)	6.733(2)
18.262(2)	14.3430(3)	14.7507(5)	18.085(4)
90	90	90	90
90	108.42(1)	90.568(2)	105.04(3)
90	90	90	90
8	8	2	4
2035.0(4)	2605.6(8)	653.1(4)	1327.5(5)
100	153	153	293
1.392	1.704	1.689	1.667
11545	6107	4261	5535
2014	6103	2706	3018
1897	4307	2243	1966
0.0425	0.0474	0.0412	0.0421
0.1038	0.1221	0.0987	0.1165
1.12	1.05	1.10	1.03

31	**37**	**38**	**39**
C14H3F10NO3	C48H36N6O6	C108H80N14O12	C30H24N4O4
423.17	792.83	1765.86	504.53
Orthorhombic	Monoclinic	Triclinic	Triclinic
Pbca	$P2_1/c$	*P-1*	*P-1*
9.8555(12)	9.8825(12)	9.4776(10)	7.3484(9)
9.3305(12)	12.5062(15)	14.1266(15)	9.2233(11)
32.741(4)	16.2270(19)	17.4609(18)	18.743(2)
90	90	70.605(2)	94.272(2)
90	100.447(2)	82.982(2)	100.101(2)
90	90	73.717(2)	94.900(2)
8	2	1	2
3010.8(6)	1972.3(4)	2115.6(4)	1240.9(3)
298	298	100	298
1.867	1.335	1.386	1.350
4261	14658	22057	9724
2916	3875	8358	4862
1892	2347	4884	1975
0.0496	0.0467	0.0769	0.0701
0.1206	0.1160	0.1580	0.1335
1.02	1.02	1.04	0.96

40	**41**	**42**	**43**
C30H22N4O3	C32H24N2O3	C25H18N3O4	C40H32N2O9
486.52	484.53	424.42	684.68
Monoclinic	Orthorhombic	Monoclinic	Orthorhombic
C2/c	$Pca2_1$	*C2/c*	$Pna2_1$
14.159(3)	12.3666(14)	18.133(3)	14.3642(9)
11.943(3)	13.7140(16)	14.960(2)	16.2055(11)
14.249(3)	14.0060(15)	15.340(2)	14.2108(9)
90	90	90	90
102.423(5)	90	102.789(2)	90
90	90	90	90
4	4	8	4
2353.1(9)	2375.4(5)	4058.0(10)	3308.0(4)
100	100	100	100
1.373	1.355	1.389	1.375
5308	5027	4818	23414
2326	2226	3469	3396
1287	1662	2672	3308
0.0636	0.0486	0.0454	0.0297
0.1590	0.1168	0.1233	0.0766
1.01	1.02	1.01	1.04

44	**45**	**48**	**49**
C94H69N7O8	C94H72N6O9	C6H6N2O2	C6H6N2O2
1424.56	1429.58	138.13	138.13
Monoclinic	Triclinic	Orthorhombic	Monoclinic
$P2_1/c$	*P-1*	*Pna*21	$P2_1/n$
15.601(4)	10.275(1)	13.467(3)	11.050(2)
14.341(4)	11.926(1)	11.722(3)	3.687(5)
16.892(5)	15.401(1)	3.737(1)	15.019(2)
90	82.408(1)	90	90
106.095(5)	71.327(1)	90	110.064(2)
90	81.211(1)	90	90
2	2	4	4
3631.2(17)	1759.9(3)	589.9(3)	574.7(2)
298	100	100	100
1.303	1.349	1.555	1.596
23046	19013	1988	3173
6387	6953	679	1136
3167	5256	625	1061
0.0753	0.0437	0.0687	0.0379
0.1643	0.1200	0.1384	0.1028
1.05	1.02	1.20	1.07

50	**51**	**52.BPNO**	**53.BPNO.H_2O**
C6H6N2O2	C5H5N3O2	C17H16N3O4	C16H14N4O6
138.13	139.12	326.33	334.29
Orthorhombic	Triclinic	Monoclinic	Orthorhombic
Pbca	*P-1*	$P2_1/c$	*Pbca*
12.940(3)	5.403(3)	10.3768(12)	16.2210(11)
7.350(2)	7.508(4)	15.8728(18)	6.5971(5)
13.087(3)	14.978(8)	9.4522(11)	27.0692(19)
90	96.838(9)	90	90
90	97.094(9)	93.165(2)	90
90	102.822(9)	90	90
8	4	4	8
1244.6(6)	581.2(6)	1554.5(3)	2896.7(4)
298	298	100	100
1.474	1.590	1.394	1.533
3790	5890	7009	17132
1219	2323	3072	2844
905	1829	2463	2270
0.0504	0.0669	0.0458	0.0510
0.1405	0.1933	0.1154	0.1204
1.04	1.09	1.02	1.07

54 (Form-I)	**54 (Form-II)**	**55**	**56**
C11H11N3O2S	C11H11N3O2S	C11H10ClN3O2S	C12H13N3O2S
249.30	249.30	283.74	263.32
Monoclinic	Monoclinic	Monoclinic	Monoclinic
$P2_1/c$	$P2_1/c$	$P2_1/c$	$P2_1/c$
8.5450 (13)	12.1099 (15)	9.232 (6)	9.169 (2)
9.0638 (17)	10.7924 (12)	8.900 (6)	8.867 (2)
15.151 (2)	17.464 (2)	15.102 (9)	15.222 (4)
90	90	90	90
91.492 (12)	97.318 (2)	96.081 (11)	96.511 (5)
90	90	90	90
4	8	4	4
1173.0 (3)	2263.9 (5)	1233.9 (14)	1229.6 (5)
293	203	298	298
1.412	1.463	1.527	1.423
3526	14219	10435	10199
3403	5443	3061	2909
2687	2871	1881	2135
0.0406	0.0579	0.0574	0.0559
0.1117	0.1525	0.1552	0.1452
1.02	0.96	0.97	1.04

58	**59**	**60**	**61**
C12H13N3O2S	C11H10FN3O2S	C11H10ClN3O2S	C11H10BrN3O2S
263.32	267.29	283.74	328.19
Monoclinic	Monoclinic	Monoclinic	Monoclinic
$P2_1/c$	$P2_1/c$	$C2/c$	$P2_1/c$
12.434 (4)	9.000 (6)	13.725 (6)	10.7941 (9)
10.396 (4)	8.618 (6)	7.312 (3)	18.2559 (15)
9.113 (3)	14.643 (10)	25.419 (11)	26.335 (2)
90	90	90	90
92.247 (6)	91.698 (17)	92.886 (8)	94.330 (2)
90	90	90	90
4	4	8	16
1177.1 (7)	1135.2 (13)	2547.7 (19)	5175.1 (7)
223	203	203	203
1.486	1.564	1.480	1.685
14514	5392	15199	65572
2916	1385	3167	12882
1971	804	2065	7255
0.0596	0.1082	0.0700	0.0656
0.1563	0.3162	0.1802	0.1848
1.04	1.02	1.06	1.04

62	63 (Form-I)	63 (Form-II)	64
C11H10IN3O2S	C12H13N3O2S	C12H13N3O2S	C12H10F3N3O2S
375.19	263.32	263.32	317.30
Orthorhombic	Monoclinic	Monoclinic	Orthorhombic
Pbca	$P2_1/n$	$P2_1/c$	*Pbca*
10.761 (5)	15.015 (6)	10.384 (3)	10.8897 (13)
18.260 (9)	10.880 (5)	17.749 (4)	18.343 (2)
26.880 (13)	17.066 (7)	26.473 (7)	26.640 (3)
90	90	90	90
90	113.457 (8)	94.531 (7)	90
90	90	90	90
16	8	16	16
5282 (4)	2557.6 (19)	5075 (2)	5321.3 (10)
183	253	203	203
1.887	1.368	1.379	1.584
61369	32477	19916	51767
6682	6436	6524	6621
2919	3422	2974	4550
0.0724	0.0565	0.0737	0.0589
0.2247	0.1688	0.2601	0.1481
0.99	1.00	0.90	1.05

65	66	67	68
C12H13N3O3S	C11H12N4O5S	C27H21N3	C27H27N3
279.32	312.32	387.47	393.52
Orthorhombic	Monoclinic	Monoclinic	Hexagonal
Pbca	$P2_1/c$	$C2/c$	$P6_5$
10.614 (3)	14.663 (16)	100	298
18.276 (5)	12.276 (16)	33.387(4)	12.8956(12)
27.402 (7)	7.589 (11)	5.8867(7)	12.8956(12)
90	90	24.412(3)	23.784(5)
90	96.16 (9)	90	90
90	90	121.61(2)	90
16	4	90	120.00
5315 (2)	1358 (3)	8	6
298	293	4085.9 (9)	3425.2(8)
1.396	1.528	1.260	1.145
48710	1925	14859	11367
4660	1763	4083	1999
3997	1241	3187	1171
0.1024	0.0781	0.0450	0.0914
0.2560	0.2323	0.1144	0.2038
1.12	1.05	1.03	1.126

List of Publications

1. Searching for polymorph: Second crystal form of 6-amino-2-phenylsulfonylimino-1,2-dihydropyridine.
   Ram K. R. Jetti, Roland Boese, Jagarlapudi A. R. P. Sarma, **L. Sreenivas Reddy**, Peddy Vishweshwar and Gautam R. Desiraju
   Angew. Chem., *Int. Ed*., **2003**, *42*, 1963–1967.

2. Phenyl-perfluorophenyl synthon mediated cocrystallization of carboxylic acids and amides
   L. Sreenivas Reddy, Ashwini Nangia and Vincent M. Lynch
   Cryst. Growth Des., **2004**, 4, 89–94.

3. Structural variations and polymorphism of some derivatives of 6-amino-2-phenylsulfonylimino-1,2-dihydropyridine
   Michael T. Kirchner, **L. Sreenivas Reddy**, Gautam R. Desiraju, Ram K. R. Jetti and Roland Boese
   Cryst. Growth Des., **2004**, 4, 701-709.

4. The rare $4^2.6^3.8$ network and a chiral, trigonal net in crystal structures of 1,3,5-tris(4-pyridyl)benzenes
   L. Sreenivas Reddy, Balakrishna R. Bhogala and Ashwini Nangia
   CrystEngComm, **2005**, *7*, 206–209.

5. Halogen trimer-mediated hexagonal host framework of 2,4,6-tris(4-halophenoxy)-1,3,5-triazine. Supramolecular isomerism from hexagonal channel (X =Cl, Br) to cage structure (X = I)
   Binoy K. Saha, Ram K. R. Jetti, **L. Sreenivas Reddy**, Srinivasulu Aitipamula and Ashwini Nangia
   Cryst. Growth Des., **2005**, *5*, 887-899.

6. Engineering the weak N–H···π hydrogen bond in 4-tritylbenzamide host and controlling the interaction through guest selection
   C. Malla Reddy, **L. Sreenivas Reddy**, Srinivasulu Aitipamula, Ashwini Nangia, Chi-Keung Lam and Thomas C. W. Mak
   CrystEngComm, **2005**, *7*, 44–52.

7. Hydrogen bonding in crystal structures of *N*,*N*'-bis(3-pyridyl)urea. Why is the N–H···O tape synthon absent in diaryl ureas with electron-withdrawing groups?
   L. Sreenivas Reddy, Srinivas Basavoju, Venu R. Vangala and Ashwini Nangia
   Cryst. Growth Des., **2006**, *6*, 161-173.

8. Carboxamide–pyridine *N*-oxide heterosynthon for crystal engineering and pharmaceutical cocrystals
   L. Sreenivas Reddy, N. Jagadeesh Babu and Ashwini Nangia
   Chem. Commun., **2006**, 1369.

9. Hydrogen bonding competition and interplay of weak interactions in crystal structures of nitro substituted diphenylureas
L. Sreenivas Reddy, Sumod George, K.C. Sreekanth and Ashwini Nangia
(Manuscript under preparation)

10. Solvent free supramolecular synthesis of some carboxylic acid and carboxamide cocrystals
L. Sreenivas Reddy, Rahul Banerjee, Prashant M. Bhatt, G. Kruger and Ashwini Nangia (Manuscript under preparation)

11. Role of hydrogen bonding and aromatic stacking in cocrystals of phenazine and acridine with multi-functional molecules
L. Sreenivas Reddy and Ashwini Nangia (Manuscript under preparation)